UNIVERSITAT
POLITÈCNICA
DE VALÈNCIA

PhD Dissertation

Doctorado en Automática, Robótica e Informática Industrial

Contributions to glucagon and pramlintide pharmacokinetics and pharmacodynamics modeling for multi-hormone artificial pancreas systems

---

Author: Clara Furió Novejarque

Supervisors: Prof. Jorge Bondia Company
Dr. José Luis Díez Ruano

Instituto Universitario de Automática e Informática Industrial

Universitat Politècnica de València

València, November 2023

This work was supported by grant FPU17/03404, grant EST19/00740,
and project PID2019-107722RB-C21, funded by MCIN/AEI/10.13039/501100011033.

Acknowledgements

No habría podido llegar a escribir estas líneas de no ser por la ayuda de mucha gente. Me siento muy afortunada de haber llegado hasta aquí y de que hayáis compartido conmigo este viaje.

En primer lugar, gracias a mis directores, Jorge Bondia y José Luis Díez. Ha sido un proceso largo pero gracias por darme la oportunidad de participar en este proyecto con vosotros. Gracias por todo vuestro apoyo y paciencia durante estos años, sois un referente para mí como profesionales y como personas.

I want to thank Danmarks Tekniske Universitet for welcoming me during my external stay. Thank you, John Bagterp Jørgensen for being my supervisor there and encouraging my ideas. I also want to thank all the people at DTU Compute that made me feel at home, especially Tobias, Asbjørn, Sarah, Morten, and Markus. Thank you to the people from the Steno Diabetes Center, Ajenthen Ranjan and Kirsten Nørgaard, for accepting to collaborate with us, and providing your clinical expertise to our work.

Gracias a mis compañeros de grupo de Tecnodiabetes, Alejandro, Ricardo y Juan David, que me han acompañado durante el proceso. También a la gente del Departamento de Ingeniería de Sistemas y Automática, tanto el cuerpo docente como la gente de la "Sala", con quienes compartí el inicio de mi doctorado.

Gracias Iván por toda tu ayuda y apoyo, esta tesis no habría salido adelante sin ti. Gracias Jose por compartir conmigo las penas del doctorado y estar siempre ahí. Gracias Cris por estar a mi lado y creer siempre en mí. Gracias a Vanessa y Michelle por ayudarme a sobrellevar todas las dificultades. Gracias a Adri, Isa, Guille, Laura, Nóbel e Iván, que

desde fuera habéis estado cuidando de mí y animándome a seguir. Gracias a Aida, que fue mi mayor alegría durante los meses que estuve lejos de casa. Y gracias a José Luis, por ser mi cuarto revisor.

Por supuesto, muchísimas gracias a mi familia. A mi madre Susi y a mi hermano Jesús, que me han apoyado incondicionalmente desde que decidí embarcarme en esta aventura. Gracias por cuidar de mí en el proceso e incluso ofreceros a completar mi tesis con un capítulo de antropología y otro de sociología. Os quiero mucho.

Gracias, JuanFer. No habría podido llegar hasta aquí sin ti, gracias por todo tu apoyo, tu ayuda y paciencia sobretodo estos últimos meses, amz.

Gracias a todos.

Abstract

English

Glucose regulation in the human body results from the coordinated secretion of hormones. Type 1 Diabetes (T1D) is a chronic disease that destroys insulin-producing cells, one of the main agents in the glucose regulation process. Consequently, people with T1D depend on exogenous insulin administration. However, therapy management is not an easy task, and it faces great variability. Artificial Pancreas systems were designed to ease the disease management, administering insulin automatically through an insulin pump based on the logic of a control algorithm that reads information from a continuous glucose monitor.

Nevertheless, insulin action is uni-directional (lowering glucose values), and sometimes, it is insufficient to maintain safe plasma glucose levels. That is why, occasionally, other hormones are also administered, with opposite (like glucagon) or complementary effects (like pramlintide) to insulin. For automatic systems to benefit from these control actions, it is necessary to study and know their dynamics to simulate their behavior, design aware controllers, and carry out in silico experiments before using the system with patients. Glucagon use in T1D has a long trajectory; and has been used in automatic systems. However, there exists a wide heterogeneity in the definitions of glucagon effect, especially related to its interaction with insulin, and it is necessary to develop models that are more physiologically accurate. On the other hand, pramlintide models have barely been studied.

This thesis' main objective is to improve T1D simulators to validate artificial pancreas systems. Specifically, a detailed analysis of the state of the art is carried out to know the physiological model proposals in the literature. Then, the focus moves to describing

the glucagon effect on endogenous glucose production and the pharmacokinetics and pharmacodynamics of pramlintide. This work includes the proposal of new physiology-based models for glucagon and pramlintide. The glucagon model was validated with individual clinical data, and the pramlintide model was validated with populational data. Both proposals improved previously existing results.

Castellano

La regulación de los niveles de glucosa en el cuerpo humano es el resultado de la secreción coordinada de hormonas. La Diabetes Tipo 1 (DT1) es una enfermedad crónica que provoca la destrucción de las células responsables de la producción de insulina, uno de los principales agentes en la regulación de glucosa. Por tanto, las personas con DT1 dependen de la administración exógena de insulina. No obstante, la gestión de la terapia no es sencilla y está sujeta a una gran variabilidad. Los sistemas de Páncreas Artificial se diseñaron con el objetivo de simplificar la gestión de la enfermedad, administrando insulina de manera automática a través de una bomba de insulina, en base a la lógica de un algoritmo de control que emplea información de un monitor continuo de glucosa.

Sin embargo, la acción de la insulina es unidireccional (disminuye el valor de la glucosa), y a veces resulta insuficiente para mantener unos niveles seguros de glucosa en sangre. Por eso, en ocasiones se administran otras hormonas, con efectos opuestos (como el glucagón), o complementarios (como la pramlintida) a la insulina. Para que los sistemas automáticos se beneficien de estas acciones de control, es necesario estudiar y conocer sus dinámicas para poder simular su comportamiento, diseñar controladores que los tengan en cuenta y realizar experimentos in silico previos a utilizar los sistemas en pacientes. El uso del glucagón ya cuenta con una larga trayectoria y ha sido utilizado en varios sistemas automáticos. Sin embargo, existe mucha heterogeneidad en las formulaciones de modelos del efecto del glucagón, sobre todo en relación con su interacción con la insulina, y es necesario profundizar en el desarrollo de modelos que reflejen mejor la fisiología subyacente. Por otra parte, los modelos de pramlintida apenas se han estudiado.

El objetivo principal de esta tesis es contribuir a mejorar simuladores para validar sistemas de páncreas artificial. En concreto, se realiza un análisis detallado del estado del arte para conocer las propuestas de modelos fisiológicos en la literatura, para luego centrarse en la descripción del efecto de glucagón en la producción endógena de glucosa y la farmacocinética y farmacodinámica de la pramlintida. El trabajo incluye la propuesta de nuevos modelos para glucagón y pramlintida basados en la fisiología, validados con datos clínicos individuales en el caso del glucagón y con datos poblacionales de la literatura en el

caso de la pramlintida, mejorando en ambos casos los resultados previamente existentes.

Valencià

La regulació dels nivells de glucosa en el cos humà és el resultat de la secreció coordinada d'hormones. La Diabetis Tipus 1 (DT1) és una malaltia crònica que provoca la destrucció de les cèl·lules responsables de la producció d'insulina, un dels principals agents en la regulació de glucosa. Per tant, les persones amb DT1 depenen de l'administració exògena d'insulina. No obstant això, la gestió de la teràpia no és senzilla i està subjecta a una gran variabilitat. Els sistemes de Pàncrees Artificial es van dissenyar amb l'objectiu de simplificar la gestió de la malaltia, administrant insulina de manera automàtica a través d'una bomba d'insulina, en funció de la lògica d'un algorisme de control que empra informació d'un monitor continu de glucosa.

No obstant això, l'acció de la insulina és unidireccional (disminueix el valor de la glucosa), i de vegades resulta insuficient per a mantindre uns nivells segurs de glucosa en sang. Per això, ocasionalment s'administren altres hormones, amb efectes oposats (com el glucagó), o complementaris (com la pramlintida) a la insulina. Perquè els sistemes automàtics es beneficien d'aquestes accions de control, és necessari estudiar i conéixer les seues dinàmiques per a poder simular el seu comportament, dissenyar controladors que els tinguen en compte i realitzar experiments in silico previs a utilitzar els sistemes en pacients. L'ús del glucagó ja compta amb una llarga trajectòria i ha sigut utilitzat en diversos sistemes automàtics. No obstant això, existeix molta heterogeneïtat en les formulacions de models de l'efecte del glucagó, sobretot en relació amb la seua interacció amb la insulina, i és necessari aprofundir en el desenvolupament de models que reflectisquen millor la fisiologia subjacent. D'altra banda, els models de pramlintida a penes s'han estudiat.

L'objectiu principal d'aquesta tesi és contribuir a millorar simuladors per a validar sistemes de pàncrees artificial. En concret, es fa una anàlisi detallada de l'estat de l'art per a conéixer les propostes de models fisiològics en la literatura, per a després centrar-se en la descripció de l'efecte de glucagó en la producció endògena de glucosa i la farmacocinètica i farmacodinàmica de la pramlintida. El treball inclou la proposta de nous models per a glucagó i pramlintida basats en la fisiologia, validats amb dades clíniques individuals en el cas del glucagó i amb dades poblacionals de la literatura en el cas de la pramlintida, millorant en tots dos casos els resultats prèviament existents.

Contents

List of Figures

List of Tables

Acronyms

AIC	Akaike Information Criterion
AP	Artificial Pancreas
BIC	Bayesian Information Criterion
CGM	Continuous Glucose Monitoring
CL	Closed-loop
DHAP	Dual-hormone Artificial Pancreas
EGP	Endogenous glucose production
FDA	U.S. Food and Drug Administration
GR	Glucagon receptors
IV	Intravenous

OL	Open-loop
PK	Pharmacokinetics
PD	Pharmacodynamics
RMSE	Root Mean Squared Error
SC	Subcutaneous
SHAP	Single-hormone Artificial Pancreas
T1D	Type 1 diabetes

Chapter 1

Introduction

"Whatever I do when I grow up, it won't be related to biology." — Me to my mum, at eight years old.

1.1 Motivation

Several physiological mechanisms are put into place in the human body to ensure that blood glucose levels are kept within a tight range ensuring glucose availability, the main energy source for cells, to every organ. The normal glucose regulation process relies on numerous physiological sensors and actuators to maintain appropriate glucose levels, with the pancreas and insulin being the main actors involved.

Type 1 Diabetes (T1D) is a chronic disease in which the body is unable to produce insulin on its own. This causes the equilibrium to crumble, and people with T1D face the titanic task of replacing the function of the pancreas with non-physiological, external devices that make glucose control burdening and challenging. As such, perfect glucose control in T1D is impossible.

Diabetes technology opens up possibilities for engineers and other technological sciences to contribute to such a medical-centered problem in the form of hardware development, control algorithms design, or, as the case of this thesis, mathematical models to serve as tools in algorithms development.

More portable glucose sensors and insulin pumps were developed to ease glucose management for people with T1D. However, the therapy is still the patients' responsibility since they are the ones coexisting with the disease every hour of their day. Artificial Pancreas (AP) systems were conceived to fill this gap. These systems provide an insulin dosing strategy based on a control algorithm that responds to glucose changes, replacing most of the patient's decision-making and alleviating their burden. AP systems are a reality, with up to seven commercial options already available in the market. However, glucose control after meals and during exercise still poses serious challenges that impede a total automatization of the system, requiring some involvement from the patients (e.g., announcing the number of carbohydrates in the meal or the start of the exercise to the system ahead enough).

Moreover, these two situations pose significant disturbances to glucose levels. Meals cause blood glucose levels to rise, whereas (aerobic) exercise drops glucose values. Deviations from the "normal" glycemic range can negatively affect the person. However, sometimes insulin control is insufficient to counter these disturbances. Consequently, a proposed strategy is the development of Dual-Hormone Artificial Pancreas (DHAP) systems. These systems use a second control action to either act in the opposite direction of insulin, such as glucagon, or to complement insulin action, easing postprandial glucose excursions, such as the case of pramlintide, an amylin analog.

Both treatments are designed to mimic the behavior of actual pancreatic hormones (glucagon and amylin) secretion since their normal behavior is also affected by T1D. Glucagon has been used in diabetes treatment for a long time, being used as a one-dose administration to help with a quick recovery from severe low-glucose values. However, several unknowns still surround its effect mechanisms and potential interactions with other hormones. On the other hand, pramlintide has been used in Type 2 Diabetes treatment, but it has only been approved for its use in T1D in the USA.

The testing and pre-clinical validation of control algorithms for AP systems require simulators that emulate the glucose responses observed in people with T1D in order to test the strategies without posing any risk to the patients. Developing new control strategies for DHAP systems requires accurate models of the adjunctive drugs' kinetics and dynamics to observe their effect and design an optimal control. Several simulators and insulin-glucose models have been proposed in the literature and are currently used by researchers to test AP strategies. However, glucagon is not often included in simulators, and the description of its effect is quite heterogeneous. On the other hand, pramlintide models are almost nonexistent in the literature.

Simulators are crucial for the development of AP algorithms, allowing for *in silico*

validations or even carrying out hardware-in-the-loop (HIL) validations of AP implementations for regulatory submissions. This technique consists of introducing real pieces of software and hardware that will be used in the clinical system and connecting them to the simulator, which allows the test of the system in "real" conditions. Since a simulation substitutes the person, it eliminates any potential risks for them and enables the possibility of performing several inexpensive tests. A HIL system of this kind was developed by the author prior to working on her thesis. The system was used to validate the AP used in the clinical trial in Viñals et al. (2021), co-authored by the candidate.

Hence, the thesis objectives are defined around the need of accurate simulators for T1D, given their importance and added value in pre-clinical experiments. These objectives are described next.

1.2 Objectives

The thesis project was conceived with the main objective of contributing to improving simulators for T1D to be used in the validation of AP systems. In order to reach it, three other sub-objectives were defined:

- To study and understand the current state and limitations of AP systems and the available simulators. This also included understanding the glucose homeostasis process and the relationships among the agents involved.
- To propose and validate a model of glucagon effect that captures glucagon dynamics observed in clinical individual data, contributing to the analysis of the physiological mechanisms surrounding glucagon effect.
- To propose and validate a pramlintide model that captures its pharmacodynamics (PD) and pharmacokinetics (PK), reflecting pramlintide behavior from the administration site until its effect becomes apparent in the rate of gastric emptying after a meal.

1.3 Structure of the thesis

Figure 1.1 depicts a summary of the thesis structure. The document is divided into three main parts, corresponding to the three sub-objectives listed above.

Part 1, *State of the art*, is composed of two chapters:

- Chapter 2 describes the normal glucose regulation process to help understand the implications of T1D. Next, the disease and the most common treatments available nowadays are presented. Among these treatments stand the AP systems, with their multi-hormone configurations. The chapter describes the contributions of these systems and their current most significant developments.

- Chapter 3 presents some of the most relevant models for T1D found in the literature, including two sections devoted to glucagon effect descriptions and pramlintide models, respectively.

The rest of the thesis presents the results of the work related to the models' development. Part 2, *Glucagon*, corresponds to the proposed glucagon model's definition and successive validations. This part is composed of three chapters:

- Chapter 4 describes glucagon receptors and glucagon's mechanism to promote glucose production. Then, the proposed model is defined. The rest of the chapter describes the identification and validation methods used in the subsequent chapters to validate the proposal.

- Chapter 5 performs the first validation of the glucagon model with a clinical dataset. Two identification methods were used, and the results are presented and discussed.

- Chapter 6 presents the second validation of the glucagon receptors model with a new clinical dataset. In this case, three different identification methods were used, and the results are presented and discussed.

Part 3, *Pramlintide*, corresponds to the development and validation of the pramlintide PK/PD model.

- Chapter 7 describes amylin physiology and presents the candidate model structures for intravenous PK, subcutaneous PK, and PD.

- Chapter 8 presents the data gathered from the literature to validate the pramlintide model, with special emphasis in datasets measuring glucose rate of appearance (tracer studies) to avoid confounding factors with insulin effect in glucose data. The chapter then describes the selection process carried out to present the model proposal.

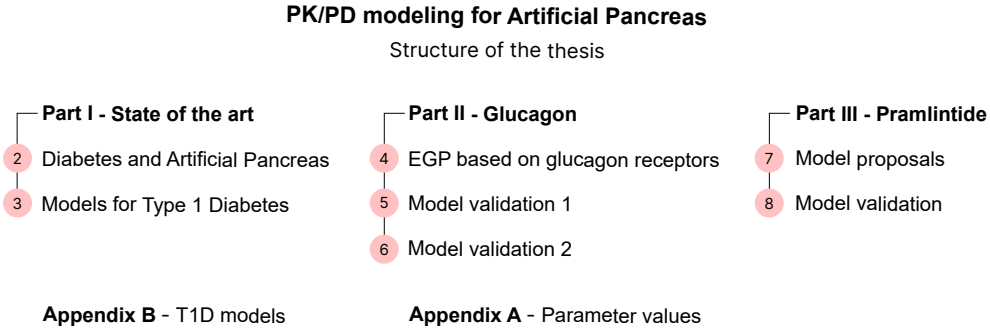

Figure 1.1: Thesis structure summary.

Finally, Chapter 9 lays out the final conclusions of the thesis. An additional final chapter lists the contributions and publications generated during the duration of the thesis.

Two appendices are included afterward. Appendix A lists the individual parameter values obtained as a result of the identifications carried out in Chapter 5 and Chapter 6. Appendix B includes a set of tables describing the states and parameters of some of the most relevant models presented in Chapter 3. The document's final pages include a set of tables that depict the complete set of equations of these models.

Part I

State of the art

Chapter 2

Diabetes and Artificial Pancreas

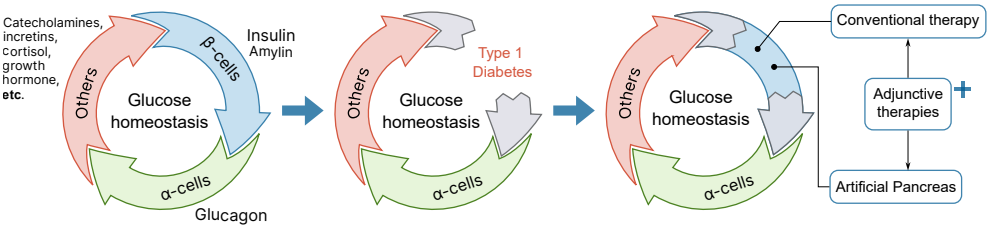

Blood glucose regulation is an intricate process that relies on several mechanisms, but the main agents are the pancreatic hormones insulin and glucagon. People with Type 1 Diabetes suffer from the autoimmune destruction of β-cells, producers of insulin, which crumbles the glucose homeostasis. In order to counter this deficiency, blood glucose has to be monitored to administer the proper amount of exogenous insulin. Some strategies have been developed to aid glucose control, such as Artificial Pancreas (AP) systems, also known as Automated Insulin Delivery systems. The use of adjunctive therapies is under investigation and can be used as an add-on to either conventional therapy or AP systems to facilitate glucose control.

2.1 Glucose regulation

Cells in the human body depend on adenosine triphosphate (ATP) as their energy source. ATP is obtained by oxidizing several metabolic fuels, but glucose is the main one. Hence, many mechanisms are implemented to guarantee that plasma glucose levels are kept within a tight healthy range (normoglycemia) to ensure glucose availability to the organism. Nevertheless, it is expected that glucose levels will change due to different factors. For instance, fasting or aerobic[1] exercise will decrease glucose levels. The contrary will happen after meals or anaerobic[2] exercise. However, many other factors could sometimes have effects on glucose levels (e.g., stress, menstruation cycles, sickness), hence the importance of glucose homeostasis to ensure that these variations do not have negative health consequences.

Glucose can appear in plasma from three possible sources: intestinal absorption after meal digestion; glycogenolysis, which breaks down glycogen in the liver; and gluconeogenesis, which forms glucose in the liver and kidney from other compounds (e.g., lactate or pyruvate). On the other hand, cells can uptake glucose from plasma, causing a decrease in plasma glucose concentration. If cells require energy, they will convert glucose into ATP through the glycolytic pathway by oxidation. However, if there is a surplus of glucose, glucose will be stored as glycogen through glycogenesis to serve as glucose reserve. On the other hand, glycolysis can also perform a non-oxidative conversion of glucose, producing lactate, that will diffuse from the muscle into capillaries and the liver. This lactate may come back later as glucose through gluconeogenesis if the liver is oxygenated and converts it into pyruvate (Shrayyef and Gerich, 2010; Woerle et al., 2003; Müller et al., 2017; Nordlie et al., 1999; Salway, 1993). Figure 2.1 summarizes these glucoregulatory metabolic processes.

The primary glucose producers are the liver and kidneys. Since the kidney contains little glycogen, its contribution is mainly through gluconeogenesis. In contrast, the liver releases glucose both by glycogenolysis and gluconeogenesis. These processes regulate plasma glucose levels and maintain them within the proper limits (see Figure 2.1).

The body's main glucose consumers are the brain, the skeletal muscle, the kidneys, blood cells, splanchnic organs (i.e., the stomach, small and large intestine, pancreas, spleen, and liver), and adipose tissue. The brain is the organ requiring the greatest consumption

[1] Aerobic exercise involves repeated and continuous movement (e.g., walking, cycling, jogging, or swimming).

[2] Anaerobic exercise refers to high-intensity interval training, alternating brief periods of intense exercise with recovery periods (e.g., sprinting, weight lifting) (Riddell et al., 2017).

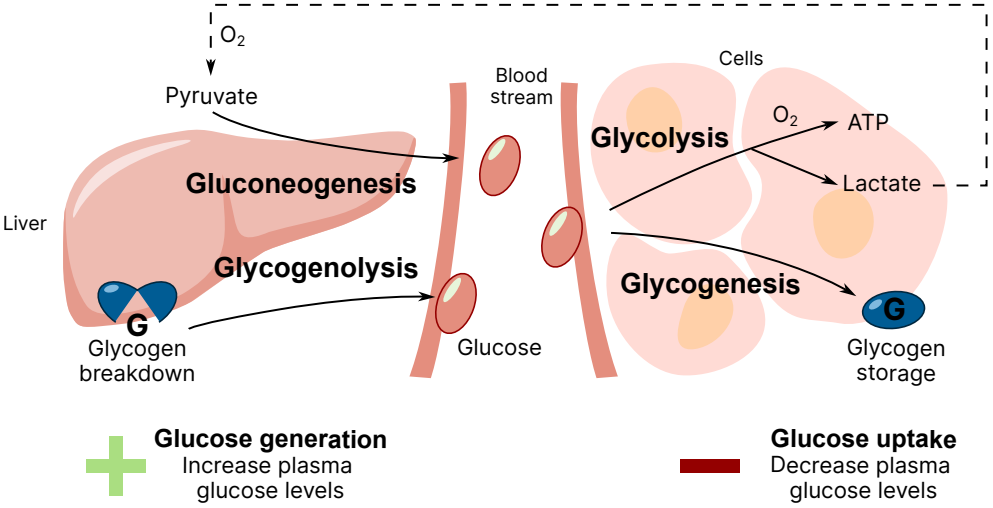

Figure 2.1: Normal glucose regulation process. Processes on the left occur mainly in the liver (gluconeogenesis also in the kidney) and increase plasma glucose levels. Processes on the right occur in most tissue cells and decrease plasma glucose. Gluconeogenesis converts pyruvate to glucose, and glycogenolysis breaks down glycogen to obtain glucose. Glycolysis converts glucose either to ATP or lactate. Glycogenesis stores glucose surplus as glycogen. Glucose conversion to ATP and lactate conversion to pyruvate are both oxidation processes that require oxygen (O_2) availability to happen.

(around 50% of glucose), followed by the muscle and kidney (around 15% each), whereas the rest utilize less than 10% of glucose available (Gerich, 1993). Nonetheless, in case of plasma glucose deficit, most organs could obtain energy from other sources, such as ketones or free fatty acids (FFA) (Bano, 2013). The notable exception to this fact is the brain. The brain activity depends entirely on plasma glucose supply since it cannot store glucose as glycogen or synthesize glucose from other sources.

Hence, extreme deviations from normoglycemia will negatively affect the person. Normoglycemia is typically defined as glucose concentration values between 70 and 180 mg/dl. Plasma glucose concentrations above 180 mg/dl mean hyperglycemia whereas values below 70 mg/dl entail hypoglycemia. Hyperglycemia has long-term consequences, especially in the cardiovascular system. Some of the complications include micro- and macro-vascular complications, retinopathy, nephropathy, neuropathy, diabetic ketoacidosis, and bone and joint problems. On the other hand, hypoglycemia consequences start at

tremors, sweating, or dizziness in the mild episodes, while prolonged glucose concentrations under 55 mg/dl could impair cerebral function, and even lower values could lead to convulsions, coma, or death.

In order to prevent these situations, numerous agents come into play to coordinate and regulate blood glucose uptake and disposal. The most relevant are pancreatic hormones insulin and glucagon.

2.1.1 Glucose-regulating agents

The pancreas contains cell clusters that form the islets of Langerhans. These islets contain five different cell types that release hormones from the endocrine system: α-cells (producing glucagon), β-cells (producing insulin, C-peptide and amylin), γ-cells (producing pancreatic polypeptide, PP), δ-cells (producing somatostatin), and ε-cells, producing ghrelin (Röder et al., 2016). Figure 2.2 summarizes the hormones secreted in each cell type and their primary functions. The reported percentage of the abundance of each cell type differs between works, but β-cells are the most abundant, followed by α-cells.

Each hormone performs a specific function in glucose homeostasis. Glucagon increases glucose levels (triggering gluconeogenesis and glycogenolysis and inhibiting glycolysis and glycogenesis), whereas insulin has the opposite effect (enhancing glycolysis and glycogenesis while inhibiting gluconeogenesis and glycogenolysis). Amylin inhibits glucagon production and slows gastric emptying, controlling the rate of exogenous glucose appearance in the circulation. It also acts as a satiety signal by accessing receptors in the area postrema of the brain (Woods et al., 2006). C-peptide, known as "connecting peptide", is co-secreted with insulin, and its main activity is related to insulin synthesis (Wahren et al., 2000). PP, similar to amylin, also has receptors in the brain and regulates gastric emptying as well as inhibiting other hormones' secretion (Katsuura et al., 2002). Somatostatin inhibits the release of both insulin and glucagon. Ghrelin production in the pancreas is small because its main secretion site is the stomach. It is known as the "hunger hormone" since it induces the sensation of hunger (Müller et al., 2015). However, our interest lies in the specific mechanisms of insulin and glucagon that will be explained next.

Insulin secretion depends on plasma glucose concentrations. A plasma glucose increase stimulates insulin secretion and inhibits glucagon secretion to avoid further increases. Moreover, after meal ingestion, the intestine will secrete specific hormones called incretins (e.g., gastrointestinal-inhibitory peptide (GIP) and glucagon-like peptide (GLP-1)) that will further increase insulin secretion and inhibit glucagon secretion. That is why plasma insulin concentrations will be higher after eating something than after get-

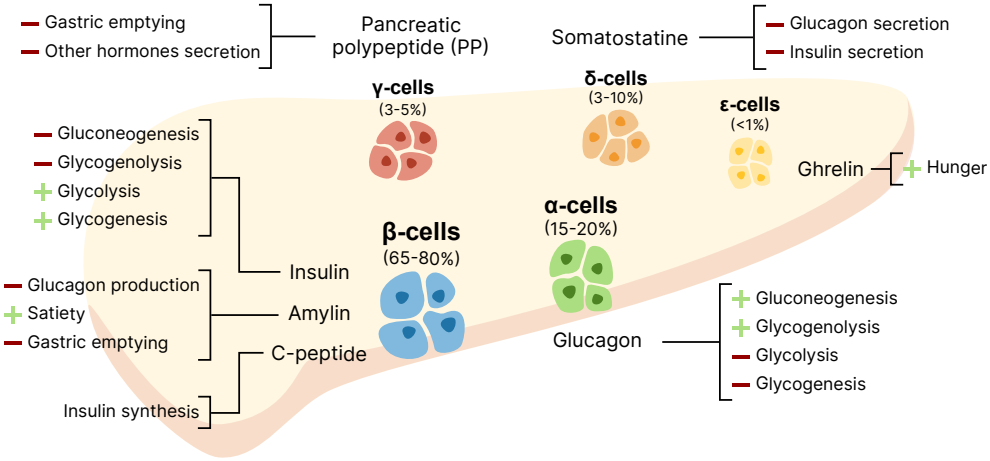

Figure 2.2: Endocrine hormones in the pancreas and their main functions. β-cells, the most abundant, produce insulin, amylin, and C-peptide. α-cells produce glucagon, γ-cells produce PP, δ-cells, somatostatin, and ε-cells, ghrelin. The effects promoted by each of these hormones are marked with a plus (+) sign, while the processes they inhibit or reduce are marked with a minus (-) sign. The approximate proportion of the islets in the pancreas of each cell type is indicated under each of them, based on Röder et al. (2016).

ting the same glucose amount delivered intravenously. Because in the former case, more agents work to increase insulin secretion than in the latter. GLP-1 also delays gastric emptying (Kruger and Gloster, 2004) and promotes satiety. These regulation processes are summarized in Figure 2.3, left-hand side.

On the other hand, in the case of a plasma glucose decrease, insulin secretion will be suppressed. Also, the sympathetic nervous system will release hormones to counter this decrease (glucagon, catecholamines, cortisol, and growth hormone). As stated by Cryer (2001): "Whereas insulin is the dominant glucose-lowering factor, there are redundant glucose-raising (counterregulatory) factors". This makes sense, considering that brain activity depends on a constant supply of glucose. Hence, a robust net of safety mechanisms will rapidly increase blood levels to avoid any endangering low-glucose consequences (Reno et al., 2013).

Insulin will cause glucose levels to decrease utilizing direct and indirect actions. After binding to its receptors, a chain of protein signaling will cause the liver and kidney to stop glucose production (gluconeogenesis and glycogenolysis). It will also promote glucose

uptake by the cells (by glycolysis and glycogenesis), inhibit FFA release, and promote glycogen accumulation (by inhibiting glucose-6-phosphatase and glycogen phosphorylase, both glycogenolysis enzymes, see Chapter 4).

Glucagon is the complementary hormone to insulin in glucose regulation. Plasma glucose increases will inhibit glucagon secretion, whereas glucose decreases will promote glucagon secretion. It will also be promoted after prolonged fasting to raise glucose levels.

Glucagon action is mediated by its receptors in the liver, which, through a complex process, stimulate glycogenolysis and gluconeogenesis, promoting glycogen breakdown (see Chapter 4 for more detail), and inhibiting glycolysis (Müller et al., 2017). A significant difference between the procedures of insulin and glucagon action is that insulin receptors are located on the surface of most cells. However, glucagon receptors are located mostly in the liver, making it the main character in glucagon action management.

Also, amylin action slows down gastric emptying, and this effect is regulated by glycemic status: gastric emptying will be slowed by hyperglycemia and accelerated by hypoglycemia (Young, 2005). This is understandable because a hypoglycemic state requires a quick availability of the ingested nutrients (Hay et al., 2015).

Other agents involved in glucose homeostasis are catecholamines, growth hormone, cortisol, and FFA. Catecholamines include hormones (epinephrine) and neurotransmitters (norepinephrine). They all work towards inhibiting insulin action, acting as counter-effective measures to glucose drops and reducing insulin effects. Changes in the sympathetic nervous system mediate their release. Catecholamines increase during stress and hypoglycemia, and their effects include inhibiting insulin secretion, decreasing insulin action, and activating hepatic glycogenolysis (Gerich, 1988). Growth hormone and cortisol also increase during hypoglycemia, with similar effects inhibiting insulin. Catecholamines have a quick response time, unlike growth hormone and cortisol, which take several hours to occur. On the other hand, FFA stimulates gluconeogenesis and works as fuel for most tissues in the body (except the brain).

There is a hierarchy among these regulatory elements. Epinephrine is only critical when glucagon is deficient. Growth hormone and cortisol are involved in defense against prolonged hypoglycemia. Threshold glucose levels at which each of these responses activate differ between works because they are dynamic (Cryer, 2001). They shift to higher plasma glucose levels during chronic hyperglycemia and to lower levels after recurrent hypoglycemia. According to a study performed on healthy volunteers, hormone secretion is the first stage in the counterregulatory response, when glucose drops around 70 mg/dl. After that, upon reaching 60 mg/dl, the next system activates, which includes epinephrine, norepinephrine, and growth hormone. Glucose drops under approximately 60 mg/dl

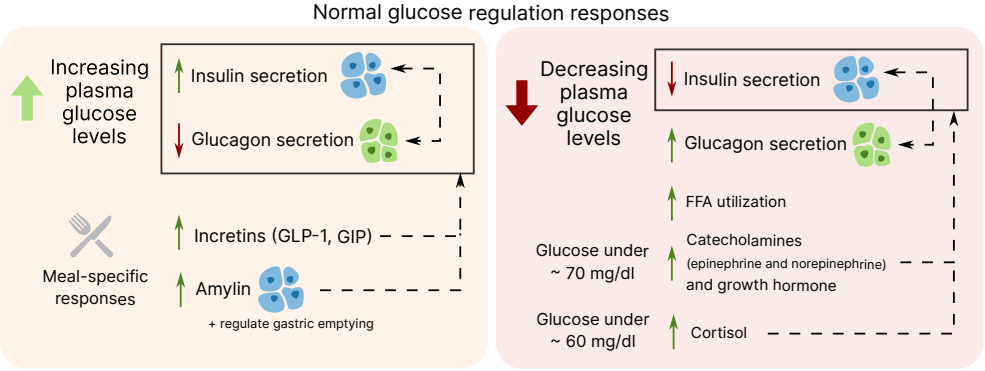

Figure 2.3: Mechanisms in the glucose regulation process. Dashed lines indicate agents promoting other processes. Green arrows facing up indicate a secretion increase and red arrows facing down indicate a reduced or inhibited secretion. Insulin secretion will be promoted, and glucagon inhibited after a glucose increase (left). After a meal, incretins and amylin will further promote insulin secretion and glucagon inhibition, among other tasks (see text for more details). In case of a glucose decrease (right), the insulin will be inhibited, and glucagon will be promoted. FFA will be used as source of energy if necessary. If certain low-glucose thresholds are reached, catecholamines, cortisol, and growth hormone will further inhibit insulin secretion.

triggered cortisol secretion. According to the authors, these thresholds were similar in previous studies devoted to this topic (Mitrakou et al., 1991).

2.1.2 Meals and interactions between hormones

With prolonged fasting, plasma insulin levels decrease, increasing its complementary hormone levels (i.e., glucagon, catecholamines, growth hormone, and cortisol). These hormones help raise (and maintain) plasma glucose levels. Fasting will consume glycogen reserves until their depletion (after around 60 hours), making gluconeogenesis the primary source of glucose (Shrayyef and Gerich, 2010).

After meal intake, insulin, glucagon, and amylin come into play. Insulin increases during and immediately after meals. Oddly enough, pancreatic glucagon is briefly secreted as food is ingested, which is thought to provide a satiety signal leading to termination of the meal (Woods et al., 2006), as observed in the clinical trial by Cooperberg and Cryer (2009). Amylin concentration rapidly increases after eating, with an increase directly proportional

to the meal size. Amylin and insulin are normally co-secreted in a fixed molecular ratio (insulin to amylin). Importantly, amylin tipically inhibits glucagon secretion, but not during hypoglycemia (Silvestre et al., 2001; Nyholm et al., 1996).

The relationship between insulin and glucagon is still a matter of study. It has been demonstrated that insulin inhibits glucagon secretion. One of the motives glucagon activates during hypoglycemia is not only that α-cells detect low glucose levels, but also that they detect the decrease in insulin secretion by β-cells (Müller et al., 2017; Cooperberg and Cryer, 2010). Moreover, high plasma insulin levels have been reported to blunt glucagon response to hypoglycemia (Banarer et al., 2002).

Another matter to consider is the relationship between glycogen and glucagon. Glycogenolysis (i.e., glycogen breakdown) is mainly initiated by glucagon. Hence, one factor that may regulate the effect of glucagon on the liver is the level of glycogen reserves. One study performed on rats showed that glycogen reserves are progressively diminished after consecutive (separated by 30 minutes) glucagon doses, regardless of the initial value of glycogen levels (Bélanger et al., 2000).

2.2 Type 1 Diabetes

Diabetes Mellitus is a metabolic disorder characterized by a dysfunction of pancreatic β-cells. While vastly heterogeneous, two main classifications of the disease exist: Type 2 Diabetes (T2D) and Type 1 Diabetes (T1D) (Leu and Zonszein, 2010). T2D accounts for 90% of diabetes cases. It is mainly characterized by insulin resistance and β-cells dysfunction, which causes higher insulin requirements in the early stages of the disease. Later on, insulin production becomes insufficient, and the person develops hyperglycemia. It is closely associated with obesity and other cardiovascular risk factors, like hypertension. On the other hand, T1D accounts for 5-10% of cases. It results from the autoimmune destruction of β-cells, leading to complete insulin deficiency. This means that people with T1D depend on exogenous insulin administration to survive. While less crucial, amylin production, which, among other things, delays gastric emptying, is also impaired since β-cells are destroyed.

T1D is an epidemic that affects 8.7 million people worldwide (JDRF, 2022). The disorder is mainly diagnosed in young people: 40% of the new diagnoses during 2022 were under 20 years old, according to the report by the International Diabetes Federation (IDF, 2022). Thanks to the isolation of insulin a hundred years ago, people with T1D can coexist with their disease as long as they can access the treatment and as they have the availability

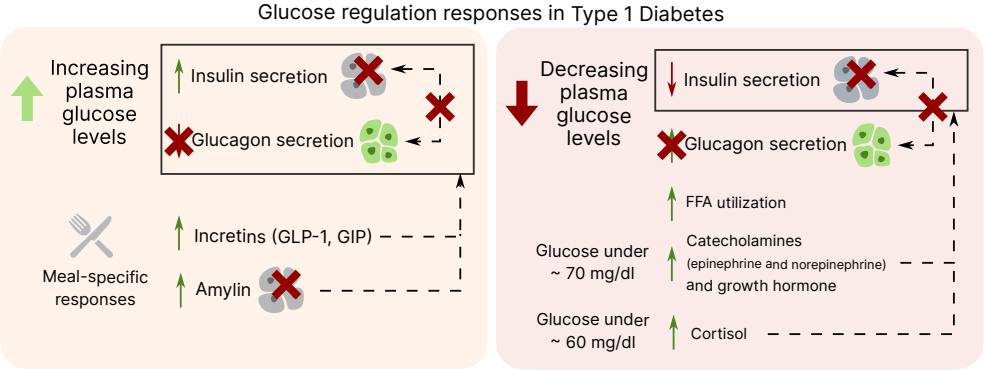

Figure 2.4: Mechanisms in the glucose regulation process in T1D. Dashed lines indicate agent promoting other processes. Green arrows facing up indicate a secretion increase and red arrows facing down indicate a reduced or inhibited secretion. Red crosses mark the elements and processes that are missing in T1D. Damaged β-cells cannot produce neither insulin nor amylin, and the communication between α-cells and β-cells is severed. Glucagon does not respond properly to glucose level changes.

of resources such as insulin dosage, glucose sensors, and diabetes education, which is sadly not the case worldwide. Some low-income countries (and some high-income countries) do not have resources for making diabetes treatment publicly available for the affected population or choose to make insulin a luxury product, available only to those who can afford it. Consequently, T1D still poses a severe threat to affected people's lives, especially undiagnosed young people. However, managing the disease in day-to-day life is not a trivial issue, even with resource availability.

As presented in the previous section, glucose homeostasis in the human body is a complex process coordinated by many agents. In the case of T1D, β-cells actions and hence, insulin action, are entirely taken away, crumbling the glucose homeostasis, which also dysregulates the behavior of other pancreatic hormones.

Figure 2.4 shows how the different regulation mechanisms are affected by T1D. With β-cells missing, mechanisms against hyperglycemia and hypoglycemia are impaired. Even if α-cells are still active, having missed their communication with β-cells, glucagon secretion does not act properly, and people with T1D typically have increased glucagon levels (Müller et al., 2017). Many studies have tried to comprehend why glucagon is unresponsive to glucose changes in T1D. Indeed, it does not activate as a response to hypoglycemia in

T1D. Likewise, it does not decrease with hyperglycemia (Gerich et al., 1973). In fact, Unger and Cherrington (2012) states that one of the main factors promoting hyperglycemia in untreated T1D is excess glucagon secretion. The exact reasons are still unknown and a matter of study. In Reiband et al. (2015), the authors theorize and summarize hypotheses of why glucagon does not work as a response to hypoglycemia in T1D. It may span from an abnormal activity of ATP-sensitive potassium channel activity to a defect of glucose sensing in α-cells, or even an impairment of signaling in the central nervous system.

This missing link between α-cells and β-cells means that glucagon secretion suppression after insulin release does not happen; neither is glucagon secreted as a response to insulin secretion suppression.

The previous section mentioned that there is a slight glucagon rise as a response to meals that may act as a satiety signal. This fact is also true for people with T1D. However, since β-cells are missing, the signaling that would constrain this glucagon production is indeed gone. These abnormally high glucagon levels after meals may also impair the organism's ability to properly replenish glycogen reserves since high glucagon levels enhance glycogen release. In fact, a study by Hwang et al. (1995) showed how the amount of stored glycogen after meals in people with T1D was significantly lower than that stored by healthy people. Moreover, glucagon and other hormones' secretion becomes increasingly damaged as the disease progresses.

The case of amylin, which is co-secreted with insulin in β-cells, is completely missing in patients with T1D. Hence, gastric emptying is dysregulated, leading to hypermotility in people with T1D regardless of the glycemic level, further contributing to the elevated postprandial glucose values (Hay et al., 2015).

Hence, people with T1D are exposed to glucose variability and the consequences that it has in all its forms: long-term complications due to hyperglycemia and the threatening consequences of hypoglycemia. The glucose regulation process becomes a manual task for patients, who have to administer insulin themselves, with all the attached difficulties it involves.

2.2.1 T1D treatment

The most essential treatment for T1D entails administering insulin and self-monitoring blood glucose levels. Insulin can be delivered using single injections (using insulin pens) or with a continuous subcutaneous insulin injection (using an insulin pump). Injections are usually administered accompanying meals or as glucose corrections at any time. Insulin pumps deliver a basal insulin infusion, with adjustable rates usually per hour (depending

on the manufacturer). This allows the person to adapt the insulin dosage to the moment of day since the insulin necessities will depend on the person's activities and insulin sensitivity, which changes following circadian rhythms. The most basic tool for glucose self-monitoring are glucose meters, which measure capillary blood glucose concentrations using finger pricks. This method is painful and burdensome for patients and does not provide information on glucose tendencies but rather a static picture of the glucose state at a given time. A more appropriate tool are continuous glucose monitoring devices (CGM). They are small, discreet sensors that attach to the body and measure interstitial[3] glucose in the subcutaneous tissue. They provide a measurement either on demand (e.g., the user has to scan the device using NFC technology) or automatically, sending measurements periodically to a receptor device (e.g., a smartphone). This allows for a more continuous, less intrusive way of glucose monitoring, providing a series of measurements every short intervals (e.g., 5 minutes), which allows for observing glucose trends and monitoring rapid glucose changes, allowing the patient to act accordingly.

The introduction of CGM devices gave place to the sensor-augmented pump therapy (SAP), which consists of combining the information of the CGM to the management of the pump insulin infusion values (Schönauer and Thomas, 2010). Still, the patient is responsible for acting and adjusting the therapy to respond to glucose changes.

Added to the complexity of continuously making therapy decisions, people with T1D can count an extra difficulty because neither the measurement point (for the glucose sensors) nor the actuators (insulin infusion) are "placed" in the ideal place. Pancreatic cells have access to many internal variables in the body, sensing even the most minor changes in glucose and even whether the other cells are starting or stopping their respective hormones' secretion. Getting scattered glucometer measurements during the day or interstitial measurements with CGM devices (instead of blood glucose) does not come close to the amount of information available to the normal glucose homeostasis process.

Moreover, interstitial glucose is related to blood glucose via a diffusion process, which allows estimating blood glucose values, but it will carry estimation errors as well as a delay (Aussedat et al., 2000; Kulcu et al., 2003). On the other hand, insulin is also administered interstitially, unlike β-cells that release insulin directly to the portal vein. In the case of insulin administration, insulin will take longer to come into effect because it is administered into the peripheral circulation (Cohan and Peters, 2010).

Appropriate diabetes treatment also involves putting special care into following a healthy diet and regular exercise to maintain healthy glucose levels and avoid hyperglycemia. Meals and exercise management come with their own difficulties, too. Neverthe-

[3] The interstice is the space between cells.

less, one of the main factors interfering with patient's management of their diabetes is fear of hypoglycemia. Low glucose values have more rapid and direct negative consequences, so people prefer being high rather than risking a hypoglycemia episode.

Fear of hypoglycemia is well-founded because regular glucose homeostasis puts into place several mechanisms to avoid it (detailed previously in Section 2.1): (1) suppression of insulin secretion, when glucose values decrease under 80 mg/dl, (2) glucagon secretion, that promotes glycogenolysis and gluconeogenesis when glucose is around 65-70 mg/dl, (3) epinephrine and other hormones may react too if necessary (Cryer et al., 2003). The other complementary hormones (epinephrine, growth hormone, and cortisol) secretion also become progressively deficient from the onset of the disease. Since insulin is not secreted within the body but administered externally, insulin suppression as a response to hypoglycemia does not happen, hence already failing the first defense mechanism. α-cells, not detecting this suppression of insulin action, do not secrete glucagon either. To make things worse, administered insulin has a persistent effect, remaining in the circulation for a considerable time and worsening the glucose decrease (Gerich, 1988). Another issue is "hypoglycemia unawareness", in which repeated hypoglycemia episodes impair the symptoms of developing hypoglycemia, which compromises the defenses against it and could lead to an acute hypoglycemic episode (Cryer, 2001). Fear of hypoglycemia makes patients lean towards higher glucose values, leading to hyperglycemia and worse overall glucose metrics.

Hypoglycemia quick treatment consists of ingesting some carbohydrates to correct and raise glucose values. These can be some juice, soft drinks, crackers, etc., or carbohydrate tablets designed for this use. They are typically known as *rescue carbohydrates*. They represent a dose usually between 15-20 g of carbohydrates, and current therapy recommendations instruct to take a dose every 15 minutes until glucose values are restored to normoglycemia. This approach is effective but increases the number of calories the patients ingest and could cause a rebound hyperglycemia later on. On the other hand, severe hypoglycemia episodes require another person to help the patient to recover, since they may be unresponsive. In those cases, the standard treatment consists on a 1-mg glucagon dose injection, to achieve a quick recovery.

2.2.2 Drugs

Insulin

Insulin is usually presented in 10-ml vials with a concentration of 100 units of insulin per ml. Then, an injection of 0.05 ml would be needed to deliver five units of insulin. This concentration is labeled as U100 (100 U per 10 ml) and is the most common. Insulin is also available in different concentrations, either more diluted or more concentrated (e.g., U40, U300, U500), designed for patients with either greater insulin sensitivity or insulin resistance (Cohan and Peters, 2010).

Different types of insulin exist, and they are characterized depending on the absorption rate after their subcutaneous administration. The main descriptive characteristics are time to onset, time to peak, and duration. Table 2.1 summarizes some of the most relevant insulin types available. The information has been adapted from the Clinical Practice Guideline for Diabetes Mellitus published in 2022 by the American Association of Clinical Endocrinology (Blonde et al., 2022).

The first fast-acting analog available was lispro, and other fast-acting insulins were developed later (aspart, glulisine). The main purpose of these rapid-acting compounds is to counter glucose increases due to meals. Patients inject the corresponding dose around 15 minutes before eating so that the onset of the insulin analog matches the start of the meal. Long-acting insulin analogs, on the other hand (e.g., glargine, determir), have less peak effect, but their effect spans several hours. Hence, conventional T1D management combines the administration of basal long-lasting insulin doses, complemented by rapid-acting analogs to counter postprandial glucose raises and administer small corrective bolus if needed (McCall and Farhy, 2013; Domingo-Lopez et al., 2022). A review of current commercially available insulin pens, CGM sensors, and other medical devices can be found in Domingo-Lopez et al. (2022). Almurashi et al. (2023) also reviews available CGM devices, adding insulin pumps.

Inhaled insulins deserve a special mention. They are administered through an inhaler instead of injections, making them a non-invasive method for insulin administration. Although the concept had a positive reception from patients and physicians, it also presents some disadvantages. Focusing on Technosphere (a brand developed by MannKind, USA), a meta-analysis of clinical trials using the drug (Pittas et al., 2015) showed that it helped to lower the risk of severe hypoglycemia, but it was less effective than subcutaneous insulin improving overall glycemic levels, making it efficient for prandial dosing, but needing basal insulin administration regardless. This could be due to the lower efficacy of absorption

	Onset time	Peak time	Duration
Basal insulins			
Long-acting analogs			
Detemir	1.5 h	near peakless	16-24 h
Glargine	1.5-2 h	near peakless	24 h
Degludec	1 h	peakless	42 h
Prandial insulins			
Short-acting			
Regular	30-60 min	2-4 h	5-8 h
Rapid-acting			
Aspart	15 min	1-1.5 h	3-5 h
Glulisine	12-30 min	1-1.5h	3.5-5 h
Lispro	15-30	1-2 h	3-4.75 h
Faster-acting			
Faster aspart	4 min	0.5-1.5 h	3-5 h
Lispro aabc	15-17 min	2 h	4.6-7.3 h
Inhaled Technosphere insulin	12 min	0.5-1 h	1.5-3 h

Table 2.1: Types of insulin. The concentrations of the preparations listed are all U100. Adapted from Blonde et al. (2022).

in inhaled insulin. In addition, there are concerns over pulmonary safety related to the long-term use of this drug. Hence, it presents a trade-off of partially getting rid of injections in return for a potential loss of normoglycemia targets and possible safety issues (Mohanty and Das, 2017).

Alternative routes for insulin delivery are intranasal insulin and intraperitoneal insulin. Intranasal insulin allows the transport of insulin to the brain more efficiently, which has been proven to improve glucose homeostasis and cognition by modulating neuroendocrine activity. However, impairments in central nervous insulin signaling have been observed; hence, advances are needed prior to the clinical application of intranasal insulin (Hallschmid, 2021). On the other hand, intraperitoneal insulin involves administering insulin by an implantable pump so that insulin is directly absorbed through the portal system (McCall and Farhy, 2013), making it the closest system to "real" pancreas behavior. However, the long-term benefits of this technique are to be determined since patients present reactions to the material, and it entails all the difficulties involved with the implantation of an external device (Renard, 2008).

Glucagon

Commercially available glucagon formulations are used to treat severe hypoglycemia. The main issues with liquid glucagon formulations are (1) the predilection to form sheets of amyloid-like fibrils in aqueous solutions that could clog the injection device and (2) the fact that glucagon spontaneously degrades (Wilson and Castle, 2018). Current stable glucagon formulations include intranasal glucagon, dasiglucagon, and non-aqueous soluble glucagon (see Table 2.2). The latter two can be administered via a pre-filled syringe, and the first is administered nasally (Blonde et al., 2022).

Glucagon emergency kits need to reconstitute glucagon before use. They consist of two-part kits, including a syringe containing a sterile water solution and a vial with glucagon powder. At the time of administration, the solution is injected into the vial, mixed, and then the fluid has to be drawn back into the syringe to be administered (Wilson and Castle, 2018). Since such a process is involved, the person cannot use this kind of emergency kit when hypoglycemia is so severe that they are feeling unwell or unconscious. Reconstituted glucagon is to be used immediately, injected intramuscularly, and discarded afterward. Currently, the available glucagon emergency kits are Glucagen HypoKit (Novo Nordisk, Denmark) and Glucagon Emergency Kit (Eli Lilly, USA) (Patil et al., 2020).

Intranasal glucagon eliminates some complexity in the process, and it is the preferred option if another person has to administer it to the patient; however, it is not as efficient (Pontiroli, 2015), as the recommended dose has to raise from 1 mg to 3 mg (Blonde et al., 2022; Beato-Víbora and Arroyo-Díez, 2019).

Dasiglucagon (Zealand Pharma, Copenhagen, Denmark) is a novel formulation that can be maintained stable for at least seven days at room temperature. Moreover, it achieves comparable effects to regular glucagon with smaller doses (Hövelmann et al., 2018, 2019). Dasiglucagon has been proven efficient in countering hypoglycemia even under free-living conditions (Laugesen et al., 2023), using small doses of 80 μg.

Other glucagon formulations are BioChaperone glucagon developed by Adocia Biotech (Lyon, France) (Glezer et al., 2018; Patil et al., 2020), and the liquid (non-aqueous) formulation developed by Xeris Pharmaceuticals (Austin, TX, USA): XeriSol. This latter formulation is stable at room temperature for up to 2 years, but patients have reported adverse reactions in the injection site, such as burning or discomfort (Haymond et al., 2016, 2017). Nevertheless, its efficacy in preventing exercise-induced hypoglycemia was tested in the trial by Rickels et al. (2018), using Xeris' G-pen mini. In a review of glucagon formulations and treatments (Hawkes et al., 2019), the authors show a comparison of the effect of the different glucagon formulations (dasiglucagon, BioChaperone glucagon, Xeris'

	Ready to use	Administration
Glucagon emergency kits	Require reconstitution	Injection
Dasiglucagon	✓	Injection
Glucagon pen (prefilled syringe)	✓	Injection
Glucagon nasal powder	✓	Nasal

Table 2.2: Types of glucagon. Adapted from Blonde et al. (2022).

G-Pen, and intranasal glucagon) on glucose. Dasiglucagon emerges as the most efficient administration, achieving the maximum effect with the lowest dose. This compound's efficacy was also proven in Hövelmann et al. (2019), where the effect of different dasiglucagon doses is compared to reconstituted glucagon. This trial showed that administration of 200 μg regular glucagon was comparable to 80 μg dasiglucagon. A recent review (Giménez et al., 2023) compared the results obtained in different clinical trials of three commercial glucagon preparations in comparison to classic injectable glucagon (requiring reconstitution). The glucagon preparations were Baqsimi (nasal glucagon, by Eli Lilly), Gvoke (glucagon injection, by Xeris Pharmaceuticals), and Zegalogue (dasiglucagon injection, by Novo Nordisk). Results show that treatment success was achieved with any of the formulations, with Gvoke reaching the highest mean maximum blood glucose values, while Bagsimi was the lowest (220 mg/dl and 168 mg/dl, respectively).

The use of glucagon is associated with some adverse effects, such as nausea or vomiting, occurring 2-3 hours after glucagon administration (Ranjan et al., 2021), although the occurrence of said effects depends on the dose and route of administration. Intranasal glucagon entails other adverse reactions such as congestion, sneezing, and headache. Nevertheless, the long-term consequences derived from chronic use of glucagon are still unknown (Ranjan et al., 2021).

However, in order to avoid adverse effects caused by large glucagon doses (1 mg), several studies have explored the possibility of using smaller doses to recover from hypoglycemia. One of the first studies testing this hypothesis was Haymond and Schreiner (2001), where they proposed using mini glucagon doses to treat mild hypoglycemia. The study was performed on children with T1D, and glucagon doses between 20 and 150 μg successfully raised glucose levels to avoid hypoglycemia. Years later, a study carried out by Ranjan et al. (2016) proved that small glucagon doses of 100, 200, or 300 μg were sufficient to treat mild-hypoglycemia in adults.

A study (Haymond et al., 2017) compared 150 μg doses of XeriSol glucagon and 16 g

carbohydrates administration as hypoglycemia treatment and found the responses were very similar, albeit for a slightly higher rise in glucose with the use of carbohydrate tablets. On the other hand, a study comparing low doses of dasiglucagon to oral glucose (Laugesen et al., 2022). Dasiglucagon doses of 80, 120 μg, or 15 g of glucose tablets were administered when participants of the trial reached induced hypoglycemia. On this occasion, there is a significant difference between the two treatments. Dasiglucagon successfully raised glucose levels 20 mg/dl in 15 minutes regardless of the doses, whereas oral glucose took 30 minutes.

Pramlintide

Pramlintide is an amylin analog that successfully delays gastric emptying (Thompson et al., 1997a; Nyholm et al., 1999; Adis, 2003; McQueen, 2005; Levetan et al., 2003). Its use is not as extended as those of insulin and glucagon, but it has proven useful in reducing postprandial hyperglycemia, and a 1-year long trial showed that pramlintide significantly helped to reduced HbA1c[4] values (Ratner et al., 2004). Pramlintide was approved for its use in T1D treatment by the FDA (U.S. Food and Drug Administration) in 2005 (Srinivasan et al., 2021). A posterior meta-analysis (Qiao et al., 2017) gathered ten clinical trials with pramlintide from 1997 to 2016, to analyze its efficacy and safety. The study concluded that pramlintide was indeed capable of reducing HbA1c levels overall (2.39% on average), as well as reducing insulin needs and body weight.

Pramlintide is administered subcutaneously using a pre-filled syringe (pramlintide pen). The pramlintide effect is dose-dependent, causing a longer delay in glucose appearance the greater the pramlintide dose (Kong et al., 1998). Pramlintide dosing usually consists of 30 to 60 μg boluses, administered 30-15 minutes before meals, accompanying the prandial insulin dose. Nevertheless, insulin dosage has to be reduced to avoid later hypoglycemia (McQueen, 2005). Pramlintide has to be readministered after each meal, since its effect does not carry on the subsequent meals (Kong et al., 1998).

Pramlintide has been tested both with regular and lispro insulin. Some differences were observed, probably due to the pharmacodynamic differences between regular and rapid-acting insulin (Weyer et al., 2003). Pramlintide has also been observed to successfully reduce glucagon increase after a meal (Fineman et al., 2002; Nyholm et al., 1999). The study by Fineman shows how small this glucagon increase is since a small dose of 100 μg

[4] Glycated hemoglobin. Measure of the overall glucose levels in the blood used as diagnostic for diabetes mellitus and assessment for glucose control quality in T1D. Therapy guidelines recommend its value should be $\leq 6.5\%$ (Blonde et al., 2022).

glucagon would cause a rise in plasma glucagon of approximately 350 pg/ml, whereas the posprandial response causes an increase of around 15 pg/ml.

Pramlintide is a drug prone to cause nausea, vomiting, or headache, with increased symptoms with increasing doses (Adis, 2003; McQueen, 2005). Symptoms seem to subside with time (Weyer et al., 2001), but patients tend to develop resistance to the drug after several years of use (Blonde et al., 2022).

Since insulin and amylin are co-secreted, some strategies propose administering them together. A clinical trial by Weyer et al. (2005) showed that both compounds could be mixed and co-administered without detriment to the effect of either drug. Recently, a novel co-formulation of insulin and pramlintide has been developed that combines the effect of both insulin and pramlintide. Clinical trials testing its viability of use and efficacy are being carried out (Andersen et al., 2021, 2023), which would pose an advancement for people with T1D, offering a more complete treatment (combining the effects of insulin and pramlintide) without the need of additional consumables or devices. Still, the studies' authors report adverse effects after this drug administration, hence it remains under development.

Adjunctive therapies in diabetes treatment

As exposed, current diabetes therapies try to replace pancreatic functions with the external administration of certain hormones. Insulin administration is the fundamental element, and even if sporadically, glucagon is also widely used. Any other hormones or medication are considered adjunctive therapies.

Apart from pramlintide, other substances are used or have been explored as potential adjunctive therapies, such as Metformin, GLP-1 agonists, DPP4 inhibitors, Sodium-glucose co-transporter inhibitors (SGLTi), verapamil, sulfonylureas, α-glucosidase inhibitors, and glitazones (Blonde et al., 2022; Avgerinos et al., 2021; von Scholten et al., 2021; Ang and Sherr, 2017; Harris et al., 2018). Table 2.3 summarizes the drugs and some of the analogs found in the literature. The center column describes the main effects of the compounds, and the right column adds information on the dosing, adverse effects, and use in T1D and T2D.

The meta-analysis in Avgerinos et al. (2021) presents a thorough review and meta-analysis of adjunctive treatments used in T1D, comparing the efficacy between treatments. The complete list of trials performed on people with T1D can be found in their supplementary material. Aberer et al. (2022) presented a narrative review that covered adjunctive therapies used in T1D, presenting a more drug-focused analysis evaluating the outcomes obtained with each drug. For instance, according to this report, the best improvements on

HbA1c, total insulin dose, and weight reduction were obtained with Metformin, Liraglutide, and the SGLTi family. The worst adverse reactions also correspond to Metformin and Liraglutide. More details on treatment outcomes can be found in both aforementioned documents.

Drug	Effect	Dosing and use
Metformin	Decreases hepatic glucose production and increases insulin-mediated glucose uptake. Reduces required amount of daily insulin.	Oral adminstration. Widely used for T2D, in trials for T1D, without clear evidence of improvements in HbA1c (Srinivasan et al., 2021; Ang and Sherr, 2017)
GLP-1-agonist (Liraglutide, Exenatide, Dulaglutide, Semaglutide)	Increase insulin secretion, decrease glucagon secretion, delay gastric emptying, promote satiety.	Administered subcutaneously. Significant adverse effects. FDA-approved for T2D, but without formal indication for T1D. (Srinivasan et al., 2021; Drucker et al., 2010; von Scholten et al., 2021)
DPP4-inhibitor (Sitagliptin, Saxagliptin, Vildagliptin, Alogliptin)	Increase GLP-1 and GIP levels (see GLP-1 effects above).	Oral administration. Cardiac risks (Blonde et al., 2022), but fewer side effects than GLP-1 (Ang and Sherr, 2017). Used in T2D, but trials in T1D do not show many potential benefits (Drucker et al., 2010; Ang and Sherr, 2017; Srinivasan et al., 2021).
SGLT-inhibitor (Dapagliflozin, Empagliflozin, Sotagliflozin, Canagliflozin, Ipragliflozin)	Lower glucose in a insulin-independent manner: increasing urinary glucose excretion (SGTL2), or restraining the absorption of glucose in the small intestine (SGTL1).	Oral administration. Used in T2D, but with significant adverse effects. (Srinivasan et al., 2021). Trials in T1D are showing positive outcomes (Ang and Sherr, 2017), but there is a risk of elevated ketones.

Continued in next page

Continued from previous page

Drug	Effect	Dosing and use
Verapamil	Calcium-channel blocker. Traditionally used as anti-hypertensive agent. Helps preserving functional β-cells. Reduces daily insulin need in T1D.	Oral administration. Useful for patients with recent onset T1D, might improve insulin sensitivity (Ovalle et al., 2018), pending on more extensive trials (von Scholten et al., 2021). Preserving C-Peptide in non-aduls with T1D (Forlenza et al., 2023).
Sulfonylureas (Glibenclamide, Glyburide)	Enhance insulin secretion (Röder et al., 2016; Cryer et al., 2003).	Oral administration. Used for T2D to prevent its progression (Blonde et al., 2022). Reduces total daily insulin in T1D, might increase insulin sensitivity (McCoy et al., 1995).
α-glucosidase inhibitors (Acarbose, Miglitol, Voglibose)	Attenuate postprandial glucose excursions (Röder et al., 2016).	Usually used in the early stage of T2D, to lower HbA1c and promote weight loss (Blonde et al., 2022).
Glitazones (Pioglitazone, Trosiglitazone, Rosiglitazone)	Insulin sensitizers (same family as Metformin).	Used in T2D. Several side effects. Even withdrawn from the market (Drucker et al., 2010; Blonde et al., 2022; Röder et al., 2016).

Table 2.3: Potential drugs for adjunctive therapies in T1D.

Among all the adjunctive therapies tested for T1D, the most promising approach currently appears to be the SGLT2i, which provide an insulin-independent approach to lower plasma glucose (Cardona-Hernandez et al., 2023). Overall results with these drugs present greater reductions of HbA1c and weight (Langford et al., 2020), although they significantly increase the risk of diabetes ketoacidosis (Garcia-Tirado et al., 2022). A review on the use of these drugs in T1D can be found in (Biester et al., 2019), separated by drug (empagliflozin, dapagliflozin, canagliflozin, and sotagliflozin) and the potential benefits of incorporating them to T1D treatment.

Many of these are only used in T2D and are still experimental therapies in T1D, pending more extensive trials and formal approvals from the corresponding Health Or-

ganizations. However, ongoing research is focused on exploring the potential benefits of incorporating these adjunctive therapies into T1D treatment since sometimes insulin is insufficient to achieve optimal glucose control. One issue surrounding these add-on proposals is the administration method. Patients may be more reluctant to add an injection-based treatment (this includes glucagon and pramlintide). Subcutaneous administration of another drug requires double the necessary consumables. Hence, therapies consisting of oral drug administration might be more well-received. Nevertheless, some of these treatments still present some serious adverse effects, especially at the start of the treatment, and the consequent contribution is not evident in some cases.

Achieving optimal glucose control in T1D is a daunting task, given the heterogeneity of the disease, making it difficult to propose a "universal" therapy. Treatment should be tailored to the patient's needs, and finding the most adequate adjunctive therapy for each condition is part of this process.

In the meantime, patients have to deal with the available tools: insulin pumps and CGM. In order to ease their management task, Artificial Pancreas systems were developed, as presented in the next section.

2.3 Artificial Pancreas

Artificial Pancreas (AP) systems are a set of interconnected elements with the purpose of aiding T1D therapies. Fundamental T1D management involves an insulin delivery system (i.e., pen or insulin pump) and a glucose monitoring device (i.e., CGM or glucometer) (Haidar, 2016). However, the patient makes insulin dosing decisions every time (e.g., deciding on the necessary prandial injection or adjusting the basal infusion). This procedure is known as an *open-loop* (OL) system in control systems terminology. AP combines an insulin pump, a CGM, and a control algorithm (see Figure 2.5). The controller governs insulin infusion values according to the glucose sensor readings. This procedure is known as a *closed-loop* (CL) system. This way, insulin doses are adjusted every few minutes, responding to glucose changes. In concept, the system tries to mimic the insulin secretion changes produced by the pancreas.

These systems have also been referred to as *automated insulin delivery* (AID) systems. However, this name leaves out some configurations that will be presented in the following sections since the name implies insulin is the only control action.

There exist very complex strategies proposed for AP devices. However, one of the most basic precursors of AP consists of suspending the pump automatically when glucose

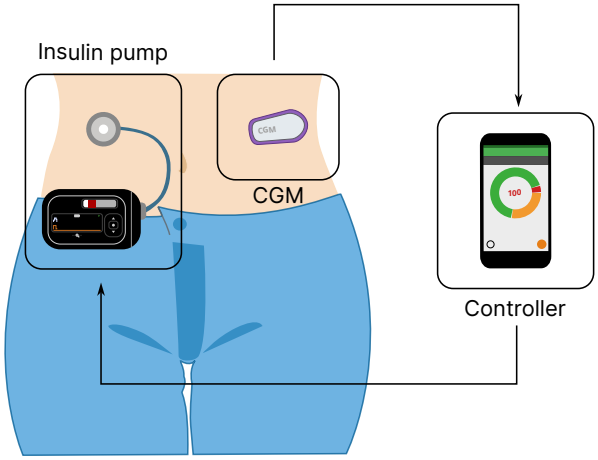

Figure 2.5: Artificial Pancreas system. The CGM (sensor) provides glucose measurements to the controller, which computes a control action to be administered by the insulin pump (actuator). The controller may be implemented in an external device (e.g., a smartphone, as depicted) or the insulin pump. The patient represents the control plant.

values are low (Harvey et al., 2012), which already helped to ease glucose control, becoming the first step in the development of closed-loop strategies (Blauw et al., 2016b; Ly et al., 2013). This system is nowadays implemented in Medtronic's AP, for instance, as *Suspend before low* and *Suspend on low* features (Collyns et al., 2021; Bosi et al., 2019).

Studies have shown an improvement in glycemic control over conventional therapy and SAP. A review from 2022 (Fang et al., 2022) evaluated the potential improvements introduced by CL systems over SAP, comparing 12 trials. The analysis found that CL performed better on glucose control overall, providing an average of 8% more time in range. Other evaluated metrics, such as average blood glucose, low and high glucose values, or a risk assessment based on adverse events, also favored the CL results. Another review (Karageorgiou et al., 2019) focused on the non-adult population collected 25 trials comparing CL to OL systems and reached similar conclusions (overall improvement of time in range of 11.2%).

In a meta-analysis of outpatient trials using AP systems in 2017 (Weisman et al., 2017) a total of 24 studies were evaluated, and the study concluded that AP systems provided a 12% greater time in normoglycemia, a 2% reduction of time in hypoglycemia and a 0.1% increase in total daily insulin needs, compared with conventional pump therapy.

Later, a review and meta-analysis evaluating over 40 AP systems (Bekiari et al., 2018) concluded that CL systems provide an improvement in at least two additional hours in normoglycemia (over 24 hours) compared with OL treatment, two hours less in hyperglycemia and 20 minutes less in hypoglycemia.

	Manufacturer	**Includes**	**Required extra devices**
Minimed 670G	**Medtronic** (Northridge, CA, USA)	Pump	Sensor Guardian 3
Minimed 780G	**Medtronic** (Northridge, CA, USA)	Pump	Sensor Guardian 4
Control-IQ Basal-IQ*	**Tandem** (San Diego, CA, USA)	t:slim X2 pump	Dexcom G6
CamAPS FX	**CamDiab** (Cambridge, UK)	CamAPS FX app	Dexcom G6 or FreeStyle Libre 3; mylife YpsoPump, Dana Diabecare RS, or DANA-i
DBLG1	**Diabeloop** (Grenoble, France)	DBLG1 app	Dexcom G6; Accu-Chek Insight pump
Insulet Omnipod 5	**Insulet** (Billerica, MA, USA)	Omnipod 5 app and Pod pump	Dexcom G6
iLet Bionic Pancreas	**BetaBionics** (CA and MA, USA)	iLet pump	Dexcom G6

Table 2.4: Commercially available Artificial Pancreas systems. *The Basal-IQ system does not incorporate a controller per se but a suspend-on-low logic.

The most extended control strategies for AP systems are model predictive control (MPC), proportional derivative integrative (PID) algorithms, and fuzzy logic (Ware and Hovorka, 2022; Quiroz, 2019; Thomas and Heinemann, 2022). Many other strategies are being developed, but they have not made it to commercial devices and have only been tested *in silico* (Tašić et al., 2022). The controller can be integrated within the insulin pump or in an external device, like a smartphone. Seven different AP systems are already available in the market, as listed in Table 2.4. Most of them integrate the controller into an insulin pump (since the pump companies develop the systems). The exceptions among the currently available systems are CamAPS FX and DBLG1's systems, whose product is an app. In those cases, agreements are needed between the developers and the pump companies to offer connectivity to commercial devices. The CamAPS FX system is the one that offers a broader range of possibilities in this regard, being able to connect to two different CGM devices and three different pumps. Medtronic's systems (Minimed 670G and Minimed 780G) use their proprietary CGM device (Sensor Guardian), with its older and newest versions, respectively. Nevertheless, one of the most extensively used CGM devices is Dexcom's, as it is the device of choice for the rest of the systems in the list. The iLet Bionic Pancreas just received FDA clearance in June 2023, which makes it the most recent one on the list. Several reviews have analyzed the performance of these systems, showing their safety and positive contributions to glucose control (Zhou and Isaacs, 2022; Lakshman et al., 2023).

While many advances have been made toward the miniaturization of the devices, technical research is still needed to reduce the patients burden, who have to rely on at least two electronic devices attached to their bodies.

Challenges of current AP systems

The main challenges surrounding AP development could be summarized into: achieving complete automatic behavior, sensor accuracy, dealing with meals and exercise, and variability.

Current AP systems are *hybrid*. This term labels their inability to be entirely automatic since they require the patient's intervention to function, announcing potential disturbances to the system such as meals (i.e., amount of carbohydrates) or exercise (intensity). Having the patients interact with the system makes it lose its "automatic" essence. Hence, significant research efforts focus on developing strategies to detect these disturbances, eliminating the patient's involvement. Also, relying on the patient's intervention makes the system more prone to errors due to mistakes or oversights (e.g., forgetting to announce a meal or physical activity).

Another of the main limitations of AP systems is the accuracy of CGM sensors. Although the latest technological advances have made them progressively more accurate, they face the difficulty of interstitial glucose being a delayed reflection of blood glucose. This poses a challenge, especially when glucose values change rapidly (McCall and Farhy, 2013), or during physical activity (Fabra et al., 2021). In that work, the authors review the MARD[5] obtained in various works, and how it increases during exercise. Previous studies and consensus on CGM accuracy determine that commercial devices should maintain their MARD around 15% (Blauw et al., 2016a; Hovorka, 2011). Kovatchev et al. (2015) performed an *in silico* study based on real data and determined that accurate clinical decisions can be made as long as the MARD is around 10%. Lower values did not significantly improve the outcomes, and larger errors negatively impacted glycemic control.

Glucose disturbances caused by meals and exercise are a challenge in themselves. The first influential factor in both cases is the delay in glucose measurements caused by the CGM, but each of them entails its own peculiarities.

As mentioned before, classic meal therapy requires administering a prandial insulin bolus between 30-15 minutes before the meal because insulin onset is significantly larger than the time it takes glucose to appear in plasma after a meal. The subcutaneous administration delays the appearance of the hormone in plasma and results in a magnitude reduction (Edgerton et al., 2021). That means patients have to administer more insulin than the amount that would be required if it was administered in the "correct" place, which can lead to complications related to hyperinsulinemia.

Another vital limitation in meals is carb (i.e., carbohydrate) counting. In order to administer an insulin prandial, patients need to determine the exact amount of carbohydrates to compute the most appropriate insulin dose based on their insulin-to-carb ratio. However, counting is a non-exact science and people are prone to make mistakes. So, much research is put towards alleviating this burden, either by detecting meal disturbances automatically and administering insulin bolus as a disturbance rejecting strategy, or simplifying the "meal announcement" by asking the patient to introduce a qualitative estimation of the meal content (e.g., small, medium or large), or just indicating the time of the start of the meal.

Regarding exercise, the greatest danger it entails is hypoglycemia. Physical activities with continuous movement (aerobic exercise) stimulate glucose uptake by the muscles, causing glucose levels to drop, and also increases insulin sensitivity (Jackson and Castle,

[5]The Mean Absolute Relative Difference (MARD) is a metric often used to assess continuous glucose monitors accuracy, expressed in %. The lower its value, the lower the difference between the measurements and the actual values.

2020). The primary endocrine response would be to suppress insulin secretion and activate counterregulatory measures (see Figure 2.3). However, people with T1D may have circulating long-acting insulin in their bodies, whose effect cannot be erased and worsens the glucose drop. Hence, pump-suspension, the primary strategy in AP systems, may be ineffective. Moreover, physical activity also entails post-activity consequences since it alters insulin sensitivity and glucose uptake, potentially causing hypoglycemia since glucose requirements can increase up to threefold (Peters and Haidar, 2018). People with T1D usually rely on consuming a snack or small amount of carbohydrates to counter the effect of hypoglycemia during exercise and reducing their basal infusion (Riddell et al., 2017), which may end up leading to hyperglycemia afterward.

An excellent review of the challenges posed by meals and exercise and the myriad of strategies presented in the literature to counter them is presented in Sala Mira (2023).

However, the main hurdle to automatic systems is variability, both inter-patient and intra-patient variability. The response to a given input may differ, even for the same patient. Also, even if the algorithm were able to detect the exact meal time, the postprandial glucose response would be different depending on various factors: meal composition, state (liquid or solid), absorption into the portal vein, extraction by the liver, suppression of endogenous glucose release, and finally, glucose uptake, storage, oxidation, and glycolysis in posthepatic tissues (Shrayyef and Gerich, 2010).

Control algorithms usually individualize their algorithms by modifying some controller parameters based on some clinical variable from the patient, such as their total daily insulin or body weight (Haidar, 2016); however, some factors such as insulin sensitivity experiment significant variation over time. Insulin absorption times oscillate 30 minutes for the same individual some weeks apart (Haidar et al., 2013b). Insulin sensitivity may also experiment variations in the same day due to stress, exercise, or food intake. Gender is another factor that may affect insulin sensitivity due to hormonal differences between men and women (Mauvais-Jarvis, 2018)

Hence, advanced adaptive algorithms may be needed to deal effectively with sudden large changes in insulin sensitivity, such as during sickness or stress periods (El Youssef et al., 2011) and menstrual cycles (Gamarra and Trimboli, 2023; Trout et al., 2007).

In short, the lack of counterregulatory measures in glucose homeostasis for people with T1D diabetes makes automatic glucose control a daunting task due to the lack of resources (i.e., unidirectionality of insulin) or lack of better tools (CGM measuring interstitial glucose, subcutaneous delivery of insulin). Moreover, many of the challenges remaining in AP development consist of finding adaptable control strategies that can deal with sudden, unexpected events and progressive changes in the control plant that is the human body.

2.3.1 Multi-hormone Artificial Pancreas

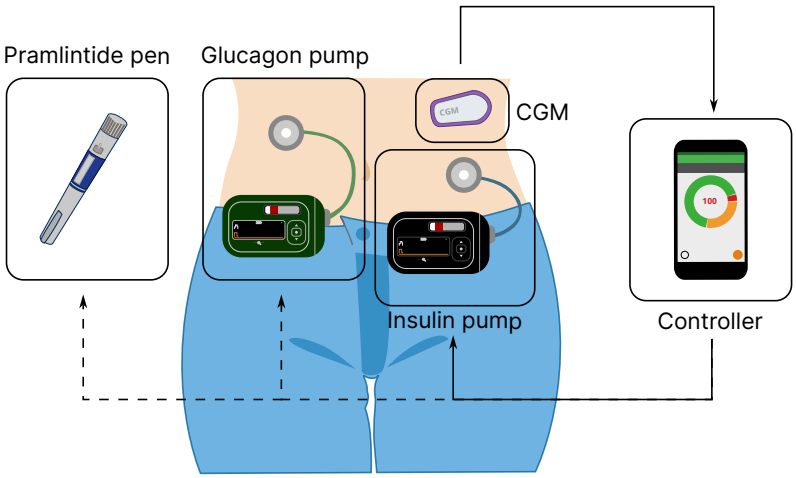

Figure 2.6: Multi-hormone Artificial Pancreas system. Additional control actions such as glucagon and pramlintide are added to the classical configuration of the system. The glucagon-insulin AP system could be implemented with a single dual-chamber pump using two catheters.

Multi-hormone AP systems were conceived to improve glycemic control by introducing additional control actions to insulin-only AP (i.e., single-hormone, SHAP), as seen in Figure 2.6. Insulin has a significant limitation: its effect is unidirectional, making it necessary to counter its effects with carbohydrate ingestion or risk hypoglycemia due to hyperinsulinemia. Consequently, one solution consists of using glucagon as a complementary hormone in the AP systems since it is the primary endocrine response to prevent hypoglycemia. With the goal of mimicking the secretion patterns of the pancreas, dual-hormone AP (DHAP) systems came to be. So, glucagon was used not only as standalone injections in case of emergency but also as a continuous low-dose infusion.

Another candidate in complementing insulin action in CL systems is pramlintide. Also co-secreted in β-cells, it is completely missing in T1D people. Hence, AP systems recently introduced pramlintide to aid postprandial glucose control and reduce the daily total amount of insulin needed.

The following sections present the most relevant aspects and examples of these hormones in CL systems, as well as the use of other adjunctive therapies.

2.3.2 Insulin-Glucagon

Glucagon in AP has now a trajectory and has been widely studied. Proven the feasibility of glucagon administration as mini doses to prevent hypoglycemia, it was incorporated into CL systems to be delivered as low-dose infusions.

Introducing glucagon in AP systems can follow two approaches: (1) using glucagon to avoid hypoglycemia, and (2) allowing more aggressive insulin dosing because glucagon can be used to counteract its effect. This strategy usually entails higher dosing of both insulin and glucagon, trying to avoid hypoglycemia and achieving tighter glucose control simultaneously. However, AP systems should aim to minimize the amount of glucagon dosing to avoid the adverse side effects (nausea and vomiting) and also because the effects of long-term glucagon dosing are unknown (Haidar et al., 2016). A variety of control strategies have been implemented in dual hormone systems, and a thorough summary can be found in Jones (2019).

Subcutaneous delivery of glucagon has a faster onset of action than insulin, making it suitable for its subcutaneous use (Wilson et al. (2020a), citing Graf et al. (1999)). Typical glucagon doses in AP range between 10-100 μg, trying not to overpass 1 mg per day as a safety measure to minimize glucagon's adverse effects.

Dual hormone trajectory and contributions

Ten years ago, Bakhtiani et al. (2013) reviewed CL systems, emphasizing bi-hormonal approaches. The most notable deficit in glucagon research was the need for a formulation stable for more than 8 hours (the reconstitution period at the time). The review also mentioned the most relevant bihormonal systems: the proposals by the Boston University group (El-Khatib et al., 2010) and the Oregon Health and Science University (OHSU) (Castle et al., 2010a). The latter compared the performance of the dual-hormone control algorithm versus delivering insulin and placebo. The glucagon arm significantly reduced time in hypoglycemia. The Boston trial consisted of only one arm, where researchers tested the performance of their bihormonal system. Glucagon administration helped to avoid hypoglycemia episodes. However, both works report a malfunction of glucagon in case of high levels of circulating insulin.

Since then, these systems have been further developed, and other research groups also have tested their own algorithms in clinical settings. Overall results show that dual-hormone systems provide an improvement over insulin-only APs.

The review by Peters and Haidar (2018) analyzes six clinical trials that directly com-

pared single versus dual hormone AP systems. One of those trials was carried out by the OHSU group (Castle et al., 2010b), whereas the remaining 5 belonged to the group led by Ahmad Haidar, in McGill University, Montreal (Haidar et al., 2015b,a, 2016, 2017; Taleb et al., 2016). The main findings in the review are: DHAP provides an overall reduction of time in hypoglycemia, helps to prevent hypoglycemia derived from physical activity, and reduces the need for pre-exercise or rescue carbohydrates, eliminating excess calorie intake. On the other hand, DHAP did not have a clear advantage over nocturnal control or the prandial period, and since the studies have been of short duration, it cannot be evaluated whether they help to reduce overall glucose levels. The review by Haidar (2019) analyzes the same works as the previous review, adding two more works: Castle et al. (2018) and Abitbol et al. (2018). Nevertheless, it reaches the same conclusions as the previous review. A recent review compared single and dual hormone AP (Wu et al., 2023). However, the authors (from the Montreal group) focused on nocturnal control in children and adolescents using three of their previous studies (Haidar et al., 2015b,a, 2016). The goal of the work was to reinforce the finding that the dual-hormone system was better at preventing hypoglycemia.

Other reviews evaluate AP systems in general, including information about some dual hormone trials, summarized in the following paragraphs.

In the review by Weisman et al. (2017), 24 studies were evaluated, of which six were DHAP. A potential comparison between single and dual AP is mentioned, but it is not trivial because two of them had an arm of SHAP, but the others were compared to conventional insulin infusion therapy (without CGM). In contrast, single-hormone trials were mostly compared against SAP. Still, DHAP improved time in range by 19.52% whereas overall improvement of single hormone systems was 11.06%.

A meta-analysis of AP systems from 2018 (Bekiari et al., 2018) also analyzes the contributions of DHAP, and from their selection of studies, they report that the weighted mean difference between DHAP and the control treatment was 15.1% over a 24h period and 2.84% overnight, versus 8.53% and 12.77% in single hormone[6]. These results reinforce the conclusions mentioned above that DHAP improves overall glucose control, but insulin-only treatment may suffice for overnight control.

The work by Wilson et al. (2020a) lists 20 dual-hormone studies published from 2010 to 2020, showing the trajectory of DHAP system development, summarizing the trials' findings, and providing a detailed overview of glucagon use in CL systems.

[6] The proportion of single hormone / dual hormone studies was 26/6 for the 24h period and 23/8 for the overnight period.

The latest review and meta-analysis on DHAP was presented in Zeng et al. (2022). The main contribution of their work is that the analysis divides the analysis depending on the control treatment used in the dual-hormone trials: single hormone AP, OL (SAP or continuous insulin infusion, i.e., with or without CGM), or pump with low suspend feature (see Section 2.3). A total of 17 trials are included in the analysis. However, one of the trials included in the DHAP versus SHAP group does not use glucagon but pramlintide, which may taint the analysis of glucagon contribution. The conclusion is that DHAP systems improve time in range and reduce time in hypoglycemia and time in hyperglycemia, regardless of the control arm. Although, the most significant improvement is found against the OL comparison. Also, the improvement on hypoglycemia is more noticeable than in hyperglycemia.

In short, almost the same conclusions are reached in every published review and meta-analysis:

- DHAP systems improve time in range and reduce time in hypoglycemia.
- Their main contribution is counteracting hypoglycemia in exercise periods since they also reduce the need for rescue carbohydrates.
- Their advantage is less marked in the overnight period.
- Using glucagon as a countermeasure after aggressive insulin dosing may not be a good strategy.
- The main challenge pending to solve is the need for a stable glucagon formulation and a dual-chamber portable pump accessible to the public.
- Longer clinical trials with glucagon are needed in order to assess glucagon's impact on HbA1c levels and account for possible long-term adverse effects. That is why DHAP systems should use low amounts of glucagon when possible, also to avoid short-term adverse effects.

Of note, the only clinical trials directly comparing SHAP to DHAP therapy are: Castle et al. (2010b)[7], Haidar et al. (2015b,a, 2016, 2017); Taleb et al. (2016); Abitbol et al. (2018); Castle et al. (2018); Wilson et al. (2020b); Castellanos et al. (2021), and Lindkvist et al. (2023).

[7] They compared using glucagon or placebo in their DHAP system. It could be considered a SHAP as long as the insulin and glucagon controllers were not coordinated.

Limitations and challenges of glucagon in AP

After their first dual hormone trials, both the Boston and OHSU groups published an article each analyzing the events observed in their trials when glucagon was not effective. The OHSU group (Castle et al., 2010b) concluded that the failures of glucagon were associated with a higher estimation of insulin on board (i.e., circulating insulin). They also considered the possibility of possible depletion of glycogen reserves and checked the amount of previously administered glucagon in the success and failure cases but found no significant differences. On the other hand, Russell et al. (2010) drew several conclusions regarding the failure episodes (with relation to the success cases): (1) the rate of decrease of plasma glucose was higher, (2) plasma insulin respect to baseline was also higher, (3) the error of the controller's estimation of plasma insulin was over 30%, and (4) plasma glucagon levels were lower. Glycogen reserves depletion was disregarded since the patients consumed sufficient carbohydrate-rich meals during the trial.

The OHSU group conducted a similar analysis in 2015 (Bakhtiani et al., 2015) revisiting four of their own clinical trials where the dual hormone AP system was used. Although they report that IOB values were higher when glucagon failed, the main analysis focuses on analyzing how their controller should be modified (e.g., the algorithm should activate at slightly higher glucagon values to avoid hypoglycemia on time and when glucose is falling more rapidly).

Another factor that these studies consider is the accuracy of the sensor since sensor readings higher than the actual glucose values could prevent the controller from acting when necessary.

A specific study by Castle et al. (2015) aimed to evaluate the consequences of repeated glucagon doses on hepatic glycogen reserves. Patients were administered eight 2 μg/kg consecutive doses (average value 140.7 μg, and total average dose 1125.8 μg over 16 hours), separated two hours each. The study found no glycogen depletion after the glucagon doses, not even in the fasting state. There was a slight decrease in glycogen stores in the fed state (observed in 6 out of 8 participants), but the difference was not statistically significant. Moreover, the rise in glucose after the last dose of glucagon was comparable to the first. These findings were useful to ensure that the typical glucagon doses administered in DHAP will not deplete glycogen reserves.

A study by Blauw et al. (2016c) tested the efficacy of different glucagon doses at different glucagon levels (glucose was clamped during intervals of 3 hours at 144, 108, 72, and 50 mg/dl). Depending on the study arm, patients were administered a different glucagon dose at each level (110, 220, or 440 μg). For the hypoglycemia stage, they were given 1 mg,

660 μg, or 330 μg. According to the study results, although the rise in plasma glucagon was consistent for every dose regardless of the glucose level, the pharmacodynamic effect of glucagon was not the same. In the case of the 50 mg/dl stage, the effect of 330 μg was comparable to the 110 μg administered previously, as well as the 660 μg to the 440 μg dose. This might be an indication of a possible glycogen depletion. Insulin influence is discarded since the authors report negligible plasma insulin levels.

In contrast to the study on repeated doses by Castle, the study by Blauw administered between 1300 and 1650 μg of glucagon over the span of 10 hours, which implies a higher glucagon administration in a shorter time. One limitation of the study was the small cohort used (ony six patients); however, the possibility of a loss of glucagon effectiveness is a matter that should be taken into consideration in DHAP design.

A different trial found that diet does have an impact on glucagon effect. The study by Ranjan et al. (2017) compared glucagon response in two different settings: (1) after a week following a high-carbohydrate diet and (2) after a week following a low-carbohydrate diet. On each study day, a 100 μg and a 500 μg dose were administered two hours apart. The study showed a statistically significant difference in the glucose rise depending on the diet, favoring the high-carbohydrate content one, meaning the low-carbohydrate diet may have depleted glycogen stores. A similar study by the same group (Ranjan et al., 2018) evaluated the effect of two 100 μg glucagon doses, once again separated two hours, after ethanol intake. The study found glucose plasma levels were higher in the control group (where placebo was consumed instead of ethanol). Still, the effect of both glucagon doses was the same, supporting Castle et al. (2015) findings. Hence, glucagon was still effective at raising glucose levels after ethanol, although it was more effective in the non-alcoholic setting.

There have been many concerns about whether a continuous use of glucagon may deplete glycogen reserves. Studies published until now seem to indicate that repeated glucagon dosing does not affect them to the point of affecting glucagon-caused glucose rises negatively. On the other hand, diet does have an effect. A poor carbohydrate content diet could affect glycogen reserves, which would reflect on glucagon response. Alcohol abuse could probably also act to the detriment of glucagon effectivity. The last general concern is the influence of plasma insulin values. Several studies have observed a loss of glucagon effectivity when their estimations of insulin on board were high. The study by El Youssef et al. (2014) seems to prove this effect since higher glucagon responses are completely blunted when administered at high plasma insulin levels.

Finally, as mentioned in Section 2.2.1, one of the main issues with glucagon is the lack of a stable formulation that does not need reconstitution. Some proposals are already being

used, but more extensive trials on their use in AP are needed. Until recently, clinical trials using glucagon had to reconstitute the hormone every 24 hours, which is inconvenient for real-life conditions. Lately, some CLs have already used dasiglucagon (Castellanos et al., 2021) and Xeris glucagon (Wilson et al., 2020a). Nevertheless, both formulations still present issues that need to be addressed.

So, the current main concerns are:

- The relationship between glucagon effect and glycogen stores.
- The blunted glucagon response in hyperinsulinemia.
- Finding a definitive stable glucagon liquid formulation.

Present of dual hormone AP

A very significant aspect of DHAP concerns the necessary devices. In order to administer a continuous subcutaneous infusion of glucagon, either a second pump or a dual-chamber pump is needed.

Currently, the most advanced dual hormone systems, product development-wise, are the ones developed by the Boston group (bihormonal iLet) (Castellanos et al., 2021; El-Khatib et al., 2017; Russell et al., 2016) and the one by Inreda, in the Netherlands (Blauw et al., 2021, 2016b; Van Bon et al., 2014).

The iLet system is commercially available in its insulin-only configuration (see Table 2.4). Their dual-hormone system uses their own dual-chamber pump, and their last published trial concludes that, given the feasibility of using dasiglucagon in AP, more extensive studies (only ten people took part in the trial in Castellanos et al. (2021)) will be performed to test the system further.

The Inreda system recently obtained CE marking in February 2020, allowing its production and supply in Europe. Nowadays, it is under development and will become available only for the Dutch market. The system consists of a dual-chamber pump (using regular glucagon at the moment, meaning patients would need to reconstitute and refill the cartridges manually every day) and two Guardian CGM sensors. This may pose a problem for its reception by the patients since T1D therapy already involves many devices, and increasing this number would make the management of diabetes even more burdensome.

T1D therapy involves constant challenges and burdens for the patients, spanning from physical to emotional burdens. Patients do not perceive diabetes devices positively

because they become a reminder of their disease, especially for younger patients, who may be more concerned with their physical image and fitting in. Even if relying on the devices becomes a relief in diabetes management, they come with their own negative perception, including actual pain or dermatological reactions, as well as the hassles derived (malfunctioning, detachment, etc.) (Tanenbaum and Commissariat, 2023).

The Boston group conducted a survey evaluating psychosocial outcomes on patients after wearing their single and dual hormone devices in Weissberg-Benchell et al. (2017). Several aspects were evaluated: quality of life, diabetes-specific emotional distress, treatment satisfaction, and their experience with the Bionic Pancreas. The system had a positive reception regarding distress reduction and improvement in quality of life. Regarding the use of the system specifically, around 70% reported a positive experience since it helped them worry less about their glucose levels. However, 77% reported that carrying around all the equipment was burdensome, and changing the glucagon every day was rated negatively by 80% of the participants. Around 60% reported that wearing all the equipment was uncomfortable and more intrusive than their typical method of diabetes care.

All things considered, DHAP provides an improvement in glucose management, but they also add to the difficulties of diabetes management by introducing an extra hormone and the subsequent extra devices. Nevertheless, it might be beneficial for certain people, such as patients suffering from recurrent hypoglycemia, especially during or after exercise, or with hypoglycemia unawareness (Infante et al., 2021).

2.3.3 Insulin-Pramlintide

Pramlintide efficacy as adjunctive therapy in T1D has been thoroughly researched and validated, proving useful in delaying gastric emptying, thus easing the management of postprandial glucose excursions.

The most common form of administration is using pens or injections before meals. In Weyer et al. (2001) it is stated that, generally, pramlintide does not need meal-dependent fine-tuning, in contrast to insulin. Hence, pramlintide administration could consist of a fixed dose most of the time. However, insulin does need to be carefully estimated depending on meal composition to avoid extreme deviations from normoglycemia, and the introduction of pramlintide forces to re-calculate insulin bolus to account for the amylin analog effect (Infante et al., 2021) and avoid insulin overdosing that could lead to hypoglycemia. That is why incorporating pramlintide into a CL system would ease the management of both hormones for the patient.

A 2009 pilot study successfully evaluated the subcutaneous administration of pramlin-

tide using a second pump (in addition to the one for insulin) in a 16-week study (Huffman et al., 2009). However, only 11 people participated in the trial, and there was no control arm. More recently, the group from OHSU performed a clinical trial co-administering continuous infusions of insulin and pramlintide at a fixed ratio, using two separate pumps (Riddle et al., 2018). Almost 30 patients participated in the two 24-hour study sessions.

Some works have started testing pramlintide in the AP context, but they are scarce.

The first trial testing pramlintide in a CL environment was the work by (Weinzimer et al., 2012), a group from New Haven, Connecticut (USA). The trial made use of the ePID CL algorithm developed by Medtronic. Participants stayed in the clinic for two days, and the three meals were identical each day. The CL insulin system was running for the entirety of the study. On one of the days (randomly assigned), each meal was accompanied by a 30 μg pramlintide bolus. Results of the trial showed a delay of approximately one hour in peak plasma glucose concentration when pramlintide was administered, and the pramlintide effect was dependent on meal type, which leads to revisit the assertion that a fixed-pramlintide dose will be sufficient regardless of the meal content.

The next work revisiting the use of pramlintide in a CL setting was the Montreal group in Haidar et al. (2020). The trial performed a double comparison: using a rapid-insulin AP system compared to rapid-insulin-plus-pramlintide AP and regular-insulin-plus-pramlinitide. Each intervention spanned 24 hours. Pramlintide was administered subcutaneously using a second pump. In every case, the insulin infusion values were governed by a control algorithm, and pramlintide was administered at a fixed ratio of 6 μg per unit of insulin.

Results of the trial show that rapid-insulin-plus pramlintide configuration improved the percentage of time in normoglycemia over a 24 hours compared to its insulin-only counterpart (84% vs 74%). On the other hand, the regular-insulin-plus pramlintide combination did not perform as well, with only a 69% time in range. The main issue was an increase of percentage time in hypoglycemia during the night period, probably due to a higher insulin dosing in said arm. The average value of total daily pramlintide delivered in the rapid-insulin arm was 278 μg and 318 μg in the regular-plus-pramlintide arm.

The Montreal group kept working on incorporating pramlintide into AP systems, and in 2021, they published the results for two other trials.

The study in Tsoukas et al. (2021b) aimed to evaluate the potential improvement after introducing pramlintide in a Fiasp (a novel faster-acting insulin) AP, comparing the performance of the system with and without pramlintide. Pramlintide was administered by a second pump in a 10 μg/U fixed ratio, both for basal and prandial boluses. The trial

reports a higher time in range using the insulin-only configuration compared to the system with pramlintide (78.1% versus 74.3%). During the day, there was a higher percentage of time spent in hyperglycemia because the first part of the postprandial response was higher in the experiments of that arm than in the control. Also, less insulin was administered during the pramlintide arm because the meals were not announced, in contrast to the control arm, where a prandial bolus was delivered at the onset of each meal. Overall, mean values for prandial boluses in the pramlintide arm were a third lower than in the control arm.

The work in Tsoukas et al. (2021a) involved two small studies: (1) an eight-participant inpatient feasibility study and (2) a four-participant outpatient pilot study (actually part of another bigger trial). The studies' chosen designs reflect their different primary aims: the feasibility study focused on glycaemic control with the DHAP system compared with the control arm. The pilot study, however, also assessed qualitative outcomes, requiring an additional arm (FiASP-and-placebo with simple meal announcements[8]) to evaluate if potential changes to the quality of life were related to pramlintide or simply to the alleviation of carbohydrate counting, irrespective of glucose control.

The feasibility study time-in-range outcomes favored the arm with pramlintide (84% of time in range versus 81% in the control arm). On the other hand, in the pilot study, the percentage of time in range between the AP with pramlintide and a simple meal announcement strategy achieved the same time in range that the insulin-only arm where the exact number of carbohydrates was introduced to the system for bolusing (around 70%).

There are no more works using pramlintide in AP systems. A recent review (Torres-Castaño et al., 2022) identified 270 publications from several databases, and after screening, only found these three works (Haidar et al., 2020; Tsoukas et al., 2021b,a).

Perspectives of pramlintide in AP

Pramlintide can offer advantages, but as seen in Haidar's results, incorporating pramlintide into AP is still a work in progress in search of the best strategy to exploit its possibilities.

Pramlintide is less studied than insulin or glucagon, which is why pramlintide clinical trials seem to be based on trial-and-error dosing strategies. However, clinical trials are expensive, so there is a need for accurate mathematical simulators that incorporate pramlintide models to test insulin-plus-pramlintide control strategies.

[8] Simple announcements do not require carbohydrate counting, but just announcing the time of the meal.

The new co-formulation of insulin and pramlintide may also delay the use of pramlintide in AP. Since the drug's pharmacokinetic and pharmacodynamic relationships are still not yet defined, no proper control strategies can be developed. However, this combined administration would avoid the complications of needing a second pump (as in the glucagon DHAP case).

Longer trials in the CL setting will be needed to assess the feasibility of the prolonged use of pramlintide.

2.3.4 Adjunctive therapies in AP

Adjunctive therapies have also reached AP systems, and some trials have incorporated some of these drugs (see Section 2.2.2) into CL systems. The ones tested until now have been: GLP-1 agonists, DDP4-inhibitors, and SGLT2-inhibitors. Additionally, one trial assessed the feasibility of a *tri-hormonal* system, combining insulin, glucagon, and pramlintide.

GLP-1 agonists

In 2014, a clinical group from New York (USA) performed a study comparing pramlintide and exenatide (GLP-1) to determine which would be more effective in attenuating postprandial glucose (Renukuntla et al., 2014). Subcutaneous insulin infusion was governed by the ePID Medtronic algorithm. Patients visited the clinic three times, and they received insulin-only therapy in one and the corresponding adjunctive therapy in the other two. The CL period lasted 24 hours in the three arms. The pramlintide visit consisted of administering a 30 μg bolus before meals, whereas in the exenatide arm, a 2.5 μg dose was administered on the same occasions. In this study, the greatest percentage of time in range was achieved with the insulin plus exenatide therapy (76%), compared to the arm with pramlintide (66%) and the control (62%). The results in the trial show how pramlintide delays (approximately 1 hour) and slightly attenuates the glucose response after meals, but the treatment with exenatide almost flattens the glucose curve.

In 2016, a study by Sherr et al. (2016), the Connecticut group, evaluated the influence of pramlintide and liraglutide in a 24-hour inpatient study after a 3-4 week outpatient period. However, the study was not designed to compare both treatments between them but each of them with the control (i.e., the CL system working with insulin only). In the adjunctive therapy arms, 60 μg of pramlintide were administered 15 minutes before each meal, and 1.8 mg of liraglutide was administered once daily at 8 AM.

The group from New York performed a second CL study (Ilkowitz et al., 2016), this time comparing liraglutide as adjunctive therapy to insulin versus insulin-only. On the treatment arm, patients were administered 1.2 mg of liraglutide at the beginning of the day. Results of the trial report a significant decrease in BG values in the treatment arm.

The work by Kobayati et al. (2022) reviewed contributions of GLP-1 agonists in T1D and listed the works in the literature that performed trials with this adjunctive therapy and CL systems. There are no more than the three trials mentioned above.

DPP4-inhibitor

Once again, the group from New York decided to test the capabilities of another adjunctive drug accompanied by an insulin-dosing CL algorithm (Underland et al., 2017). The inpatient study lasted for 25 hours, which covered dinner, breakfast, lunch, and dinner again. Patients participated in two trial arms, one where they took 100 mg sitagliptin just before the first dinner and another where the dose was placebo. Although a difference can be observed in the glucose concentrations between the treatment and the control arm after the first two meals (around 20 mg/dl difference after dinner and breakfast), the statistical analysis concluded the difference was not statistically significant. Postprandial glucose concentrations after the lunch and second dinner were almost identical. Overall, glucose concentrations and insulin requirements were lower during the treatment arm, but a better dosing time (e.g., before breakfast) or a second administration of sitagliptin during the day would help prolong its effect to cover all daily meals.

SGLT2-inhibitor

Trials testing SGLT2-inhibitors in the CL context are fairly recent, the first works in the literature dating from 2021.

In the review by Srinivasan et al. (2021), there is a reference to a 2019 conference abstract of a CL study with dapagliflozin. The proper results of the trial were later presented in the work by Biester et al. (2021). The trial was carried out by a consortium including groups from Germany, Israel, and Slovenia. They aimed to observe the contribution of dapagliflozin on unannounced meals with an insulin CL system versus a control arm where placebo was administered. The treatment arm administered 10 mg of dapagliflozin twice over the 27-hour inpatient study (at 7 PM the first day and 6.30 AM the next morning). A total of 30 participants completed the study (15 young adults and 15 adolescents). The results show an improvement in time in range in the treatment group (68% versus 50% in

the placebo arm) and a reduction of delivered insulin since fewer correction boluses were necessary. The main improvement is observed in the reduction of nocturnal variability.

The group for Montreal conducted a trial with empagliflozin (Haidar et al., 2021), performing several comparisons: the trial consisted of two insulin-only and three insulin-plus-empagliflozin arms. The insulin CL strategy was the same for all the trials. 25 mg of empagliflozin were consumed daily on the corresponding days. The difference among the trials of the same type was the meal announcement strategy. For the insulin only, either the patients introduced the amount of carbohydrates in the system or performed a simple meal announcement, simply pressing a button at the start of the meal. The same strategies were followed in the empagliflozin arm, adding a non-announcement strategy and letting the insulin dosing algorithm react on its own. The main results presented in the paper compare the control arm with carbohydrate counting against each empagliflozin strategy. In comparison, not announcing the meals with empagliflozin worsened glucose control. The simple meal announcement performed similarly to the baseline case, and finally, the carbohydrate counting with empagliflozin significantly improved time in range compared to its insulin-only counterpart.

The same group carried out a second trial with empagliflozin a year later (Haidar et al., 2022). This trial compared the addition of 25 mg of empagliflozin or placebo to a CL or a SAP system. The addition of empagliflozin improved time in range in CL by 7.2% and 11.4% in the SAP counterpart, with respect to placebo administration. They also performed a trial testing low-dose (2.5 or 5 mg) empagliflozin (Pasqua et al., 2022).

Finally, the group from the University of Virginia (Garcia-Tirado et al., 2022) recently conducted a trial to observe the potential benefits of low-dose empagliflozin (5 mg/day) as a complement to the AP systems Control-IQ and Basal-IQ (see Table 2.4), versus placebo administration. The study was done in an outpatient context for 1-2 weeks. Results report a 10% improvement in *daytime* time in range after adding the SGTL2 inhibitor to the Control-IQ therapy (81% versus 71%). The study also demonstrated that empagliflozin use improved the performance of both Control-IQ and Basal-IQ overnight and overall (Control-IQ maintaining superiority over Basal-IQ). The trial also noted the risk of diabetic ketoacidosis derived from the use of the drug.

Insulin-glucagon-pramlintide

As the last representative of adjunctive therapy, we find the trial (once again) by the Montreal group in which they tested insulin-glucagon and pramlintide intending to obtain a full automated AP that does not require carbohydrate counting (Majdpour et al., 2021).

Nine patients underwent a control arm with the insulin-alone AP with full carbohydrate counting and another arm with the fully automated multi-hormone pancreas. The inpatient study lasted 24 hours.

There was a run-in period of 3 to 6 days, in which patients started using pramlintide in a fixed ratio fashion (3 μg/U the first two days and 6 μg/U thereafter) in order to avoid the onset of treatment adverse effects the day of the study. During the 24-hour visit to the clinic, patients used a total of three pumps in the multihormone visits. Pramlintide and insulin were administered in a basal-bolus manner with a fixed ratio to mimic a co-formulation and the normal physiology of the pancreas. Glucagon was administered as miniboluses based on heuristic logical rules using glucose levels and their trends.

The study performs an iterative tuning process of the control strategy every two or three patients: increasing and reducing the pramlintide to insulin ratio, adding a meal-detection algorithm, increasing the controller aggressiveness, or eliminating glucagon. All these changes aimed to reduce postprandial hyperglycemia, reduce gastrointestinal symptoms, and avoid hypoglycemia. Based on the best results obtained, their final proposal would be an insulin-plus-pramlintide (ratio of 10 μg/U) AP with a meal detection algorithm to trigger meal boluses without glucagon.

This is an interesting trial but with several limitations, and further research on this matter should be done to see the potential benefits of using three hormones. The main disadvantage of the system, patient-wise, would be the need for three different infusion sets and the side effects attached to the continuous drug administration.

2.4 Conclusion

T1D hinders normal glucose regulation in the body, making people dependent on exogenous insulin administration. However, managing insulin dosing and the subsequent inconveniences of the disease (avoiding hyperglycemia and hypoglycemia while achieving as much time in normoglycemia as possible) is not a trivial task. Many strategies have been developed to aid patients in this task:

- Administering additional drugs to help manage glucose values. The candidates are glucagon, which has an opposite effect to insulin, and adjunctive therapies (e.g., pramlintide, GLP-1 agonists, SGTL-inhibitors) that aim to ease insulin's task, attenuating disturbances' impact on glucose.

- Developing AP systems that manage insulin dosing semi-automatically. The ulti-

mate goal for these systems is to be able to manage the disease without the patient's intervention.

These two approaches complement each other. The introduction of adjunctive therapies or additional control actions would provide supplementary tools and ease the task of the AP system since insulin-only therapy can be insufficient to properly manage T1D in some cases.

However, extended access to these therapies to the public is still a long-term project. Pramlintide has only been approved for use in T1D in the USA, whereas SGLT inhibitors are only approved in Europe and Japan (Srinivasan et al., 2021). Moreover, many of these drugs still present severe adverse effects that the manufacturers should address, and the consequences of their prolonged use must be thoroughly assessed.

AP systems will need to adapt their strategies to consider these additional elements. In the case of oral agents (usually administered once a day), the system will need to take into account the changes in dynamics introduced by the drugs, which will primarly affect the model-based control strategies. Subcutaneously-administered drugs pose a greater change to the system since they introduce an additional control action, so their mechanisms need to be well-known.

These AP developments demand an improvement in T1D simulators. There is no consensus on the glucagon effect description, and pramlintide models are scarce. Moreover, the effect of other adjunctive therapies has not been included in any T1D simulator. There is also a necessity for simulators that describe different cohorts of patients with different characteristics and necessities that would benefit from one specific treatment or another.

Chapter 3

T1D simulation models

Mathematical models allow to reproduce the behavior of biological systems. Glucose dynamics have been studied for a long time, and many proposals are devoted to describing its physiology. This chapter presents some of the most relevant models used to simulate T1D glucose dynamics, including a summary of the relationships among them. The analysis then focuses on descriptions of glucagon effect and, finally, on pramlintide models.

3.1 Introduction

Mathematical representations of biological processes allow replicating their behavior using computer simulations. This facilitates faster experimentation and reduces costs and efforts of biological or clinical experiments (Balsa-Canto et al., 2010), which is especially useful when access to the real process is unavailable or experimentation is too complex or expensive. Mathematical models also help to understand the underlying dynamics of complex biological systems, and they are used in applications from cellular biology to health service research (Ajmera et al., 2013).

In the context of human clinical experiments, whole-body models are often too complex, and including every biological interaction and reaction is virtually impossible. Hence, many models focus on a specific route or pathway, simplifying the model to the magnitudes

of interest. For instance, some models are often used to describe how a certain substance or drug affects the body. In those cases, the definitions are divided into pharmacokinetics (PK) and pharmacodynamics (PD).

As stated in Rimmington (2020), PK could be simply explained as "what the body does to the drug", while PD would be "what the drug does to the body". Indeed, PK describes the transport of a certain substance from the point where it is administered (e.g., subcutaneously, orally) to the site of measurement (usually concentration in plasma). Many factors, both on the part of the body and on the drug characteristics themselves, can influence drug absorption. After absorption, the drug is transported from one location to another by a rate-limited process of perfusion or permeability. These rates can be later used to define compartmental models. On the other hand, PD relates the concentration of the drug and its effect, which includes the binding of drugs to cells, drug uptake, and intracellular drug metabolism (Rimmington, 2020).

One of the most common ways of defining this kind of model is using compartmental structures. A compartment represents a certain amount of material, which may or may not be an actual physical volume. The particles of each compartment are influenced by forces that make them transfer from one compartment to another, through some physical barrier, or by undergoing some physical or chemical transformation (Anderson, 1983). A compartmental system comprises two or more compartments, with certain transfer rates describing the material transfer from one to another. These systems are usually modeled using ordinary differential equations (ODEs), using first-order kinetics to describe mass balance equations (Ajmera et al., 2013).

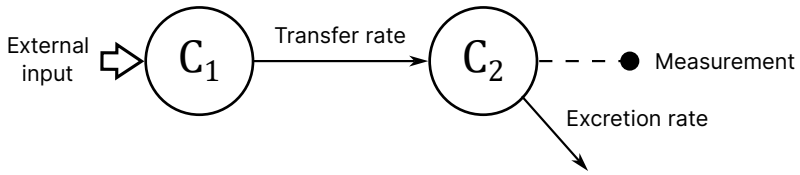

Figure 3.1: Generic compartmental model structure.

A classical representation of compartmental systems includes boxes or circles to represent each compartment, as illustrated in Figure 3.1. Pointed arrows illustrate the transfer from one compartment to the other, and the magnitude usually written on them symbolizes the aforementioned transfer rates. These transfers could also represent any amount of material lost by excretion, metabolism, etc. In those cases, arrows just draw an output flux from the compartment. On the other hand, there might be external inputs to

the system (e.g., the subcutaneous drug administration), as illustrated by the arrow on the left. The input sometimes is modulated by a bioavailability coefficient because some portion of the drug might be lost following administration, and only part of the initial dose reaches blood circulation. This coefficient will depend on the route of administration. For instance, intravenous dosing should have an availability coefficient of 1 since the drug is directly delivered to plasma (Rimmington, 2020).

The line with a point on the right represents a compartment where measurements are taken (e.g., the plasma compartment). Compartmental system representation may include the formula of the concentration as a function of the compartment mass, which is usually obtained as the quotient between said mass and the distribution volume of the specific magnitude. The volume of distribution represents the volume into which a drug dose would need to be distributed in order to produce the observed plasma concentration (Rimmington, 2020), being calculated as:

$$V_d = \frac{\text{total amount of drug in body or dose}}{\text{concentration of drug in plasma}}$$

The graphical representations of compartmental models considered in this chapter follow a set of rules:

- Compartments are drawn using circles, and they represent an ODE.
- Certain arithmetic relationships used to calculate intermediate or auxiliary signals are represented with a square.
- White arrows represent exogenous inputs to the system.
- Thin black arrows indicate a transference or influence from one element to another.
- Small black circles indicate where plasma measurements are taken.
- A variable without any circle or square represents a constant value.

T1D is not an exception to benefit from the use of mathematical models and simulators (Kovatchev et al., 2009). The work of Ajmera et al. (2013) reviewed the advances and contributions of mathematical models in the study of T1D in the last 50 years. Their work analyzes the published models, studying the relationships and inheritances from one to the others and classifying them depending on their purpose (e.g., models for diagnostic tests, models for control, models for describing specific physiological dynamics). This

chapter presents a simpler review, aiming to provide an overview of some of the most relevant or widely used diabetes models in the T1D literature, highlighting their structural differences.

3.2 Models in Type 1 Diabetes

Mathematical models are also a key tool in developing and implementing AP technologies, both for developing model-based control strategies and the pre-clinical testing algorithms (McCall and Farhy, 2013; Haidar, 2016). Several works in the literature have provided descriptions of physiology and the processes involved in glucose regulation, allowing the development of T1D simulators that simplify the insulin-glucose relationship (in their most basic version) to test different insulin administration strategies without resorting to clinical trials. These models allow the evaluation of extreme situations in a controlled environment without entailing any risk for the patients.

However, their capabilities are limited since they are, after all, just an approximation. There are a myriad of other mechanisms and reactions involved that are not included in these representations. Moreover, as mentioned in the previous chapter (Section 2.3), the patients show a lot of variability, which depends on internal and external factors that are usually not included in mathematical models. Nevertheless, simulators are very valuable since this approximation already provides a ground for technological developments.

Mathematical models for T1D focus mainly on insulin PK and its effect on glucose. Glucose dynamics might include additional considerations, such as the contribution of endogenous glucose production (EGP) in the liver or renal excretion.

Some of the most relevant models in the literature are Bergman's Minimal Model, the Hovorka Model, and the Dalla Man model, which are the most mentioned in reviews of T1D models (Kushner et al., 2019; Wilinska and Hovorka, 2014; Chandrasekhar and Padhi, 2023). Hence, this section will include a description of those models and some relevant extensions derived from them.

A selection of the presented models is represented in the central pages of this chapter (Figure 3.2 to 3.5) in order to provide an overview of their structures and main features. The compartments are classified into sections which are:

- Insulin PK.
- Glucagon PK.

- EGP. This block also includes the glucagon effect (glucagon PD) since glucagon is one of the main agents involved in hepatic glucose production, as presented in the previous chapter (Section 2.1).

- Glucose regulation. This block may include insulin PD compartments. An extra section for insulin effect was not included for simplicity. Also, one of the focus points is the analysis of different glucagon definitions, hence, separating insulin action mechanisms was not as relevant to this analysis.

- Glucose absorption (meal model).

- Physical activity (exercise model).

These are the most relevant parts found in most T1D mathematical models. Insulin and glucose regulation will always be present. Some models might include glucagon as a control action, hence describing its effect on glucose. The two most common disturbances in diabetes control are meals and physical activity, which is why they have their corresponding blocks.

The selected models are reported in more detail in Appendix B, where a collection of tables describe their states and parameters. Also, their complete equations are reported at the end of the document.

Nevertheless, the collection of models described in this chapter is a sample of the numerous works and proposals in the literature. Models that included glucagon PK/PD definitions were favored in the selection process.

3.2.1 Bergman Minimal Model

One of the simplest and earliest models available was the model developed by Bergman (Bergman et al., 1979), known as the *Minimal Model*. This model was designed to estimate insulin sensitivity based on the response to an intravenous glucose injection. The insulin sensitivity value could be inferred as the relation between two model parameters ($S_I = -p_3/p_2$).

It employs three differential equations (Bergman et al., 1981), that describe plasma glucose concentration ($G(t)$), plasma insulin concentration ($I(t)$), and a state proportional to insulin in a remote compartment ($X(t)$), which was later defined as the interstitial compartment (Bergman, 2005).

$$\dot{G}(t) = (p_1 - X(t))\, G(t) - p_1 G_b \tag{3.1a}$$
$$\dot{X}(t) = p_2 X(t) + p_3 I(t) \tag{3.1b}$$
$$\dot{I}(t) = \gamma\, (G(t) - h)\, t - n I(t) \tag{3.1c}$$

The first two equations correspond to glucose dynamics, whereas the third represents insulin kinetics. The parameters in these equations do not describe actual rates between compartments, but they aggregate arithmetic relationships between those rates, as described in the original work of Bergman et al. (1979). See Table B.7 for more details on the model parameters. Equation (3.1c) assumes an endogenous insulin production. Hence, this term has to be modified when modeling T1D glucose dynamics, where insulin contributions are due to external administration only.

However, this model has had great importance in T1D literature, given its simplicity and effectivity in describing insulin-glucose dynamics (Bergman, 2005). Many works have taken this model as a foundation to propose extensions, adding equations to account for additional effects. A small sample of said works is described next.

One of the first extensions of the Minimal Model was presented in Cobelli et al. (1999), where they introduced the *Two-compartment Minimal Model* (2CMM). This structure introduces an extra state for the glucose dynamics in a non-accessible compartment.

Another example, Patek et al. (2016), used an extension of the Minimal Model to analyze glucose variability as a consequence of carbohydrate ingestion, naming it the *Subcutaneous Oral Glucose Minimal Model* (SOGMM). They expanded Equation (3.1a) to include: (1) the effect of meals, adding a meal subsystem composed of two compartments, (2) the transport of insulin from the subcutaneous administration to plasma, with a three-compartment subsystem, and (3) subcutaneous glucose measurements, adding an extra state representing the delay when measuring subcutaneously instead of in plasma.

The work in Breton (2008) extends the minimal model, adding a term to introduce the effect of exercise using heart rate (HR) value as input to the system. Another example is the extended model by Roy and Parker (2006), which includes FFA dynamics and interactions among FFA, glucose, and insulin. The extension adds three extra compartments: (1) one compartment for the remote insulin dynamics, where insulin promotes uptake of FFA for storage, (2) one state to describe plasma FFA concentrations, and (3) one compartment to represent the remote FFA dynamics.

The same authors then performed a second extension of the minimal model (Roy and Parker, 2007), including the effect of exercise by adding three extra compartments. Two

of them represent the rates of glucose uptake and hepatic glucose production induced by exercise, which contribute with two additional terms in Equation (3.1a). The third extra state represents the rate of insulin removal from the circulation due to exercise-related physiological changes, and it adds a subtracting term on Equation (3.1c). The input to the exercise subsystem is the exercise level, expressed as the oxygen consumption (VO_2^{max}).

More recently, a Minimal Model including glucagon was proposed in Kelly et al. (2019). The *Nonlinear Glucagon Minimal Model formulation* (NLGMM) describes the relationship between insulin and glucagon the same way as the Minimal Model but includes a subsystem of glucose-insulin-glucagon dynamics. Insulin compartments $I(t)$ and $X(t)$ are replicated to describe plasma and active glucagon, respectively. A linear version of the model, where the effect of glucagon on glucose is simplified to a linear relationship, is also proposed in the same paper. However, the system does not include PK dynamics for either insulin or glucagon since the available inputs are an external infusion of insulin and glucose directly introduced to plasma. See Table B.10 for more details on the model structure.

The work in Fabietti et al. (2006) presents a glucoregulatory model that includes insulin and glucose metabolism, based on Bergman's Minimal Model, adding an extra insulin compartment to describe external insulin administration and exogenous glucose intake. Meal absorption is modeled by dividing the meal into three components filtered through three transfer functions. The filter characteristics were determined based on fittings of clinical data. The model was designed for control applications to use a simple enough identifiable model useful for control applications but capable of describing glucose dynamics accurately. Its parameters are described in Table B.12.

However, the most relevant extension of the Minimal model is the Hovorka model, presented in the next section.

3.2.2 Hovorka model

This model was first presented in Hovorka et al. (2002). One of its main characteristics is using an accessible (Q_1) and non-accessible (Q_2) compartment to describe glucose dynamics. The former is where measurements are made, while the latter represents an equilibrating pool containing the remaining interstitial and intracellular distribution space. Two output rates depart from the accessible compartment, one representing the insulin-independent glucose flux (F_{01}), and the other representing renal glucose clearance happening in hyperglycemia (F_R). Insulin has an effect on the glucose transfer from the accessible to the non-accessible compartment, as well as glucose transport or distribution, which is

represented as an output flux from the non-accessible compartment. The complete model equations are listed at the end of Appendix B.

Hence, the insulin effect derived from plasma insulin concentration is divided into three compartments, each affecting a different aspect. Apart from its influence on glucose disposal (x_1) and transport (x_2), the third effect (x_3) influences EGP. EGP symbolizes the glucose production from the liver, and insulin diminishes its effect.

A submodel describing insulin PK was added in Hovorka et al. (2004). The model uses a three-compartment system: two for the subcutaneous transport of insulin to the third compartment, representing the plasma concentration. An exploration of different models to describe the kinetics of insulin lispro was carried out in Wilinska et al. (2005), where a series of model proposals were evaluated using the Akaike Information Criterion (AIC) and the Bayesian Information Criterion (BIC)[1]. The model that provided the best fit to their data consisted of two parallel chains (to account for fast and slow transport), as well as a degradation of the input in the injection site (bioavailability coefficient). However, most implementations favor the simpler version with just two consecutive compartments.

Additionally, the authors added a two-compartment model to represent glucose absorption from the gut (after meal ingestion). Since the transfer rates between compartments were identical, the expression could be expressed as:

$$U_G(t) = \frac{D_G A_G t e^{-t/t_{max,G}}}{t^2_{max.G}} \tag{3.2}$$

The compartmental representation equations are reported in Wilinska et al. (2010), but both expressions are equivalent.

This model has become one of the most widely used models in the literature, and several works have proposed extensions to this structure, including subsystems for additional inputs such as glucagon or physical activity.

Wendt model

The work by Wendt et al. (2017b) proposed an extension of the Hovorka model in which they did not include the meal model. However, they replicated the insulin subcutaneous PK system to include glucagon kinetics. Of note, plasma insulin and glucagon compartments were not defined as ODEs but as arithmetic relationships. Their other contribution was the

[1] AIC and BIC are two metrics commonly used to evaluate the performance of biological models. More details on the definition of these criteria will be given in Section 7.4.

definition of an EGP expression that combined both the influence of insulin and glucagon, applying a saturation on the latter (more details will be given in Section 3.3). The model parameters are listed in Table B.2.

Herrero model

Herrero et al. (2013) proposed a model that is actually based both on Hovorka and the Bergman model: glucose dynamics are based on the Bergman model, whereas insulin PK and the gastrointestinal absorption model were based on Hovorka et al. (2004). Moreover, the insulin subcutaneous absorption subsystem was replicated to add glucagon PK to the model. Model parameters are described in B.8.

Jacobs model

This model was described first in Jacobs et al. (2015), where an exercise model was incorporated into the Hovorka model. The exercise model was proposed in Hernández-Ordoñez and Campos-Delgado (2008). This model modifies the insulin action states to reflect insulin sensitivity changes associated with exercise. The inputs to the system are the percentage of oxygen consumption (PVO_2^{max}), and the percentage of active muscle mass. During the model validation, the value of PVO_2^{max} was estimated based on HR and accelerometry data recorded in the clinic. The model also includes a remote compartment ($Y(t)$) and a glucagon action compartment ($Z(t)$) to account for the plasma glucagon effect on glucose.

The authors later added glucagon kinetics to the model based on the glucagon PK model proposed in Lv et al. (2013). This work presented a set of eight different proposals to approach glucagon kinetics and selected the best structure according to the obtained BIC results. Their proposal consisted of a chain of three compartments from the subcutaneous administration of glucagon to the plasma compartment. This subsystem was incorporated into a Bergman-based glucose dynamics equation, following the work of Herrero et al. (2013).

Hence, a later version of the model presented as the *Virtual Patient Population* (VPP) in Resalat et al. (2019) incorporated the three-compartment glucagon PK subsystem to the Jacobs et al. (2015) model. With this, the authors achieved a complete insulin-glucagon PK/PD proposal, including physical activity. Table B.4 gives more details on the model parameters and states.

A simulator with an implementation of this model is available online in Jacobs (2019).

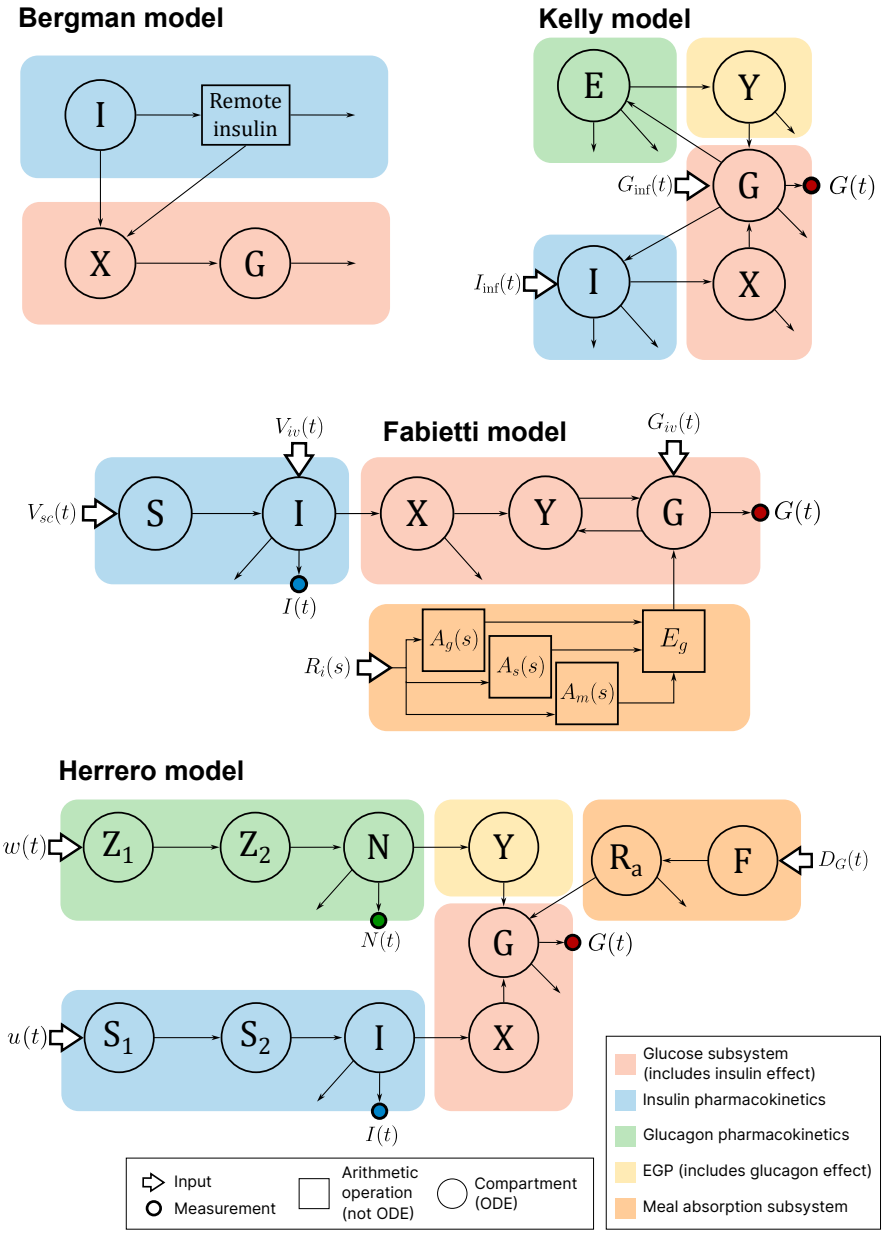

Figure 3.2: Compartmental diagrams of the Bergman model (Bergman et al., 1981), Kelly model (Kelly et al., 2019), Fabietti model (Fabietti et al., 2006), and Herrero model (Herrero et al., 2013).

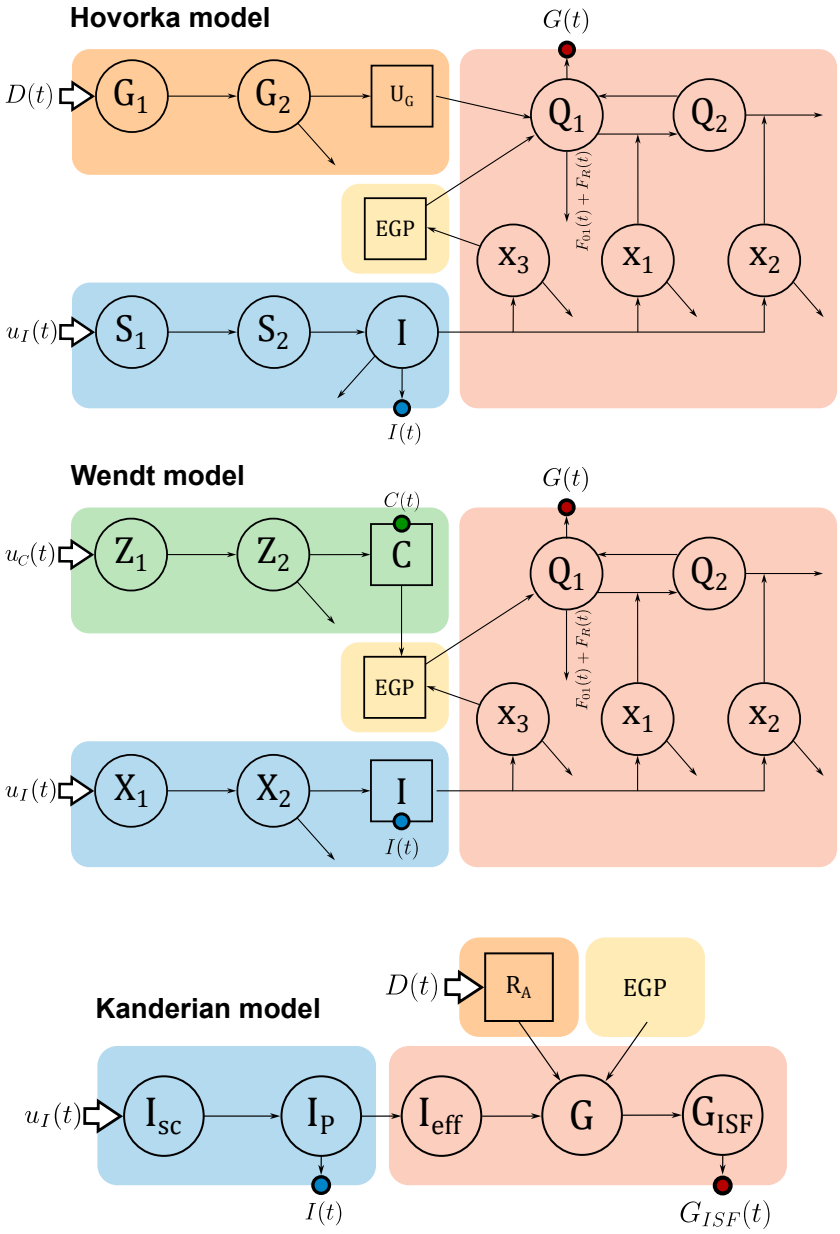

Figure 3.3: Compartmental diagrams of the Hovorka model (Wilinska et al., 2010), Wendt model (Wendt et al., 2017b), and Kanderian model (Kanderian et al., 2012).

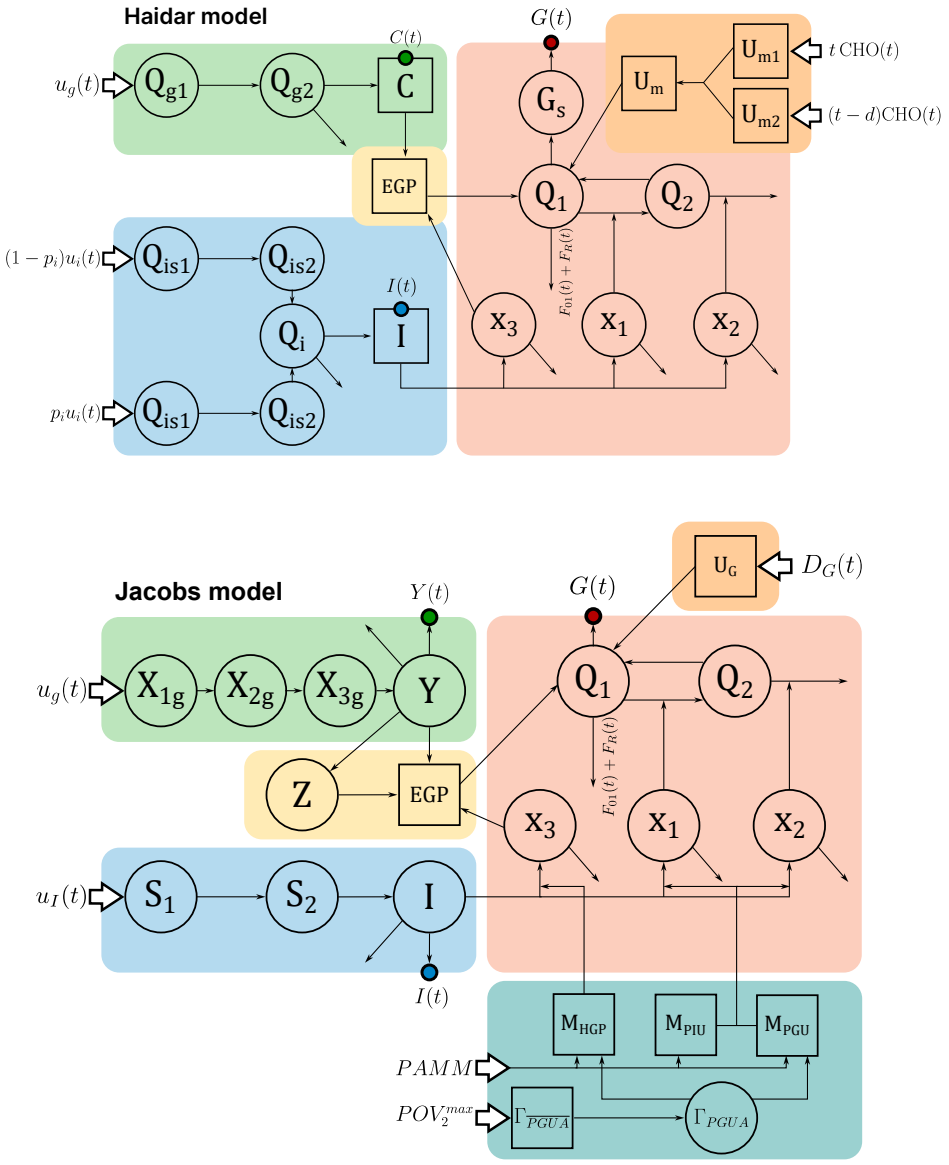

Figure 3.4: Compartmental diagrams of the Haidar model (Smaoui et al., 2020a) and the Jacobs model (Resalat et al., 2019).

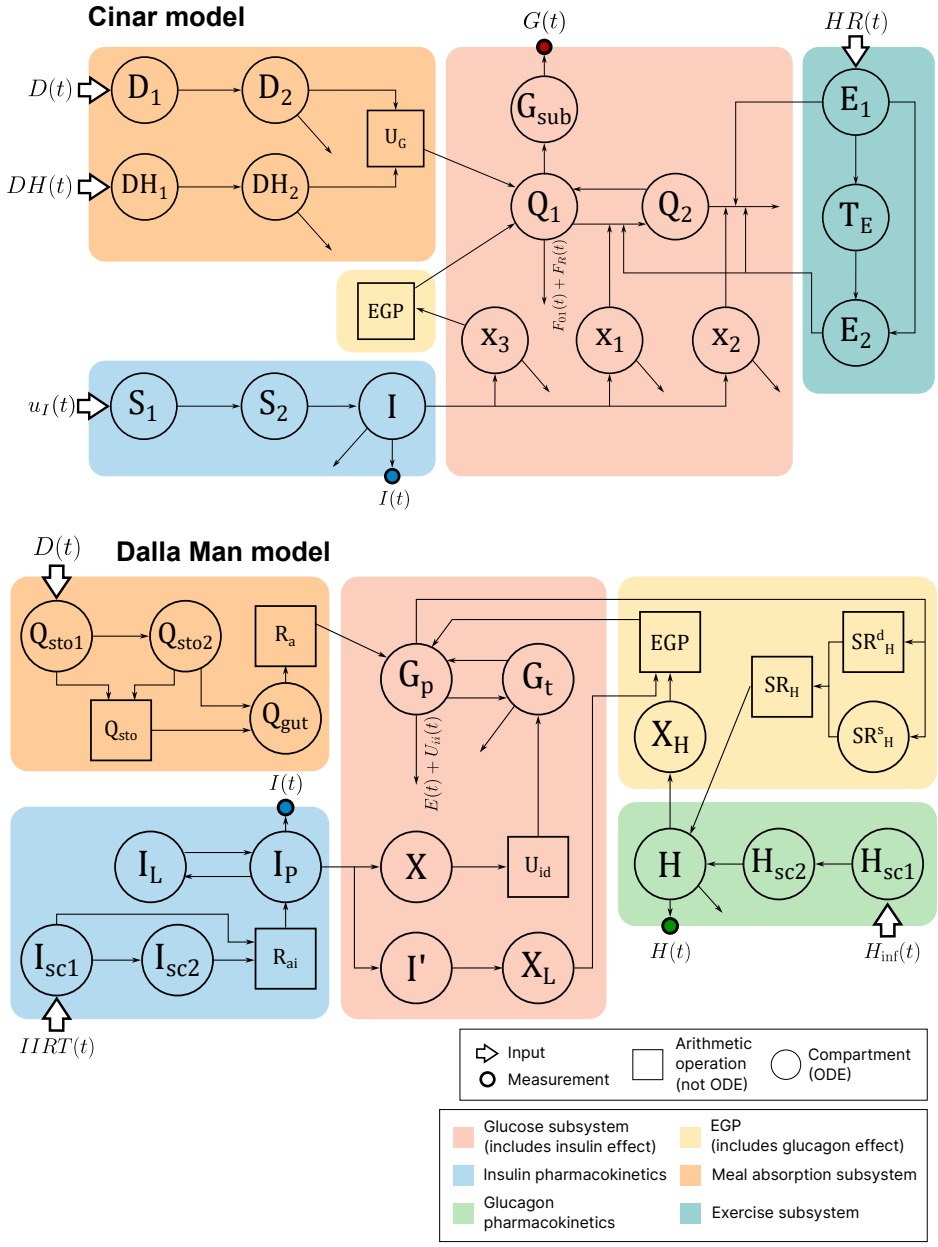

Figure 3.5: Compartmental diagrams of the Cinar model (Rashid et al., 2019) and the Dalla Man model (Dalla Man et al., 2014).

Haidar model

Haidar and colleagues have also proposed a model (Smaoui et al., 2020a) based on the Hovorka model that has been expanded over successive works. The insulin PK subsystem consists of two parallel chains (slow and fast channels) and an additional compartment for plasma concentration, proposed initially in Haidar et al. (2013c). In this same work, a meal model is included with two parallel channels to describe glucose absorption. Glucagon kinetics are taken from Haidar et al. (2013a), where a more simple two-chain compartment was validated both for insulin and glucagon PK. Nevertheless, the insulin subsystem was later modified.

The same authors carried out a work evaluating different definitions for EGP, testing different relationships and interactions between insulin and glucagon. They came up with a proposal based on the model that provided the lowest error. However, the EGP presented in Smaoui et al. (2020a) corresponds to a different, simpler proposal. More details on the EGP definitions will be given in Section 3.3.

Both the glucose dynamics and the glucose appearance rate in this model incorporate time-varying functions ($f_g(t)$, $f_m(t)$) to introduce variability and flexibility in the model dynamics, trying to replicate the variability between subjects.

A development platform has been implemented with this model named *Ulna*, described in Smaoui et al. (2020b). The model is detailed in Table B.6.

Kanderian - IVP model

The *Identifiable Virtual Patient Model* (IVP) model is one of the most used models in control applications. The IVP model was developed to aid the development of Medtronic's CL algorithm (Kanderian et al., 2012). It assembles information from three different previous works.

Their insulin PK subsystem is reported to belong to Sherwin and colleagues, who worked on proposing an insulin kinetics model (Insel et al., 1974). The model consists of a two-compartment chain, including an additional compartment to account for insulin effect ($I_{EFF}(t)$). Glucose dynamics are based on Bergman's minimal model, and the meal model is from Hovorka (Wilinska et al., 2010). A compartment was added to represent the subcutaneous interstitial fluid ($G_{ISF}(t)$) and account for the glucose sensor reading delays. See Table B.9 for more detail.

Cinar model

The group led by Ali Cinar, which has a trajectory studying exercise in T1D, presented an extension of the Hovorka model that included exercise (Rashid et al., 2019). The *multivariable Glucose-Insulin-Physiological Variable Simulator* (mGIPsim) also has the peculiarity that includes additional "measured" variables, that is, HR, energy expenditure (EE), skin temperature (ST), and accelerometer readings, that complement glucose concentration measurements.

The HR is computed through a physiological model as a function of the exercise intensity. Another model computes the mechanical work rate from the exercise intensity information and translates it to energy expenditure through a first-order filter. The skin temperature is obtained with a partial differential equation that relates the core body temperature to skin temperature dynamics.

The insulin PK model and insulin effect equations are based on Hovorka's model. The glucose absorption subsystem includes two subsystems: one for regular meals and another for rescue carbohydrates. Both subsystems present the same two-compartment structures, but the latter has a much faster absorption rate. Glucose dynamics are also based on the Hovorka model, with introduced modifications to account for the exercise effect. The exercise model, which takes the HR signal as input, was proposed in Svendby (2016). It consists of three states that describe the immediate effect of physical activity on glucose ($E_1(t)$), a characteristic time to represent the differing long-lasting effects of exercise ($T_E(t)$), and the nonlinear prolonged effect of physical activity ($E_2(t)$).

An implementation of the simulator in Matlab is available upon request to the authors. More details can be found in Table B.11. The skin temperature model has not been included in the table details since it falls out of the scope of this work.

3.2.3 Dalla Man model - UVA/Padova simulator

The UVA/Padova simulator, containing the Dalla Man model, is the most well-known simulator for glucose dynamics in T1D since it is the only one currently accepted by the FDA as a substitute to pre-clinical trials of AP systems since 2008 (version S2008) (Kovatchev et al., 2009). The model has had a long trajectory, with different subsystems being added, improved, and updated over the years. The first development of the Dalla Man model is reported in Dalla Man et al. (2006), where the authors modeled the glucose absorption as a response to a meal, validated with healthy people data. The (for now) final version of the model consists of almost 20 ODEs that include PK subsystems of insulin

and glucagon and their effects, oral glucose absorption, and glucose dynamics.

The insulin and glucagon PK both consist of two-compartment chains before reaching their respective plasma compartments. The EGP signal considers independent contributions of insulin and glucagon with opposite effects on glucose. The glucose subsystem considers two compartments: plasma glucose and glucose measured in tissues. Lastly, the meal model defines two compartments to model the initial glucose absorption in the stomach, and the rate of glucose appearance is a function of the mass of glucose in the gut. The input term to the gut compartment is a function of the stomach's rate of gastric emptying.

Some curiosities about the model: the glucagon subsystem does not only contemplate the dynamics of the externally administered glucagon, but it also accounts for its internal secretion. This subsystem was introduced in Dalla Man et al. (2014) (S2013 version). The model also includes a subsystem focused on glucose utilization during hypoglycemia. The authors refer to an increased effect of insulin action observed when glucose decreases under a specific threshold. In order to account for this effect, a *risk* function is defined as a piecewise function that increases insulin-dependent glucose utilization, making glucose to drop more rapidly in hypoglycemia (Kovatchev et al., 1999). The most recent version, published in Visentin et al. (2018) (S2017 version), allows simulating not just one meal but a complete day, and introduces variability in the insulin sensitivity (varying parameters k_{p3} and V_{mx}).

The software includes 300 virtual patients (100 adults, 100 adolescents, and 100 children). An "academic" version of the simulator was available for third-party use some years ago that included 30 virtual patients (10 in each age group). Nowadays, many researchers still use this version to present their validations of their proposed control algorithms for AP systems. Moreover, some open source projects offer an implementation of the model with the parameters of the open version, such as Xie (2018), that provides a Python implementation of the UVA/Padova simulator.

Table B.5 includes a description of the model states and parameters. Although the latest version of the model includes subsystems for intradermal and inhaled insulin PK, they have been left out for simplicity.

As a summary of this section, Figure 3.6 presents a diagram simplifying the relationships between the models mentioned here. Models are labeled as the first author's name and the year of publication, which correspond to the bibliographic references presented throughout this section. References surrounded by a gray box correspond to the models selected for the diagrams presented before, and their name is indicated in bold.

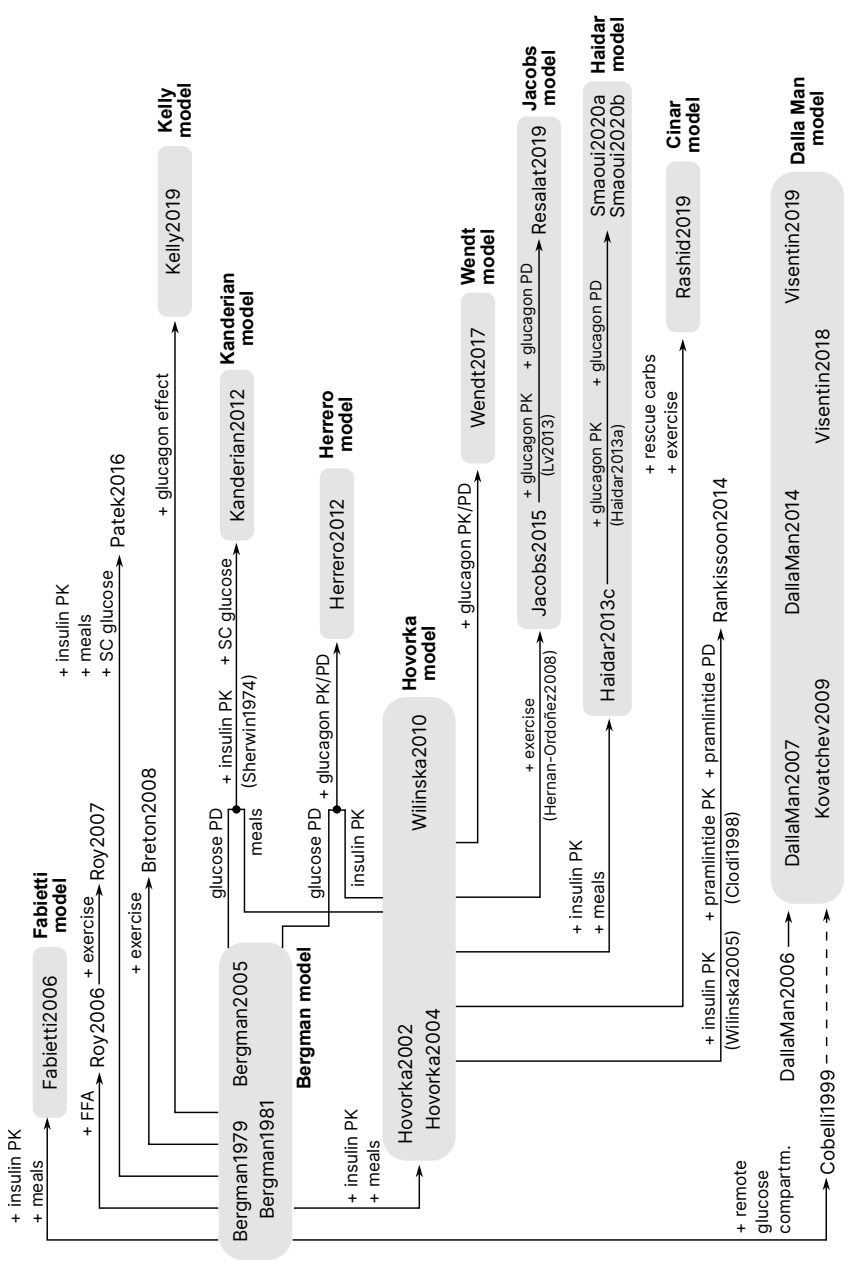

Figure 3.6: Overview of the relationships between the T1D models presented in this section. Models' labels correspond to the first author of the paper where they were presented and the year of publication. The contributions of each extension are indicated preceeded by a + sign on each of the arrows.

Some models might be the results of more than one work, which is why some of the boxes include more than one reference. Arrows link each "base" model to their extensions. A text preceded by a plus sign (+) on top of the arrow indicates the main addition or contribution of the result model. Some of these contributions also have a reference underneath between brackets if they were based on a specific work. In the case of the Kanderian model and the Herrero model, they are both based on the Bergman model and the Hovorka model, so the text on the line indicates which aspect, in particular, was used for their development. The dashed line between the model in "Cobelli1999" and the Dalla Man model block represents that was not the only work to influence the development of the Dalla Man model. There were many others that have not been included in this qualitative analysis.

3.2.4 Other models

The model by Liu and Tang (2008) models the glucoregulatory system with the peculiarity of describing insulin and glucagon intracellular concentration based on their receptors binding. Their proposal for this effect is a simplification of the detailed model proposed for insulin binding presented in Sedaghat et al. (2002). Liu's work proposes an eight-compartment system, where three of them describe insulin plasma concentration, insulin intracellular concentration, and the concentration of insulin-bound receptors, respectively. The same structure is replicated for glucagon. The two remaining compartments are devoted to the glycogen concentration and glucose blood concentration. The effect of meals is not modeled but included as a disturbance input.

Lehmann and Deutsch (1992) present a glucoregulatory model based on the glucose PD model described in Guyton et al. (1978), and the insulin PK proposed in Berger and Rodbard (1989). Their model includes insulin kinetics and follows its trajectory from plasma absorption to an insulin *active* pool. The other two ODEs in the system describe glucose dynamics and the amount of glucose in the gut after a meal. The model was implemented in the AIDA (*An interactive diabetes advisor*) platform (Lehmann et al., 1994), which was conceived as a decision support system for clinicians. An extension of the model incorporated insulin kinetics models to describe long-acting insulin analogs (Lehmann et al., 2007).

Other proposals present more complex models that aim to include more detailed metabolic processes. Such is the case of the work in Neelakanta (2006). They model the glucoregulatory system, including the kinetics of exogenous insulin administration. The glucose subsystem considers the effect of glucose uptake by the skeleton, muscles, cells,

kidneys, and liver. Likewise, it considers liver glucose production. The second available input to their system is glucose exogenous administration, either in the form of intravenous infusion or oral ingestion. A glucagon subsystem is included that accounts for glucagon concentration in plasma and interstitial fluid, but only the endogenous production is considered. The system consists of 7 differential equations. However, the contributions to each term in the glucose dynamics equation are modeled as nonlinear relationships using Bernoulli-Langevin functions (Neelakanta et al., 1991).

One of the most relevant models in the diabetes literature is the Sorensen model (Sorensen, 1985). This model was designed to simulate the normal glucose regulation process and was then adapted to the dynamics observed in people with T1D. The model is divided into six physiological sections: brain, heart and lungs, periphery (which includes skeletal muscle and adipose tissue), gut, liver, and kidney. As an overview, the glucose source in the model is the hepatic glucose production, and its destinations include red blood cell uptake, brain uptake, gut uptake, peripheral uptake, hepatic uptake, and urinary excretion. Each of the blocks also includes insulin effect, whose source is the pancreatic insulin release, and it has an effect (sinks) in the liver, kidneys, and peripheral clearance. The described metabolic processes for glucagon only consist of one compartment, considering pancreatic glucagon release and plasma clearance. The complete model is composed of 19 states.

The Sorensen model was later extended to include a physiology-based PK model for glucose, insulin, and glucagon in Schaller (2014); Schaller et al. (2013). The insulin and glucagon subcutaneous absorption subsystems consisted of two compartments each and were adapted from Tarín et al. (2005).

Nevertheless, there are several models in the literature that describe glucose dynamics, all with their own contributions, but not all can be included here. The review presented in Rathee and Nilam (2017) provides an overview of ODE-based models in the literature used to describe T1D glucose dynamics, providing an analysis of each of their main results and limitations. The work in Cobelli and Dalla Man (2022) also reviews the literature glucose models, separating minimal and maximal approaches. The maximal model analysis focuses on their own proposal, the UVA/Padova T1D simulator, whereas the minimal models' analysis presents approaches to modeling different specific relations, such as a glucose minimal model, C-peptide minimal model, as well as an analysis of insulin action based on the information provided by tracer studies.

Other works have focused on analyzing the simulation differences of some of the aforementioned proposals. For instance, the work in Steil et al. (2005) compares the output magnitudes provided by Bergman's Minimal model, the AIDA model, and the

Sorensen model since they model glucose uptake based on different assumptions. They conclude that, even if the direct comparison of models is not trivial, given the systematic differences in each model and the wide variation in form and detail, significant differences are observed in the glucose response behavior among the three selected models. Still, the three of them provide a stable steady-state response in glucose following a basal change in insulin, making them suitable candidates to be used as base in the development of CL algorithms. This analysis was carried out prior to the development and publication of the UVA/Padova simulator. Later on, a similar (in concept) work by Colmegna and Sánchez Peña (2014) compared the Dalla Man model (the S2008 version), along with Hovorka's and the Sorensen model. A shared limitation of the three models is that none of them considers both inter and intra-patient variability. Only the Sorensen model considers the glucagon effect, but none of the versions account for its administration either. The three of them have received eventual extensions that consider glucagon: the S2013 version of the UVA/Padova simulator, the Schaller extensions of the Sorensen model, and multiple works based on Hovorka's model (e.g., Wendt, Haidar or Jacobs model).

3.3 Glucagon effect definitions

This section focuses on how glucagon effect is usually represented in the literature. Glucagon becomes effective through the terms in the model that comprise glycogenesis and gluconeogenesis (i.e., glucose production in the liver). Based on the overview of models presented in the previous sections, the glucagon effect is usually a part of the EGP(t) signal in the Hovorka-based models, or it replicates insulin mechanics in the Bergman-based models, including a remote compartment to account for glucagon effect prior being incorporated into the plasma glucose compartment.

Definitions of EGP are diverse. Models typically consider at least a constant value for hepatic glucose production (usually labeled EGP_0), and it might be influenced by some amount of circulating insulin (x_i):

$$EGP(t) = EGP_0 \left(1 - x_i(t)\right)$$

Most models that include glucagon use this term as a base to add the contribution of exogenous glucagon. One of the simplest considerations consists of considering insulin and glucagon effects independent, such as in the case of the Jacobs model (Resalat et al., 2019), the Dalla Man model (Dalla Man et al., 2014), the Herrero model (Herrero et al., 2013), or the Kelly model (Kelly et al., 2019).

The Jacobs model defines EGP as:

$$EGP(t) = EGP_0(1 - X_3(t) + Y(t) + k_{g3}Z(t)),$$

where $X_3(t)$ is the effect of insulin concentration on EGP, $Y(t)$ is the effect of glucagon on EGP, and $Z(t)$ is an extra signal representing the derivative of $Y(t)$.

The EGP definition in the Dalla Man model,

$$EGP(t) = k_{p1} - k_{p2}G_p(t) - k_{p3}X_L(t) + \xi X_H(t),$$

includes plasma glucose mass ($G_p(t)$), the delayed insulin action in the liver ($X_L(t)$), and the delayed glucagon action on EGP ($X_H(t)$).

The Herrero model does not provide a explicit definition of EGP, but the effects of insulin and glucagon on glucose are expressed in the equation for glucose ($G(t)$) dynamics as:

$$\dot{G}(t) = -\left(S_G + X(t) - Y(t)\right)G(t) + S_G G_b + \frac{R_a(t)}{V}$$

where insulin action ($X(t)$) and glucagon action ($Y(t)$), present an additive relationship between them.

The same relationship is used in the Kelly model, which was also based on the Bergman model (Bergman et al., 1981), where insulin effect ($X(t)$) and glucagon effect ($Y(t)$) influence glucose such that:

$$\dot{G}(t) = -p_1\left(G(t) - G_b\right) + \left(Y(t) - X(t)\right)G(t) + G_{inf}(t)$$

On the other hand, other definitions consider a potential interference between insulin and glucagon (beyond the balance in the above equations). For instance, the work by Haidar and colleagues in Emami et al. (2017) proposes an EGP definition based on the identification of a set of clinical data from El Youssef et al. (2014). This work showed in a clamp study that high circulating levels of insulin could blunt glucagon response. The EGP proposal in Emami's work was defined as follows:

$$EGP(t) = \mathcal{H}\left(1 - S \cdot X(t)\right) \cdot \mathcal{H}\left(EGP_{Gluc(t)} + T \cdot Gluc(t)\right) + G_{ng}$$
$$\dot{EGP}_{Gluc(t)} = -k_{Gd} \cdot EGP_{Gluc(t)} - k_{Gd}T_{Gd} \cdot \left(\frac{\mathrm{d}Gluc(t)}{\mathrm{d}t}\right)$$

Notice how insulin effect ($X(t)$) and glucagon ($Gluc(t)$) have a nonlinear relationship in this model, and it also incorporates a term ($EGP_{Gluc(t)}$) that depends on the derivative of glucagon concentration. The function $\mathcal{H}$ represents a unit step function intended to keep the expression positive. This was the model proposal that provided the best fit results among nine different candidate model structures. Note that it is a different definition from the one used in the simulator by the same authors (Smaoui et al., 2020a), where the authors opted for a much simpler expression, although they maintained the multiplicative relationship between insulin effect and plasma glucagon ($x_3(t)$ and $C_p(t)$):

$$EGP(t) = C_p(t)S_g\left(1 - x_3(t)S_e\right)$$

Another model considering an interaction between both hormones is the Wendt model:

$$EGP(t) = \frac{1 - S_e x_3(t)}{1 - S_e I_b}\left((E_{max} - G_{GNG})\frac{C(t)}{C_{E50} + C(t)}\right) + G_{GNG}$$

In this case, a Michaelis-Menten[2] structure is used to bound glucagon ($C(t)$) effect and limit its maximum value depending on insulin ($x_3(t)$).

The parameters and state variables of the models listed in this subsection are described in Appendix B.

A more physiology-based glucagon action model was proposed in Hinshaw et al. (2015), in which the proposed EGP definition includes the processes of glycogenolysis and gluconeogenesis, based on the dephosphorylation of glucose-6-phosphate (see Section 4.2).

[2]The Michaelis-Menten equation is used to describe kinetics of substances that are bound over time. It is a widely-used structure to describe the behavior of biological processes since its development by Leonor Michaelis and Maud Menten in 1913 (Cornish-Bowden, 2015).

$$
\begin{aligned}
EGP(t) =& a \cdot G6P \\
\dot{G6P} =& -a \cdot G6P + Glys + Gng \\
Glys =& \begin{cases} [Glys_b + b \cdot (Gn - G_{th})] \cdot E & \text{if} \quad G_n \geq G_{th} \\ Glys_b \cdot E & \text{if} \quad G_n \leq G_{th} \end{cases} \\
E =& \frac{1}{2} \cdot \left[1 - \tanh\left(\frac{t = t_0}{\tau} \right) \right] \\
Gng =& \begin{cases} Gng_b + XGn & \text{in hypoglycemia} \\ Gng_b + OF & \text{in normoglycemia} \end{cases}
\end{aligned}
$$

Some effects are modulated by the term E, which accounts for the "evanescence" effect observed in glucagon (i.e., the hormone effect tends to decrease with time). The definition of glycogenolysis ($Glys$) depends on the glucagon concentration (Gn) when it reaches a specific threshold (G_{th}); otherwise, its value is constant. On the other hand, gluconeogenesis is a function of XGn, which comprises a chain of compartments representing delays with respect to the plasma glucagon concentration as input. The term OF represents "other factors" that might stimulate gluconeogenesis during normoglycemia. Note that this EGP definition focuses on glucagon only and does not consider insulin influence.

A research group from the Norwegian University of Science and Technology has directed many efforts into the concept of the intraperitoneal dual hormone AP, conducting trials on animal models, including the work of a recent PhD thesis (Teigen, 2023). The work in Benam et al. (2023) presents their glucoregulatory model, which considers intraperitoneal delivery of both insulin and glucagon. They account for the glucagon effect on plasma glucose through a term representing hepatic glucose production (HGP), defined as:

$$
HGP \triangleq k_{g_1} E_{h,l} \sqrt{\xi} \cdot \exp\left(-k_{\xi_0} \cdot E_{i,l}\right)
$$

In this expression, $E_{h,l}$ and $E_{i,l}$ represent the effective glucagon and insulin rates in the liver. As a novelty, the term ξ represents the glycogen store levels (expressed as a percentage). It is assumed that some amount of glucose is stored as glycogen, which increases glycogen stores, defining ξ as:

$$
\dot{\xi} = k_{\xi_1} E_{i,l} G - k_{\xi_2} E_{h,l} f\left(\xi, E_{i,l}\right)
$$

This is the only model included in this analysis that accounts for the influence of glycogen reserves on the glucagon effect. However, the model has only been validated using data from non-diabetic pigs.

3.4 Pramlintide models

As presented in the previous sections, glucoregulatory models (glucose-insulin) and glucagon models have had a long trajectory. A solid foundation has been built over the years that has allowed the development of new proposals and models that progressively complement the understanding of the regulation process and the interactions among hormones. However, pramlintide has fallen out of the T1D modeling scope. Even if its use along AP systems is fairly recent (see Section 2.3.3), pramlintide use is not new. However, there is a lack of mathematical models that describe its dynamics, and the four proposals detailed in this section are the only ones present in the literature.

3.4.1 Clodi model

The first pramlintide model proposal that can be found in the literature is the work of Clodi et al. (1998). This work proposes an intravenous pramlintide kinetics model that uses three compartments to represent pramlintide distribution along different pools after entering the plasma compartment. Figure 3.7 presents a schematic of the model.

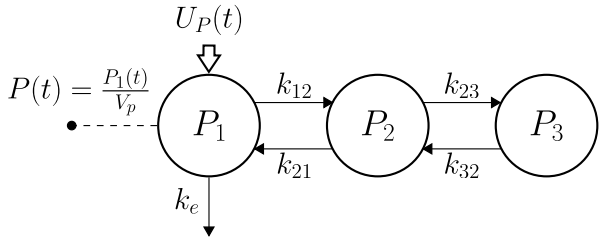

Figure 3.7: Pramlintide PK model structure proposed in Clodi et al. (1998). $U_P(t)$ represents the intravenous pramlintide input. $P(t)$ is the pramlintide concentration measurement. P_i are each of the successive compartments of the model. k_{ij} represent the transfer rates from compartment i to j. k_e is the excretion rate from the plasma compartment.

3.4.2 Fang model

The first model describing pramlintide PD was the work by Fang et al. (2013). They validate the model using a dataset from Colburn et al. (1996), where different intravenous pramlintide doses were administered. Fang proposes a non-compartmental model to describe pramlintide kinetics and pramlintide development is based on an indirect response (IDR) model[3]. Hence, the authors delay the appearance of glucose in plasma from the intestine in a dose-independent manner, modifying their T_{max} parameter.

$$\frac{\mathrm{d}Int}{\mathrm{d}t} = k_0 \left(-T_{in} \times S\right) - k_a \times Int \tag{3.3a}$$

$$k_0 = \frac{D \times F}{T_{in} \times S} \tag{3.3b}$$

$$\frac{\mathrm{d}G_c}{\mathrm{d}t} = k_{in} \times I + k_a \times Int - k_{out} \times G_c + \frac{Q_G}{V_{Gp}} \times G_p - \frac{Q_G}{VGp} \times G_c \tag{3.3c}$$

$$\frac{\mathrm{d}G_p}{\mathrm{d}t} = \frac{Q_G}{VGp} \times G_c - \frac{Q_G}{V_{Gp}} \times G_p \tag{3.3d}$$

Equations (3.3) are reproduced as reported in Fang et al. (2013). $Int(t)$ is the amount of glucose in the intestine, $G_c(t)$ is glucose central compartment and $G_p(t)$ is the amount of glucose in the peripheral compartment. Pramlintide has an effect inhibiting k_{in} and prolonging the glucose input by modifying k_0. Parameter D in Equation (3.3c) represents the glucose input, F is the glucose bioavailability, and T_{in} is the duration of the glucose input. For more details on the model operation, the reader is referred to the original work.

3.4.3 Ramkissoon model

The other pramlintide PD model in the literature was presented in Ramkissoon et al. (2014). A complete insulin-pramlintide-glucose PK/PD model is set up based on the glucoregulatory model by Hovorka. The authors substituted the insulin PK subsystem by the proposal in Wilinska et al. (2005) instead of the simpler subsystem usually associated with the Hovorka model. To account for pramlintide PK, they use the system proposed in Clodi et al. (1998), mentioned above, for pramlintide intravenous kinetics (Plasma$_P$, P_2, P_3). An extra compartment is added to represent subcutaneous PK (SQ_p). Hence, the complete pramlintide PK subsystem is described as:

[3] IDR models describe those physiological systems where a certain drug inhibits or stimulates production, synthesis, secretion, or removal of a variable, usually with a delay (Sharma and Jusko, 1998).

$$\frac{\mathrm{d}SQ_p}{\mathrm{d}t} = u_{Pram} - kSQ_pSQ_p \tag{3.4a}$$

$$\frac{\mathrm{d}\text{Plasma}_P}{\mathrm{d}t} = kSQ_pSQ_p - (k_{ep} + k_{p21})\,\text{Plasma}_P + k_{p12}P_2 \tag{3.4b}$$

$$\frac{\mathrm{d}P_2}{\mathrm{d}t} = k_{p21}\text{Plasma}_P - (k_{p12} + k_{p32})\,P_2 + k_{p23}P_3 \tag{3.4c}$$

$$\frac{\mathrm{d}P_3}{\mathrm{d}t} = k_{p32}P_2 - k_{p23}P_3 \tag{3.4d}$$

$$P = \frac{\text{Plasma}_P}{V_P} \tag{3.4e}$$

The input to the system is represented as u_{Pram}. The constants k_{pij} represent the rates between compartments (i to j), and P is the plasma pramlintide concentration, measured in the Plasma$_P$ compartment.

Their proposed PD model effect is based on modifying the meal peak absorption time (t_{max}) in the equation describing the oral absorption of glucose (U_G, see Equation 3.2). The PD subsystem is constituted as:

$$P_{eff}(t) = \begin{cases} 0 & 0 \le t \le p_\theta \\ P(t - p_\theta) & t > p_\theta \end{cases} \tag{3.5a}$$

$$t_{\max,G,\text{new}} = t_{\max,G,\text{old}}\left(1 + k_{\text{lag}}\left(P_{\text{eff}}(t)\right)\right) \tag{3.5b}$$

$$Gap = \int_0^{t_{sw}} \frac{D_G A_G\,(t - n_\theta)\,e^{-\frac{(t-n_\theta)}{t_{\max,G,\text{old}}}}}{t^2_{\max,G,\text{old}}} - \int_0^{t_{sw}} \frac{D_G A_G\,(t - n_\theta)\,e^{-\frac{(t-n_\theta)}{t_{\max,,\text{new}}}}}{t^2_{\max,G,\text{new}}} \tag{3.5c}$$

The value P_{eff} represents the effective pramlintide concentration after the displacement of pramlintide from the administration site to its effective site, delayed by p_θ. The delay in the meal observed in the presence of pramlintide is represented as n_θ. The value t_{sw} is the time at which $t > n_\theta$ and P_{eff} raises over a certain threshold ($P_{eff} > P_{min}$). The time constant $t_{\max,G,\text{new}}$ is the peak meal absorption time at the current instant, whereas $t_{\max,G,\text{old}}$ refers to the previous time point. k_{lag} is a lag constant that acts in the presence of pramlintide. Then, U_G is modified such that:

$$U_G = \begin{cases} \frac{(D_G A_G - Gap)(t-n_\theta)e^{-\frac{(t-n_\theta)}{t_{\max,G}}}}{t_{\max,G}^2} & t > n_\theta \text{ and } P_{\text{eff}} > P_{\min} \\ \frac{D_G A_G t e^{-\frac{t}{t_{\max,G}}}}{t_{\max,G}^2} & 0 \leq t \leq n_\theta \text{ and } P_{\text{eff}} \leq P_{\min} \end{cases} \tag{3.6}$$

This model was then validated using a collection of clinical data gathered from the literature. Hence, average values were used as a reference.

3.4.4 Pramlintide effect in the UVA/Padova simulator

The work by Micheletto et al. (2013) introduced the pramlintide effect on the UVA/Padova simulator. Based on the clinical data presented in Woerle et al. (2008), the glucose rate of appearance was modified to delay its effect.

However, according to the paper, the parameters of the model were re-identified to accommodate the new dynamics, and no PK model is proposed to describe the appearance of pramlintide in plasma, nor is a PD model to explain how the concentration of pramlintide modulates gastric emptying. Nevertheless, they report dose-dependent results in the paper.

3.5 Conclusions

This chapter has presented some of the glucoregulatory models devoted to T1D present in the literature. Some relevant points can be highlighted in each one of the main sections.

Models devoted to glucose regulation have a long history, and, as with many scientific developments, they are usually built based on previous knowledge, improving certain aspects or extending them with new submodels that broaden their capabilities. Figure 3.6 helps to get a general perception of this kind of development, even if the models included in this chapter's analysis are just a sample of the works found in the literature.

Glucagon is not often considered in glucoregulatory models or is only considered in later developments. Given the nature of this thesis, there was an emphasis on models that included glucagon, but most works usually consider just the insulin-glucose relationship. Section 3.3 has offered an overview of the most common ways to incorporate the glucagon effect into the glucoregulatory models. Given the close relationship between pancreatic hormones, as seen in Chapter 2, it would make sense to consider some kind of interaction

between insulin and glucagon effects. However, most definitions consider their contributions independent of one another. On the other hand, the definitions that deviate from this norm are diverse, as seen in the presented examples.

Pramlintide models lie on opposite sides of the spectrum, with very few PK/PD models in existence. Moreover, defining the PK of pramlintide might be complex, especially if future therapies are going to use the co-formulation of insulin and pramlintide. New clinical data reporting the PK/PD effects of the drug will be needed to propose a reliable simulation model.

Part II

Glucagon

Chapter 4

EGP based on glucagon receptor dynamics

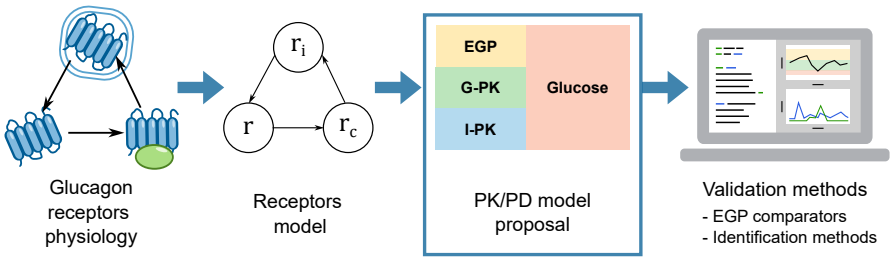

This chapter presents the mechanisms of receptors in general and glucagon receptors in particular. Given a precedent model that described the glucagon receptors lifecyle, a complete PK/PD model is proposed to be used for describing glucagon dynamics in Type 1 Diabetes. The last sections of the chapter present the validation tools that will be used in the subsequent chapters to validate the proposal: EGP models from the literature that will be used for comparison and the identification methods followed.

4.1 Introduction

Accurate mathematical models are a keystone in AP development. Not only for model-based control algorithms but especially to define T1D simulators to perform *in silico* evaluations of the controllers. Models of the glucagon effect are needed for controllers designed for therapies that combine insulin and glucagon administration. However, glucagon models in the literature are diverse, and the community has not reached a consensus about the most appropriate way to describe the effect of glucagon on glucose. This thesis aims to explore the possibility of a more physiologically-accurate glucagon model that is still not too complex and is identifiable using glucose data.

This chapter provides an overview of glucagon receptors in order to gather some insight into their mechanisms and lifecycle. Receptors are cellular components that bind to hormones in plasma, triggering a chain of effects. Glucagon receptors, in particular, are responsible for activating glycogenolysis and gluconeogenesis processes as a reaction to plasma glucagon binding. Then, the model proposed in this work is presented, introducing in first place the models from the literature used as the base for the glucagon receptor dynamics and as the baseline glucoregulatory model. The complete pharmacokinetics and pharmacodynamics (PK/PD) model is validated in the following chapters, identifying the models' parameters based on clinical data. The last section of this chapter presents the tools that will be used to validate the model: endogenous glucose production (EGP) models from the literature that serve as comparators, and the general identification procedures and software used.

4.2 Glucagon receptors

A receptor is a cellular component capable of recognizing and binding to a particular hormone. Binding is a fast and usually reversible process that triggers a chain of events, leading to a biological response that spans from activation or inhibition of enzymes to protein synthesis or membrane effects (Ronald Kahn, 1976).

Receptors are located on the plasma membranes of cells, and after activation, they are transported to endosomes through an internalization process (Koenig, 2004). In this internalized stage, most receptors are then recycled back to the cell surface, but some are sent to lysosomes for degradation in a process called sequestration (Yu et al., 1993). Afterward, new receptors can be synthesized and added to the cell membrane. This lifecycle is summarized in Figure 4.1.

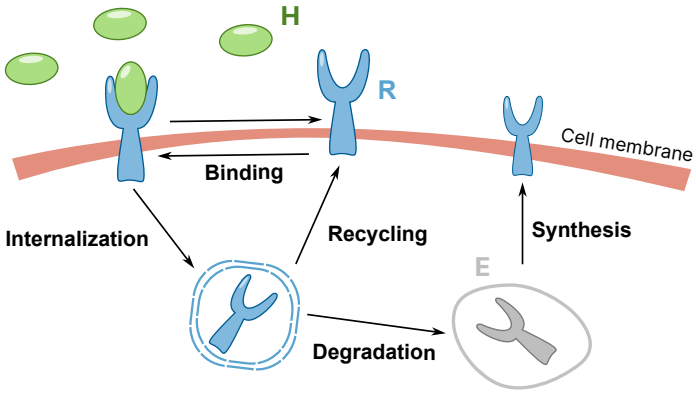

Figure 4.1: Receptors trafficking diagram. Receptors (R) on the cell membrane, bind to the hormone (H) in plasma. Afterwards they become internalized either to recycle back to the surface, or to degrade on the endosomes (E). New receptors can be synthesized to the cell surface.

Due to the synthesis and degradation processes, the receptors' concentration is not constant. In fact, some studies have observed that the amount of receptors is inversely proportional to the concentration of the corresponding hormone. For instance, studies performed on insulin-deficient mice showed an increase of insulin receptors on the cell membrane, whereas hyperinsulinemic insulin-resistant mice showed a decrease (Hepp et al., 1975). However, variations in the number of receptors are a consequence of a chronic state or conditions prolonged in time (i.e., several hours). This phenomenon is reported in Gavin et al. (1974), Kahn et al. (1973), and Goldfine (1975), among others. These variations are a mechanism for the cell to regulate the sensitivity to the hormone (i.e., the more abundant receptors are, the higher the sensitivity). Hence, if a high hormone concentration is maintained for a long time, the cell will regulate the number of receptors as a defense mechanism. Likewise, the studies mentioned above also prove that a prolonged subnormal concentration will increase the number of receptors. However, an acute short-timed variation in plasma hormone concentration will not affect the number of receptors (Kahn et al., 1973).

Receptors are also the mediators for the glucagon effect. Glucagon receptors (GRs) belong to the family of G protein-coupled receptors (GPCRs). These receptors' primary purpose is to transmit information from the environment to the interior of the cell, being a key component of intercellular signaling and regulation processes (Böhm et al., 1997). GRs are mainly found on the liver cell membrane. However, they can also be found in small

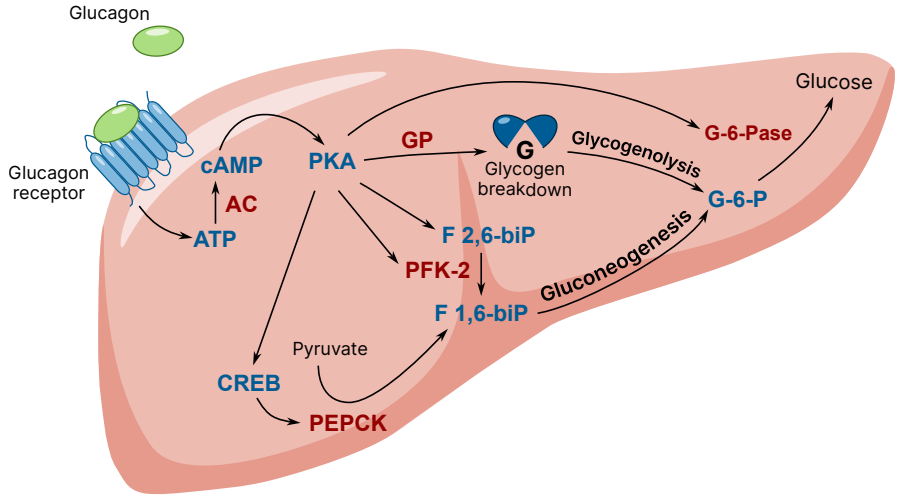

Figure 4.2: Regulation of glycogenolysis and gluconeogenesis in the liver after glucagon binding to its receptors. Acronyms in red represent enzymes catalyzing reactions and initials in blue represent other proteins or compounds. Receptors on the liver surface cell membrane bind to glucagon in plasma, activating AC, which results in PKA production and opens several pathways to promote glycogenolysis and gluconeogenesis. Initials' meanings and descriptions are listed in Table 4.1.

amounts in the kidney, adipose tissue, lymphoblasts, spleen, pancreas, brain, adrenal gland, and the gastrointestinal tract (Svoboda et al., 1994). Glucagon binding to its receptors in the liver has a direct effect of promoting glycogenolysis and gluconeogenesis (see Section 2.1) and, as other peptide hormones' receptors, they undergo the aforementioned processes of binding, internalization, and recycling.

The work by Krilov et al. (2008) analyzed glucagon receptors specifically, focusing on their internalization process in several *in vitro* experiments. Experiments performed on transfected[1] human cells showed that 30-40% of glucagon receptors had internalized after 30 minutes of treatment with $\sim$350 μg of glucagon. Thirty minutes after the removal of glucagon, 70% of internalized receptors had recycled back to the cell membrane, and nearly 100% had recovered after 60 minutes. This short stimulation with glucagon did not impact the concentration of receptors, and the authors report that more prolonged exposure to the hormone (3 hours) was necessary to observe degradation in the level

[1]Transfection is a gene transfer technology that introduces foreign DNA into cultured cells to produce genetically modified cells. It allows to study the gene function and protein expression in a cellular environment (Kim and Eberwine, 2010).

Symbol	Name	Description
ATP	adenosite triphosphate	Energy source for molecules. Mainly synthesized from carbohydrates and fats (Salway, 1993).
PKA	protein kinase A	Family of enzymes which activity depends on cAMP, with several functions, such as regulation of glycogen, sugar, and lipid metabolism. It activates glycogenolysis and inhibits glycogen synthesis (Salway, 1993).
AC	adenyl cyclase	A membrane-bound enzyme that catalyzes the conversion of ATP to cAMP (Ishikawa and Homcy, 1997).
cAMP	cyclic AMP	AMP (adenosine monophosphate) is an intracellular messenger, that activates PKA (Ishikawa and Homcy, 1997).
GP	glycogen phosphorylase	Enzyme catalyzing the glucogenolysis process.
CREB	cAMP-response element-binding	Protein that acts as a transcription factor, involved in numerous metabolic pathways (Wang et al., 2018).
PEPCK	phosphoenolpyruvate carboxykinase	Enzyme whose main role is related to glucose synthesis in gluconeogenesis (Yang et al., 2009).
PFK-2	phosphofructokinase-2	Enzyme that catalyzes formation or degradation of fructose 2,6-biPase (Payne et al., 2005).
G-6-P	Glucose-6-phosphate	Glucose substrate (precursor of glucose) (Müller et al., 2017).
G-6-Pase	Glucose-6-phosphatase	Enzyme that hydrolyses G-6-P to glucose (Van Schaftingen and Gerin, 2002).
F 2,6-biP	Fructose-2,6-bisphosphate	A metabolite that affects glycoslysis and gluconeogenesis processes.
F 1,6-biP	Fructose-1,6-bisphosphate	A type of sugar phosphate based upon fructose, used to store or transfer energy.

Table 4.1: Meanings and descriptions of the main agents involved in glycogenolysis and gluconeogenesis processes after glucagon binding, as depicted in Figure 4.2.

of glucagon receptors, which agrees with the works mentioned earlier. So, according to these studies, a great number of receptors will internalize after a short exposure to the hormone, but they will recycle back to the surface some time later, without affecting the total concentration of receptors.

Glucagon effect on glucose is a consequence of glucagon binding to its receptors. This union triggers a cascade of protein reactions leading to glycogenolysis and gluconeogenesis. Figure 4.2 summarizes the proteins' pathways. Texts in red represent enzymes catalyzing reactions and texts in blue represent other proteins involved in the process. The meanings of the initials used in the figure and the next paragraphs are detailed in Table 4.1.

Glucagon binding activates enzyme AC. This leads to an increase of cAMP, which in turn activates PKA. PKA is one of the key components in glucogenolysis and gluconeogenesis processes, since it opens several pathways to promote both processes.

Glycogenolysis is the result of two possible sequences: (1) the activation of GP, which promotes glycogen breakdown, or (2) the production of glucose-6-phosphate (G-6-P), which is later translated to glucose. This process also inhibits glycolysis.

On the other hand, several pathways lead to gluconeogenesis. (1) PKA enhances the activity and expression of the G-6-Pase. (2) Active PKA removes F 2,6-biP, which increases F 1,6-biP activity, and promotes G-6-Pase, that catalyzes G-6-P to glucose. Second, PKA leads to the phosphorylation of a CREB, which promotes PEPCK. This enzyme stimulates pyruvate conversion into glucose. Third, PKA also inhibits PFK-2, which lowers values of F 2,6-biP, following the same path described in the first point.

The endpoint of both processes is to raise plasma glucose levels, which is the keystone of glucagon action. The triggering element is the binding to the receptors, so it makes sense to include their dynamics in a glucagon action model. Some proposals from the literature have simplified the description of these processes by approximating the relationship between glucagon binding and glucose production by the liver, which is the focus of the next section.

4.3 EGP model proposal

4.3.1 Glucagon receptors model precedent

As presented in Chapter 3, some glucagon effect models existing in the literature try to provide an accurate description of the glucagon receptors' physiology, such as the model by González-Vélez et al. (2012) that focuses on secretion of glucagon model based on Ca^{2+} dynamics. The model proposed by Schaller (2014) is a detailed physiology-focused insulin model that includes glucagon receptor dynamics, considering the PK from interstitial glucagon and defining a system with two differential equations to describe the dynamics between receptors. The PD of glucagon on glucose is defined with a Michaelis-Menten

expression. The model proposed by Liu and Tang (2008) uses parallel structures for insulin and glucagon, proposing two equations to describe the intracellular concentration and the concentration of the respective hormone-bound receptors, respectively. The effect of glucagon is then incorporated into the plasma glucose equation, modulating the maximum value of two Michaelis-Menten terms describing the conversion of glycogen into glucose and glucose into glycogen (see equations (8) and (9) in the paper). On the other hand, Masroor et al. (2019) proposed a three-compartment model to describe the concentration of receptors in each of their main lifecycle stages: available, bound, and internalized. The model defines hepatic glucose production based on the concentration of bound receptors, modulated through a Michaelis-Menten expression. Their model was incorporated into a glucoregulatory model based on the Minimal Model and validated using data from a Glucagon Challenge test. Their work presented an easy-to-follow scalable model (i.e., it was easily implementable into other models since the glucagon effect is localized in the definition of hepatic glucose production). Consequently, it was chosen as the base for our development of an EGP definition to test the capabilities of glucagon receptors dynamics to describe the glucagon effect on people with T1D.

The system of equations for glucagon receptors dynamics, as presented in Masroor's work, is described next:

$$\frac{\mathrm{d}R}{\mathrm{d}t} = -k_{on} \cdot V_h \cdot C(t) \cdot R(t) + k_{off} \cdot RC(t) - k'_{in} \cdot R(t) + k_{rec} \cdot R_i(t) \tag{4.1a}$$

$$\frac{\mathrm{d}RC}{\mathrm{d}t} = k_{on} \cdot V_h \cdot C(t) \cdot R(t) - k_{off} \cdot RC(t) - k_{in} \cdot RC(t) \tag{4.1b}$$

$$\frac{\mathrm{d}R_i}{\mathrm{d}t} = k_{in} \cdot RC(t) + k'_{in} \cdot R(t) - k_{rec} \cdot R_i(t) \tag{4.1c}$$

$R(t)$, $RC(t)$, and $R_i(t)$ represent the number of available, bound, and internalized receptors. The signal $C(t)$ represents the concentration of plasma glucagon, and it affects the rate of activation of receptors. V_h is the volume of the hepatic interstitial space. The constants denoted by k represent the transfer rates between compartments.

Some studies have found that only a small percentage of receptors are actually activated when the binding occurs. Ronald Kahn (1976) reviews a series of works that prove that the maximum effect is achieved when 2-3% of receptors are bound, so the majority of receptors are just in "reserve" (Kono and Barham, 1971; Megyesi et al., 1975). Consequently, it is assumed that the glucagon concentration in plasma does not change even after binding to receptors.

Similarly to the model by Liu and Tang (2008), synthesis and degradation are considered equal, assuming that the total number of receptors remains constant. Since the data

used for validation both in Masroor et al. (2019) and Liu and Tang's work do not expose receptors to long periods of high glucagon concentrations, there should be no alteration to the concentration of receptors. Hence, the total number of receptors remains constant, which leads to considering the following relationship: $R(t) + RC(t) + R_i(t) = R_{tot}$.

With this premise, two modifications are performed on the system in Equation (4.1). First, the signal of the number of receptors in each state is substituted by a unitless concentration value $(r(t))$, equal to the corresponding number of receptors over the total receptors (R/R^{tot}):

$$r(t) = R(t)/R_{tot}, \quad r_c(t) = RC(t)/R_{tot}, \quad r_i(t) = R_i(t)/R_{tot}$$

Second, since the number of receptors remains constant, the three states can be simplified into two so that the system becomes:

$$\begin{aligned} \frac{\mathrm{d}r(t)}{\mathrm{d}t} &= -k_{on} \cdot V_h \cdot C(t) \cdot r(t) + k_{off} \cdot r_c(t) - k'_{in} \cdot r(t) \\ &\quad + k_{rec}\,(1 - r(t) - r_c(t)) \qquad (4.2a) \\ \frac{\mathrm{d}r_c(t)}{\mathrm{d}t} &= k_{on} \cdot V_h \cdot C(t) \cdot r(t) - k_{off} \cdot r_c(t) - k_{in} \cdot r_c(t) \qquad (4.2b) \end{aligned}$$

The concentration of bound receptors is later translated into hepatic glucose production $(F_{hgp}(t))$. In the original work, the shape of $F_{hgp}(t)$ was investigated considering three different possibilities: a linear relationship with $r_c(t)$, a Michaelis-Menten, or a Hill-type expression. Their results concluded that the Hill equation, with a value of n fixed to 2, was the best option for fitting their data, as shown in Equation (4.3).

$$F_{hgp}(t) = b_G + \frac{V_1 \cdot r_c(t)^n}{K_1^n + r_c(t)^n} \qquad (4.3)$$

Constants V_1 and K_1 are the characteristic parameters of the Hill equation, and b_G is the baseline hepatic glucose production. This expression is later added to the equation describing glucose, where the insulin-dependent and insulin-independent productions of glucose were also included.

Figure 4.3 presents a schematic representation of the receptors' states and the transfer rates between them. Receptors on the liver membrane (r) can bind to glucagon molecules at rate k_{on}. Active receptors (r_c) can either unbind (k_{off}) or internalize (k_{in}). Internalized receptors (r_i) then recycle back to the surface at rate k_{rec}. In some cases, free receptors could also internalize, represented with rate k'_{in}.

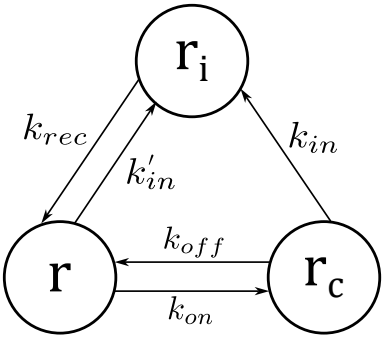

Figure 4.3: Receptors rates diagram. Compartment r represents the available receptors; r_c, the active/bound receptors, and r_i, the internalized receptors.

In Masroor's work, some rate values were fixed to constants obtained from the literature to avoid identifiability issues. k_{on} and k_{off} values were taken from Ronald Kahn (1976), where association and dissociation values for different hormone and neurotransmitter receptors are listed. Glucagon rate values specifically were initially described in Rodbell et al. (1971). The magnitude of the values agrees with the study by Strasser et al. (2017), where they present activation and deactivation rate values for 28 different GPCRs. They report that association rate constants range from 10^5 to 10^{10} (M min)$^{-1}$, and dissociation rates range from 0.0001 to 10 min^{-1}.

The value of the recycling constant for glucagon receptors (k_{rec}) is assumed to be equal to insulin receptors, and they use the value reported in Sedaghat et al. (2002). The remaining parameters were identified, although the value of k'_{in} collapsed to zero during the preliminary estimation process. Based on those results, we will also assume the transfer of receptors from the *available* state to the internalization endosome is negligible. The final parameter values used in Masroor's work are listed in Table 4.2.

A dataset from a clinical trial performing a Glucagon Challenge Test (Van Dongen et al., 2015) was used to identify and validate the model. The clinical trial aimed to test a specific glucagon receptors antisense drug for its use in Type 2 Diabetes (T2D) treatment. The drug should block glucagon receptors, limiting glucagon production, hence avoiding hyperglycemia, one of the main consequences of T2D. In order to test the drug capabilities, the glucagon challenge test procedure was used (Van Dongen et al., 2014). The test is a procedure used to measure the glucagon effect on hepatic glucose production. It lasts a total of 6 hours. The first half of the trial aims to stabilize and measure basal concentrations. In the

last three hours, somatostatin is used to inhibit pancreatic insulin and glucagon secretion while administering exogenous insulin and glucagon so that insulin concentrations remain at basal levels, but glucagon levels rise 2 or 3 times over their baseline values.

In the identification performed in Masroor's work, datasets from both parts of the clinical trial were used: before treatment with the antisense drug and after a 6-week treatment with 400 μg doses. Although 58 healthy subjects participated in the clinical trial, the subset used included eight patients. Regarding the parameters identified for the receptors model, different values were obtained before and after treatment with the drug. However, only the parameters prior to the drug treatment have been used as references here. The identified parameters included in Table 4.2 present this distinction with the (B) or (A) indication.

Parameter	k_{on}	k_{off}	k_{rec}	k_{in}	V_h
Units	$(\text{pmol h})^{-1}$	min^{-1}	min^{-1}	h^{-1}	l
Value	0.0036	0.24	0.003	(B) 21.5 ± 15.2 (A) 12.1 ± 3.15	(B) 4.65 ± 2.28 (A) 4.96 ± 1.77

Table 4.2: Glucagon receptors model rate values fixed (k_{on}, k_{off}, k_{rec}) or identified (k_{in}, V_h) in Masroor et al. (2019). Only the parameters relevant to the receptors model have been included in this list. (B) and (A) refer to "Before" and "After" treatment with the antisense drug tested in the clinical trial by Van Dongen et al. (2015).

Notice that the value for k_{in} is the one that experiments a greater difference before and after the antisense drug. Since the drug was designed to inhibit glucagon receptors, it is reflected in the model with a lower internalization rate. The goal is to check this model in receptor dynamics with data from people with T1D. However, this disease is fundamentally based on a deficiency of insulin secretion, so receptor behavior should not be affected. That is why the model proposal uses as a reference the values corresponding to the state prior to any medication being administered.

Masroor and colleagues validated the model by incorporating it into a simple glucoregulatory model based on the Minimal Model (Bergman et al., 1981). It yielded a good fit to the datasets used, and the authors leave as open work exploring this model's capabilities to be used in AP development. Given the simple structure of the model and the good results observed in describing glucagon receptor dynamics, an interest arose in evaluating it with a more detailed glucoregulatory model and describing the glucagon effect observed in data from people with T1D.

4.3.2 Model proposal

The model proposal consists of a definition of $EGP(t)$ that incorporates the effect of glucagon mediated by glucagon receptors. Equation (4.4) presents the final expressions used for the states $r(t)$ and $r_c(t)$.

$$\frac{\mathrm{d}r(t)}{\mathrm{d}t} = -k_{on} \cdot V_h \cdot C(t) \cdot r(t) + k_{off} \cdot r_c(t) + k_{rec}\left(1 - r(t) - r_c(t)\right) \tag{4.4a}$$

$$\frac{\mathrm{d}r_c(t)}{\mathrm{d}t} = k_{on} \cdot V_h \cdot C(t) \cdot r(t) - k_{off} \cdot r_c(t) - k_{in} \cdot r_c(t) \tag{4.4b}$$

Note that the term $-k'_{in} \cdot r(t)$ has been omitted compared to the expression in Equation (4.2) since the value of k'_{in} is assumed to be negligible.

Even though Masroor's work employed a Hill equation to describe receptors' dynamics (see Equation (4.3)), a more straightforward structure was considered, substituting it with a Michaelis-Menten structure:

$$F_{hgp}(t) = \frac{V \cdot r_c(t)}{K + r_c(t)} \tag{4.5}$$

This expression represents glucose production from the liver, grouping the effect of the glycogenolysis and gluconeogenesis processes. Their effects are approximated, associating the increase in glucose with the concentration of active receptors. Then, the EGP definition was complemented by adding an additive effect of insulin on glucose production by the liver (Hovorka et al., 2002), which was not considered in Masroor's proposal. With this, the expression of EGP is written as:

$$EGP(t) = F_{hgp}(t) + EGP_0\left(1 - S_I \cdot x_3(t)\right) \tag{4.6}$$

where S_I is the hepatic insulin sensitivity, and EGP_0 is the EGP at basal insulin concentration.

A PK/PD model from the literature was chosen as the base to test this model. The model proposed in Wendt et al. (2017b) gathered a series of appealing aspects that led to its use in this work. First, it is based on the Hovorka PK/PD model (Hovorka et al., 2002), which is a widely used and accepted model in diabetes-related modeling. Wendt incorporated the PK of glucagon to include its effect on glucose. They also provided a definition of EGP in which insulin limits the effect of glucagon. Its development was inspired by the conclusions gathered in El Youssef et al. (2014), where high concentrations of insulin blunt glucagon response.

Table 4.3 at the end of this section presents each state and parameter of the complete model, including the EGP proposal, along with their units and description.

The insulin PK model is composed of a chain of two compartments ($X_1(t)$ and $X_2(t)$) and a signal ($I(t)$) used to describe insulin PK:

$$\frac{\mathrm{d}X_1(t)}{\mathrm{d}t} = u_I(t) - \frac{X_1(t)}{t_{max}} \tag{4.7a}$$

$$\frac{\mathrm{d}X_2(t)}{\mathrm{d}t} = \frac{X_1(t)}{t_{max}} - \frac{X_2(t)}{t_{max}} \tag{4.7b}$$

$$I(t) = \frac{1}{t_{max}} \frac{X_2(t)}{W \cdot Cl_{F,I}} \cdot 10^6 + I_b \tag{4.7c}$$

$u_I(t)$ is the insulin infusion, expressed as a deviation with respect to the basal insulin infusion. The system's output is plasma insulin concentration ($I(t)$). The factor 10^6 in Equation (4.7c) acts as a unit conversion from U/ml to mU/l. This structure was replicated to describe the PK of glucagon:

$$\frac{\mathrm{d}Z_1(t)}{\mathrm{d}t} = u_C(t) - k_1 \cdot Z_1(t) \tag{4.8a}$$

$$\frac{\mathrm{d}Z_2(t)}{\mathrm{d}t} = k_1 \cdot Z_1(t) - k_2 \cdot Z_2(t) \tag{4.8b}$$

$$C(t) = \frac{k_2 \cdot Z_2(t)}{W \cdot Cl_{F,C}} + C_b \tag{4.8c}$$

$Z_1(t)$ and $Z_2(t)$ represent the glucagon mass in subcutaneous tissue and plasma, respectively, with input the glucagon infusion ($u_C(t)$), expressed as a deviation from basal glucagon infusion (which is expected to be zero), and output plasma glucagon concentration ($C(t)$).

The glucose regulation subsystem follows the Hovorka model. It comprises three states representing insulin's effects on EGP, glucose transport, and glucose uptake, respectively:

$$\frac{\mathrm{d}x_1(t)}{\mathrm{d}t} = k_{a1}\left(I(t) - x_1(t)\right) \tag{4.9a}$$

$$\frac{\mathrm{d}x_2(t)}{\mathrm{d}t} = k_{a2}\left(I(t) - x_2(t)\right) \tag{4.9b}$$

$$\frac{\mathrm{d}x_3(t)}{\mathrm{d}t} = k_{a3}\left(I(t) - x_3(t)\right) \tag{4.9c}$$

Finally, the glucose dynamics for the accessible, $Q_1(t)$, and non-accessible, $Q_2(t)$, compartments, are described as follows:

$$\frac{\mathrm{d}Q_1(t)}{\mathrm{d}t} = -F_{01}(t) - F_R(t) - S_T \cdot x_1(t) \cdot Q_1(t) + k_{12} \cdot Q_2(t) + EGP(t) \tag{4.10a}$$

$$\frac{\mathrm{d}Q_2(t)}{\mathrm{d}t} = S_T \cdot x_1(t) \cdot Q_1(t) - Q_2(t) \cdot (k_{12} + S_D \cdot x_2(t)) \tag{4.10b}$$

$$G(t) = \frac{Q_1(t)}{V} \tag{4.10c}$$

The expression for EGP is defined as the proposal described in Equation (4.6). The original formula for EGP used in Wendt et al. (2017b) will be detailed in Section 4.4.1. Note that, as compared to Hovorka et al. (2002), equations (4.9a)-(4.9c) have unit static gain, being insulin sensitivities (gains) for glucose transport and uptake described by parameters S_T and S_D, respectively, in equations (4.10a)-(4.10b).

The value of $F_{01}(t)$ is zero unless glucose falls under 80 mg/dl, in which case its value will be $F_{01} \cdot G(t)/4.5$. Likewise, $F_R(t)$ will be zero until glucose reaches 160 mg/dl, in which case its value will be $0.003 \cdot (G(t) - 9) \cdot V$.

The end goal is to evaluate the capabilities of the receptors model structure in describing glucagon dynamics. To do so, the validation of the model proposal is based on two main pillars:

1. Using clinical data from patients with T1D to identify the model's parameters,
2. Comparing its behavior to EGP models from the literature.

As a result of a research stay that initiated a collaboration between our group and the Technical University of Denmark and Steno Diabetes Center in Copenhagen, we were able to use two clinical datasets for the validation of our model proposal. The clinical data are described in Sections 5.1 and 6.1.

Given the variety of glucagon effect definitions in the literature (see Section 3.3), an appropriate validation method would be to compare the performance of the proposal against other models from the literature, to better analyze the potential contributions of considering the relation between the glucagon receptors' lifecyle and the glucagon effect. Hence, three EGP models were selected to serve as comparators.

Magnitude	Units	Description
$u_I(t)$	U/min	Insulin infusion (as a deviation from basal)
$X_1(t)$	U	Insulin mass due to exogenous dosing in subcutaneous tissue
$X_2(t)$	U	Insulin mass due to exogenous dosing in plasma
$I(t)$	mU/l	Insulin plasma concentration
t_{max}	min	Time from dose to maximum plasma concentration
W	kg	Weight
Cl_{FI}	ml/kg/min	Apparent insulin clearance
I_b	mU/l	Basal insulin concentration
$u_C(t)$	pg/min	Glucagon infusion (as a deviation from basal)
$Z_1(t)$	pg	Glucagon mass due to exogenous dosing in subcutaneous tissue
$Z_2(t)$	pg	Glucagon mass due to exogenous dosing in plasma
$C(t)$	pg/ml	Glucagon concentration in plasma
k_1, k_2	min^{-1}	Absorption elimination rate constants
Cl_{FC}	ml/kg/min	Apparent glucagon clearance
C_b	pg/ml	Basal glucagon concentration
$x_1(t)$	mU/l	Effect of insulin on glucose distribution
$x_2(t)$	mU/l	Effect of insulin on glucose disposal
$x_3(t)$	mU/l	Effect of insulin on EGP
$EGP(t)$	μmol/kg/min	Endogenous glucose production
$Q_1(t)$	μmol/kg	Glucose mass in the accessible compartment
$Q_2(t)$	μmol/kg	Glucose mass in the non-accessible compartment
$G(t)$	mmol/l	Blood glucose
k_{a1}, k_{a2}, k_{a3}	min^{-1}	Deactivation rate constants
F_{01}	μmol/kg/min	Insulin-independent glucose flux
F_R	μmol/kg/min	Renal glucose clearance
S_T	min^{-1}/(mU/l)	Insulin sensitivity to glucose transport
S_D	min^{-1}/(mU/l)	Insulin sensitivity to glucose disposal
k_{12}	min^{-1}	Transfer rate constant from the nonaccessible to the accessible compartment
V	ml/kg	Glucose distribution volume

Continued in next page

Continued from previous page

Magnitude	Units	Description
$r(t), r_C(t)$	unitless	Normalized amount of free and bonded receptors
$F_{hgp}(t)$	μmol/kg/min	Hepatic glucose production
k_{off}	min^{-1}	Dissociation rate
k_{rec}	min^{-1}	Recycling rate
k_{in}	min^{-1}	Internalization rate of the glucagon-bonded receptor
k_{on}	$(\text{pg/min})^{-1}$	Association rate of glucagon to the receptor
V_h	ml	Volume of the hepatic interstitial space
K_r	unitless	Apparent dissociation constant
V_r	μmol/kg/min	Maximal glucagon-dependent hepatic glucose production rate
EGP_0	μmol/kg/min	EGP extrapolated to zero insulin concentration
S_I	$(\text{mU/l})^{-1}$	Hepatic insulin sensitivity

Table 4.3: Units and description of the states and parameters in the PK/PD model proposal. The table contains the following groups: insulin PK states and signals, insulin PK parameters, glucagon PK states and signals, glucagon PK parameters, glucose regulation states and signals, glucose regulation parameters, EGP states and signals, and EGP parameters.

4.4 Validation methods

4.4.1 EGP comparators

The validation process aims to replace the EGP definitions keeping the same baseline model (i.e., insulin PK, glucagon PK, and glucose regulation should be the same regardless of the EGP model). The baseline model, as described in the previous section, will be the one proposed by Wendt, which is based on Hovorka's.

Hence, in order to ensure the comparison process was as fair as possible, the selection of the EGP comparators was based on (1) using models that included glucagon dynamics, and (2) models whose underlying dynamics were based on Hovorka's PK/PD model. If the selected EGP model is already designed based on a model structure similar to the one used in the proposal, there is a smaller chance that the change of base model has a negative impact on their performance.

Among the models presented in Chapter 3, the ones that fitted the criteria (they were based on Hovorka's structure and also included glucagon PK and glucagon dynamics in their EGP description) were the following:

1. DTU's model: definition by Wendt et al. (2017b) that accompanies the baseline model, as described in the previous section. It will be labeled as *DTU* (Technical University of Denmark), which was Wendt's affiliation at the time of publication.

2. McGill's model: EGP model proposed by Emami et al. (2017). The paper evaluates several definitions of EGP and presents a solution (their proposal number 8) that is the one used in this work. It will be labeled as *McGill*, for McGill University in Montreal. The Montreal group has a significant trajectory working on multi-hormonal systems and different hormones applied to the treatment of T1D, as seen thorough Section 2.3.1.

3. OHSU's model: proposal by Resalat et al. (2019), which was first presented in Jacobs et al. (2015). It will be referred to as *OHSU* model for the Oregon Health and Science University. This research group also has contributed with many significant developments in the area of multi-hormone APs, especially in insulin plus glucagon systems.

The following sections present the equations for each EGP model, and Table 4.4 details each model-specific parameters and signals' units and descriptions. All the models will use two inputs and one output. The inputs are the portion of plasma insulin that influences hepatic glucose production (gluconeogenesis and glycogenesis), given by the state $x_3(t)$, and plasma glucagon concentration, given by $C(t)$. Every model provides the amount of glucose produced in the liver, $EGP(t)$, as output.

DTU EGP model

The original Wendt model described EGP as:

$$EGP(t) = G_{gg}(t) + G_{GNG}, \tag{4.11a}$$

where the signal $G_{gg}(t)$ determines the combined effect of glucagon and insulin on hepatic glucose production. A Michaelis-Menten expression links their relationship with a maximum rate inhibited by insulin effect $(x_3(t))$ above basal insulin concentration I_b,

	Magnitude	Units	Description
DTU	S_E	$(\text{mU/l})^{-1}$	Hepatic insulin sensitivity
	E_{max}	μmol/kg/min	Maximum EGP at basal insulin concentration
	C_{E50}	pg/ml	Glucagon concentration yielding half of maximum EGP
	G_{GNG}	μmol/kg/min	Glucose production by gluconeogenesis
	$G_{gg}(t)$	μmol/kg/min	Glucose production due to glycogenolysis
McGill	S	$(\text{mU/l})^{-1}$	Insulin sensitivity
	T	$(\text{pg/ml})^{-1}$	Glucagon sensitivity
	K_{Gd}	$(\mu\text{mol/kg})^{-1}$	Fractional deactivation rate constant
	T_{Gd}	μmol/kg	Glucagon rate of change sensitivity
	G_{ng}	μmol/kg/min	Effect due to gluconeogenesis
	$EGP_G(t)$	μmol/kg/min	Contribution to EGP from the rate of change of glucagon
OHSU	S_f	$(\text{mU/l})^{-1}$	Hepatic insulin sensitivity
	k_c	$(\text{ng/l})^{-1}/\text{min}$	Glucagon sensitivity
	k_{g3}	unitless	Glucagon rate of change sensitivity
	k_d	min^{-1}	Clearance rate of glucagon from the remote compartment
	EGP_0	μmol/kg/min	Basal endogenous glucose production at zero insulin concentration
	$Y(t)$	unitless	Effect of glucagon on EGP

Table 4.4: Units and description of states and parameters associated to each EGP definition selected as comparator. The upper group describes the DTU EGP parameters, the second group describes McGill EGP, and the bottom group describes the OHSU EGP parameters and states.

with hepatic insulin sensitivity S_E:

$$G_{gg}(t) = \frac{1 - S_E \cdot x_3(t)}{1 - S_E \cdot I_b} \cdot \left((E_{max} - G_{GNG}) \frac{C(t)}{C_{E50} + C(t)} \right) \tag{4.11b}$$

As mentioned before, this goal of this EGP definition is capturing the glucagon effect limitation caused by high circulating plasma insulin levels.

McGill EGP model

Emami et al. (2017) compared nine different descriptions of $EGP(t)$ and validated them with a set of clinical data (El Youssef et al., 2014). The model concluded as the best

description for EGP corresponds to model number 8, defined as follows:

$$EGP(t) = \mathcal{H}\left(1 - S \cdot x_3(t)\right) \cdot \mathcal{H}\left(EGP_G(t) + T \cdot C(t)\right) + G_{ng}, \tag{4.12a}$$

where $\mathcal{H}(\cdot)$ is a unit step function, included to keep the expression positive. They consider that not only the level of plasma glucagon contributes to hepatic glucose production but also its rate of change, defining the derivative of $EGP_G(t)$ as:

$$\frac{\mathrm{d}EGP_G(t)}{\mathrm{d}t} = -k_{Gd} \cdot EGP_G(t) - k_{Gd} \cdot T_{Gd} \left(\frac{\mathrm{d}C(t)}{\mathrm{d}t}\right) \tag{4.12b}$$

In this expression, hepatic insulin sensitivity is given by parameter S. Similarly to Wendt et al. (2017b), insulin effect $x_3(t)$ inhibits glucagon effect on EGP as a multiplicative factor.

Later work by the same authors presented the Ulna simulator (Smaoui et al., 2020b,a), where they also incorporated insulin and glucagon dynamics. However, they used a different definition of EGP among the ones presented in Emami et al. (2017). Specifically, their proposal number 5. However, for this evaluation, proposal 8 was used as the EGP comparator since it was the one that provided the best fit to clinical data according to their analyses.

OHSU EGP model

Jacobs et al. (2015) proposed a model based on Hovorka's model, incorporating glucagon dynamics, similar to the procedure followed in Wendt et al. (2017b). However, their EGP is significantly different :

$$EGP(t) = EGP_0 \left(1 - S_f \cdot x_3(t) + Y(t) + k_{g3} \cdot \frac{\mathrm{d}Y(t)}{\mathrm{d}t}\right) \tag{4.13a}$$

where $Y(t)$ represents glucagon effect with dynamics given by:

$$\frac{\mathrm{d}Y(t)}{\mathrm{d}t} = k_c \cdot C(t) - k_d \cdot Y(t) \tag{4.13b}$$

Note that the parameter S_f in Equation (4.13a) was added to the original formulation of the model (see Section 3.3) to match our definition of the unit-gain $x_3(t)$, as compared to Jacobs et al. (2015). Also, the units of k_c are different with respect to the original definition in order to match the units of the plasma glucagon signal. This is because glucagon PK in Resalat et al. (2019) is defined as a chain of three compartments as opposed to Wendt's model, which uses two, and they are expressed in terms of glucagon mass, instead of

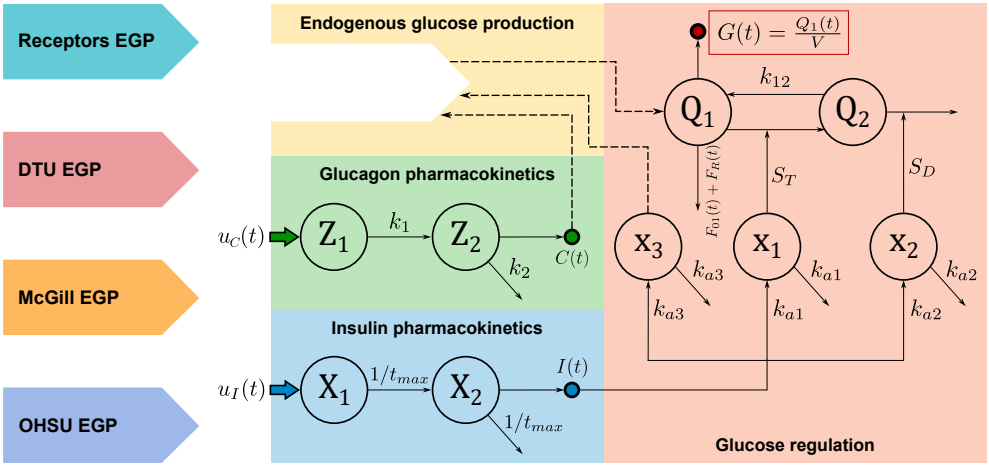

Figure 4.4: EGP model validation setup. The baseline model by Wendt et al. (2017b) includes descriptions for insulin PK (blue blox), glucagon PK (green box), and glucose regulation(red box). The EGP definition will be interchanged depending on the model being evaluated: our proposal (Receptors EGP), the EGP model by Wendt et al. (2017b) (DTU EGP), the proposal by Emami et al. (2017) (McGill EGP), or the definition by Jacobs et al. (2015) (OHSU EGP).

concentration. Remark that contrary to Wendt's and Emami's proposals, insulin and glucagon effects on EGP in this model are considered additive instead of multiplicative. This means that the contribution of glucagon to EGP is independent of insulin and that the balance between glucagon and insulin antagonistic effects will determine EGP.

Validation setup

Once all the actors have been presented, the validation layout can be set up, as described in Figure 4.4. The model by Wendt was used as a baseline, which means that the descriptions of insulin PK, glucagon PK and glucose regulation will be kept the same through the process. The block dedicated to the EGP model receives two inputs, $x_3(t)$ and $C(t)$, and provides the $EGP(t)$ value as output, that will be added as a contribution to the glucose in the accessible compartment, $Q_1(t)$ (Equation (4.10a)). In each validation stage, the EGP definition was substituted with the corresponding model (the receptors EGP proposal, DTU EGP, McGill EGP, or OHSU EGP).

The performance of each structure was evaluated as a function of their goodness of fit to

the data. The validation procedure involved identifying the parameters of each of the EGP models using different procedures that are described in chapters 5 and 6. Nevertheless, Section 4.4.2 describes the common aspects in the identification methodology, including the description of the performance index, as well as the different software tools used in the optimization and identification process, since they are shared by all the identifications carried out throughout the document.

The main reason of choosing to re-identify various EGP structures was to evaluate, on equal grounds, the performance of different model structures and analyze whether the proposed structure based on glucagon receptors provided any improvements. The same identification methods were followed with each EGP definition to ensure a fair process.

4.4.2 Identification methodology

Performance index

In order to identify the parameters of each EGP model, the optimization process assessed the difference between the simulation output and the data points. This difference was evaluated using the Root Mean Squared Error (RMSE), which is defined as follows:

$$RMSE_P^v = \sqrt{\frac{1}{n_v}\sum_{i=1}^{n_v}(e^v)^2} \qquad \text{where} \quad e^v = \hat{y}_{i,P}^v - y_{i,P}^v \tag{4.14}$$

In the datasets available, a given patient would participate in more than one arm of the clinical trial. Hence, multiple visits to the clinic ensued. The subscript P in Equation (4.14) denotes a specific patient, whereas v denotes a visit of that patient. The number of data points in the specific experiment is indicated by n_v, $\hat{y}_{i,P}$ is the model output, and $y_{i,P}^v$ represents the set of data points.

Optimization procedure

The parameter identification process consists of finding the set of parameters that would minimize the error between the data and the simulation as much as possible. Then, to identify the system's parameters, the model will be run multiple times within an optimization function that will vary the parameter values, searching for the combination that will minimize the specified cost index.

All identification processes were carried out in MATLAB (versions R2018b and R2022a), and the optimization function used was `fmincon`, which makes use of the interior point algorithm (Nocedal and Wright, 2006). This algorithm is the default solver in the `fmincon` function, and it is widely used for solving optimization problems. The interior point algorithm tries to iteratively approach the optimal solution from the interior of a feasible set to find the minimum of a function $f(\theta)$ (where θ represents the parameter set). To utilize the `fmincon` function, the user must define a function that computes $f(\theta)$ and returns a scalar value, which will represent the amount to minimize (i.e., the cost index). It is also required that a set of initial values for each parameter is provided (θ_0). Additionally, the function allows defining upper and lower bounds for the parameters, as well as equality or inequality constraints. Parameter limits will be set in the successive identifications, to avoid finding solutions that fall out of physiological thresholds.

The definition of the function $f(\theta)$ will contain the simulation of the models and the computation of the cost index (J_P). One parameter set will be obtained per patient in each optimization process, hence the subscript P. The selected solution was the result which provided the lowest index value. This index was defined differently for each identification stage, as it will be presented in the next chapters. Nevertheless, it is always defined as a function of the RMSE:

$$J_P = g(RMSE_P^v) \tag{4.15}$$

`fmincon` is a local optimization solver, which means that it will assume the function $f(\theta)$ has a unique minimum in a local area or region, close to the inital points. However, this might not always be the case, and there exists the risk that the function will stop the optimization on a local minimum. In order to avoid this problem, the identifications were executed several times, with different initial points selected within the parameter bounds. The number of times the identification was repeated was different in each identification stage.

Initially, the starting points for the optimization were sampled randomly within the defined parameters' bounds. These bounds were based on the parameter values provided in each EGP model's respective original work. Later on, the initial parameter values were drawn from Latin hypercube sampling (LHS). This technique allows obtaining distributed points along the parameter space with a relatively small number of samples (McKay et al., 2000). An alternative would be using Monte Carlo sampling, but LHS requires less computational resources (Balsa-Canto et al., 2010).

The models used in this work consist of systems of differential equations. In order

to solve them, Matlab provides the function `ode45`, that makes use of a Runga-Kutta method to solve the system over a specific time step. Specifically, the Dormand-Prince method (Dormand and Prince, 1980). In this work, the `ode45` function runs over 5 minutes intervals, with the solver applying a variable simulation step size within each interval.

In summary, the models will be simulated within the function $f(\theta)$, where the cost index J_P will be computed, and the `fmincon` function will find the values of θ that provide the lowest RMSE between the models' execution and the data.

Structural identifiability and parameter sensitivity analysis

Prior to carrying out the parameter identification process, the structural identifiability of the models should be addressed.

Structural identifiability is a theoretical property of the model structure that evaluates whether the parameters can be assigned unique values under ideal experimental conditions, i.e., noise-free and continuous. It depends only on the system dynamics, the observation and the stimuli functions, being independent of the parameter values (Balsa-Canto et al., 2010; Chiş et al., 2011b).

There are multiple answers we can obtain in this analysis. If the structural identifiability problem has a unique solution, the model is structurally *globally* identifiable (SGI). However, if there are several parameter sets that provide the same solution, the model is structurally *locally* identifiable (SLI). If the number of those parameter sets is infinite, the system becomes structurally unidentifiable. Checking local identifiability is usually easier than assessing global identifiability, and a recent work by Barreiro and Villaverde (2023) posed whether ensuring SLI would suffice since it is often the case that an SLI parameter is SGI too. The work analyzes 102 biological models from the literature to analyze their structural identifiability, and concluded that in 92.4% of the cases, a SLI parameter was also SGI. Hence, were we not able to perform a global identifiability analysis, a local analysis would suffice.

Some of the most common methods for testing the structural identifiability are the Taylor series approach and the generating series system. The first is a well-known extensively-used method, since it is more general and can be applied to any nonlinear model. However, it might be more computationally demanding, since the number of needed derivatives is usually unknown. On the other hand, the generating series approach requires a lower number of derivatives, meeting halfway between resources consumption and applicability.

In order to apply the generating series strategy to find the model's structural iden-

tifiability the software GenSSI was employed. GenSSI (*Generating Series approach for testing Structural Identifiability*) is a free toolbox available for MATLAB (Chiş et al., 2011a), that implements the generating series approach accompanied by the use of identifiability tableaus. The software accepts both linear and nonlinear systems of the form:

$$\Sigma(p): \begin{cases} \dot{x}(t) = f'(x(t),\theta) + g'(x(t),\theta)u(t), \quad x(t_0) = x_0(\theta), \\ y(t,\theta) = h(x(t),\theta), \end{cases} \tag{4.16}$$

In the above equation, θ represents the unknown set of parameters, x is the state vector, u is the control or input vector, y is the output vector, and x_0 are the initial conditions (that could depend on the parameters). The software requires the user to define a function where they specify the model equations, the input and output variables, the initial conditions and the relevant parameters. The software generates a nonlinear system of equations from the computation of the successive Lie derivatives of f' and g'. If the solution of the system of equations is unique, then the parameters are GSI. GenSSI later provides the solution in the form of identifiability tableaus and a textual description of which parameters are locally identifiable, globally identifiable, or unidentifiable.

Identifiability tableaus are a graphical tool to easily visualize structural identifiability of a system. It consists of a grid that represents the non-zero elements of the Jacobian of the series coefficients with respect to the parameters. The grid has as many columns as parameters and as many rows as non-zero series coefficients, which could be, in principle, infinite (Balsa-Canto et al., 2010). If the tableau has any empty columns, the corresponding parameters may be unidentifiable. Results presenting identifiability tableaus are presented in Section 5.2.2.

Identification can be an iterative process if the proposed model turns out to be unidentifiable. According to Balsa-Canto et al. (2010), there are two possible courses of action in that case: (1) reducing the number of parameters in the model, or (2) reformulating the model equations. Since the second option might be more complex or not possible, the former alternative should be the first to be addressed by fixing some parameters to literature values, for example. However, deciding which parameters should be constant might not be trivial. A sensitivity analysis of the parameters could provide information to assess the influence of each parameter on the output, thus allowing to elaborate a ranking (Garcia-Tirado et al., 2018).

The software AMIGO2 (Balsa-Canto et al., 2016), which is available as a Matlab toolbox, can be used to perform the parameters' global sensitivity analysis. The software suite actually implements many other features such as tools for parameter estimation, identifia-

bility analysis, optimal experimental design, optimal control solvers, etc. Regarding the sensitivity analysis feature, the software requires the user to define the system of equations conforming the model, a nominal value per parameter, and the subset of parameters to be included in the analysis. Additionally, at least one *experiment* has to be defined. The user has to specify one or more experimental benchmarks to run the model in. The experiments require information about the states initial values, the observable magnitudes, duration and sampling time, and input signals to stimulate the system. The software then proceeds to perform the sensitivity analysis.

The local parameter sensitivity of a parameter θ (from a total of p parameters), with respect to an output y_o, is computed as:

$$S_p^o(\theta) = \left.\frac{\partial y_o}{\partial \theta_p}\right|_{\theta=\hat{\theta}, y_o=y_o(t,\hat{\theta})} \tag{4.17}$$

The analysis is made based on a nominal value of the parameter, $\hat{\theta}$, hence it will be valid in the neighborhood region of said value. To extend the analysis to a global domain, the sensitivities of a wide spectrum of parameters (within the defined bound) should be analyzed. The authors use LHS to obtain samples of parameters and perform the corresponding sensitivity calculations.

The total importance factor for a parameter θ_p is then calculated as:

$$\delta_{\theta_p}^{msqr} = \frac{1}{n_D}\sqrt{\sum_{l=1}^{n_{lhs}}\sum_{e=1}^{n_e}\sum_{j=1}^{n_o}\sum_{t_{si}=1}^{n_s}\left(s_{\theta_p,j}^{l,e}\left(t_{s_p}\right)\right)^2} \tag{4.18}$$

where the subscript e denotes the number of experiments, o refers to the obserbables (outputs), n_{lhs} is the number of samples provided by the LHS algorithm, and n_s is the number of sampling times used in a given experiment, with a given observable.

Each parameter in the set is assigned a $\delta_{\theta_p}^{msqr}$ value, and then the set is sorted according to their values, usually in decreasing order. The higher the value, the greatest influence of the parameter in the output. This will help to assess the parameter discrimination process.

4.5 Conclusion

This chapter presents the first contribution of this thesis: a model of endogenous glucose production including glucagon receptor dynamics. Even though glucagon receptors'

pathways to glycogenolysis and gluconeogenesis are complex, the increment in hepatic glucose production is simplified as a function of the amount of receptors that bind to plasma glucagon.

Finally, we have presented the tools that are going to be used to identify the models, presenting the metric used for the optimization process, as well as the software suites that will be used to analyze the structural identifiability and sensitivity of the parameters later on.

The subsequent chapters present the validation of the proposed model, which will be identified along with the models selected for comparison using clinical datasets. Chapter 5 uses a dataset where three different single glucagon doses were administered to T1D patients. It will be generally referred to as *dataset 1*, and the final results are labeled as *Validation 1*. Next, Chapter 6 utilizes a dataset where two consecutive glucagon doses were administered. Data and final results of this second validation will be referred to as *dataset 2* and *Validation 2*.

Chapter 5

Glucagon model validation against single glucagon doses

The present chapter presents the first validation performed on the EGP model proposal using a clinical dataset where single glucagon doses were administered (100, 200, or 300 μg). A preliminary validation compared the model's performance against one other EGP definition. After the obtained positive results, a more thorough process was carried out to compare the proposed model to three other definitions from the literature. The results of the procedures obtained in this chapter lead to the publication of a conference paper, a conference abstract, and one journal paper:

- *Furió-Novejarque, C., Sanz, R., Reenberg, A.T., et al. (2022a). Assessment of a new model of glucagon action with glucagon receptor dynamics. 10th Vienna International Conference on Mathematical Modelling (MATHMOD 2022). Viena (Austria). IFAC-PapersOnLine, 55(20):647 – 652.*
- *Furió-Novejarque, C., Sanz, R., Reenberg, A.T., et al (2022b). Validation of a novel model of glucagon effect including glucagon receptor dynamics. 15th International Conference on Advanced Technologies & Treatments for Diabetes (ATTD 2022). Barcelona (Spain). In Diabetes Technology and Therapeutics, 24(S1):A-27.*
- *Furió-Novejarque, C., Sanz, R., Ritschel, T.K., et al. (2023). Modeling the effect of glucagon on endogenous glucose production in type 1 diabetes: On the role of glucagon receptor dynamics. Computers in Biology and Medicine, 154(January): 106605.*

5.1 Data collection

The data used for the models' evaluation was obtained in the clinical trial performed by Ranjan et al. (2016). The purpose of the trial was to test the efficacy of different glucagon doses in recovering from mild hypoglycemia. Eight people with T1D took part in the study, who underwent four different arms in the trial.

Patients arrived at the clinic after fasting for 12 hours. After retrieving initial blood samples, patients received an insulin bolus (Novorapid, Novo Nordisk) to reach mild hypoglycemic conditions (blood glucose concentration lower than 70 mg/dl). At that point, they received either saline or a glucagon bolus (GlucaGen, Novo Nordisk). Depending on the trial arm, the glucagon boluses were either 100, 200, or 300 μg. A summary of the protocol is shown in Figure 5.1. Plasma glucose, plasma glucagon, plasma insulin, plasma growth hormone, cortisol, free fatty acids, triglycerides, blood pressure, and heart rate were measured throughout the study.

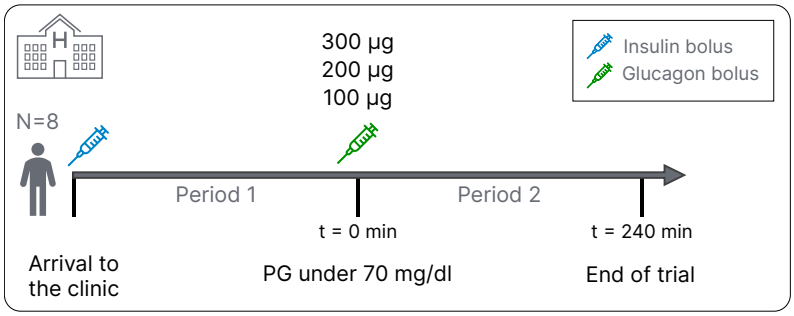

Figure 5.1: Summary of the clinical trial in Ranjan et al. (2016).

For the purpose of validating the EGP model, only the information about plasma glucose, glucagon, and insulin was used. Also, since the main interest was the modeling of the glucagon effect, only the visits where glucagon was administered (either the 100 μg, 200 μg, or 300 μg dose) have been considered. They will be labeled visits A, B, and C henceforth. Figure 5.2 summarizes the data at our disposal from the trial.

On average, plasma glucagon peak response occurred between 12 and 16 minutes after the bolus administration. Plasma glucagon peak concentrations had mean values of 100, 217, and 358 pmol/l (348, 755, and 1245 pg/ml, approximately). The study found that peak plasma glucagon values were inversely correlated with weight and positively correlated with the duration of diabetes. Its effect also had a fast effect on glucose, increasing

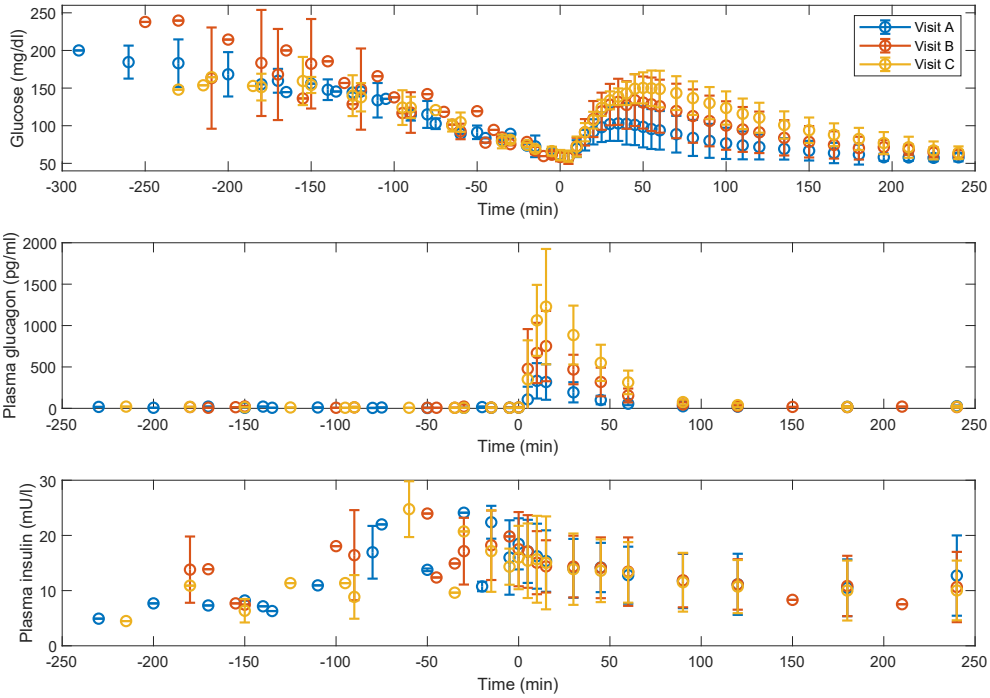

Figure 5.2: Mean values and standard deviation of the data from the clinical trial in Ranjan et al. (2016). Available data included plasma glucose (upper graph), plasma glucagon (middle graph), and plasma insulin (bottom graph). Data in blue represent Visit A (100 μg glucagon dose), data in orange represent Visit B (200 μg dose), and data in yellow represent Visit C (300 μg dose).

plasma glucose levels within 15 minutes at least 10 mg/dl over its value at the moment of bolus administration. The trial also discussed how glucose response did not significantly increase with doses larger than 250 μg. The study by Graf et al. (1999) also observed that intravenous doses of glucagon between 250 μg and 2 mg provided a linear increment in plasma glucagon concentration. However, the dose response was quite similar regardless of the dose size. Indeed, for intravenous glucagon doses of 0.25, 0.5, 1, and 2 mg, average peak glucose values were 131, 138, 132, and 129 mg/dl, respectively.

The study by Ranjan did not use any clamp technique, so neither insulin nor glucagon levels were constant throughout the study. This is both a limitation and an advantage. As a limitation, it does not allow a study of the effect of prolonged exposure to the hormone.

As mentioned in Section 4.2, several hours of high plasma glucagon concentrations could affect the number of receptors. Moreover, the work by El Youssef et al. (2014) reported a loss of glucagon effectivity in a clamped high insulin concentration setting, which cannot be corroborated with this dataset. On the other hand, clamped concentrations of either hormone do not represent physiological conditions, giving insight into more close-to-life conditions.

Data sampling in the trial was constant and thorough from the moment of the glucagon infusion (from $t = 0$ onwards). However, the *Period 1* (Figure 5.1) sampling was irregular, especially for plasma insulin and glucagon. Since the insulin bolus was administered at the time of arrival in the clinic, the bolus effect on plasma insulin concentration is not reflected in the data. This lack of information would pose a problem if insulin dynamics had to be analyzed.

This dataset provides a compelling testbench to validate the glucagon effect model proposed in the previous chapter, offering data on three different glucagon doses in the typically used range of glucagon AP doses.

5.2 Preliminary validation

This section will present the preliminary method used to identify the EGP models and the obtained results. The work was presented in Furió-Novejarque et al. (2022a) and Furió-Novejarque et al. (2022b).

5.2.1 Parameter Identification

Pre-identified values and PK adjustment

The work where the DTU PK/PD model was introduced (Wendt et al., 2017b) identified the model parameters using the same dataset as the present work, presented in the previous section. Hence, individual parameter sets for each patient for the baseline model and DTU EGP were already available. The known parameters are listed in Appendix A, Table A.3. As described in Wendt's work, the values of V and G_{GNG} were constant for all the patients, with a value of 160 ml/kg and 6 μmol/kg/min, respectively. The existence of this pre-identified parameter set simplified the identification process because it allowed us to focus on the EGP-concerning parameters.

However, in a preliminary analysis, it was observed that the given parameter set

Patient	1	2	3	4	5	6	7	8
$k_{2\text{-}A}$	0.14	0.10	0.19	0.25	0.26	0.06	0.28	0.09
$k_{2\text{-}B}$	0.14	0.12	0.19	0.25	0.41	0.06	0.28	0.14
$k_{2\text{-}C}$	0.14	0.50	0.17	0.25	0.19	0.07	0.09	0.06
$Cl_{F,C\text{-}A}$	94.0	114.0	200.0	136.0	106.0	159.0	125.0	91.0
$Cl_{F,C\text{-}B}$	94.0	75.6	200.0	136.0	97.8	159.0	125.0	78.0
$Cl_{F,C\text{-}C}$	94.0	90.1	130.6	136.0	84.8	89.5	86.8	68.7

Table 5.1: Glucagon PK parameters used with dataset 1. Gray-shaded cells highlight the original values. The subscript in each parameter name indicates the visit (A, B, or C).

provided an adequate average fit, but glucagon dynamics on glucose were not properly described on some occasions, further motivating the search for a more adequate model structure.

Furthermore, some of the predefined values for the PK glucagon system did not simultaneously produce an accurate fit for the three glucagon doses. Figure 5.3 provides some illustrative examples of the cases of patients 2 and 8. The blue lines represent the simulation using the pre-identified values. The small doses (100 μg) do not present any discrepancies. However, the simulation for the 200 and 300 μg doses shows some deviations with respect to the data. This may indicate that the dose-response to glucagon is not entirely linear in some cases. Hence, an adjustment of glucagon PK parameters (k_2 and $Cl_{F,C}$, see Equations (4.8b) and (4.8c)) was carried out, searching for a different value for each visit, if necessary. Table 5.1 shows the results for this parameter tuning, where shaded cells represent the original parameter values. Some patients did not need any adjustment of their parameters (i.e., patients 1 and 4), and the provided values were adequate for all 100 μg doses. On the other hand, most patients required tuning for the greater dose, and some needed a parameter change for both visits B and C (e.g., patients 2 and 8, as depicted in Figure 5.3).

Figure 5.4 shows the average resulting simulation output for plasma insulin and glucagon. The fit to the plasma insulin signal with the provided parameter values was adequate. However, for Period 1, the accuracy of the fit could not be assessed due to the data undersampling, as mentioned earlier.

Values for basal insulin and basal glucagon (I_b in Equation 4.7c, and C_b in Equation (4.8c)) were based on the first data measurements of plasma insulin and glucagon when patients had just arrived to the clinic.

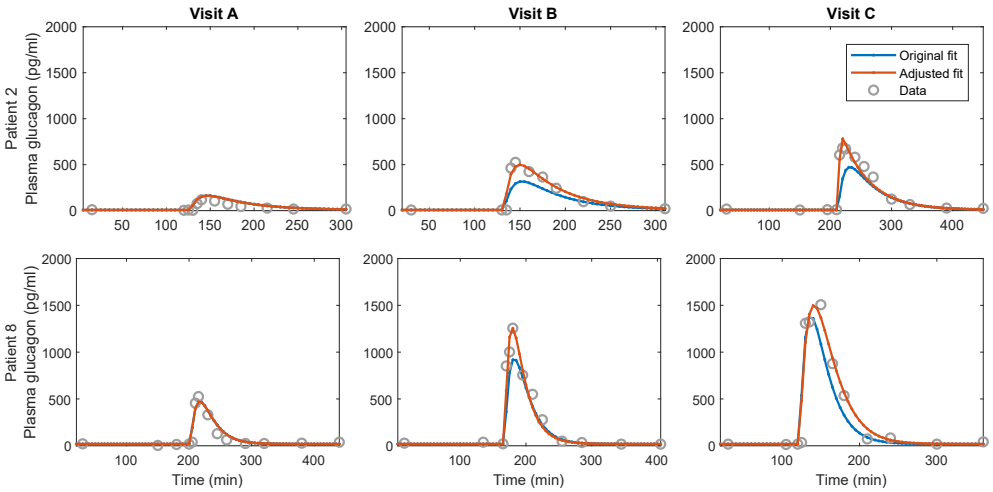

Figure 5.3: Glucagon PK parameters per-visit adjustment for patient 2 (upper row) and patient 8 (lower row) for visit A (left column), visit B (middle column), and visit C (right column). Blue circles represent plasma glucagon data points. Blue lines show the simulation results with the pre-identified parameters provided in Wendt et al. (2017a). Orange lines represent the simulation output after the parameter tuning. Time in the x-axis starts on arrival at the clinic.

Having defined a set of parameters that fits the data as closely as possible will allow to focus the analysis on EGP without the hindering of confounding factors, such as inaccuracy of the inputs to the EGP submodel (plasma insulin and glucagon).

EGP parameter identification

The preliminary identification method consisted of performing an independent optimization for each EGP definition considered. Each EGP model had a reduced parameter set, between three and five parameters each. Although the parameters from the baseline model were pre-identified in a previous work, some of them were included in the identification process, as described in the following sections.

Setting up the optimization framework required the definition of a set of upper and lower bounds for the parameters being identified. These limits were based upon Wendt's previously identified values for the base model parameters and on the reported value in the corresponding original work for each EGP definition (see Section 4.4.1). Hence, the

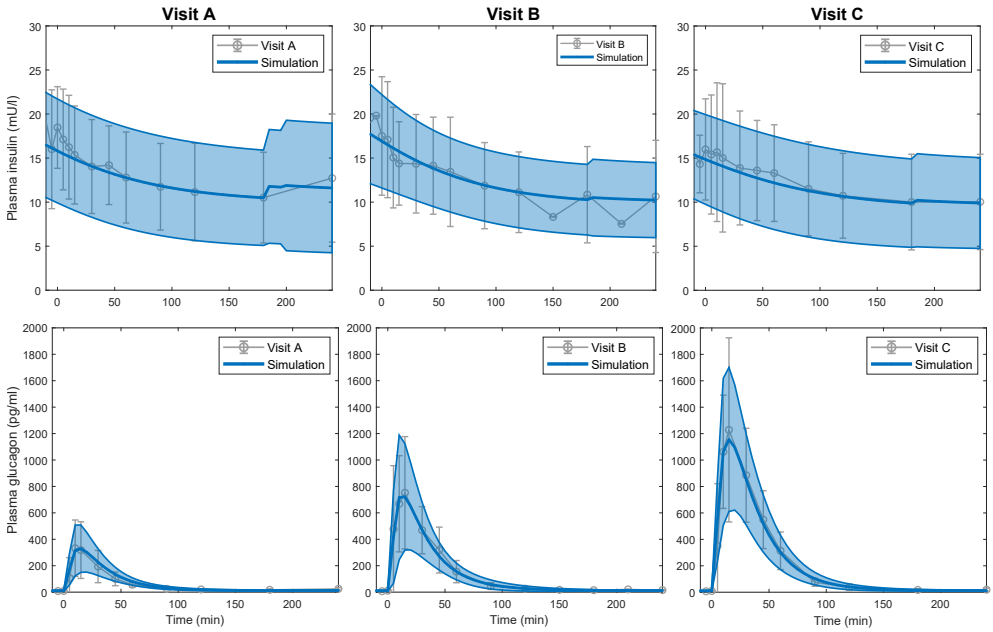

Figure 5.4: Plasma insulin (top row) and glucagon (bottom row) simulation results. Gray error bars correspond to the mean and standard deviation of the data, and continuous colored lines show the simulation results. The gray circles and the central line represent the average of the eight patients, whereas the shaded area encloses the standard deviation. Graphs show the response from $t = 0$ min to 240 min.

bounds for a specific parameter being estimated ($\hat{\theta}$) were defined such that:

$$\hat{\theta}_u = (1 + \alpha) \cdot \max \theta$$
$$\hat{\theta}_l = (1 - \beta) \cdot \min \theta$$

In this expression, the upper limit ($\hat{\theta}_u$) is a deviation from the maximum value reported in the corresponding original works for that specific parameter (θ). Likewise, the lower bound ($\hat{\theta}_l$) is based on the minimum reported value. Values of α and β had a value between 0 and 1 and were adjusted based on the identification results, if necessary.

The main confounding factor in glucose dynamics could be the patient's insulin sensi-

tivity, which can present a wide variability and change over time for a myriad of reasons (Heinemann, 2002). The baseline model incorporates three insulin sensitivity parameters, of which S_T and S_D affect processes unrelated to EGP. Consequently, these parameters were identified not only per patient but also per visit (i.e., each patient gets a different insulin sensitivity in each visit to the clinic).

Along with these parameters, the initial condition for the state $Q_2(t)$ (named Q_{20} henceforth) was also identified for each visit. This allowed for a better fit to the data of each visit, especially in the first part of the trial, where only the insulin effect was present. In simulation studies, the initial state is sometimes associated with equilibrium. However, achieving steady-state conditions in real life is challenging, i.e., the study's starting point is not in equilibrium. Contrary to the value of $Q_1(t = 0)$, which is known from glucose measurements, Q_{20} should be identified for each visit. The rest of the model states were considered to be at equilibrium.

Therefore, the following set of parameters (θ_1) must be identified, for each patient P, and each visit v:

$$\theta_{1P}^{v} = \{S_T, S_D, Q_{20}\}, \quad v = A, B, C;\ P = 1, 2, ..., 8$$

The EGP model subsystem must be able to explain the dose-response from data in Visit A, B, and C, so individualized parameter values must be considered. These sets of parameters for each EGP model are identified per patient. However, they are shared across visits (the same EGP model should be able to explain the response of different glucagon doses).

Regarding the glucagon receptors model, parameters k_{on}, K_r, and V_r were considered in the identification process, representing the activation rate of receptors and the Michaelis-Menten parameters. Since the patients that underwent the glucagon challenge test in Masroor et al. (2019) were healthy people, it was deemed appropriate to tune the activation rate of the receptors. It could be argued that glucagon action is impaired in people with diabetes, which could be explained by a deficit in the activation rate. The remaining parameters in Equation (4.4) were fixed based on the values used in Masroor's work. Parameters EGP_0 and S_I affecting insulin influence on EGP were also identified.

$$\theta_{2P}^{R} = \{k_{on}, K_r, V_r, EGP_0, S_I\}, \quad P = 1, 2, ..., 8$$

Thus, for each patient P, the parameter vector to be optimized for the model with the receptors (R) subsystem is:

$$\Theta_{P}^{R} = \left\{\theta_{1P}^{A}, \theta_{1P}^{B}, \theta_{1P}^{C}, \theta_{2P}^{R}\right\}$$

The cost index J_P (4.15) for the optimization was defined as the aggregated sum of the RMSE (4.14) obtained in each visit.

$$J_P = \sum_{v=1}^{3} RMSE_v \tag{5.2}$$

Having defined the procedure using the receptors EGP model, the next step consisted of identifying the selected EGP models for comparison. As described in Section 4.4.1, the base model equations (insulin PK, glucagon PK, and PD) will be kept the same, and the EGP subsystem will be interchanged according to the evaluated submodel.

The same considerations regarding the insulin sensitivity parameters (i.e., identifying S_T and S_D per visit) and Q_{20} are kept for the other EGP definitions. Hence, the parameter vector for the DTU EGP model will be:

$$\theta_{2P}^{DTU} = \{S_E, E_{max}, C_{E50}, (G_{GNG})\}, \quad P = 1, 2, ..., 8$$

The G_{GNG} parameter is left between brackets because it was considered in the preliminary identification but not in the proof-of-concept described next. The total resulting parameter vector is:

$$\Theta_P^{DTU} = \left\{\theta_{1P}^A, \theta_{1P}^B, \theta_{1P}^C, \theta_{2P}^{DTU}\right\}$$

Then, the corresponding parameter vectors for the McGill EGP will be:

$$\Theta_P^{MG} = \left\{\theta_{1P}^A, \theta_{1P}^B, \theta_{1P}^C, \theta_{2P}^{MG}\right\}$$

where,

$$\theta_{2P}^{MG} = \left\{G_{ng}, S, T, K_{Gd}, T_{Gd}\right\}, \quad P = 1, 2, ..., 8$$

And for the OHSU EGP:

$$\Theta_P^{OU} = \left\{\theta_{1P}^A, \theta_{1P}^B, \theta_{1P}^C, \theta_{2P}^{OU}\right\}$$

where,

$$\theta_{2P}^{OU} = \{EGP_0, S_f, k_{g3}, k_g, k_c\}, \quad P = 1, 2, ..., 8$$

The optimization was performed with Matlab R2018b using the `fmincon` function, as described in Section 4.4.2, and, in order to avoid local minima, the process was repeated ten times per patient, assigning different random initial guesses of the parameter values within predefined limits based on the pre-identified values.

5.2.2 Structural identifiability analysis

Once the parameter collection had been selected for the identification process, a structural identifiability analysis was carried out to ensure that the models were at least structurally locally identifiable regardless of the EGP definition used.

A separate analysis was carried out for each combination of the baseline model plus EGP submodel. The parameters included in the analysis were the corresponding to each EGP model along with S_T and S_D. The identifiability tableaus provided by the GenSSI software (Section 4.4.2) are presented in Figure 5.5. As no parameter presents an empty column in the tableaus, all parameters are structurally identifiable. This conclusion is also confirmed by the software output text, which stated that all parameters in each analysis were structurally globally identifiable.

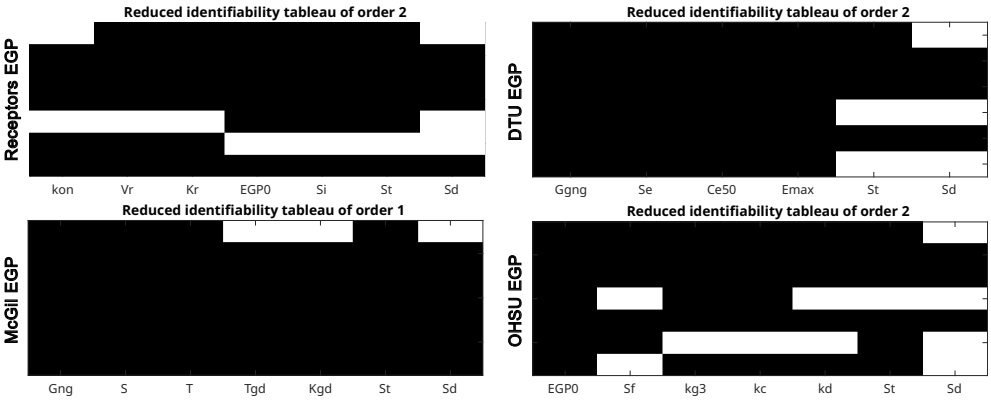

Figure 5.5: Identifiability tableaus for each EGP model obtained with the GenSSI Matlab toolbox. A not-colored column would indicate an unidentifiable parameter. Since there are no empty columns, all models are globally structurally identifiable.

5.2.3 Results

Proof-of-concept results

In order to obtain a quick assessment of whether the use of the glucagon receptors in the description of glucagon action provided any improvements, a proof-of-concept validation was carried out. The process compared the proposed model to the base model with the DTU EGP. For this identification, the G_{GNG} parameter in θ_{2P}^{DTU} was left constant. The parameter values obtained per patient in this analysis can be found in Table A.1 (Receptors EGP parameters) and Table A.2 (DTU EGP parameters). The parameters used in the baseline model were taken from the previous identification by Wendt, and they are detailed in Table A.3.

	Receptors RMSE	DTU RMSE	t	p	Cohen's d
Overall	19.65 ± 5.45	25.57 ± 0.55	3.20	0.015*	1.13
Visit A	5.54 ± 1.46	6.48 ± 1.44	-2.17	0.066	-0.77
Visit B	8.55 ± 3.28	9.47 ± 3.00	-1.57	0.161	-0.55
Visit C	5.56 ± 2.32	9.61 ± 3.85	-3.10	0.017*	-1.10

Table 5.2: RMSE results (expressed in mg/dl) and statistical analysis for the proof-of-concept validation, separated per visit. Results, expressed as mean $\pm$ standard deviations, provide the J_P index of the receptors EGP and DTU EGP, t-test analysis, and Cohen's d. d.f.=7. The symbol * indicates a p-value lower than 0.05.

After simulating all eight patients, the results for index J_P (5.2) were analyzed. The overall mean J_P value with the glucagon receptors proposal was 19.65 $\pm$ 5.45 mg/dl whereas the mean result with the DTU EGP was 25.57 $\pm$ 5.5 mg/dl. A statistical analysis was performed using R (version 4.2.1). Three different normality tests (Shapiro-Wilk, Kolmogorov-Smirnov, and Anderson-Darling) were performed, which confirmed that both data distributions were normal. Next, a t-test was applied to see if there were statistically significant difference between both approaches, providing as a result, the t-test value and its p-value. As shown in Table 5.2, the analysis provided a p-value of 0.015, proving that there was a statistically significant difference. Cohen's d size effect measurement was also included to complement these results. This metric quantifies the size of the difference between two sets. The conventional interpretation of Cohen's d values considers a 0.2 absolute value represents a small difference, 0.5 is a medium effect, and 0.8 or a higher value indicates a large difference (McGough and Faraone, 2009).

The difference in the J_P values per visit was also analyzed. The results show that the average error value is lower in every visit for the proposed EGP, especially in visit C (300 μg glucagon dose), where there is the most significant difference between both models. Note that a trend to increase residuals with respect to the glucagon dose is observed in the DTU model, contrary to our proposal. As a matter of fact, there was a statistically significant difference between the RMSE in Visit C. Visit A results provided a Cohen's d size effect close to 0.8 also indicate that the difference is not negligible.

Preliminary validation results

Given the positive results of the receptors EGP model, the comparison was extended to include McGill EGP and OHSU EGP models in the identification. These two models, as the receptors proposal, add five parameters each to the parameter vectors to be identified (see θ_{2P}^{R}, θ_{2P}^{MG}, and θ_{2P}^{OU}). Consequently, the parameter G_{GNG} was added to the DTU model identification to raise its parameter count to four to be closer to the other EGP definitions, making the process more fair.

The identifications were carried out according to the procedure described above, optimizing index J_P, which provided four separate parameter sets accompanying each EGP submodel. Table 5.3 presents the average value and standard deviation for each identified parameter. Each quadrant of the table presents each of the evaluated models. The parameter results for the receptors EGP were virtually identical to the ones obtained in the proof-of-concept identification. Parameters for the DTU EGP experimented a more significant change since a new parameter was added. The individual parameter values for each model are detailed in Tables A.4 to A.7. The parameters for the baseline model were the same as the proof-of-concept validation.

Table 5.4 shows the RMSE results as mean $\pm$ standard deviation of each EGP comparator, separated per visit. The mean values aggregate the results obtained for the eight patients of the dataset. Each result was compared against the results obtained with the receptors proposal, and paired t-tests were performed to assess the differences between them. An ANOVA test could have been used to explore the existence of statistically significant difference between all the groups of models in the work. However, the focus of the analysis was whether there were differences between the receptors model and every other pair, so a series of t-tests were obtained instead applied to the cases of interest only. The same evaluation was performed separating the results per period, presented in Table 5.5.

As seen in Table 5.4, there are no statistically significant differences between the receptors model and the comparators in Visit B. For Visit A, there is only a statistically

significant difference between the OHSU and receptors EGP. This would indicate that any of the models would adequately describe the dynamics of small glucagon doses. Nevertheless, note that the lowest RMSE was obtained with the receptors model on every occasion. On the other hand, there is a statistically significant difference with every comparator in Visit C, where the 300 μg dose was administered.

Receptors	Parameter	Value	DTU	Parameter	Value
EGP	$k_{on} \cdot 10^{-6}$	41.88 ± 33.92	EGP	E_{max}	87.17 ± 13.76
	V_r	103.40 ± 47.24		C_{E50}	688.9 ± 225.5
	$K_r \cdot 10^{-3}$	75.98 ± 97.49		$S_E \cdot 10^{-4}$	93.15 ± 125.05
	$S_I \cdot 10^{-3}$	25.39 ± 16.66		G_{GNG}	5.62 ± 1.62
	EGP_0	7.63 ± 2.84			
BM	$S_{T\text{-}A} \cdot 10^{-4}$	37.54 ± 11.06	BM	$S_{T\text{-}A} \cdot 10^{-4}$	28.92 ± 14.13
	$S_{T\text{-}B} \cdot 10^{-4}$	28.07 ± 6.90		$S_{T\text{-}B} \cdot 10^{-4}$	25.93 ± 6.38
	$S_{T\text{-}C} \cdot 10^{-4}$	32.43 ± 15.41		$S_{T\text{-}C} \cdot 10^{-4}$	41.09 ± 10.57
	$S_{D\text{-}A} \cdot 10^{-4}$	2.47 ± 1.88		$S_{D\text{-}A} \cdot 10^{-4}$	2.39 ± 1.76
	$S_{D\text{-}B} \cdot 10^{-4}$	3.33 ± 2.29		$S_{D\text{-}B} \cdot 10^{-4}$	3.30 ± 1.98
	$S_{D\text{-}C} \cdot 10^{-4}$	3.06 ± 1.90		$S_{D\text{-}C} \cdot 10^{-4}$	3.25 ± 2.04
	$Q_{20\text{-}A}$	2040.0 ± 544.0		$Q_{20\text{-}A}$	1734.0 ± 730.0
	$Q_{20\text{-}B}$	1772.0 ± 619.0		$Q_{20\text{-}B}$	1732.0 ± 545.0
	$Q_{20\text{-}C}$	1477.0 ± 687.0		$Q_{20\text{-}C}$	1880.0 ± 729.0
McGill	Parameter	Value	OHSU	Parameter	Value
EGP	$T \cdot 10^{-2}$	11.65 ± 9.94	EGP	$k_{g3} \cdot 10^{-6}$	8.50 ± 3.90
	K_{Gd}	2.32 ± 4.09		k_d	25.61 ± 16.15
	$T_{Gd} \cdot 10^{-2}$	22.38 ± 26.77		$k_c \cdot 10^{-2}$	65.04 ± 34.12
	$S \cdot 10^{-3}$	21.57 ± 16.58		$S_f \cdot 10^{-6}$	26.48 ± 45.23
	G_{ng}	7.03 ± 1.18		EGP_0	7.58 ± 1.72
BM	$S_{T\text{-}A} \cdot 10^{-4}$	22.16 ± 15.88	BM	$S_{T\text{-}A} \cdot 10^{-4}$	19.83 ± 14.47
	$S_{T\text{-}B} \cdot 10^{-4}$	20.84 ± 7.33		$S_{T\text{-}B} \cdot 10^{-4}$	21.16 ± 8.99
	$S_{T\text{-}C} \cdot 10^{-4}$	43.76 ± 8.43		$S_{T\text{-}C} \cdot 10^{-4}$	43.16 ± 8.41
	$S_{D\text{-}A} \cdot 10^{-4}$	1.51 ± 0.67		$S_{D\text{-}A} \cdot 10^{-4}$	1.72 ± 1.05
	$S_{D\text{-}B} \cdot 10^{-4}$	3.48 ± 1.84		$S_{D\text{-}B} \cdot 10^{-4}$	4.08 ± 1.52
	$S_{D\text{-}C} \cdot 10^{-4}$	3.40 ± 1.88		$S_{D\text{-}C} \cdot 10^{-4}$	3.27 ± 2.02
	$Q_{20\text{-}A}$	1291.0 ± 782.0		$Q_{20\text{-}A}$	1190.0 ± 668.0
	$Q_{20\text{-}B}$	1386.0 ± 579.0		$Q_{20\text{-}B}$	1445.0 ± 777.0
	$Q_{20\text{-}C}$	1880.0 ± 705.0		$Q_{20\text{-}C}$	1774.0 ± 759.0

Table 5.3: Preliminary validation parameter values summary. Values are expressed as mean $\pm$ standard deviation. Parameters S_T, S_D, and Q_{20} were adjusted per visit (A, B, C). The identification of each model was performed separately. *EGP* sections include the EGP-related parameters, and *BM* sections include the parameters related to the base model.

Visit	Model	Comparators RMSE	Receptors RMSE	t	p	Cohen's d
A	DTU	6.35 ± 1.34	5.54 ± 1.46	1.72	0.128	0.61
	McGill	8.74 ± 3.58		2.27	0.058	0.80
	OHSU	8.27 ± 2.71		2.44	0.045*	0.86
B	DTU	9.23 ± 3.18	8.55 ± 3.28	1.72	0.128	0.61
	McGill	8.64 ± 3.43		0.16	0.880	0.06
	OHSU	10.32 ± 5.14		1.60	0.153	0.57
C	DTU	8.03 ± 2.65	5.56 ± 2.32	3.11	0.017*	1.10
	McGill	7.54 ± 2.09		2.42	0.046*	0.86
	OHSU	8.27 ± 2.15		3.25	0.014*	1.15

Table 5.4: RMSE results (mg/dl) and statistical analysis for the preliminary validation. Results include mean $\pm$ standard deviation of the receptors EGP, DTU EGP, McGill EGP, and OHSU EGP. Paired t-test are used to compare the performance of the receptors EGP against each EGP comparator per **visit**. The symbol * indicates a p-value lower than 0.05.

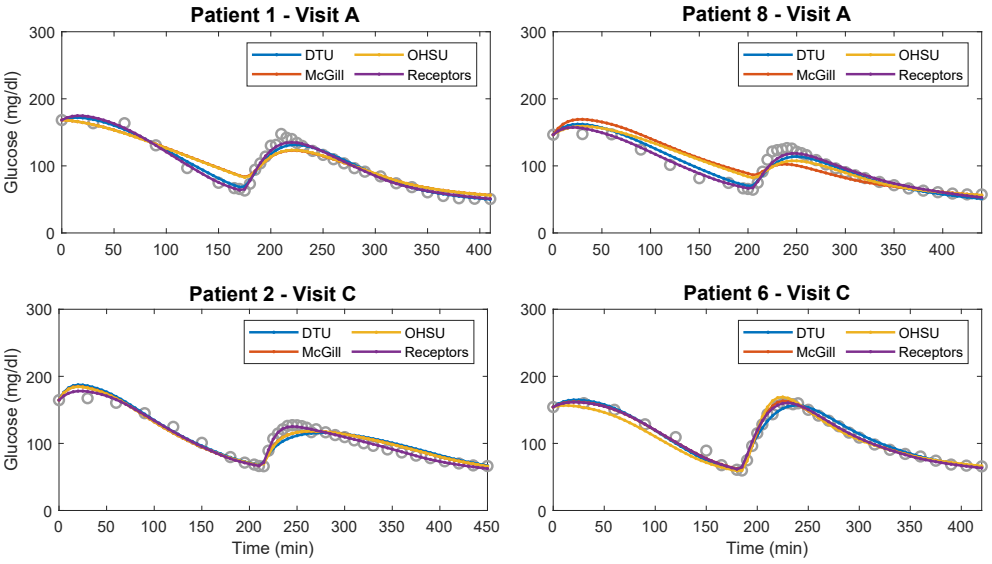

Figure 5.6: Simulation results sample from the preliminary validation. Gray circles represent data points. Upper row plots present visit A results with the four tested models for patients 1 and 8. Lower row plots show visit C results for patients 2 and 6.

Period	Model	Comparators RMSE	Receptors RMSE	t	p	Cohen's d
1	DTU	7.57 ± 3.03	6.63 ± 2.53	2.90	0.023*	1.02
	McGill	9.17 ± 4.73		2.36	0.051	0.83
	OHSU	9.58 ± 4.43		3.41	0.011*	1.21
2	DTU	6.74 ± 1.56	5.47 ± 1.72	2.70	0.031*	0.95
	McGill	6.85 ± 1.40		2.60	0.035*	0.92
	OHSU	7.47 ± 1.55		4.72	0.002*	1.67
Total	DTU	7.87 ± 1.69	6.55 ± 1.82	3.01	0.020*	1.06
	McGill	8.31 ± 1.99		2.78	0.027*	0.98
	OHSU	8.95 ± 2.05		5.58	<0.001*	1.97

Table 5.5: RMSE results (mg/dl) and statistical analysis for the preliminary validation. Results include mean $\pm$ standard deviation of the receptors EGP, DTU EGP, McGill EGP, and OHSU EGP. Paired t-test are used to compare the performance of the receptors EGP against each EGP comparator per **period**. The symbol * indicates a p-value lower than 0.05.

Table 5.5 shows the analysis of RMSE values at three different periods: (1) considering the first part only (*Period 1*), from the start time of the clinical trial until the glucagon bolus was administered (from the arrival to the clinic to $t = 0$ min, see Figure 5.1); (2) from the moment the glucagon was administered onward (*Period 2*), from t = 0 to t = 240 min. This period is the main area of interest in this study, where the glucagon effect comes into play; (3) along all the time of the experiment (*Total time*).

The results presented in this table aggregate the average error values from the three visits. The results over the total time of the experiment (bottom section of Table 5.5) show that the receptors proposal provides a better fit to the data, with a statistically significant difference against all three comparators. On the other hand, the glucagon receptors proposal in Period 2, which focuses on describing the glucagon dynamics, also presents the lowest RMSE, with statistically significant differences between it and each of the comparators. Nevertheless, Period 1 also presents significant differences with two of the comparators. This difference will contribute to the overall error differences. However, there is no glucagon action but the basal EGP values, which should be similar regardless of the EGP definition.

This highlights some limitations of the procedure since there seems to be a greater source of error in the first period of the experiments, which may taint the interpretation of the overall results. Also, although the parameter set chosen for identification is structurally identifiable, there is much variability between each model identification. This means the

differences observed between the models cannot only be attributed to the EGP definitions but also to the differences in S_T, S_D, and Q_{20}, which are different for every model. This situation motivated the next work, which modified the identification process.

Figure 5.6 shows some sample simulation results for a selection of patients. The upper row graphs show some examples where the difference in fit made that the first part of the data was not so well-adjusted for some models, and the initial point for the models at $t = 0$ is not the same. On the other hand, the lower row depicts two examples at the higher glucagon dose (visit C), where the glucagon receptors model provided a better fit than the comparators.

5.3 Validation 1

This section presents the identification procedure and final identification results as published in Furió-Novejarque et al. (2023b).

5.3.1 Parameter Identification

In the preliminary validation of the receptors-based EGP proposal, each model was identified independently. However, since multiple EGP definitions are used in the validation, but the baseline model is common to all of them, the identification method was revised taking into account that:

1. The parameters in the baseline model should be the same for each one of the complete models.
2. Instead of carrying out separate optimizations for each one of the models, the required set of parameters should be found for all models in the same optimization problem. This way, the parameters of the base model will be shared by all EGP definitions.
3. The aim is to test each model structure, not finding a global model for all the patients. Hence, a different set of parameters will still be identified for each patient.

With these premises in mind, the identification procedure was updated in order to find the best fit for the data for all the models while being equally fair and minimizing the potential confounding factors. This way, the parameter differences among executions with different EGP definitions will only be attributed to the EGP definitions themselves.

In solving the optimization problem, each model was executed three times, one for each visit (v) to the clinic. Then, for each model (m), an index was calculated as the aggregated sum of the RMSE per visit:

$$J_m = \sum_{v=1}^{3} RMSE_v \tag{5.3}$$

The total optimization index obtained per patient (P) for the optimization function was defined as the average value of J_m for the four models.

$$J_P = \frac{1}{4} \sum_{m=1}^{4} J_m \tag{5.4}$$

As in the previous validation, insulin sensitivity-related parameters, S_T and S_D, were identified per visit. Also, the initial condition for the state $Q_2(t)$ (Q_{20}). Defining once again the total parameter vector to be identified, the first element will contain the parameters from the base model:

$$\theta_{1P}^{v} = \{S_T^v, S_D^v, Q_{20}^v\}, \quad v = 1, 2, 3;\ P = 1, 2, ..., 8$$

Then, a different subset of parameters is defined for the receptors EGP model: the DTU EGP, the McGill EGP, and the OHSU EGP, respectively.

$$\theta_{2P} = \{EGP_0, S_I, k_{on}, K_r, V_r\}, \quad P = 1, 2, ..., 8$$

$$\theta_{3P} = \{G_{GNG}, S_E, E_{max}, C_{E50}\}, \quad P = 1, 2, ..., 8$$

$$\theta_{4P} = \{G_{ng}, S, T, K_{Gd}, T_{Gd}\}, \quad P = 1, 2, ..., 8$$

$$\theta_{5P} = \{EGP_0, S_f, k_{g3}, k_g, k_c\}, \quad P = 1, 2, ..., 8$$

With this, the total parameter vector will consist of 28 parameters to be identified per patient.

$$\Theta_P = \left\{\theta_{1P}^A, \theta_{1P}^B, \theta_{1P}^C, \theta_{2P}, \theta_{3P}, \theta_{4P}, \theta_{5P}\right\}$$

The four models were simulated within the same optimization process, but the baseline model parameters were common regardless of the EGP definition. The structural identifiability was not assessed once again because the subset of parameters "per model" remains the same as in the previous identification.

Due to the longer computation times caused by the significant increase in the number of parameters, the identification was repeated only five times per patient (instead of the previous ten).

5.3.2 Results

Table 5.6 presents a summary of the parameter values obtained in the optimization process. In this case, only one set of parameters related to the baseline model is reported since it was common to all EGP definitions. The individual parameters obtained for each patient for each EGP model are listed in Tables A.8 to A.11. The identified baseline model parameters can be found in Table A.12. The rest of the model's parameters remain as described in Table A.3. The overall performance of each model in describing glucose dynamics is described in Figure 5.7.

The statistical analysis performed in the preliminary validation was replicated to analyze the present results. Table 5.7 shows the comparison of RMSE between the receptors model and each EGP comparator, separated by visit. In these results, the only statistically significant differences are found in visit A, against the McGill and OHSU model, and the DTU model in visit C. In this identification, the base model accompanying each EGP definition was the same (see BM parameters in Table 5.6), which equalizes the model outputs.

However, the main interest of the analysis lies in the time period differences since the analysis of Period 2 would provide more insight into the contributions of the receptors model, which is precisely the period where there are more noticeable differences. Table 5.8 presents the results of this analysis, where the outcomes favor the proposed EGP model. In contrast to the previous identification, there are no statistically significant differences in the Period 1 of the data. This solves one of the limitations assessed in the previous validation. Having the same baseline model has contributed making the models' execution closer to each other in the first part of the data so that their behavior on basal glucagon conditions is consistent independently of the EGP model. On the other hand, considering the total

Receptors	Parameter	Value	DTU	Parameter	Value
EGP	$k_{on} \cdot 10^{-6}$	12.80 ± 17.31	EGP	E_{max}	92.25 ± 10.32
	V_r	140.38 ± 50.19		C_{E50}	792.7 ± 209.2
	$K_r \cdot 10^{-3}$	49.37 ± 76.39		$S_E \cdot 10^{-4}$	63.36 ± 75.84
	$S_I \cdot 10^{-3}$	23.68 ± 19.69		G_{GNG}	5.63 ± 2.78
	EGP_0	7.72 ± 2.49			
McGill	**Parameter**	**Value**	**OHSU**	**Parameter**	**Value**
EGP	$T \cdot 10^{-2}$	8.67 ± 6.33	EGP	$k_{g3} \cdot 10^{-6}$	10.55 ± 1.62
	K_{Gd}	2.68 ± 3.37		k_d	0.44 ± 0.35
	$T_{Gd} \cdot 10^{-2}$	31.54 ± 22.38		$k_c \cdot 10^{-2}$	0.41 ± 0.46
	$S \cdot 10^{-3}$	15.90 ± 10.97		$S_f \cdot 10^{-6}$	39.19 ± 41.05
	G_{ng}	7.12 ± 2.34		EGP_0	7.42 ± 2.81

	Parameter	Value
BM	$S_{T\text{-}A} \cdot 10^{-4}$	33.68 ± 22.14
	$S_{T\text{-}B} \cdot 10^{-4}$	27.12 ± 14.38
	$S_{T\text{-}C} \cdot 10^{-4}$	50.54 ± 28.71
	$S_{D\text{-}A} \cdot 10^{-4}$	1.31 ± 0.96
	$S_{D\text{-}B} \cdot 10^{-4}$	27.97 ± 70.32
	$S_{D\text{-}C} \cdot 10^{-4}$	447.10 ± 1253.90
	$Q_{20\text{-}A}$	1828.0 ± 1033.0
	$Q_{20\text{-}B}$	1952.0 ± 798.0
	$Q_{20\text{-}C}$	2289.0 ± 991.0

Table 5.6: Validation 1 parameter values summary. Values are expressed as mean $\pm$ standard deviation. Parameters S_T, S_D, and Q_{20} were adjusted per visit in the dataset (A, B, C). The identification of each model was performed in the same optimization process. *EGP* sections include the EGP-related parameters, and the *BM* section includes the parameters related to the base model.

experiment time, we find a statistically significant difference between each comparator and the receptors model. This means that the lack of significance in the results per visit may be hindered by the contribution of the first part of the data, where the behavior of the models has been regularized.

Having no statistically significant difference in Period 1 agrees with the expected results since, in that interval, the EGP model only contributes as a constant (basal value) to the general model. Our hypothesis was that no matter the EGP model used, the behavior in Period 1 should be similar across models in order to provide a fair comparison. The first period also shows the greater standard deviation in the error values. This is due to

Visit	Model	Comparators RMSE	Receptors RMSE	t	p	Cohen's d
A	DTU	6.36 ± 1.36	6.26 ± 1.18	0.48	0.644	0.17
	McGill	9.27 ± 2.43		3.68	0.008*	1.30
	OHSU	8.88 ± 2.48		3.17	0.016*	1.12
B	DTU	9.22 ± 2.78	8.92 ± 3.39	0.76	0.474	0.27
	McGill	9.60 ± 3.43		1.30	0.235	0.46
	OHSU	11.11 ± 4.99		2.20	0.063	0.78
C	DTU	7.70 ± 1.79	6.21 ± 2.07	2.58	0.036*	0.91
	McGill	6.48 ± 1.69		0.39	0.712	0.14
	OHSU	6.96 ± 1.70		0.96	0.370	0.34

Table 5.7: RMSE results (mg/dl) and statistical analysis for Validation 1. Results include means $\pm$ standard deviations of the receptors EGP, DTU EGP, McGill EGP, and OHSU EGP. Paired t-test are used to compare the performance of the receptors EGP against each EGP comparator per **visit**. The symbol * indicates a p-value lower than 0.05.

the scarce data available in the first part of the experiment, which caused the fits to have greater RMSEs, and also the significant variability in the initial conditions (i.e., there is no information about the patients' state prior to arriving at the clinic).

Finally, considering the total time of the experiments across the three visits, there is a statistically significant difference comparing the receptors EGP performance to the McGill and the OHSU model. Also, Cohen's d values (larger than 0.8) confirm that there is a noticeable difference in the behavior between the analyzed pairs. Although the difference was not significant compared to the DTU model, the p-value is close to being lower than 0.05, and Cohen's d is also close to 0.8, meaning that the difference is not negligible. Additionally, regardless of the statistical analyses, the average error obtained with the receptors model was lower on every occasion, both in the analysis per time period and per visit.

5.4 Discussion

This work's results show how including glucagon receptor dynamics in the EGP model provides an improvement in describing the glucagon effect when compared with other EGP models from the literature. The RMSE results tables in this chapter reflect this fact, showing a lower average error value for the glucagon receptors model and a statistically

Period	Model	Comparators RMSE	Receptors RMSE	t	p	Cohen's d
1	DTU	7.22 ± 2.15	7.21 ± 2.36	0.02	0.985	0.01
	McGill	8.84 ± 3.01		1.78	0.118	0.63
	OHSU	8.64 ± 2.82		1.58	0.159	0.56
2	DTU	6.64 ± 1.58	5.90 ± 1.75	2.43	0.046*	0.86
	McGill	7.18 ± 1.32		3.85	0.006*	1.36
	OHSU	7.81 ± 1.75		3.06	0.018*	1.08
Total	DTU	7.76 ± 1.45	7.13 ± 1.71	2.18	0.066	0.77
	McGill	8.45 ± 1.38		3.44	0.011*	1.22
	OHSU	8.99 ± 1.62		3.74	0.007*	1.32

Table 5.8: RMSE results (mg/dl) and statistical analysis for Validation 1. Results include mean $\pm$ standard deviations of the receptors EGP, DTU EGP, McGill EGP, and OHSU EGP. Paired t-test are used to compare the performance of the receptors EGP against each EGP comparator per **period**. The symbol * indicates a p-value lower than 0.05.

significant difference for each of the comparisons in Period 2, which is the main area of interest of this analysis.

The validation framework was designed to ensure fairness in the process comparison, using the same baseline model (same equations in the preliminary validation and the same equations and parameters in Validation 1) and the same optimization process for each of them. Three out of four EGP definitions use five parameters to adjust glucose behavior, while the remaining model (DTU EGP) uses four. While having one parameter less, it does not act to the detriment of its performance since it produces the second-best results in the evaluated scenarios.

The two identification procedures presented in this chapter present significant differences. In the preliminary identification, the EGP models were given independence from each other, and the adjusted parameters from the base model were allowed to take different values. Still, the optimization seemed to converge to similar results since the pair of S_t - S_d values per visit is in a similar order of magnitude for the four models (see Table 5.3). On the other hand, the Validation 1 method forced the base model parameters to be the same in every case, and that causes a change of parameters both for the base model and the EGP model parameters (Table 5.6).

Figure 5.8 shows a comparison of the average RMSE values obtained for the two validations in this chapter, separated by visit (columns) and period (rows). The analyses

presented in Table 5.4 and Table 5.7 would correspond to boxplots for Visit A, B, and C, in the "Total time" row. On the other hand, results in Table 5.5 and Table 5.8 correspond to the "Overall" column of Period 1, Period 2 and, Total time results.

The second validation method constrained the models' behavior, so the outputs of the models are more alike between them. However, it helps ensure that the observed differences are indeed due to the EGP definitions only and that no other confounding factors are involved. The RMSE overall results were lower with the preliminary validation since the optimizer had the liberty to assign parameter values and provided the best fit to each model individually. In contrast, in Validation 1, the optimizer had to find a compromise in the base model parameters to adequate the results to the four EGP definitions. The second method resulted in a lower number of identified parameters in total, but it obtained them all in the same identification, increasing the computational cost of the problem.

This dataset provides the chance to analyze the performance of different EGP models in a setting where single small glucagon doses are delivered. These could reflect the scenario of a dual-hormone AP glucagon delivery, using glucagon dosing to prevent mild hypoglycemia. The RMSE variability for all four definitions seems to be reduced for the greatest glucagon dose. It may also be due to the fact that it is the dose with the greatest variability in the dataset, compared to the 100 and 200 μg doses (see Figure 5.7).

With this dataset, the influence of circulating insulin on glucagon effect could not be assessed. As shown in Figure 5.4, plasma insulin levels were stable during Period 2, when glucagon was in effect, with an average value of approximately 15 mU/l. According to the results reported by El Youssef et al. (2014), maintained high plasma insulin may impair glucagon effect. Their results report a high plasma insulin concentration of around 40 mU/l, which is not close to the conditions of the data in Ranjan et al. (2016).

Even after the second validation performed, this work presents some limitations, which include:

- The reduced number of patients in the clinical dataset only allows for drawing preliminary conclusions. An added difficulty is the fact that clinical trials devoted to studying physiological characteristics (i.e., that require patients to be in-clinic) are usually performed with a reduced sample of patients (typically between 10 and 20, (Ranjan et al., 2017; El Youssef et al., 2014; Castle et al., 2015)).
- There is a slight inaccuracy in the fit to the data close to $t = 0$. As seen in Figure 5.7, some models did not exactly reach the point of interest at t = 0, which might also indicate a limitation in the insulin pharmacokinetics models.

- The large number of parameters to be identified. A long time was needed to solve the optimization problem, which makes it infeasible to solve online within an AP algorithm.
- Further validation should include different datasets in a variety of conditions, such as larger glucagon doses, higher plasma insulin concentrations, close-in-time repeated glucagon doses, a larger number of patients, or using several datasets.

5.5 Conclusion

This chapter has performed the validation of the EGP model based on glucagon receptors proposed in the previous chapter. A set of clinical data has allowed testing the model against single glucagon doses of 100, 200, and 300 μg. The validation consisted of identifying the model and three other EGP definitions from the literature and comparing their performance based on the RMSE. Two different identification methods were used, and the receptors model provided the lowest error on both occasions.

The results obtained in this study will open for consideration incorporating EGP models that include glucagon receptor dynamics into other T1D simulators. To our knowledge, it has yet to be incorporated into any widely-used simulator. However, it could improve the accuracy of the *in silico* experiments, providing a more physiology-based definition.

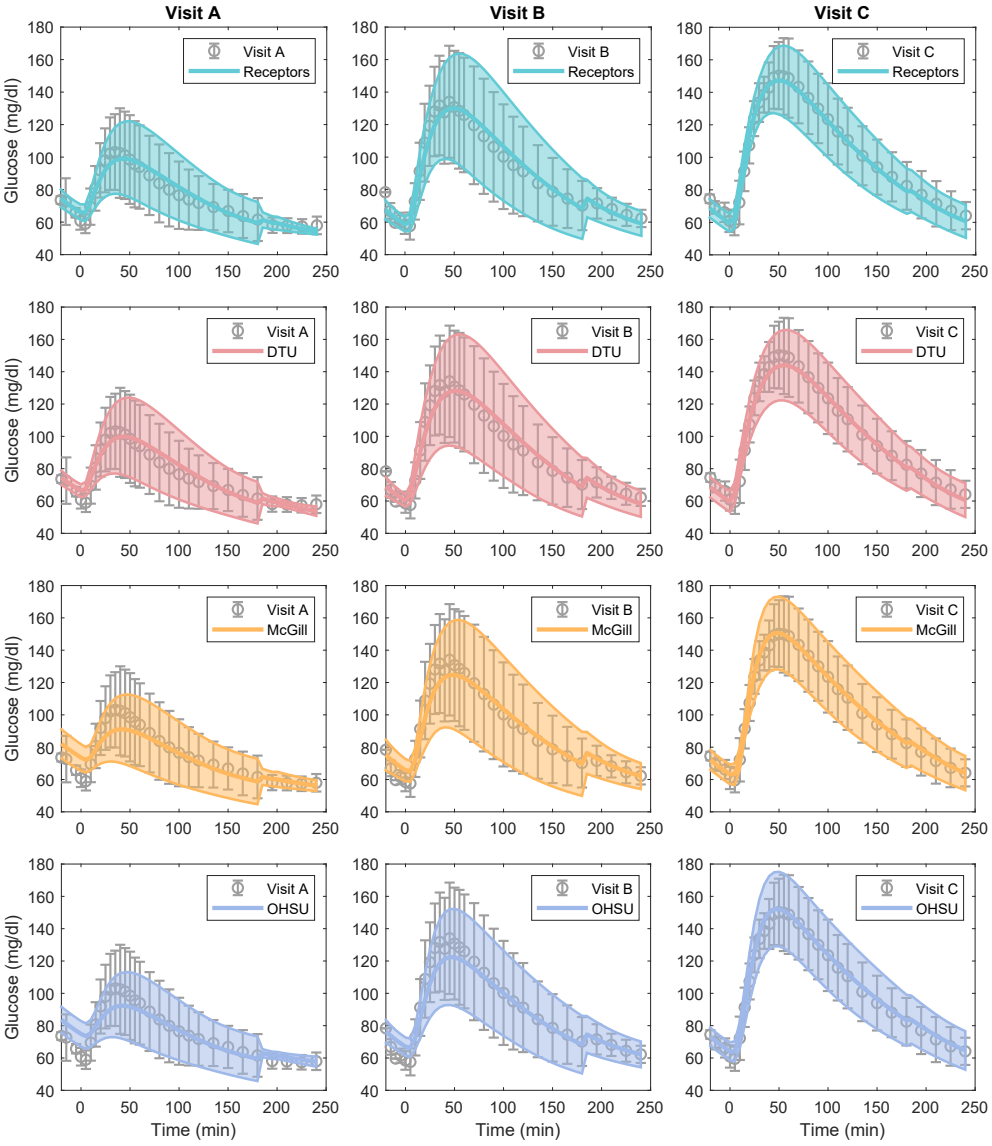

Figure 5.7: Overall glucose outcomes in Validation 1. Gray error bars represent the data mean and standard deviation. Colored lines represent the mean simulation results, and colored areas enclose their standard deviation. Each row presents the results for a different EGP model. Columns correspond to the data from each visit.

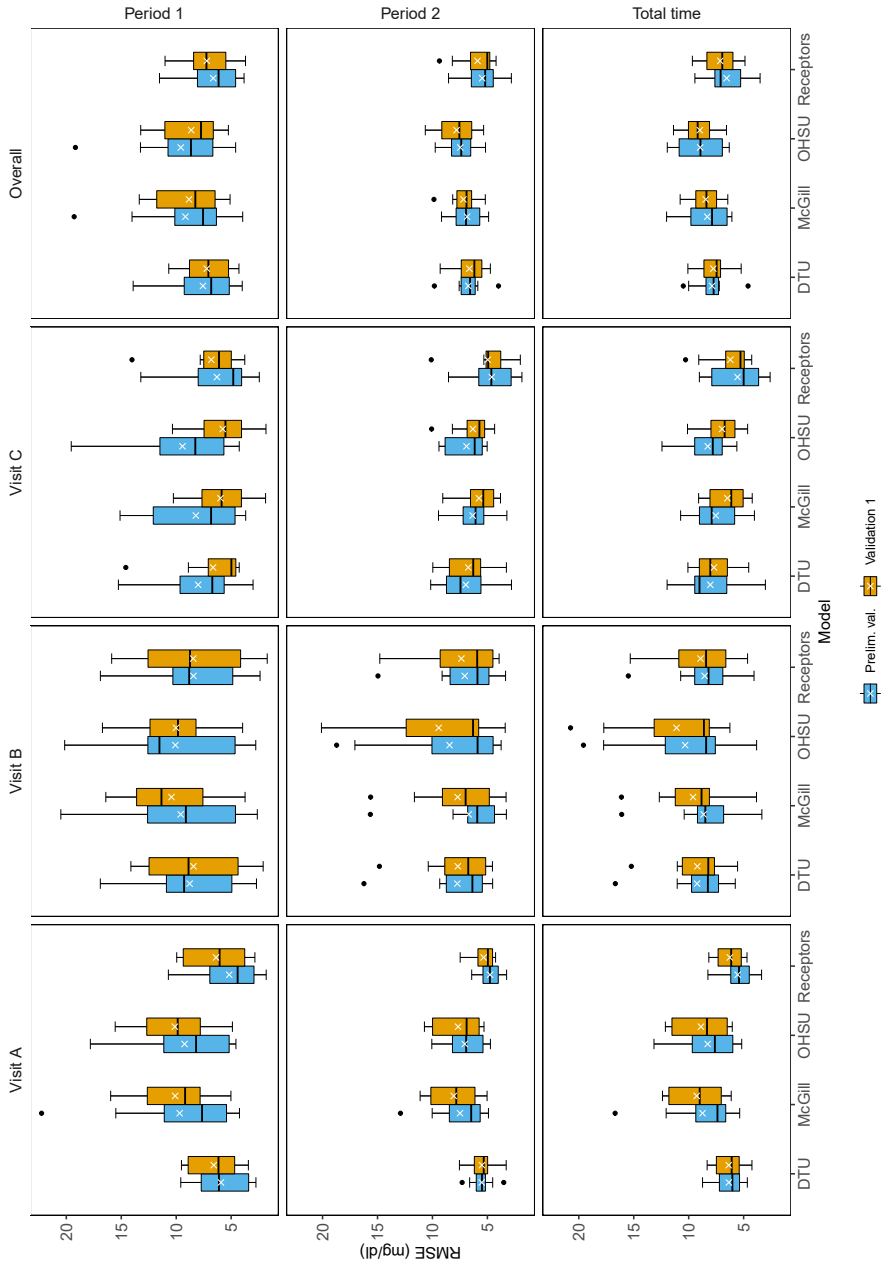

Figure 5.8: General RMSE comparison between the preliminary validation method (blue boxes) and Validation 1 (orange boxes). Rows represent the considered period times. Columns represent the visits. The "Overall" column considers the average values of the visits.

Chapter 6

Glucagon model validation against multiple doses with different diets

This chapter offers a second validation of the glucagon receptors-based EGP model using a new clinical data set. In contrast to the previous work, the data includes ten patients and consecutive glucagon doses (100 and 500 μg) in the same experiment. Three different identification methods are carried out to test the proposed model structure. The results of the procedures obtained in this chapter lead to the publication of a conference paper:

- *Furió-Novejarque, C., Sala-Mira, I., Ranjan, A.G., et al. (2023). Validation of a model of glucagon action including glucagon receptor dynamics under consecutive doses in low and high-carb diets. 22nd World Congress of the International Federation of Automatic Control (IFAC WC 2023). Yokohama (Japan). IFAC-PapersOnLine, 56(2):9666–9671.*

Additionally, a journal paper expanding the results of the previous publication is under review:

- *Furió-Novejarque, C., Sala-Mira, I., Ranjan, A.G., et al. Analysis on the contribution of glucagon receptors to glucose dynamics in type 1 diabetes. IFAC Journal of Systems and Control - Invitation to Special Issue. Submitted.*

6.1 Data collection

The clinical datasets used in this chapter were obtained in the clinical trial by Ranjan et al. (2017) and were provided by the Steno Diabetes Center in Copenhagen. Several factors could affect glucagon effectivity, such as a depletion of glycogen reserves caused by prolonged glucagon administration or a deficit of carbohydrate availability (see Section 2.3.2). This trial was conceived to observe how marked of a difference would cause the carbohydrate content on the impact of glucagon over glucose. Ten people with T1D took part in the study.

The trial had two arms, each consisting of an outpatient week followed by a visit to the clinic. Depending on the trial arm, the week prior to the clinical trial, participants were instructed to follow a high (HCD) or low (LCD) carbohydrate content diet following the dietitian's guidelines. The HCD was designed so that carbohydrate intake was over 250 g/day, whereas the LCD involved less than 50 g/day.

The trial protocol in the clinic was the same for both arms of the study (see Figure 6.1). Patients were administered an insulin bolus on arrival to lower their glucose values to 70 mg/dl. At that moment, they were administered a 100 μg glucagon bolus (GlucaGen, Novo Nordisk, Denmark). Two hours later, a second dose of 500 μg followed. Patients were monitored for two more hours after the second dose.

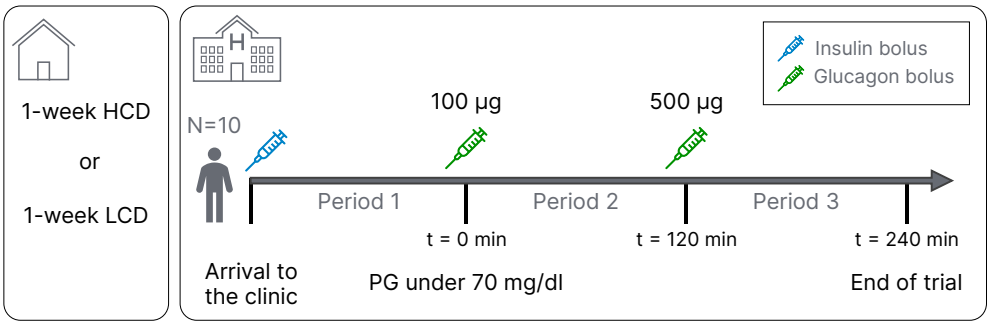

Figure 6.1: Summary of the clinical trial in Ranjan et al. (2017).

The primary outcome of the trial was plasma glucose, but additionally, analysis of blood samples included serum insulin and glucagon, plasma ketones, serum free fatty acids, and triglycerides. As in the previous chapter, the data used in this work will include

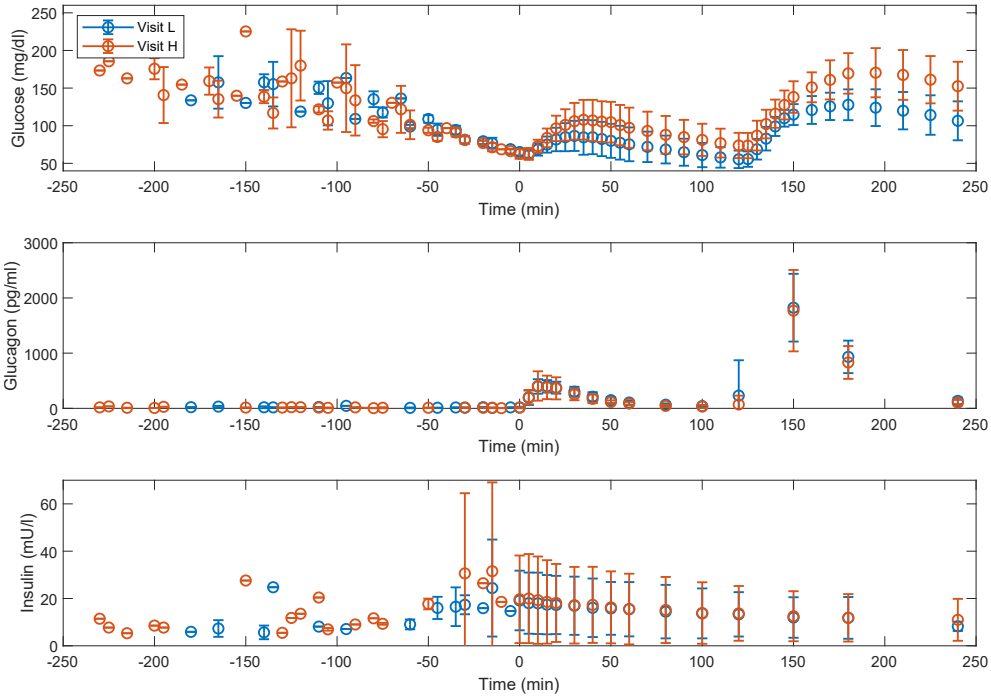

Figure 6.2: Mean values and standard deviation of the data from the clinical trial in Ranjan et al. (2017). Available data included plasma glucose (upper graph), plasma glucagon (middle graph), and plasma insulin (bottom graph). Data in blue represent Visit L (low carbohydrate content diet arm), and data in orange represent Visit H (high carbohydrate content diet arm).

glucose, plasma insulin, and plasma glucagon. A summary of the available data is shown in Figure 6.2, separated by the results obtained in each visit to the clinic after the LCD (labeled Visit L) or the HCD (labeled Visit H). Similarly to the previous dataset, there is a severe undersampling in the first part of the insulin data, but also in plasma glucagon data after the second dose (t between 120 and 240 min).

Results reported by the trial show that glucose response to glucagon after one week of the HCD was higher than after the LCD for both of the administered doses. This could be explained by LCD reducing hepatic glycogen stores, one of the main mediators of glucagon effect during glycogenolysis.

The difference in diet allows for analyzing the consequences of glycogen depletion.

Trial arm	G_{100}	ΔG_{100}	G_{500}	ΔG_{500}
LCD	65.02 ± 4.47	22.87 ± 19.90	55.36 ± 11.62	73.23 ± 11.15
HCD	62.64 ± 6.49	47.28 ± 23.25	73.76 ± 16.80	100.66 ± 25.63

Table 6.1: Glucose values and increments depending on the dose. All glucose values are expressed in mg/dl as mean $\pm$ standard deviation. G_{100} represents the glucose value at the time of the 100 μg administration. ΔG_{100} is the maximum increment observed after the 100 μg dose. G_{500} and ΔG_{500} represent the same concepts for the 500 μg counterpart.

Table 6.1 summarizes the differences in the maximum glucose increase achieved with both glucagon doses in the two experimental settings. The most affected dose due to the diet difference is the 100 μg dose, which has its average value reduced to half in the LCD arm (ΔG_{100}), compared to the HCD. This reduction is not so abrupt in the 500 μg dose, where there is an approximate reduction of 27% (ΔG_{500}). Also note that, although several trials have demonstrated that small glucagon doses (i.e., 100 μg) are sufficient to help recover from hypoglycemia (Haymond and Schreiner, 2001; Ranjan et al., 2016; Haymond et al., 2017; Laugesen et al., 2022), said dose was ineffective in the LCD setting, since 2 hours later to the administration of the dose (value at G_{500}) glucose values are below the hypoglycemia range (average of 55.36 mg/dl).

The relationship between glucagon administration and glycogen reserve depletion has been a matter of study for years, and it remains under investigation. As reviewed in Chapter 2, Bélanger et al. (2000) observed a depletion of glycogen reserves under repeated glucagon doses separated by 30 minutes. The study was performed on rats with 20 μg/kg doses. In Castle et al. (2015), eleven people with T1D participated in a trial where they were administered eight glucagon doses separated by two-hour periods. The study reported a slight, not statistically significant decrease in glycogen reserves. Their doses were 2 μg/kg, with an average of 140 μg per dose. Compared to the previous study, in Castle's trial, glucagon doses were ten times smaller and were separated further apart (2 hours versus 30 minutes). In the study by Blauw et al. (2016c), glycogen reserves were not measured, but the authors observed the effect of repeated glucagon doses on glucose. They administered four glucagon doses between 110 and 440 μg, each of them separated by three hours. The study reported a reduction of glucagon effectivity towards the second half of the trial. The total amount of administered glucagon was higher than in Castle's study (total dose between 1300 and 1650 μg over 10 hours, versus 1125 μg over 16 hours).

The present study lies somewhere in between. The difference in the diet allows us to observe the consequences of glycogen depletion on glucagon effect. However, given

the small first dose administered and the sufficient 2-hour separation between doses, there seems to be no further glycogen depletion due to the dose consecutivity. Hence, the response of the 500 μg dose is not significantly bounded. Given the magnitude of this second dose (which may have affected glycogen reserves), it would be interesting to observe the possible consequences over a third latter dose.

This kind of physiological studies have the limitation that they are usually expensive and hence only performed on small cohorts, as the case of this study, and do not allow drawing generalizable conclusions.

Nonetheless, the results from this clinical trial provide a very interesting dataset to evaluate different glucagon effect descriptions. The previous chapter validated the receptors proposal against single doses of 100, 200, and 300 μg of glucagon. This new dataset provides a broader range of doses (100 μg and 500 μg) under different settings (LCD and HCD). Testing consecutive administration is important since internalization of glucagon receptors could affect the dynamics of newly administered doses of glucagon.

6.2 Identification procedure

Contrary to the case with the dataset used in Chapter 5, no previous work had identified the parameter values for the patients of this dataset. Hence, all the parameters had to be identified. The only parameters assumed a priori were the body weight and the glucose volume of distribution (V). Unfortunately, no information was available about the patients' actual weight. Hence, the value was fixed to the median weight reported in the clinical trial data (75 kg, as reported in Table 1 in the Supplementary Material from Ranjan et al. (2017)). On the other hand, the value of V was considered common to all patients, as in the previous chapter, with a value of 160 ml/kg.

The first part of this section describes a series of preliminary approaches followed to identify the parameters for the baseline model and why they were abandoned. The following section presents the tuning and identification of insulin and glucagon PK parameters, and finally, the third subsection lays out the main identification procedures in this validation. Three different identification strategies were used to adapt the fit of the models to the present dataset and provide the best framework to evaluate their structures.

6.2.1 Initial approaches

At first, we considered using plasma insulin and glucagon data directly as inputs to the system (substituting the signals from equations (4.7c) and (4.8c), respectively). However, due to the undersampling present in both signals (see Figure 6.2), this was not a viable option.

Individual model parameters for this set of participants were unknown. However, the pre-identified parameter values were available, providing information about the probable distribution of their values: values identified in (Wendt et al., 2017b) for the base model and the EGP-related parameters identified in the previous validations.

Looking to make the most out of the a priori parameter knowledge, a Bayesian-inspired approach was considered, based on the work by Visentin et al. (2016). This approach was based on constraining the parameter values so that they would stay close to the already-identified average values. An additional term was added to the cost index. The proposal from Visentin's work was adapted so that a cost was associated with each estimated parameter, penalizing deviations from the average of the known parameters. This method was also applied in Wilinska et al. (2005). The index, named J_{pms} was added to the cost function, defined as:

$$J_{pms}(\theta) = \frac{1}{\sigma_\theta} \cdot (\hat{\theta} - \mu_\theta)^2$$

in which $\hat{\theta}$ was the estimated parameter value in a particular iteration of the optimization process, and μ_θ and σ_θ were the average and standard deviation values previously recorded for that parameter.

On the other hand, the model structure allows the identification of both PK subsystems independently, with their corresponding plasma signal as the system's output, using Equations (4.7a) - (4.7c) for the insulin subsystem, and Equations (4.8a) - (4.8c) for the glucagon subsystem. Hence, the first identification approach tried identifying PK parameters for insulin and glucagon, adding a Bayesian constraint to the cost index. The RMSE between the data and the simulation output was normalized to avoid issues derived from magnitude discrepancies, yielding the following cost function:

$$J_P = \sum_{v=1}^{2} {E_{nC}}^v + \sum_{v=1}^{2} {E_{nI}}^v + \sum_{i=1}^{p} J_{pms}(\hat{\theta}_i)$$

where E_{nC} and E_{nI} are the normalized error measurement of the plasma glucagon ($C(t)$) and the insulin ($I(t)$), respectively for visit v. The parameter values were common for

both visits. The total contribution of the J_{pms} was equal to the sum of the cost associated with each estimated parameter, where p is the total number of parameters.

The normalization of the error was first achieved by apply a logarithm function to the RMSE value,

$$E_n = \log(RMSE^v)$$

however it was then modified to applying the RMSE to a normalized error value ($\bar{e}$), obtained as:

$$\bar{e} = \frac{e - \min e}{\max e - \min e} \qquad \text{where} \quad e = \hat{y}_{i,P}^v - y_{i,P}^v$$

Nevertheless, this approach did not provide adequate results. In a subsequent step, it was decided to include information about the glucose performance so that all parameters (PK and PD) were identified in the same optimization process. The cost index was modified by adding the RMSE associated with the glucose (G):

$$J_P = \sum_{v=1}^{2} E_{nG}^{\ v} + \sum_{v=1}^{2} E_{nC}^{\ v} + \sum_{v=1}^{2} E_{nI}^{\ v} + \sum_{i=1}^{p} J_{pms}(\hat{\theta}_i)$$

Given the poor performance of the results (none of the strategies provided adequate fits to the data for the ten patients) and the uncertainty surrounding the plasma insulin and glucagon signals, the process was re-oriented to focus on the PK subsystem only, working on insulin and glucagon separately.

6.2.2 PK identification

This section will provide a deeper analysis of the insulin and glucagon data and the proposed solutions to find suitable parameter sets for the PK submodels.

Insulin PK

An insulin bolus was administered to every patient on arrival at the clinic. However, as mentioned in the first section of this chapter, sampling in the first part of plasma insulin data is irregular and scarce. This makes the pharmacokinetics of insulin completely unknown since only the "tail" of the bolus is captured (see Plasma Insulin in Figure 6.2). However, that does not provide enough information to model insulin kinetics properly.

At this point, several identifications had already been performed, and multiple pairs of values for t_{max} and $Cl_{F,I}$ were available. Hence, the values used for the insulin PK model for each patient were selected from the previous identifications. The performance of several pairs of parameters on their respective patients was reviewed, and a series of parameter pairs were selected.

Specifically, the parameters for patients 1, 3, 6, and 8 were obtained from an identification that fixed the glucagon PK model and optimized the parameters for the insulin subsystem and the glucose regulation model without any Bayesian constraints. On the other hand, parameters for patients 2, 4, 5, 7, 9, and 10 were selected from a PK-only optimization that used normalized RMSE values for insulin and glucagon, and it did not consider the added weight of J_{pms} in the parameters either.

The resulting parameter values are summarized in 6.2, and the individual results obtained per participant are listed in Table A.18. The overview of the plasma insulin signal against the available data is presented in Figure 6.4, upper row, separated by visit.

Glucagon PK

Glucagon PK identification also posed a series of issues. Although not perceptible in the general data overview, analyzing the individual datasets, there were differences in glucagon PK in the same patients from visit to visit. See, for instance, data points (gray circles) for Patient 8 in Figure 6.3. The measurement right after the 500 μg dose has a value of 2958 pg/ml in visit L and 1496 pg/ml in visit H. Seeing these differences, a single tuple of $k_2 - Cl_{F,C}$ values was not sufficient to fit adequately the signal in both visits. These differences may be caused by inadequate data sampling or measurement, or they may represent actual differences. Unfortunately, it is not possible to discern a priori which might be the case.

In the clinical trial used in the previous chapter, the same authors found that plasma glucagon concentrations were inversely correlated to weight. In this work, the weight of the patients had to be set to a constant value since the individual data was not available. That information might have helped to identify glucagon response since the phenomena caused by weight differences would not have been described by the glucagon PK parameters.

Another issue is that the peak value of plasma glucagon for the 500 μg dose is not captured. Blood samples were taken 30, 60, and 120 minutes after the second glucagon dose. However, it takes GlucaGen 15 minutes to reach its peak concentration after administration (Hövelmann et al., 2018). So, given the sampling times of the trial, there was no information available on the actual dimensions of the glucagon peak. GlucaGen PK for a 500 μg dose in Hovelmann's study reached an average maximum concentration of 1100 pmol/l

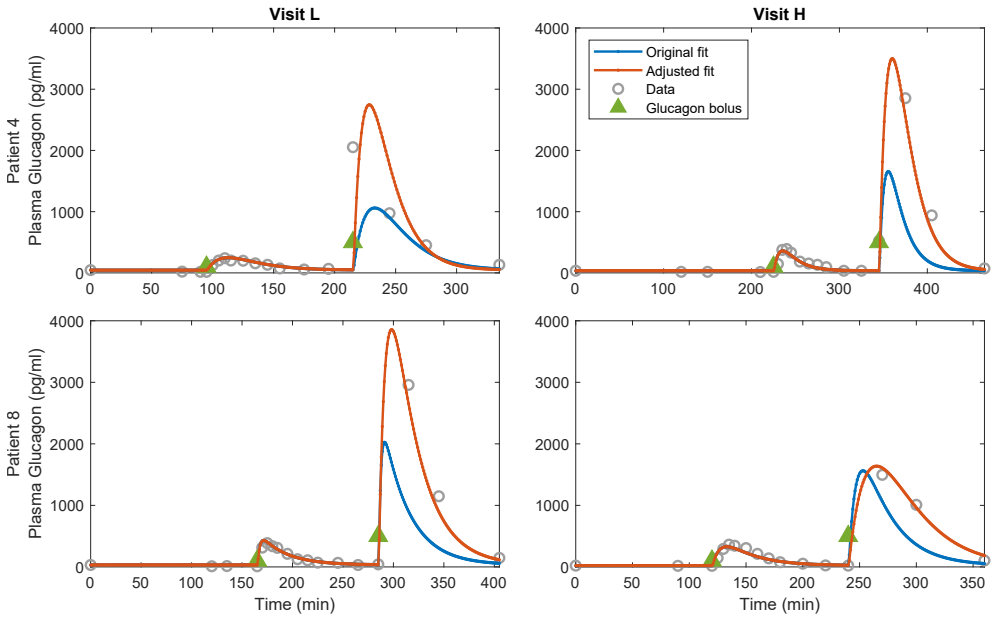

Figure 6.3: Glucagon PK parameters per-visit adjustment. Gray circles represent plasma glucagon data points. Blue lines show the simulation results. Orange lines represent the simulation output after the parameter tuning. Time in the x-axis starts on arrival at the clinic. Green triangles mark the administration of the 100 μg and 500 μg doses.

(approximately 3828 pg/ml), and its half-life time was reached less than one hour after the bolus administration. Observing the average value of the 30-minute-after data point in Figure 6.2, around 1800 pg/ml on average, that value might correspond to the tail of the signal. However, there is no certainty about how close that value is to the peak concentration.

Glucagon PK data is not very reliable in this study because the sampling might give the impression of the existence of some differences that are not there. However, as mentioned, not enough tools are available to discern the data's "real" values. Hence, we opted to try to fit the simulation to the data.

In the previous chapter, it was observed how a single set of parameters in the glucagon model might not correctly describe bigger glucagon doses (e.g., 300 μg). So, for this study, the same issue becomes more accentuated with the introduction of the 500 μg dose. There

might be a nonlinearity in glucagon PK that cannot be captured with the present glucagon PK model. A proper description of the bigger dose pharmacokinetics would have posed an excellent opportunity to try to explore this relationship. However, the aforementioned limitations in sampling times turned this into a fruitless task.

Given that the sampling of the first dose was frequent enough, a glucagon-PK-only identification was carried out that reduced the weight of the error corresponding to the second dose to focus on obtaining an accurate description of the first dose. However, these results had to be adjusted later on to adapt the parameters not only per visit but also per dose, allowing to obtain results such as the ones presented in Figure 5.3 (orange lines representing the adjusted fit). Table 6.2 lists a summary of the final k_2 and $Cl_{F,C}$ values. The results of the average fit of the plasma glucagon simulation to the data are included in the bottom row of Figure 6.4 for both visits L and H.

Parameter	Value (mean $\pm$ SD)	Units
t_{max}	73.5 ± 17.1	min
$Cl_{F,I}$	17.2 ± 7.8	ml/kg/min
$k_1 \cdot 10^{-4}$	483 ± 140	min^{-1}
$k_{2L\text{-}100} \cdot 10^{-2}$	17.39 ± 13.55	min^{-1}
$k_{2L\text{-}500} \cdot 10^{-2}$	11.04 ± 7.77	min^{-1}
$k_{2H\text{-}100} \cdot 10^{-2}$	19.06 ± 17.09	min^{-1}
$k_{2H\text{-}500} \cdot 10^{-2}$	8.73 ± 5.27	min^{-1}
$Cl_{F,C\text{-}100}$	91.11 ± 22.96	ml/kg/min
$Cl_{F,C\,L\text{-}500}$	57.37 ± 13.34	ml/kg/min
$Cl_{F,C\,H\text{-}500}$	66.32 ± 18.02	ml/kg/min

Table 6.2: Insulin and glucagon PK parameters summary for Validation 2. The values of k_2 were adjusted per visit (L or H) and per dose (100 or 500). $Cl_{F,C}$ was kept the same for the first dose regardless of the visit, but it was also adjusted for the 500 μg dose. Value of k_1 was just identified per patient.

6.2.3 Identification of EGP and baseline model

Once the PK subsystem had been defined, the next step consisted of identifying the parameters corresponding to the glucose regulation subsystem of the base model and the EGP-related parameters for the receptors model proposal and the three EGP comparators.

The identification procedure for this section was based on the method followed in the

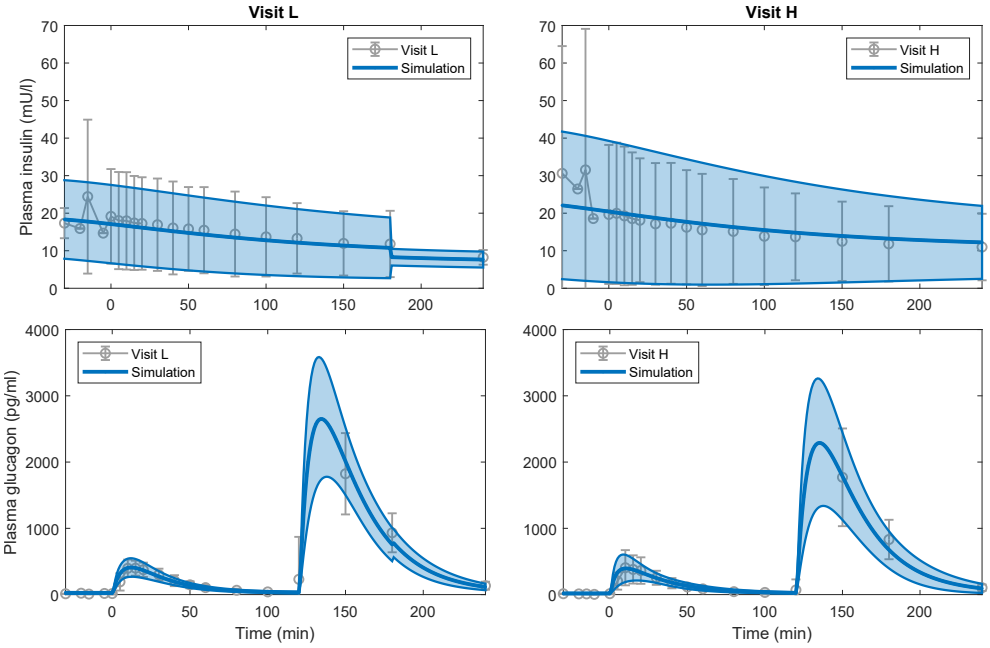

Figure 6.4: Plasma insulin (top row) and glucagon (bottom row) simulation results. Gray error bars correspond to the mean and standard deviation of the data, and continuous colored lines encase the mean and standard deviation of the simulation results. Graphs show the response from $t = 0$ min to 240 min, which is the main period of interest of the study.

previous chapter. Since all EGP models share the same baseline model (comprised of the glucose regulation, insulin PK, and glucagon PK subsystems), to avoid differences in the baseline models confounding the effects of the EGP model, the baseline model is forced to have the same parameters regardless of the EGP definition. This leads to an identification process where all the parameters (for the baseline model and each EGP model) have to be obtained in the same optimization.

In setting up the optimization process, parameter bounds had to be defined. For this validation, the parameter bounds were expressed as a function of the previously identified average parameter values ($\mu_{\hat{\theta}}$), either from Wendt's identified values for the base model, or from the previous validation for the EGP-specific parameters.

$$\hat{\theta}_u = (1+\alpha)\cdot\mu_{\hat{\theta}}$$
$$\hat{\theta}_l = (1-\beta)\cdot\mu_{\hat{\theta}}$$

Values of α and β were defined between 0 and 1 and were often equal in this validation.

Due to the often observed variability in the patients' insulin sensitivity, related parameters (S_T and S_D) were identified for each visit to the clinic (LCD or HCD). In contrast to the previous validation, Q_{20} was no longer identified but calculated based on the other states' initial values. With this, two parameters were removed from the parameter vector to identify. Also, since the glucose-regulation parameters also have to be identified, there are sufficient degrees of freedom to adapt to the initial conditions of the data without having to identify the initial conditions themselves.

Hence, the list of parameters to be identified from the baseline model becomes:

$$\theta_{1P} = \{S_T^v, S_D^v, F_{01}, k_{12}, k_{a1}, k_{a2}, k_{a3}\}$$
$$P = 1, 2, ..., 10; \quad v = \text{LCD}, \text{HCD}$$

As in the previous validations, a different identification is carried out for each patient (P). Note that the superscript v refers to the visit for which the parameter has been individualized. The parameters without this superscript are common to both visits.

Next, the parameters to identify for each EGP definition are described, starting with the receptors proposal.

At this point, a global parameter sensitivity analysis was performed, using the AMIGO-2 Matlab toolbox, to study whether another rate parameter would be more influential on glucose instead of the activation rate, k_{on}. The values of k_{on}, k_{off}, k_{rec} and k_{in} (see Section 4.3) were included in the analysis. The sensitivity analysis returned that the most sensitive parameters were k_{rec}, k_{off}, k_{in} and k_{on}, in that order. Consequently, some identifications were carried out substituting k_{on} by k_{rec}, but the fits of the model to the glucose signal worsened significantly; hence, the change was reverted.

Consequently, the parameters to identify in the receptors model become:

$$\theta_{2P} = \{EGP_0, S_I, k_{on}, K_r, V_r\}, \quad P = 1, 2, ..., 10$$

For the DTU model:

$$\theta_{3P} = \{G_{GNG}, S_E, E_{max}, C_{E50}\}, \quad P = 1, 2, ..., 10$$

For the McGill model:

$$\theta_{4P} = \left\{G_{ng}, S, T, K_{Gd}, T_{Gd}\right\}, \quad P = 1, 2, ..., 10$$

And finally the OHSU EGP model:

$$\theta_{5P} = \left\{EGP_0, S_f, k_{g3}, k_d, k_c\right\}, \quad P = 1, 2, ..., 10$$

The resulting parameter vector contains a total of 28 parameters:

$$\Theta_P = \{\theta_{1P}^v, \theta_{2P}, \theta_{3P}, \theta_{4P}, \theta_{5P}\}$$

Method A

Having defined the set of parameters to identify, the combination of the baseline model plus each EGP model (m) is used to simulate both visits (L and H). Then, the optimization cost index (J_P) is computed as the average of the total RMSE of each simulation:

$$J_P = \frac{1}{4}\sum_{m=1}^{4}\left(RMSE_m^L + RMSE_m^H\right) \tag{6.2}$$

For this validation, the optimization was carried out in MATLAB R2022a, using the `fmincon` function for the parameter optimization. The identification for each patient was repeated ten times, with a different initial point each time, to reduce the risk of finding a local solution. Initial points were drawn from Latin hypercube sampling.

Figure 6.9, left plot, summarizes the RMSE results obtained with each model using Method A. Each boxplot represents the average RMSE obtained across all 20 datasets (10 patients, two visits each). Figure 6.5 shows some sample results for Patient 3 in visits L and H.

The primary takeaway from the results is that the average error obtained with the receptors model is lower than the other EGP definitions. However, this difference is mainly due to discrepancies in the first part of the data, as observed in Figure 6.10 (from the start time of the study, when the insulin bolus was administered until the administration of the first glucagon dose). During this phase, the only role of EGP models is the contribution of basal EGP, which will depend on the identified parameters. This taints the interpretation of the results since the optimizer tends to fit glucagon doses to the detriment of an accurate basal EGP to avoid overall larger errors. In the absence of glucagon infusion, the basal EGP value should be independent of the EGP model used, which is the same criteria that was applied in the previous validation.

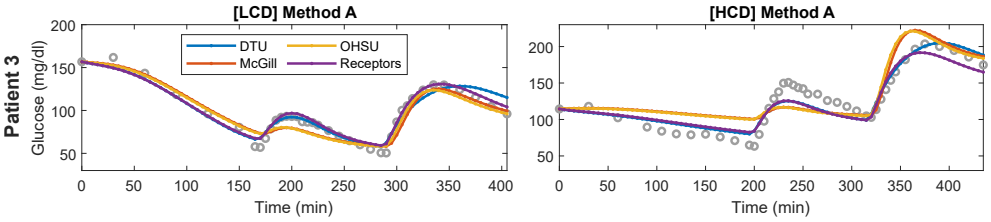

Figure 6.5: Patient 3 results for identification method A. Gray points represent the glucose data points. Continuous lines represent the simulations of the baseline model plus the DTU EGP (blue line), the McGill EGP (orange line), the OHSU EGP (yellow line), and the receptors EGP (purple line); for visit L (left), and visit H (right).

Method B

Using the same parameters in the baseline model was insufficient to eliminate the errors between models in Period 1 (i.e., before the first glucagon dose, see Figure 6.1). Hence, a second approach to the identification was followed, in which the error in this period is penalized more than the others. With this, the error calculation, e^v in Equation (4.14), is redefined as:

$$e^v = \begin{cases} \omega \cdot (\hat{y}^v_{i,P} - y^v_{i,P}), & \text{if } t \leq t_{100} \\ (\hat{y}^v_{i,P} - y^v_{i,P}) & \text{if } t > t_{100} \end{cases} \tag{6.3}$$

The value of ω was set to 10, and t_{100} refers to the time of the first glucagon dose. The results for this identification are labeled as Method B.

The overall RMSE results obtained with this method can be found in Figure 6.9, center plot. Overall, RMSE values have increased, which makes sense considering the optimizer does not provide the best average result, but it is obliged to improve the fit in the first part. However, that allows for highlighting the differences between the models in the second part, where the glucagon doses are administered. Figure 6.6 shows results for Patient 3 results in visits L and H. In contrast to the results presented with the previous method, there is an improvement in the models fit to the first period of the data.

It becomes relevant now to see how the different models behave after the glucagon doses. For instance, DTU and the receptors proposal are able to fit both glucagon doses adequately. However, the McGill and OHSU models sacrifice the fit of the first data to fit

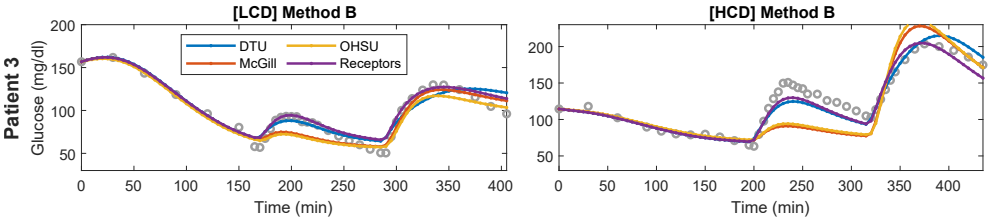

Figure 6.6: Patient 3 results for identification method B. Gray points represent the glucose data points. Continuous lines represent the simulations of the baseline model plus the DTU EGP (blue line), the McGill EGP (orange line), the OHSU EGP (yellow line), and the receptors EGP (purple line); for visit L (left), and visit H (right).

the second (because it is the option that provides the lowest RMSE since they cannot fit both simultaneously). In addition, as it was mentioned during the data analysis in Section 6.1, glucose behaves differently depending on the diet. Here, even the models that provide the best fit in visit L present an error increase in visit H since the behavior of glucose has changed. This motivated the definition of the last validation method.

Method C

The main characteristic of this dataset is the difference in glucose response to glucagon caused by the diet. Methods A and B aimed to fit every situation (LCD and HCD) with the same glucagon model. However, the results show that the RMSE values for the HCD are always higher than for the LCD (see Figure 6.10). The difference in diets is not described in any of the models, so one of the visits is favored to the detriment of the other in the identifications. The last optimization carried out in this work tries to describe this difference in diet, optimizing a variable gain in each of the EGP models per visit.

In order to select the parameters, a global parameter sensitivity analysis was performed on each EGP model, using the Matlab toolbox AMIGO2, as described in Section 4.4.2. The combination of the baseline model plus each EGP model was analyzed individually, and the parameters included in the analysis were the corresponding parameters of each EGP definition only. A total of 10^5 samples (n_{lhs}, in Equation (4.18)) were considered. A constraint was introduced in the simulations to discard the experiment if glucose reached values under 32.5 mg/dl or above 450 mg/dl. This way, the software discarded the parameter combinations that resulted in non-physiological results for the given inputs: 100 and

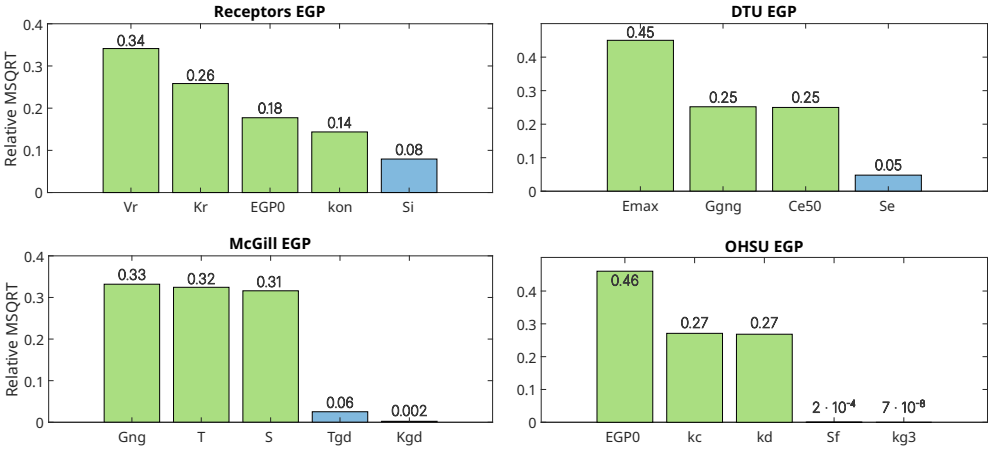

Figure 6.7: Parameter sensitivity analysis results for each EGP model.

500 μg of glucagon.

Figure 6.7 presents the results of the parameter sensitivity analysis, plotting the relative value of $\delta_{\theta_p}^{msqr}$ (4.18). Parameters are sorted from left to right from most to least influential on the glucose result, according to the relative mean square sensitivity measure (MSQRT). Color codes correspond to these output-related sensitivity intervals: green bars correspond to the most sensitive values, followed by blue bars, and red bars represent parameters with a low sensitivity index. Some parameters' bars might not be visible if the relative sensitivity was too small. The parameters with the highest value of $\delta_{\theta_p}^{msqr}$ were the ones selected to be tailored per visit. The only exception was the parameter for the McGill EGP. According to the sensitivity analysis, the candidate was G_{ng} (see Equation (4.12a) and Table 4.4). However, this parameter represents a constant contribution to EGP from gluconeogenesis as an offset in the $EGP(t)$ equation. It was decided to use the parameter T instead since it presents a similar relative $\delta_{\theta_p}^{msqr}$ value (i.e., the magnitude of its influence is comparable to G_{ng}). Also, parameter T may have a more significant influence on glucose shape since it represents glucagon sensitivity and is found both in $EGP(t)$ (4.12a) and $EGP_G(t)$ (4.12b) equations as a multiplying factor.

With the conclusions of this analysis, the selected parameters were: V_r for the receptors model, E_{max} for the DTU model, T for the McGill model, and EGP_0 for the OHSU model. Results are labeled as Method C.

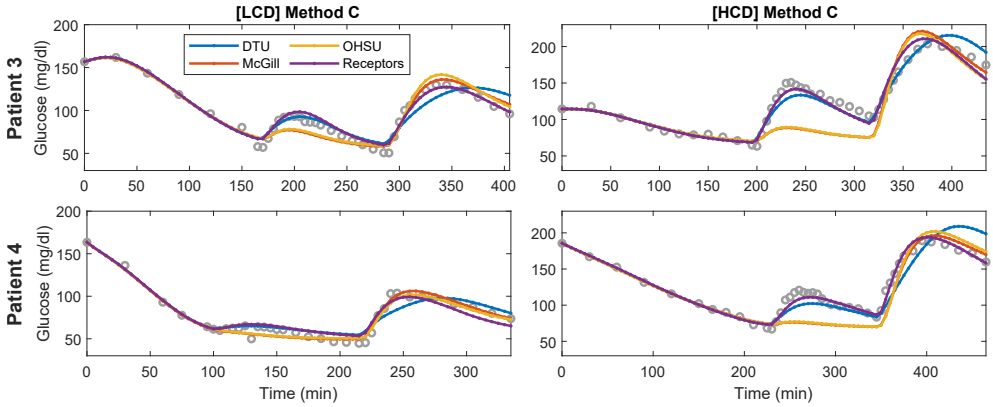

Figure 6.8: Patient 3 and Patient 4 results for identification method C. Gray points represent the glucose data points. Continuous lines represent the simulations of the baseline model plus the DTU EGP (blue line), the McGill EGP (orange line), the OHSU EGP (yellow line), and the receptors EGP (purple line); for visit L (left column), and visit H (right column).

Figure 6.8 shows the simulation results generated with Method C's identification for patients 3 and 4 in both visits L and H. The improvement introduced in the receptors and DTU model in visit H is readily appreciated since now the models are able to fit both glucagon doses. Likewise, patient 4 has a differentiated glucose response in each visit that is well described with this parameter change. However, McGill and OHSU EGP models are still not able to fit both glucagon doses.

Boxplots in Figure 6.9, right plot, summarize the RMSE obtained with this method. Since the constraint to improve the fit in Period 1 is still present, average RMSE results are higher than those obtained with Method A, similar to those in Method B. Nevertheless, the receptors proposal still provides the most accurate fit to the data.

6.3 Validation 2 results

Table 6.3 summarizes the identified parameter values in this validation for each EGP model. Each column corresponds to the specific method. In the third column, a different value was identified for visit L and H for some parameters, indicated by the corresponding label at their right. Table 6.4 presents the same information for the parameters belonging

Model	Parameters	Method A	Method B	Method C	
Receptors	$k_{on} \cdot 10^{-6}$	6.43 ± 6.32	22.15 ± 18.45	22.81 ± 17.13	
	V_r	75.40 ± 26.18	74.70 ± 54.25	66.61 ± 49.08	L
				107.25 ± 89.33	H
	$K_r \cdot 10^{-3}$	11.71 ± 7.53	64.84 ± 88.88	73.52 ± 93.99	
	$S_I \cdot 10^{-3}$	33.87 ± 32.94	20.08 ± 14.96	15.16 ± 9.99	
	EGP_0	9.40 ± 2.68	12.88 ± 2.42	13.43 ± 2.10	
DTU	E_{max}	67.02 ± 13.06	54.92 ± 35.12	45.08 ± 13.50	L
				66.63 ± 39.64	H
	C_{E50}	920.3 ± 335.2	460.2 ± 374.3	561.4 ± 507.3	
	$S_E \cdot 10^{-4}$	127.5 ± 115.7	190.7 ± 138.9	246.8 ± 103.6	
	G_{GNG}	6.09 ± 3.42	9.44 ± 3.06	10.12 ± 3.06	
McGill	$T \cdot 10^{-2}$	2.87 ± 0.54	4.74 ± 7.38	3.47 ± 2.85	L
				7.93 ± 8.98	H
	K_{Gd}	0.70 ± 1.99	0.06 ± 0.09	0.11 ± 0.24	
	$T_{Gd} \cdot 10^{-2}$	31.89 ± 21.56	35.48 ± 40.14	48.10 ± 40.18	
	$S \cdot 10^{-3}$	19.27 ± 11.56	22.58 ± 22.19	42.18 ± 17.23	
	G_{ng}	8.88 ± 2.99	10.93 ± 3.06	11.68 ± 3.18	
OHSU	$k_{g3} \cdot 10^{-6}$	10.26 ± 0.15	9.17 ± 0.20	9.09 ± 0.14	
	k_d	0.47 ± 0.20	0.92 ± 0.61	0.98 ± 0.58	
	$k_c \cdot 10^{-3}$	1.05 ± 0.38	1.29 ± 1.02	1.24 ± 0.86	
	$S_f \cdot 10^{-6}$	41.63 ± 33.13	111.76 ± 53.51	103.31 ± 54.43	
	EGP_0	8.86 ± 3.03	11.04 ± 3.11	11.84 ± 3.16	L
				11.98 ± 3.36	H

Table 6.3: Validation 2 EGP parameter values summary for the three identification methods presented in this chapter (A, B, C). Values are expressed as mean $\pm$ standard deviation. Parameters V_r, E_{max}, T, and EGP_0 were adjusted per visit (L, H) in method C.

to the baseline model.

As mentioned thorough the previous section, Figure 6.9 shows an overview of the RMSE of each model for identification of Method A (left), Method B (center), and Method C (right).

Table 6.5 presents the mean and standard deviation of the overall RMSE values obtained with the corresponding identification method in this validation. A statistical analysis was carried out in R (version 4.1.3) to analyze the differences between the results obtained with the receptors model and the comparators. After applying normality tests to ensure the data distributions were normal (Kolmogorov-Smirnov test), paired t-tests were performed comparing each pair of results. Of note, the RMSE difference in the overall

Parameters	Method A	Method B	Method C	
F_{01}	11.5 ± 3.0	7.9 ± 3.2	8.3 ± 3.5	
$k_{12} \cdot 10^{-4}$	242 ± 111	447 ± 207	595 ± 1	
$k_{a1} \cdot 10^{-4}$	21 ± 19	55 ± 23	53 ± 21	
$k_{a2} \cdot 10^{-4}$	474 ± 223	492 ± 306	503 ± 322	
$k_{a3} \cdot 10^{-4}$	95 ± 103	150 ± 145	111 ± 146	
$S_T \cdot 10^{-4}$	79.66 ± 34.79	71.47 ± 48.16	44.77 ± 27.08	L
	36.13 ± 32.31	16.26 ± 11.54	26.95 ± 25.42	H
$S_D \cdot 10^{-4}$	3.72 ± 3.98	16.67 ± 17.21	556.45 ± 1645.27	L
	424.12 ± 1326.52	507.92 ± 1379.81	550.68 ± 1478.12	H

Table 6.4: Validation 2 base model parameter values summary for the three identification methods presented in this chapter (A, B, C). Values are expressed as mean $\pm$ standard deviation. Parameters S_T and S_D were adjusted per visit (L, H).

results of each method is statistically significant in every case according to the p-value results. The significance of the difference between the results obtained with the receptors proposal and the EGP comparators is further reinforced by Cohen's d values greater than 0.8 in the overall results obtained with the three methods.

A similar analysis is presented in Table 6.6, where the analysis is applied to the RMSE values separated per visit and method. These results allow for observing how the main contributions of the receptors are related to the HCD, where the effect of glucagon is more pronounced. This agrees with the conclusions gathered in Validation 1 that the receptors proposal provides better results for bigger glucagon doses. Likewise, the RMSE differences in visits L are less notable. As observed in the overall results, the DTU EGP performance is similar to the receptors EGP, although the latter achieves the lowest RMSE in every evaluation of this validation.

The analysis is extended in Figure 6.10, which differentiates the results per visit but also considers the three time periods given by the data (see Figure 6.1):

- Period 1: from the start of the trial to the administration of the first glucagon dose (100 μg), where only the insulin effect is significant, and EGP contribution is limited to its basal value.
- Period 2: from the administration of the first glucagon dose to the second (500 μg).
- Period 3: from the second glucagon dose to the end of the visit.

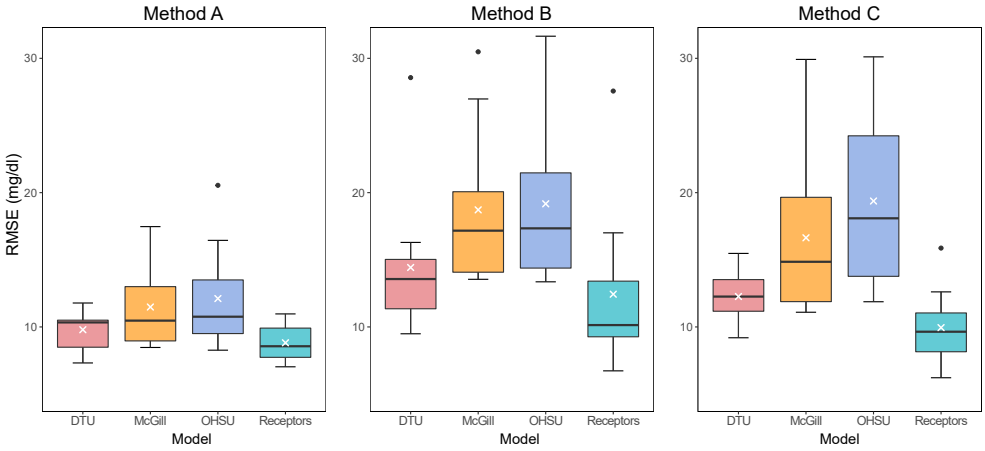

Figure 6.9: Boxplots of overall RMSE obtained in Validation 2 for each identification method.

Method	Model	Comparators RMSE	Receptors RMSE	t	p	Cohen's d
A	DTU	9.79 ± 1.43	8.82 ± 1.29	3.59	0.006*	1.13
	McGill	11.48 ± 2.98		3.73	0.005*	1.18
	OHSU	12.11 ± 3.67		3.65	0.005*	1.15
B	DTU	14.43 ± 5.12	12.44 ± 5.75	2.57	0.030*	0.81
	McGill	18.72 ± 5.58		3.26	0.010*	1.03
	OHSU	19.17 ± 5.82		3.37	0.008*	1.07
C	DTU	12.27 ± 1.76	9.95 ± 2.63	2.95	0.016*	0.93
	McGill	16.64 ± 5.73		3.37	0.008*	1.06
	OHSU	19.38 ± 6.25		4.98	<0.001*	1.57

Table 6.5: Comparison of overall RMSE for each model and identification method, considering the average RMSE in visits L and H during all the experiment time. The symbol * indicates a p-value lower than 0.05.

Some general conclusions can be drawn from Figure 6.10, in accordance with the observations made until now: (a) The mean RMSE values are lower in the LCD identification than in the HCD; (b) In the LCD, the error values for the smaller dose (Period 2) are similar to those for the second dose (Period 3), but in the HCD, the difference between

Method	Visit	Model	Comparators RMSE	Receptors RMSE	t	p	Cohen's d
A	L	DTU	8.38 ± 2.37	7.59 ± 1.88	2.19	0.056	0.69
		McGill	9.39 ± 3.58		2.44	0.037*	0.77
		OHSU	9.73 ± 4.53		1.97	0.081	0.62
	H	DTU	11.20 ± 2.36	10.05 ± 2.54	2.50	0.034*	0.79
		McGill	13.57 ± 4.56		3.86	0.004*	1.22
		OHSU	14.50 ± 4.92		4.77	0.001*	1.51
B	L	DTU	13.81 ± 7.27	12.52 ± 6.84	1.62	0.139	0.51
		McGill	15.21 ± 8.20		1.00	0.341	0.32
		OHSU	15.20 ± 8.32		0.92	0.383	0.29
	H	DTU	15.04 ± 4.27	12.36 ± 5.56	1.54	0.158	0.49
		McGill	22.22 ± 5.48		4.47	0.002*	1.41
		OHSU	23.13 ± 5.76		5.06	<0.001*	1.60
C	L	DTU	11.09 ± 3.13	9.14 ± 2.70	2.19	0.056	0.69
		McGill	12.90 ± 8.02		1.30	0.225	0.41
		OHSU	15.27 ± 8.81		2.11	0.064	0.67
	H	DTU	13.45 ± 3.40	10.76 ± 4.65	1.56	0.154	0.49
		McGill	20.38 ± 6.76		4.03	0.003*	1.27
		OHSU	23.48 ± 6.13		6.85	<0.001*	2.16

Table 6.6: Comparison of RMSE for each model and identification method, considering the average RMSE in visits L and H separated by visits. The symbol * indicates a p-value lower than 0.05.

errors in periods 2 and 3 is larger; (c) The receptors model provides the lowest mean values in each studied situation, regardless of the identification method used.

6.4 Discussion

The results obtained in this chapter reassure the conclusion that using the receptors model structure can contribute to providing a more accurate description of the glucagon effect over glucose. The introduction of a larger glucagon dose, even if the settings were challenging (different diet compositions in each trial arm), has made the potential contributions of the receptors model more apparent compared to the previous validation.

Indeed, the final analysis of overall results obtained in Validation 1 concluded that the receptors EGP provided a statistically significant difference compared to the McGill and OHSU EGP models (see *Total* results in Table 5.8).

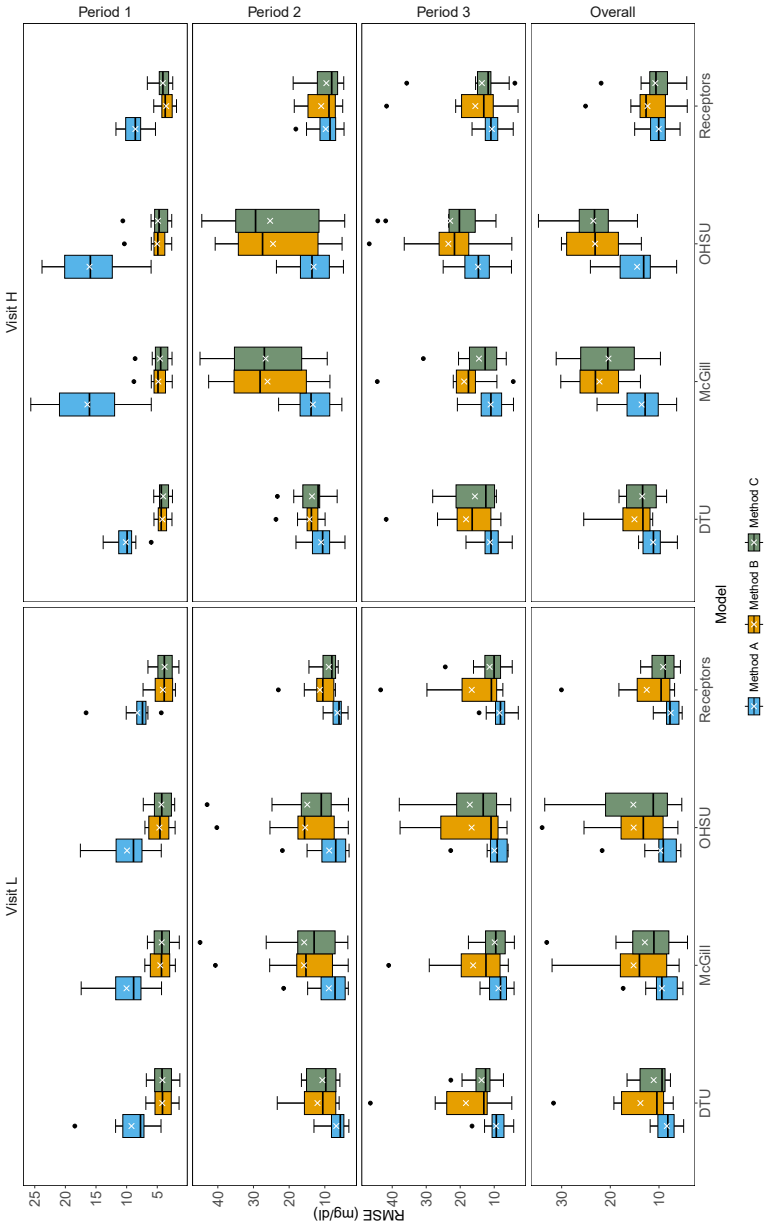

Figure 6.10: General RMSE comparison between Method A (blue boxes), Method B (orange boxes), and Method C (green boxes). Rows represent the considered period times. Columns represent the visits. The "Overall" column considers the total time of each visit.

However, in this validation, a statistically significant difference with all the comparators is observed favoring the receptors results regardless of the identification method used.

Method A Looking at results for Method A in Table 6.5, the mean values obtained with the receptors model are lower across all periods. However, the largest differences correspond to the first part (Figure 6.10, Period 1), whose absolute error values are higher than periods 2 and 3.

Focusing on periods 2 and 3, all models behave similarly, with close average RMSE values. This shows that, in general, the optimization tried to reduce possible errors in these periods by sacrificing the fit in the first part. This justifies weighting the first part of the data as proposed in Methods B and C.

Method B The results show that overall errors with the receptors model are lower compared with the rest (Method B, Table 6.5). The most noticeable fact from these results is that the overall RMSE has increased for all the models. This optimization strategy ensures a more accurate fit for the first part of the data. As shown in Figure 6.10, the RMSE for Period 1 has been notoriously reduced compared to Method A. However, this acted to the detriment of periods 2 and 3.

This situation emphasizes the capabilities of each EGP model in describing the glucagon effect. For instance, the OHSU and McGill models misfit the second part (when glucagon is active) if they are forced to fit the first part, meaning that their structure cannot adequately describe the observed glucagon behavior.

Method C The main feature of this optimization method was tailoring a parameter to try to capture the differences introduced by the variation of the carbohydrate content in the patients' diet.

The aim of Method C was to attenuate the differences in error between visits L and H. Overall, mean values of RMSE are reduced when incorporating a variable parameter in each EGP model, except for the OHSU model (see Method C in Table 6.5).

This shows that differences in diet could be explained by an associated gain change in the EGP model only in some specific model structures (e.g., the receptors or the DTU approach). However, a better representation of the dynamics might involve some nonlinear relationships (i.e., the behavior of glucose response is fairly similar in Period 2 both in visit L and H but presents a more acute response in the HCD case).

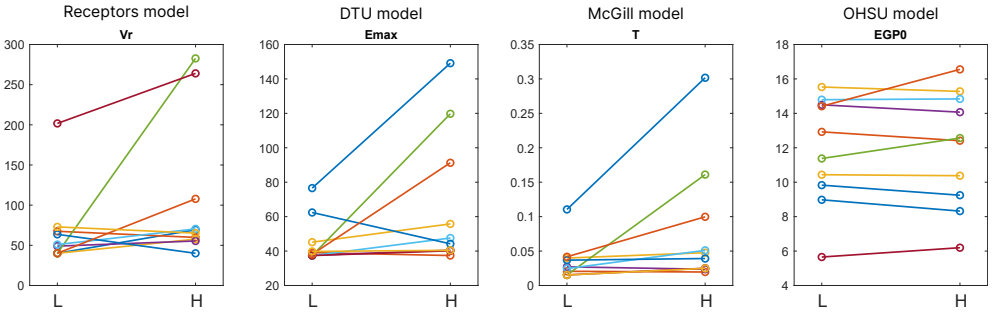

Figure 6.11: Parameter variation in absolute value between the identification of visit L and visit H in Method C.

Percent parameter changes between diets (Method C)										
Patient	1	2	3	4	5	6	7	8	9	10
Vr	73.0	−11.3	44.0	13.1	605.4	38.3	30.9	−37.1	168.8	−10.6
Emax	94.8	−4.3	23.5	8.0	220.5	27.3	7.5	−29.2	139.7	1.7
T	173.1	−5.0	19.6	−12.7	954.0	108.2	63.7	6.4	139.1	62.4
EGP0	−6.0	−4.0	−1.6	−2.9	10.4	0.3	9.6	−7.3	14.9	−0.6

Table 6.7: Percent parameter changes between diets in identification Method C. Values represent the percent relative change of the EGP parameters from L to H parameters.

Table 6.7 summarizes the relative change of the parameters from visit L to H. Figure 6.11 illustrates these parameter values variations graphically. Most parameters increased their value to adapt to the greater glucagon doses. However, almost one-third of them (13 out of 40) decreased their values, albeit in a more reduced proportion with respect to the percentage magnitudes observed in the increases. An increase in their values was expected since the selected values will directly affect glucose values, which will increase in the HCD setting.

The values of the OHSU EGP are the ones that experiment the smallest changes, which would explain why its fit did not improve even with the parameter change, resulting in the lowest performance in the results of Method C. There might be some issues in the design of the identification procedure. Nevertheless, neither of the processes used in these chapters favored one model over the others.

Certainly, attempting to describe diet peculiarities with a single parameter in the EGP

definition is just an approximation to test whether this approach would improve the fit in any way. To properly capture this kind of influence on physiology, a meal model would be needed, as well as defining a relationship between meal content and the glucagon effect model parameters. However, this proof-of-concept may serve as a baseline in future works.

6.5 Conclusion

This chapter has presented a second validation of the EGP definition based on glucagon receptor dynamics. The dataset used for evaluation included consecutive doses of 100 and 500 μg in two different settings: LCD and HCD. Three identification methods are used to identify the proposed model parameters and compare its performance to three EGP models from the literature. The proposed EGP and the comparators share the parameters of the PK/PD model used as the baseline.

Results show how the proposed EGP model outperforms the comparators, providing a lower RMSE, hence performing an appropriate description of glycogenolysis and gluconeogenesis since the model describes glucose dynamics observed in clinical data. The previous chapter showed a tendency of the proposal to improve the fit in higher glucagon doses (300 μg), which is further differentiated in this validation with the 500 μg doses. This validation did not allow for validating insulin-glucagon interactions since the available data did not describe this effect.

The proposed model offers the possibility of incorporating a not-too-complex, more physiologically accurate description of glucagon into the current T1D simulators. It is, however, more complex than other proposals from the literature that achieve a similar performance level (e.g., the DTU EGP model). Nevertheless, the proposed EGP introduces new dynamics that have shown significant improvements in describing clinical data.

Part III

Pramlintide

Chapter 7

Pramlintide model

This chapter lays the ground for developing a pramlintide PK/PD model. The first part describes amylin physiology and its receptors. Then, different hypotheses for model structures are laid out, depending on the model stage (intravenous PK, subcutaneous PK, and PD). Finally, the validation methods are presented, including the identification methodology and the assessment metrics.

7.1 Introduction

As presented in Chapter 2, pramlintide is an amylin analog that has allowed to administer amylin externally to counter its absence in people with T1D (Lutz, 2022). Several clinical trials have proved pramlintide's efficacy in reducing postprandial excursions, thus easing glucose control (Kong et al., 1997; Kolterman et al., 1996; Hinshaw et al., 2016). Pramlintide has also been tested in CL trials administered with a fixed ratio with respect to insulin, emulating an insulin-pramlintide co-formulation (Haidar et al., 2020; Tsoukas et al., 2021b). Its main advantage is that it removes the need to provide the algorithm with accurate estimations of the amount of ingested carbohydrates each meal. However, pramlintide dosing is sometimes accompanied by adverse effects such as nausea or vomiting, especially during the first weeks of treatment (Edelman et al., 2007). Hence, new control algorithms need to be investigated to minimize pramlintide infusion and avoid potential side effects.

Simulators describing pramlintide and its effect on glucose are essential in validating control strategies in a pre-clinical phase. However, there is a lack of simulators that include pramlintide and provide a set of PK/PD relations, as exposed in Chapter 3.

With the goal of proposing a pramlintide PK/PD model for T1D, this chapter presents an overview of the physiology surrounding amylin and its receptors. Then, Section 7.3 describes the different model structures considered for the PK/PD model proposal, and Section 7.4 presents the methodology and tools that will be used for the validation of the model in the next chapter.

7.2 Amylin physiology

Amylin is a hormone segregated by β-cells in the pancreas, alongside insulin. Its functions include energy expenditure management, inhibition of glucagon secretion, inducing satiation, and slowing down gastric emptying, as presented in Section 2.1. Amylin works in coordination with insulin to regulate glucose after a meal: insulin reduces the amount of glucose in the blood, whereas amylin slows down gastric emptying, hence delaying the appearance of glucose in plasma. This prevents blood glucose from staying in hyperglycemia for long periods of time. Both hormones are usually co-secreted in a ratio of approximately 15:1 (insulin:amylin) (Hay et al., 2015). Of note, in healthy people, fasting plasma amylin concentrations are in the range of 4 - 8 pmol/l and between 15 - 25 pmol/l in the postprandial state (Nyholm et al., 2001).

Amylin physiology is understudied in many aspects, and many of its behaviors have only been studied on animal models. This section summarizes some of the most relevant knowledge gathered on the matter.

Similar to glucagon, amylin action is mediated by amylin receptors. These receptors also belong to the family of G protein-coupled receptors (GPCRs). However, there is not a unique amylin receptor gene. Furthermore, investigation of amylin binding sites showed an overlap with calcitonin[1] binding sites (Hay et al., 2015). As it turns out, the functional amylin receptor is actually composed of a calcitonin receptor (CTR) that has been coupled with *receptor activity modifying proteins* (RAMPs), that enhance the binding capabilities of the receptors (Woods et al., 2006). The prototypical amylin receptor results from the interaction of RAMP1, RAMP2, or RAMP3 with the CTR (Hay et al., 2018).

The characterization of the amylin receptor is complex since there exist three types

[1] Calcitonin is a hormone secreted in C-cells in the thyroid that helps calcium homeostasis by decreasing calcium levels.

of RAMPs and several subtypes of the CTR. Hence, there are multiple possible amylin receptor subtypes with distinctive pharmacology, signaling, and regulation profiles (Hay et al., 2015). Most studies of amylin receptor signaling derive from transfected model cellular studies. However, mixed populations of free and RAMP-complexed calcitonin receptors may be activated simultaneously by amylin (depending on the concentration). Thus, it is not possible so far to know the exact receptor that triggers the activation of a particular signaling pathway. Gluconeogenesis and glycogenolysis pathways in the liver have been thoroughly studied, but this is not the case with amylin signaling, given the significant increase in system complexity. Hence, more extensive research is needed to narrow down which intracellular signals are triggered by amylin and which of them are sufficient to mediate amylin's effect.

Even if amylin receptors belong to the family of GPCRs, they share few distinctive features with other receptors, such as glucagon receptors. In the manner of glucagon GPCRs, amylin can stimulate intracellular cAMP and CREB production (see Table 4.1) by binding to its receptors. However, the regulation of amylin receptor subtypes has not been studied. Although CTR regulation processes have been studied more, and it is tempting to infer that amylin receptors could behave similarly, RAMPs are known to alter the receptor fate in terms of regulation. Hence, it cannot be assumed that their behavior will be similar even though their "core" is the same (Hay et al., 2015). Indeed, the work by Gingell et al. (2020) showed that amylin receptors undergo very little internalization compared to CTR. As mentioned in Section 4.2, glucagon receptors may experience degradation when exposed to high concentrations of the hormone for long periods of time. However, studies of continuous infusion of amylin in rats for 3-7 days still showed an evident responsiveness to amylin, hinting at a maintained effect even under the effect of prolonged circulating amylin levels (Young, 2005).

Amylin and CTR receptors are mainly located in distinct parts of the brain, such as the area postrema, the nucleus accumbens, and the hypothalamus (Hay et al., 2015). The main characteristic of the area postrema is that it is directly exposed to glucose and glucose-regulatory peptides in plasma due to the lack of a blood-brain barrier. In fact, in this area, there is an overlap of glucose-sensing and amylin receptor-expressing neurons (Weyer et al., 2001).

On the other hand, some amylin binding sites have been detected in pancreatic β-cells, which could indicate how amylin is able to inhibit its own and insulin secretion. In contrast, no amylin receptors have been found in α-cells or the stomach (Samsom et al., 2000), further confirming the fact that amylin acts as a neuroendocrine hormone that takes action via a central pathway.

The mediation of the central nervous system in amylin's effect had already been studied in rats, where the studies concluded that (1) amylin does not affect motility of gastric funds ex vivo, (2) an intact vagus nerve is necessary for amylin to be effective, (3) the effectiveness of amylin to inhibit gastric emptying depends upon the intracranial location of injection, (4) ablation of the area postrema nullifies amylin effect, and (5) there is a high density of amylin receptors in the area postrema. More details about the specific experiments in each case can be found in Young (2005).

The major brain site regulating gastric motility is the dorsal vagal complex of the brain stem, which is composed of the nucleus tractus solitarius (NTS), dorsal motor nucleus of the vagus (DMV), and area postrema (Young, 2005). Altogether, the dorsal vagal complex receives many signals from cardiovascular, respiratory, and gastrointestinal receptors and modulates numerous autonomic functions (Bauer et al., 2005). Amylin appears to directly activate neurons in the area postrema, which is indeed one of the key actuators in gastric motility and amylin's satiation effect (Hay et al., 2015). In fact, the area postrema contains the highest density of amylin-binding receptors. This area of the brain receives different stimuli through the nerves and generates vagal responses that originate in the DMV (Weyer et al., 2001).

Gastric motility is controlled predominantly by the vagus nerve (Horowitz et al., 2004). From the DMV there are efferent projections to the stomach, which modulate the activity of muscle cells through activation of motor neurones. This circuit has been called a vago-vagal reflex. Gastric flow is the product of pressure increases in certain areas that cause contractions, modulating the flow through the pylorus.

In summary, amylin receptor mechanisms are unknown, and their real behavior may be masked by its core component, calcitonin receptors. Also, there seem to be many different subtypes of receptors (depending on the CTR core and depending on the RAMP). Hence, the modeling approach cannot focus on amylin receptors since there are numerous information gaps.

Moreover, in the current simulators, there is no model of neurological signals, making the direct translation of the amylin effect very complex. Instead, it is possible to act over functional descriptions of the modulation on gastric emptying described in meal models, which is the end goal of amylin action. Hence, the pramlintide model definition will be based on proposing structure hypothesis inspired by PK/PD models in the literature and selecting the one providing the best fitting.

7.3 Proposed model structures

This work aims to describe both the PK and PD behavior of pramlintide. The first part of the work will focus on describing the drug's appearance in plasma after subcutaneous administration. On the other hand, the PD subsystem will modulate gastric emptying as a function of plasma pramlintide concentration since, as described in Section 2.2.2, the pramlintide effect is dose-dependent. Although pramlintide administration has chronic effects, reducing body adiposity and increasing energy expenditure (Boyle et al., 2022), this work will aim to cover the description of gastric emptying only.

More detail will be given on the datasets used for validation in the next chapter, but since we had no access to complete clinical datasets, a literature search was conducted in order to gather average data from published works. The development of the model was based on the available datasets, so three differentiated stages were defined:

1. Intravenous pharmacokinetics, which describes how pramlintide appears in plasma after an intravenous input.

2. Subcutaneous pharmacokinetics, that defines pramlintide appearance in plasma from a subcutaneous input and will integrate intravenous PK as a submodel.

3. Pharmacodynamics, which describes the effect of plasma concentration of pramlintide on gastric emptying.

Given that there was availability of PK intravenous data, it was decided to add it as a complementary stage to the description of PK, to be combined with the subcutaneous stage.

The modeling approach consisted of proposing several model structures based on commonly observed structures in the literature. The process of selecting and combining the candidate structures will be explained in the next chapter. This section presents the base ground of the model composition, listing all the considered model structures.

The structures selected for each stage will be interconnected in the progression shown in Figure 7.1, where $U_{sc}(t)$ represents the input of subcutaneous pramlintide to the system. $P(t)$ is the plasma concentration that is measured in the intravenous PK block. Said magnitude is later translated to the PD model, where the gastric emptying is modulated. This model is integrated with a meal model chosen from the literature and will be described in the following subsections.

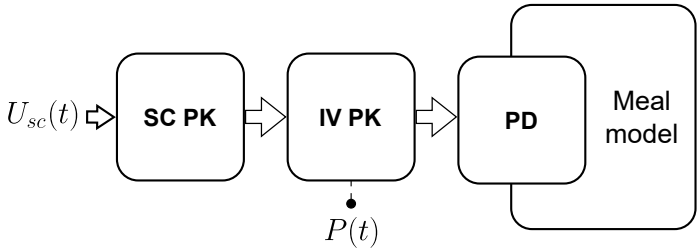

Figure 7.1: Pramlintide modeling summary.

The procedure followed in this section starts with the description of intravenous PK. Since the available data are plasma measurements, the proposal for intravenous kinetics should be defined before the subcutaneous kinetics are analyzed. Hence, the following subsections will present the candidate structures considered for intravenous PK, subcutaneous PK, and PD in that order. The letters IV and SC are used throughout the chapter as abbreviations for intravenous and subcutaneous, respectively.

7.3.1 Intravenous pharmacokinetics model

Intravenous PK describes plasma pramlintide behavior after a pramlintide input is administered directly into plasma. Said input could either be an intravenous injection or the amount of pramlintide coming from the subcutaneous compartments, as it will be later in our case.

A relevant precedent of intravenous PK model in the literature is the one presented by Clodi et al. (1998) (see Section 3.4). This model comprised a chain of three compartments and was validated using plasma pramlintide clinical data. Clodi's model is used in Ramkissoon et al. (2014), with the same parameters used in the original work.

IV structure 1 The first hypothesis (labeled 1) is based upon Clodi's model, following the same model structure. Originally, the system was determined to have as many compartments as exponentials were needed to fit the data. The system is composed by three compartments ($P_1(t), P_2(t)$, and $P_3(t)$). The input pramlintide ($U_p(t)$) enters the system through P_1, which is where the plasma measurements are taken ($P(t)$).

$$\dot{P}_1(t) = U_p(t) - (k_{pe} + k_{p12}) \cdot P_1(t) + k_{p21} \cdot P_2(t) \tag{7.1a}$$
$$\dot{P}_2(t) = k_{p12} \cdot P_1(t) - (k_{p21} - k_{p23}) \cdot P_2(t) + k_{p32} \cdot P_3(t) \tag{7.1b}$$
$$\dot{P}_3(t) = k_{p23} \cdot P_2(t) - k_{p32} \cdot P_3(t) \tag{7.1c}$$

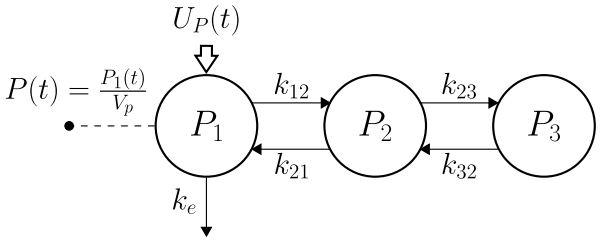

A series of transfer rates (k_{ij}, where i is the origin compartment and j is the destination) describe the transfer of material from one compartment to another in the system. Although the original paper already provides values for the transfer rates between compartments, they will be re-identified because the original dataset belonged to data from people without T1D. The rate k_e represents the pramlintide clearance rate.

IV structure 2 The above proposal is simplified to include two compartments only. The pramlintide degradation in plasma may not require three compartments, and a simpler solution may suffice.

$$\dot{P}_1(t) = U_p(t) - (k_{pe} + k_{p12}) \cdot P_1(t) + k_{p21} \cdot P_2(t) \tag{7.2a}$$
$$\dot{P}_2(t) = k_{p12} \cdot P_1(t) - k_{p21} \cdot P_2(t) \tag{7.2b}$$

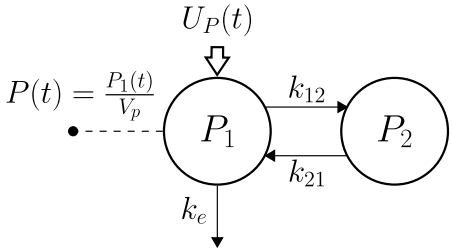

IV structure 3 Similar to other proposals in the literature for insulin kinetics (such as Wilinska et al. (2010) or Kanderian et al. (2012)), only one compartment is used for describing pramlintide PK intravenously.

$$\dot{P}_1(t) = U_p(t) - k_{pe} \cdot P_1(t) \tag{7.3}$$

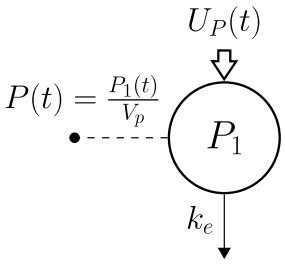

Some other options were also considered, as add-ons to the previously described structures, that do not modify the base structures of the model.

IV structure A This structure contemplates the addition of a compartment ($P_0(t)$) prior to $P_1(t)$, representing a delay in the displacement of pramlintide either from the site of injection or from the subcutaneous stage.

$$\dot{P}_0(t) = U_p(t) - k_{p01} \cdot P_0(t) \tag{7.4a}$$
$$\dot{P}_1(t) = k_{p01} \cdot P_0(t) - (...) \tag{7.4b}$$

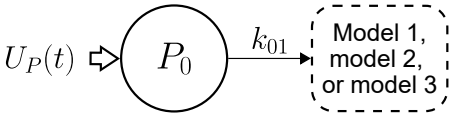

Equation (7.4b) is left incomplete since the definition of $\dot{P}_1(t)$ will depend on the selected base structure (1, 2, or 3, as seen in the upper diagram), which will be modified according to the new input coming from the $P_0(t)$ compartment ($k_{p01} \cdot P_0(t)$).

Each of the numbered structures will be combined with structure A, or be left on its own, potentially providing up to six model combinations.

In every case, plasma pramlintide concentration is obtained the same way regardless of the underlying structure, as described by Equation (7.5).

$$P(t) = \frac{P_1(t)}{V_P} \tag{7.5}$$

7.3.2 Subcutaneous pharmacokinetics model

The second section comprises the subcutaneous PK stage. Subcutaneous kinetics describes how the drug behaves from the subcutaneous infusion point until the compartment where plasma concentration measurements are taken. This is the stage of more interest since it will simulate the subcutaneous infusion of pramlintide, which is the intended use in AP systems, to which the potential model will be aimed.

Subcutaneous pramlintide PK models are scarce in the literature. The most relevant precedent is the work in Ramkissoon et al. (2014). In that paper, the authors model intravenous PK with the Clodi model and base the design of subcutaneous PK on previous work focused on testing insulin PK structures (Wilinska et al., 2005).

Similar to the approach followed in the previous section, a series of hypotheses are laid out to test their capability of describing the data. In every case, the signal $U_p(t)$ describes the magnitude leaving the subcutaneous block and going into the intravenous PK stage.

SC structure 1 This structure assumes only one compartment needs to be added between the subcutaneous infusion ($U_{sc}(t)$) and the intravenous PK model.

$$\dot{Q}_1(t) = U_{sc}(t) - k_q \cdot Q_1(t) \tag{7.6a}$$
$$U_p(t) = k_q \cdot Q_1(t) \tag{7.6b}$$

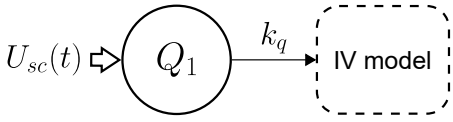

SC structure 2 The second considered structure assumes a consecutive chain of two compartments.

$$\dot{Q}_1(t) = U_{sc}(t) - k_{q1} \cdot Q_1(t) \tag{7.7a}$$
$$\dot{Q}_2(t) = k_{q1} \cdot Q_1(t) - k_{q2} \cdot Q_2(t) \tag{7.7b}$$
$$U_p(t) = k_{q2} \cdot Q_2(t) \tag{7.7c}$$
$$\tag{7.7d}$$

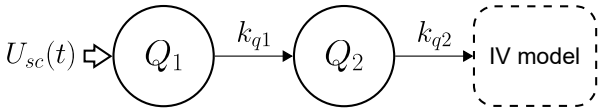

SC structure 3 The next candidate also considers two compartments but distributes the flow of pramlintide in a triangular structure:

$$\dot{Q}_1(t) = U_{sc}(t) - (k_{qe1} + k_{q12}) \cdot Q_1(t) \tag{7.8a}$$
$$\dot{Q}_2(t) = k_{q12} \cdot Q_1(t) - k_{qe2} \cdot Q_2(t) \tag{7.8b}$$
$$U_p(t) = k_{qe1} \cdot Q_1(t) + k_{qe2} \cdot Q_2(t) \tag{7.8c}$$

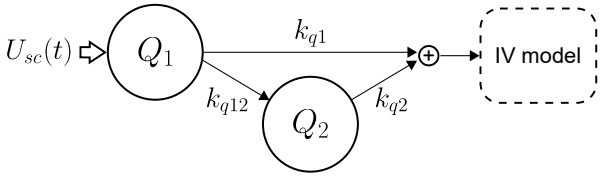

SC structure 4 Similar to the insulin PK structure used in Smaoui et al. (2020a) for the insulin, the following hypothesis presents two parallel chains, assuming a fast and a slow channel in the subcutaneous absorption.

$$\dot{Q}_1(t) = k_f \cdot U_{sc}(t) - k_{q1} \cdot Q_1(t) \tag{7.9a}$$
$$\dot{Q}_2(t) = (1 - k_f) \cdot U_{sc}(t) - k_{q2} \cdot Q_2(t) \tag{7.9b}$$
$$\dot{Q}_3(t) = k_{q2} \cdot Q_2(t) - k_{q3} \cdot Q_3(t) \tag{7.9c}$$
$$U_p(t) = k_{q1} \cdot Q_1(t) + k_{q3} \cdot Q_3(t) \tag{7.9d}$$

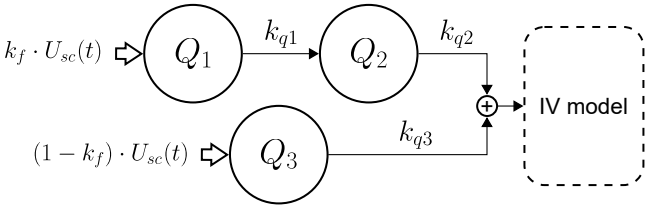

SC structure A Introduces a bioavailability coefficient (a_s) to account for some hypothetical loss of pramlintide at the infusion site.

$$\dot{Q}_1(t) = a_s \cdot U_{sc}(t) - (...) \tag{7.10}$$

In this case, the input to all variants will be the subcutaneous pramlintide input, $U_{sc}(t)$, and the output will be the amount of pramlintide going into plasma, $U_p(t)$.

The aforementioned structures are combined to form eight different model candidates.

7.3.3 Pharmacodynamics model

Pharmacodynamics describes the effects on the organism of a certain substance in plasma. As mentioned in the introduction, amylin has many effects, mainly regulated by the central nervous system since amylin receptors are located in the brain (Lutz, 2022). Even so, this work aims to find a relationship between the concentration of plasma pramlintide and its effect on the gastric emptying process after a meal.

Precedents in literature modeling pramlintide PD can be found in Fang et al. (2013), Micheletto et al. (2013), or Ramkissoon et al. (2014). However, the model proposed by Fang et al. (2013) has a main limitation: the pramlintide effect on gastric emptying is independent of the amount of the pramlintide dose. The authors in Micheletto et al. (2013) modify an existing meal model, reidentifying its parameters to fit glucose rate of appearance clinical data (data from Woerle et al. (2008)). However, no new PD model is proposed, and the mechanics to emulate the effect of different pramlintide doses are not described in the paper. The model in Ramkissoon et al. (2014) is a complete PK/PD model that describes the effect of pramlintide modifying the meal action t_{max} parameter. These modifications are incorporated to the meal model proposed in Hovorka et al. (2004), but they introduce a piecewise function that produces a discontinuity and implementing the model requires an analytical solution of the meal model used.

The pramlintide PD model proposed in this work modifies the glucose rate of appearance after a meal. The meal model used in this work was presented in Dalla Man et al.

(2006), and three differential equations describe it (see Table 8.10 for the description of parameters and values):

$$\dot{Q}_{sto1}(t) = U_g(t) - k_{g21} \cdot Q_{sto1}(t) \tag{7.11a}$$
$$\dot{Q}_{sto2}(t) = k_{g21} \cdot Q_{sto1}(t) - k_{empt}(Q_{sto}) \cdot Q_{sto2}(t) \tag{7.11b}$$
$$\dot{Q}_{gut}(t) = k_{empt}(Q_{sto}) \cdot Q_{sto2}(t) - k_{abs} \cdot Q_{gut}(t) \tag{7.11c}$$

where $Q_{sto}(t), k_{empt}(Q_{sto})$, and α are defined as:

$$Q_{sto}(t) = Q_{sto1}(t) + Q_{sto2}(t) \tag{7.11d}$$
$$k_{empt}(Q_{sto}) = k_{min} + \frac{k_{max} - k_{min}}{2} \cdot (\tanh(\alpha \cdot (Q_{sto}(t) - b \cdot D)) + 1) \tag{7.11e}$$
$$\alpha = \frac{5}{2 \cdot D \cdot (1 - b)} \tag{7.11f}$$

The system's output is the meal rate of glucose appearance $(R_a(t))$, defined as follows.

$$R_a(t) = \frac{f \cdot k_{abs} \cdot Q_{gut}(t)}{BW} \tag{7.11g}$$

The purpose of the developed pramlintide PD model is to modulate the rate of gastric emptying, $k_{empt}(Q_{sto})$, applying a multiplying factor that we have defined as:

$$\eta(\mathcal{P}) = \frac{1}{1 + h(\mathcal{P})} \tag{7.12}$$

where $\mathcal{P}$ is the input variable to the function, which will be related to the plasma pramlintide concentration $P(t)$, and $h(\mathcal{P})$ is a monotonically increasing function, with $h(0) = 0$, such that the larger the pramlintide concentration is, the slower the gastric emptying.

Similar to the previous sections, a series of structures have been studied to describe pramlintide dynamics. Structures 1 to 3 refer to the definition of $\mathcal{P}$, whereas structures A to D refer to the form of h.

PD structure 1 This structure assumes $\mathcal{P}$ is just equal to the amount of pramlintide in the compartment where plasma pramlintide is measured (P_1).

$$\mathcal{P} = P_1(t) \tag{7.13}$$

PD structure 2 The second structure introduces a delay in the form of an extra compartment (P_{eff}) between the intravenous stage and the PD subsystem.

$$P_{\mathit{eff}} = k_a \cdot (P_1(t) - P_{\mathit{eff}}(t)) \tag{7.14a}$$
$$\mathcal{P} = P_{\mathit{eff}}(t) \tag{7.14b}$$

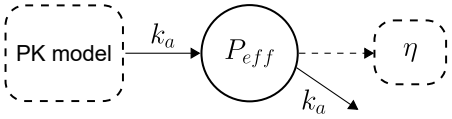

PD structure 3 Structure 3 uses a double-compartment chain.

$$P_{\mathit{eff1}} = k_a \cdot P_1(t) - k_b \cdot P_{\mathit{eff1}}(t) \tag{7.15a}$$
$$P_{\mathit{eff2}} = k_b \cdot (P_{\mathit{eff1}}(t) - P_{\mathit{eff2}}(t)) \tag{7.15b}$$
$$\mathcal{P} = P_{\mathit{eff2}}(t) \tag{7.15c}$$

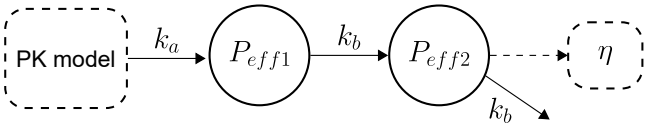

Once the different inputs ($\mathcal{P}$) are laid out, the following structures propose different definitions for the function h.

PD structure A Assumes $h(\mathcal{P})$ does not perform any modifications on the input signal.

$$h(\mathcal{P}) = \mathcal{P} \tag{7.16}$$

PD structure B Introduces a linear modification of $\mathcal{P}$ using a constant value, α:

$$h(\mathcal{P}) = \alpha \cdot \mathcal{P} \tag{7.17}$$

PD structure C Proposes a transformation based on a Michaelis-Menten structure.

$$h(\mathcal{P}) = \frac{n \cdot \mathcal{P}}{d + \mathcal{P}} \tag{7.18}$$

PD structure D Defines h as a Hill equation. Both this and the previous structures were considered in the development of the glucagon receptors model since they are widely used structures to describe saturation in biological processes (Goutelle et al., 2008).

$$h(\mathcal{P}) = \frac{n \cdot \mathcal{P}^e}{d^e + \mathcal{P}^e} \tag{7.19}$$

Based on these model structures, a total of 12 combinations are available to test their performance.

7.4 Validation methods

This section describes the methods and tools used in the next chapter to evaluate the model structures and find the most adequate pramlintide model. Some of the resources are shared with those used in the evaluation of the glucagon receptors model. Hence, those elements will be mentioned but not described in the same detail as in Section 4.4.2.

There are significant differences between the development of the glucagon model in the previous part and the present one. In the case of the glucagon model, many model structures have been tested and proposed in the literature. That is why a comparison against different structures from the literature was deemed an appropriate way to validate the glucagon model proposal. However, pramlintide models are a rarity, as presented in Section 3.4. There are few precedents to compare to, making it difficult to reproduce the same procedure. In this section, a series of hypotheses regarding the optimal model structures are presented, and the validation process will evaluate each model's performance.

Given the limited amount of available data, a series of combinations have been made (presented in Chapter 8) to distribute the data into identification and validation datasets. Then, model structures were evaluated based on performance metrics that are described in this section. The specifics of the methods followed in each stage will be detailed in the next chapter. Nevertheless, the general procedure consisted of the following:

1. Defining the model structures to evaluate based on combining the hypotheses presented in the previous section.

2. Asses their individual structural identifiability to ensure the identification was possible.

3. Identify its parameters based on the selected datasets for identification by optimization of the performance index (J), which was based on RMSE values.

4. Evaluate the performance of each model structure based on the results of the assessment metrics obtained with the validation datasets.

7.4.1 Identification and optimization process

Similarly to the identification of the glucagon models, an optimization was carried out, with the goal of minimizing the RMSE between the simulation and the data. In this occasion, a value of RMSE was obtained per dataset, according to the following formula:

$$\text{RMSE}_d = \sqrt{\frac{1}{N_d}\sum_{i=1}^{N_d}(\hat{y}_i^d - y_i^d)^2} \tag{7.20}$$

where d refers to the specific dataset, $\hat{y}_i^d$ are the simulation points, y_i^d are the data points, and N_d is the total number of samples.

Additionally, there were some sets of identification data with significant magnitude differences between them. In those cases, the normalized RMSE (NRMSE) was used instead to measure the simulation errors:

$$\text{NRMSE}_d = \frac{\text{RMSE}_d}{\max(y^d) - \min(y^d)} \tag{7.21}$$

Then, the optimization index (J) for a specific model was calculated as the sum of RMSEs obtained for each set of data used (total number denoted by D):

$$J = \sum_{d=1}^{D} \text{RMSE}_d \tag{7.22}$$

Replicating the identification carried out for the glucagon model, a parameter set was obtained per model, minimizing the RMSE obtained in a set of identification-selected datasets.

The evaluated model structures follow a compartmental model structure; hence, they were implemented as differential equations and solved using the `ode45` function (see Section 4.4.2). The optimization process was carried out in MATLAB (version R2021b). However, Matlab's genetic algorithm (`ga`) was used to solve the optimization process instead of `fmincon`. This algorithm is population-based and searches randomly across the population, which may avoid providing a solution on a local minimum and finding the global minimum instead. This algorithm also is able to run without specifying parameter boundaries, which is useful when there is no precedent on what the parameter values might be, as in the present case.

The structural identifiability of the models was evaluated using Matlab's toolbox GenSSI (Chiş et al., 2011a), also described in Section 4.4.2. This software applies the Generating Series Approach (Walter and Lecourtier, 1982) to determine whether a model is structurally globally identifiable (all the parameters are uniquely determined with the given inputs and output in the absence of noise), structurally locally identifiable (some of the model parameters have a finite set of values), or structurally unidentifiable (at least one parameter has infinite solutions).

7.4.2 Performance evaluation

After identifying the parameter values for the *identification* sets of data, their performance was compared to the data in the *validation* datasets. In the evaluation of the glucagon model, the analysis was limited to the differences between the obtained RMSE values. However, in this case, we also wanted to weigh in additional aspects that would evaluate the model structures per se (e.g., including the number of identified parameters in the index calculation).

A collection of metrics for model evaluation was gathered from Moscardó García (2019) (Chapter 5) and Pham (2019), where different metrics are reviewed and tested. A total of six criteria were selected for consideration in the analysis of the proposed model. The first one included was the R-squared (R^2) metric,

$$R^2 = 1 - \frac{\sum_{i=1}^{n} (y_i - \hat{y}_i)^2}{\sum_{i=1}^{n} (y_i - \bar{y})^2}$$

which measures the amount of variation accounted for in the fitted model. Variable $\hat{y}_i$ represents the simulation points, y_i are the data points, and $\bar{y}$ is the average value of the data. A variation of this metric is the Adjusted R-squared (Adj R^2), defined as:

$$R^2_{adj} = 1 - \left(\frac{n-1}{n-k}\right)\left(1 - R^2\right)$$

where n is the number of data points and k is the number of parameters. This metric adds a weight to account for the number of parameters in the model. The *mean absolute percentage error* (MAPE) was also considered:

$$\text{MAPE} = \frac{\sum_{i=1}^{n} \frac{|y_i - \hat{y}_i|}{y_i}}{n}$$

This metric measures the model prediction accuracy. A new criterion was proposed in Pham (2019), PIC (PIC, *Pham Information Criterion*), which combines an assessment of the error obtained with the model and a penalty based on the number of parameters with respect to the number of data samples.

$$\text{PIC} = SSR + k\left(\frac{n-1}{n-k}\right)$$

Additionally, the Akaike Information Criterion (AIC) and the Bayesian Information Criterion (BIC) were also considered. These two metrics commonly serve as selection criteria when proposing different biological models (e.g., van Sloun et al. (2023); Faggionato et al. (2023); Wilinska et al. (2005); Lv et al. (2013)). Their formulae are defined as follows:

$$\text{AIC} = n \cdot \ln\left(\frac{SSR}{n}\right) + 2 \cdot k \tag{7.23}$$

$$\text{BIC} = n \cdot \ln\left(\frac{SSR}{n}\right) + \ln(n) \cdot k \tag{7.24}$$

SSR stands for *sum of squared residuals* and is calculated as:

$$\text{SSR} = \sum_{i=1}^{n} (\hat{y}_i - y_i)^2$$

The interpretation of the presented metrics is usually related to their absolute value: the lower the value obtained, the better the performance of the model. The R^2 and Adj R^2 are the exceptions to this since their values span from 0 to 1 (or in percentage, from 0 to 100%), and the closer they are to 1, the more accurate the fit of the model to the data.

The preliminary assessment of the model structures included results obtained with each one of these metrics (including the RMSE). However, those analyses have not been included in this work for brevity, and the final evaluation was limited to the information provided by the AIC and BIC indexes since they were the most significant and are some of the most extensively used for model evaluation.

7.5 Conclusions

This chapter has presented the different hypotheses considered in order to define the proposed pramlintide PK/PD model. Since the physiology surrounding amylin receptor regulation and signaling is not well-known, the proposed model structures are based on structures commonly used in the literature to define biological models. The last part of the chapter lays out the general methodology and tools that will be used in the following chapter to assess the capabilities of each model combination in describing pramlintide data.

Chapter 8

Pramlintide model validation

This chapter presents the consecutive identification and validation processes performed to evaluate the candidate pramlintide model structures and propose a PK|PD model. First, the collection of literature data used is presented. Then, the procedures are divided into each evaluated stage: subcutaneous PK, intravenous PK, and PD. Finally, the complete model is presented, and the results are discussed. A preliminary approach to the model proposal was presented in a conference abstract:

- *Miragall, J. , Furió-Novejarque, C., Sala-Mira, I., Díez, J.L., Bondia, J. (2023). A new pharmacokinetics and pharmacodynamics model of subcutaneous pramlintide infusion. 16th International Conference on Advanced Technologies & Treatments for Diabetes (ATTD 2023). Berlin (Germany). In Diabetes Technology and Therapeutics, 25(S2):A-136.*

And the results of the procedures obtained in this chapter have been published in a journal paper:

- *Furió-Novejarque, C., Sala-Mira, I., Díez, J.L., Bondia, J. (2024). A model of subcutaneous pramlintide pharmacokinetics and its effect on gastric emptying: Proof-of-concept based on populational data. Computer Methods and Programs in Biomedicine, 244(February): 107968.*

8.1 Data collection

Identification and validation of any model is based on data availability to compare the simulation results against. Unfortunately, we did not have access to clinical individual datasets from pramlintide trials. Hence, some datasets were gathered from the literature based on published data plots. Since individual graphs were not usually disclosed, only average values could be picked up. Data points were collected using the software *WebPlot-Digitizer* (Rohatgi, 2022). This allowed obtaining a collection of datasets that helped to validate pramlintide average behavior.

Parallel to the three stages that compose the model, three kinds of data were searched for:

- plasma pramlintide concentration after intravenous pramlintide injections,
- plasma pramlintide concentration after subcutaneous pramlintide administration, and
- rate of glucose appearance after a meal accompanied by pramlintide administration.

Unlike other works in the literature (Ramkissoon et al., 2014; Fang et al., 2013), this validation considers the meal rate of glucose appearance rather than glucose values to validate the PD model proposals. Manipulating the rate of glucose appearance allows decoupling the PD pramlintide model from other subsystems in the glucoregulatory model (e.g., insulin effect, endogenous glucose production). However, obtaining the rate of glucose appearance values requires a tracer study, meaning that it is neither trivial nor inexpensive, so only a few works in the literature were found to report this kind of data.

After a thorough literature revision, a total of 17 datasets were selected for this work. Some other works were discarded because of data undersampling in some periods of interest or lack of data of interest (e.g., only glucose values were reported, which is helpful to observe the effect of pramlintide on glucose but did not provide enough information for our modeling purposes) (Weyer et al., 2003, 2001; Thompson et al., 1997b; Rodriguez et al., 2007; Huffman et al., 2009). As mentioned, mean values are used since no individual curves were available, meaning that the final result is a set of parameters describing pramlintide's average behavior. This same procedure was followed in Ramkissoon et al. (2014). Table 8.1 provides a summary of the trial protocol followed in each selected work (second column), a description of the data of interest available (third column), and a list of names used as keys to refer to each of the datasets (fourth column).

Source	Trial summary	Data description	Datasets ID
Colburn et al. (1996)	Study evaluating the effect of bolus and infusion administration of pramlintide on 24 men with T1D.	Plasma pramlintide data for 2-minute boluses (30 μg, 100 μg, 300 μg) and 2-hour infusions (30 μg, 100 μg, 300 μg).	Col-B-30, Col-B-100, Col-B-300, Col-I-30, Col-I-100, Col-I-300
Kong et al. (1998)	Study aimed to observe the effect of single doses of pramlintide on two separate meals. 11 men with T1D participated in the study.	Plasma pramlintide data for boluses (30 μg, 60 μg, 90 μg).	Kon-30, Kon-60, Kon-90
Kolterman et al. (1996)	Effect of pramlintide after accompanying meals with a pramlintide bolus for 14 days on 84 people with T1D.	Plasma pramlintide concentrations on the first study day (30 μg, 100 μg, 300 μg).	Kol-30, Kol-100, Kol-300
Ahren et al. (2002)	Study of pramlintide and GLP-1 relationship on 9 people with T1D.	Plasma pramlintide concentrations after a 30 μg bolus.	Ahr-30
Chase et al. (2009)	Evaluation of pramlintide PK/PD in 12 adolescents with T1D.	Plasma pramlintide data after pramlintide boluses (30 μg and 15 μg*).	Cha-30
Hassan and Heptulla (2009)	Study of pramlintide effect on 8 adolescents with T1D.	Plasma pramlintide data result of a 30 μg pramlintide bolus.	Has-30

Continued in next page

Continued from previous page

Source	Trial summary	Data description	Datasets ID
Woerle et al. (2008)	Evaluation of pramlintide effect on gastric emptying on 15 people with T1D.	Glucose rate of appearance data (after a meal of 53 g of CHO plus a 30 μg pramlintide bolus or placebo).	Woe-30, Woe-Placebo
Hinshaw et al. (2016)	Study on pramlintide effect on postprandial glucose on 12 people with T1D.	Glucose rate of appearance data (meal of 75 g CHO plus 30 μg pramlintide bolus or placebo).	Hin-30, Hin-Placebo

*The data corresponding to the 15 μg bolus was not used because few data points were available.

Table 8.1: Summary of datasets used for identification and validation in this work.

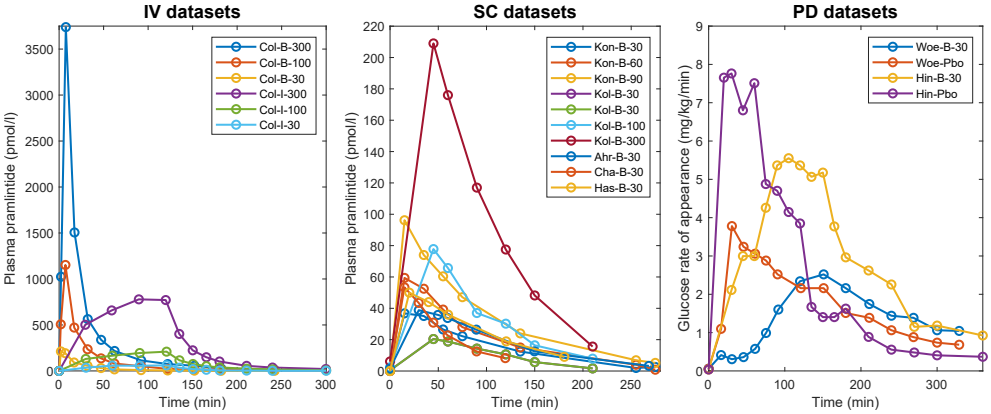

Figure 8.1: Pramlintide datasets summary. The plot on the left shows the datasets of plasma pramlintide extracted from the Colburn study for the intravenous stage. The center plot aggregates the data gathered for the subcutaneous validation, and the right plot shows the two pairs of datasets for glucose rate of appearance, both the placebo and the pramlintide. Datasets' keys listed in the legend are defined in Table 8.1.

Figure 8.1 summarizes the datasets gathered, divided into each studied stage. Legend in the three plots shows the data IDs as listed in Table 8.1. Most of the datasets in the subcutaneous stage include a 30 μg dose; however, it can be seen how there is a significant magnitude disparity among the collected average values. Lastly, in the PD datasets plots it can be observed the significant difference that pramlintide introduces in the rate of glucose appearance compared to its absence (Woe-B-30 (blue) versus Woe-Pbo (orange), and Hin-B-30 (yellow) versus Hin-Pbo (purple)).

8.2 Identification procedure

This section describes the modeling process for each stage. As mentioned in Section 7.4, the basic procedure for the model structures' selection will be similar in each stage, and it is summarized in Figure 8.2. First, the model combinations based on the possibilities presented in Section 7.3 will be set up. A structural identifiability analysis will check whether all parameters in each model combination are structurally identifiable. Then, the parameters will be identified, and the selection will be carried out based on the results of AIC and BIC with the validation datasets. However, each stage required some variations from this procedure that will be explained in their corresponding subsections.

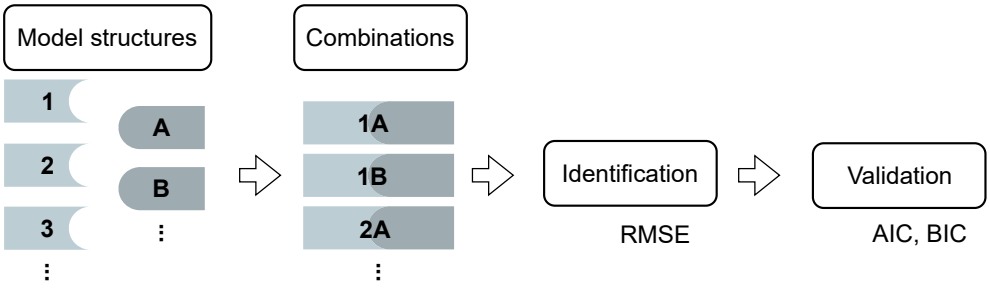

Figure 8.2: Pramlintide models selection procedure summary. Different model structure candidates are assembled to form model combinations that are identified based on the RMSE, and the most adequate model is selected based on the validation AIC and BIC results.

Table 8.2 provides an overview of the selected data for the identification and validation of each stage. Datasets are listed according to the identifiers defined in Table 8.1. The first group corresponds to intravenous PK (IV), the second to subcutaneous PK (SC), and the third to PD. More details about each of them will be provided in the following sections.

Stage	Identification data	Validation data
STAGE-IV1	Col-B-30, Col-B-100, Col-B-300	Col-I-30,Col-I-100,Col-I-300
STAGE-IV2	Col-I-30, Col-I-100, Col-I-300	Col-B-30, Col-B-100, Col-B-300
STAGE-IV3	Col-I-30, Col-I-100, Col-I-300, Col-B-30, Col-B-100, Col-B-300	
STAGE-SC	Kon-30, Kon-60, Kon-90	Kol-30, Kol-100, Kol-300, Ahr-30, Cha-30, Has-30
STAGE-PD0	Woe-Placebo, Hin-Placebo	
STAGE-PD1	Woe-30	
STAGE-PD2	Hin-30	

Table 8.2: Identification and validation data summary. IV refers to the intravenous pharmacokinetics stage, SC to the subcutaneous pharmacokinetics, and PD to the pharmacodynamics stage. Datasets keys are defined in Table 8.1.

8.2.1 Intravenous PK model

Plasma pramlintide data from Colburn et al. (1996) is used to identify and validate the proposal (see the first three rows of Table 8.2). The same dataset was used in Fang et al. (2013) to propose and validate a PK/PD pramlintide model. The trial by Colburn involved 24 people with insulin-dependent diabetes mellitus (i.e., T1D) that were divided into three groups and were administered 30 μg, 100 μg, or 300 μg, in bolus or infusion form, depending on the study arm.

In order to best describe pramlintide kinetics, a series of hypotheses have been made, described in Section 7.3.1. In total, three different structures were proposed for the general structure of the model (1, 2, and 3), and one affecting the input to the system (A). Combining these hypotheses leaves us with six models to evaluate, as listed in Table 8.3. This table also indicates the total number of parameters to identify, as well as the results of the structural identifiability analysis provided by GenSSI. All parameters for every structure were globally structurally identifiable. Of note, for structure 1A only parameters V_p and k_{p01} were globally identifiable, with the remaining parameters being locally identifiable. However, since there were no unidentifiable parameters, the identification was carried out without issues.

Since there were plasma pramlintide data for three doses of intravenous boluses

IV model combinations	1	1A	2	2A	3	3A
Number of parameters	6	7	4	5	2	3
Structurally globally identifiable	✓	V_p, k_{p01} *	✓	✓	✓	✓

*Parameters V_p and k_{p01} in structure 1A were globally identifiable. The remaining parameters ($k_e, k_{12}, k_{21}, k_{23}, k_{32}$) were locally identifiable.

Table 8.3: Evaluated model structures for pramlintide intravenous pharmacokinetics.

and three doses of intravenous infusion, cross-validation was performed, using the bolus data to identify first and validate second, and vice versa with the infusion data (see rows STAGE-IV1 and STAGE-IV2 in Table 8.2).

The selection of the best model structures for intravenous PK consisted of three steps. First, AIC and BIC values were calculated for validation results in STAGE-IV1. Second, AIC and BIC were calculated for validation in STAGE-IV2 (see row STAGE-IV1 and STAGE-IV2 in Table 8.4 for the results). Then, a combination metric was obtained to integrate the results of both validations. This metric was based on calculating the mean of the means ($\bar{\mu}$) and the median of the medians ($\overline{M}$), as shown in Equation (8.1):

$$\bar{\mu}_C = \text{mean}\left(\mu^C_{\text{STAGE-IV1}}, \mu^C_{\text{STAGE-IV2}}\right) \tag{8.1a}$$

$$\overline{M}_C = \text{median}\left(M^C_{\text{STAGE-IV1}}, M^C_{\text{STAGE-IV2}}\right) \tag{8.1b}$$

The variable C represents the criterion considered (either AIC or BIC); μ^C is the mean value of the criterion obtained for STAGE-IV1 or STAGE-IV2; M^C represents the median AIC or BIC value for each stage. The results obtained with these metrics are detailed in Table 8.4, under the "Combination of STAGE-IV1 and STAGE-IV2" section. Based on these results, the three structures with the lowest index values were selected for the next stage. The selection was not limited to one structure because some were more appropriate to describe infusion behavior, whereas others worked better for bolus data.

Model structures 2, 2A, and 3 consistently provided the three lowest index values, making them the selected structures for this stage. These selected structures are used as the

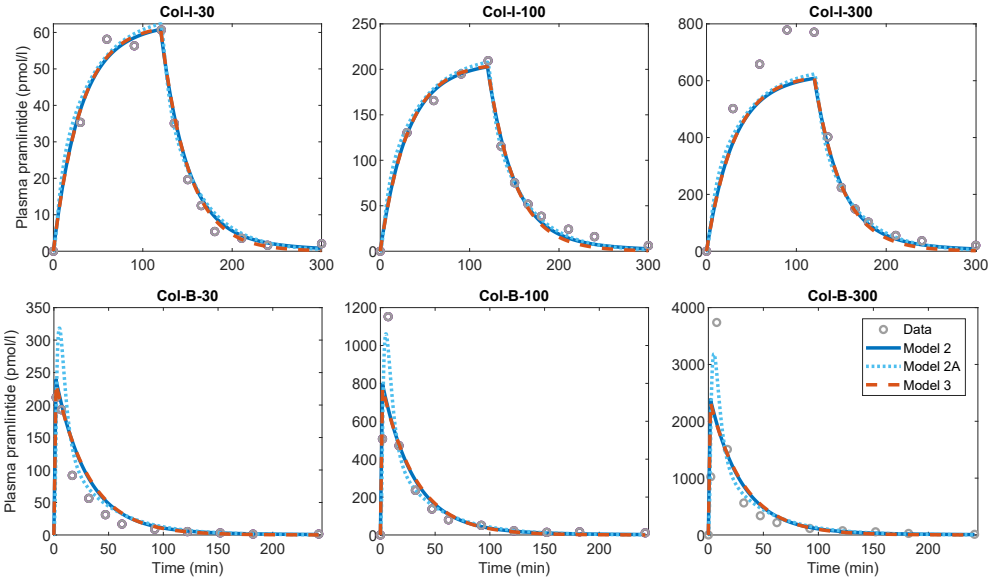

Figure 8.3: Plasma pramlintide simulation results of identification STAGE-IV3. The three selected intravenous pharmacokinetics structures are identified using data from the six datasets available from Colburn et al. (1996) (30, 100, and 300 μg 2-hour intravenous infusion doses, and 30, 100, and 300 μg 2-min intravenous boluses). The depicted models are used as base models in the subcutaneous pharmacokinetics modeling.

base for evaluating subcutaneous PK models. Since both of the performed identifications (STAGE-IV1 and STAGE-IV2) were focused on either infusion or boluses, we wanted to move forward with a set of parameters for each IV structure that adequately described both behaviors (infusion and boluses). Consequently, using both data collections, a third identification was carried out (STAGE-IV3). The NRMSE is used for calculating J (Equation (7.22)) in this stage since there is a significant magnitude difference between infusion and bolus data. The resulting parameter values are used for the intravenous PK models in the next stage.

The simulation outputs of the three models after identifying STAGE-IV3 against Colburn data are shown in Figure 8.3. Note that the models describe the smaller doses (30, 100 μg) better than the largest one, which indicates that the models may not capture certain nonlinearities in the pharmacokinetics. However, therapeutic doses are closer to 30 μg (see Table 8.1); hence the goal was to achieve a better description of those doses.

STAGE-IV1	1	1A	2	2A	3	3A
Mean AIC	74.30	94.93	70.18	89.37	**66.20***	97.95
Median AIC	65.69	88.78	61.32	82.64	**57.41***	96.50
Mean BIC	75.21	96.32	70.12	89.80	**65.17***	97.41
Median BIC	66.60	90.17	61.26	83.06	**56.38***	95.96
STAGE-IV2	1	1A	2	2A	3	3A
Mean AIC	152.64	132.72	138.96	130.74	131.09	**123.23***
Median AIC	152.42	122.16	137.37	121.26	129.74	**117.17***
Mean BIC	153.55	134.12	138.90	131.16	130.06	**122.69***
Median BIC	153.33	123.55	137.31	121.69	128.71	**116.62***
Combination of IV1 and IV2	1	1A	2	2A	3	3A
$\bar{\mu}_{\text{AIC}}$	113.47	113.83	104.57	110.06	**98.65***	110.59
$\overline{M}_{\text{AIC}}$	109.06	105.47	99.35	101.95	**93.57***	106.84
$\bar{\mu}_{\text{BIC}}$	114.38	115.22	104.51	110.48	**97.62***	110.05
$\overline{M}_{\text{BIC}}$	109.97	106.86	99.28	102.37	**92.54***	106.29
STAGE-IV3	2	2A	3			
Mean AIC	97.86	94.86	94.37			
Median AIC	100.40	102.19	96.33			
Mean BIC	97.80	95.29	93.34			
Median BIC	100.34	102.61	95.30			

Table 8.4: Pramlintide intravenous PK AIC and BIC results for STAGE-IV1 validation, STAGE-IV2 validation, and identification results of STAGE-IV3. The section "Combination of IV1 and IV2" presents the metric results obtained to select the model structures used in STAGE-IV3 (see the expressions of $\bar{\mu}$ and $\overline{M}$ in Equation (8.1)). The asterisks (*) highlight the lowest value in each row.

8.2.2 Subcutaneous PK model

Subcutaneous kinetics describes how the drug behaves from the subcutaneous infusion point until the compartment where plasma concentration measurements are taken. Similar to the approach followed in the previous section, a series of hypotheses are laid out to test their capability of describing the data (see Section 7.3.2).

The structures are combined to form eight different model candidates. Each structure was identified three times, using each selected IV structure as the base. Information about

SC model combinations	1	1A	2	2A	3	3A	4	4A
Number of parameters	1	2	2	3	3	4	4	5
Structurally globally identifiable	✓	✓	✓	✓	✓	L*	✓	✓

* Parameters were all locally identifiable for structure 3A. However, the analysis could not conclude on structural global identifiability.

Table 8.5: Evaluated model structures for pramlintide subcutaneous pharmacokinetics.

the number of parameters for each structure and their structural global identifiability is also included.

Most literature works reporting plasma pramlintide clinical data use subcutaneous boluses. The procedence of the data is listed in the second section of Table 8.1. As detailed in Table 8.2, the three datasets from Kong et al. (1998) were used for identification since they captured the concentration peak better than Kolterman et al. (1996), which is undersampled for the initial trial period.

The subcutaneous model combinations were identified three times, using each selected intravenous structure as the base. In order to evaluate these results, AIC and BIC were used, with a modification to account for the number of parameters in the base intravenous model. Parameter K in equations (7.23) and (7.24) is substituted by $k+k_{IV}$, where k is the number of parameters in the subcutaneous PK model and k_{IV} is the number of parameters introduced by the intravenous PK model. AIC and BIC values for each identification are included in Table 8.6.

The final model was selected analyzing the best mean and median AIC and BIC values. The lowest AIC and BIC values were achieved when using intravenous model 3 as the base (see Table 8.6). In turn, the best AIC and BIC results were produced by subcutaneous models 3 and 3A. Figure 8.4 shows the output produced by both models. Their behavior is quite similar, but the subcutaneous model 3A fits the tail more accurately, making it the selected model.

The final equations for the PK model, comprised of intravenous submodel 3 and subcutaneous submodel 3A, are presented in Section 8.3.

STAGE-SC (IV model 2)	1	1A	2	2A	3	3A	4	4A
Mean AIC	53.47	50.50	55.56	47.58	43.91	**43.33***	45.91	48.00
Median AIC	50.58	49.42	52.78	46.71	**46.46***	48.50	48.43	50.42
Mean BIC	53.18	50.15	55.22	47.18	43.51	**42.87***	45.45	47.48
Median BIC	50.26	48.63	52.39	46.14	**45.54***	47.45	47.38	49.24
STAGE-SC (IV model 2A)	1	1A	2	2A	3	3A	4	4A
Mean AIC	55.37	52.21	57.48	46.99	**43.84***	45.28	45.82	47.03
Median AIC	52.07	51.17	54.19	48.40	**48.34***	50.40	50.35	52.66
Mean BIC	55.02	51.81	57.07	46.53	**43.38***	44.76	45.30	46.45
Median BIC	51.68	50.25	53.73	47.35	**47.30***	49.22	49.17	51.35
STAGE-SC (IV model 3)	1	1A	2	2A	3	3A	4	4A
Mean AIC	49.43	46.47	51.53	44.06	39.85	**39.36***	41.90	41.48
Median AIC	46.60	45.40	48.79	43.15	**42.45***	44.44	44.44	46.47
Mean BIC	49.25	46.24	51.30	43.77	39.56	**39.01***	41.56	41.08
Median BIC	46.41	44.88	48.54	42.88	**41.80***	43.65	43.66	45.55

Table 8.6: Pramlintide subcutaneous pharmacokinetics AIC and BIC results for STAGE-SC validation, with each of the selected IV structures (2, 2A, and 3). The asterisks (*) highlight the lowest value in each row.

8.2.3 PD model

Pharmacodynamics describes the effects on the organism of a certain substance in plasma. As the introduction mentions, amylin has many effects, mainly regulated by the central nervous system since amylin receptors are located in the brain (Lutz, 2022). Even so, this work aims to find a relationship between the concentration of plasma pramlintide and its effect on the gastric emptying process after a meal.

The proposed model describes the effect of pramlintide on gastric emptying by multiplying the gastric emptying rate, $k_{empt}(Q_{sto})$, as described in Equation (7.12):

$$\eta(\mathcal{P}) = \frac{1}{1 + h(\mathcal{P})}$$

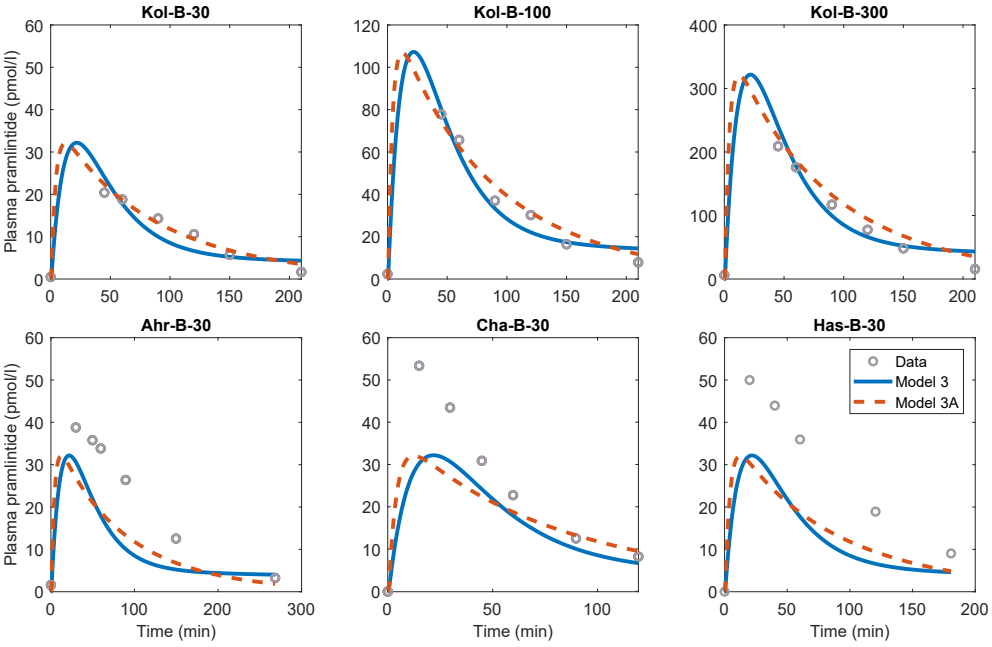

Figure 8.4: Plasma pramlintide simulation results of the STAGE-SC validation. Validation was performed with a variety of datasets (30, 100, and 300 μg subcutaneous boluses from Kolterman et al. (1996) and 30 μg boluses from Ahren et al. (2002); Chase et al. (2009); Hassan and Heptulla (2009)).

$\mathcal{P}$ is the input variable to the function, and $h(\mathcal{P})$ is the function used to modulate gastric emptying.

A series of structures have been studied to describe pramlintide dynamics, presented in Section 7.3.3. Structures 1 to 3 refer to the definition of $\mathcal{P}$, whereas structures A to D refer to the form of h.

Each of the possible inputs is paired up with each of the possible function forms, as listed in Table 8.7. Of note, combination 1A introduces no new parameters to be identified, so no identifiability analysis was performed for this structure.

Data on glucose rate of appearance is more scarce in the literature than glucose data. This is due to the complexity of the analysis and infrastructure involved (i.e., triple-tracer study (Basu et al., 2003)). The only works in the literature that perform this kind of analysis,

PD model combinations	1A	1B	1C	1D	2A	2B	2C	2D	3A	3B	3C	3D
Number of parameters	–	1	2	3	1	2	3	4	2	3	4	5
Globally identifiable	–	✓	✓	✓	✓	✓	✓	L*	✓	✓	✓	✓

* Parameters were all locally identifiable for structure 2D. However, the analysis could not conclude on structural global identifiability.

Table 8.7: Evaluated model structures for pramlintide pharmacodynamics.

including pramlintide, are the works by Woerle et al. (2008) and Hinshaw et al. (2016). In both clinical trials, the protocol follows two arms: administering a 30 μg pramlintide dose alongside a meal or a placebo dose. The glucose rate of appearance is reported for both experiments. Placebo datasets were used to identify two distinct sets of parameters for the meal model (identification STAGE-PD0, Table 8.2) before introducing any pramlintide model. Parameter values are reported in Table 8.10. Of note, $R_a(t)$ in Dalla Man et al. (2006) is defined in mg/kg/min. Hence, the appropriate transformations have been applied to the datasets used in this section to express them in said units.

Two different meal model parameters were necessary to describe each placebo dataset because the behavior of the observed signals is noticeably different (see data in Figure 8.5, upper row). Woerle data reaches a peak value of around 4 mg/kg/min, whereas Hinshaw data doubles that amount. In addition, the rate of disappearance from Woerle et al. (2008) has a value of around 160 minutes, whereas, for Hinshaw's, its value is 100 min, meaning the food leaves the stomach much faster in the second dataset. Meal composition is known to have a significant effect on the shape of glucose in the postprandial period, with faster higher responses in meals with high carbohydrate content, whereas the responses

Dataset	kcal	Carbohydrates	Fat	Protein	D
Woerle	450	45%	30%	25%	53 g
Hinshaw	703.2	55%	30%	15%	75 g

Table 8.8: Meal composition reported in Woerle et al. (2008) and Hinshaw et al. (2016). "D" denotes the number of carbohydrates used as input to the meal model for the simulations carried out in this work.

		1A	1B	1C	1D	2A	2B	2C	2D
STAGE-PD1	AIC	12.31	-13.70	-11.69	-36.18	10.20	-11.71	-9.70	**-38.51***
	BIC	11.01	-14.99	-12.28	-36.06	8.91	-12.29	-9.57	**-37.68***
		3A	3B	3C	3D				
	AIC	-11.70	-9.71	-7.69	-35.93				
	BIC	-12.29	-9.58	-6.86	-34.38				
STAGE-PD2		1A	1B	1C	1D	2A	2B	2C	2D
	AIC	46.49	17.72	7.45	**-9.64***	44.10	19.93	9.38	-8.05
	BIC	45.32	16.55	7.12	**-9.14***	42.93	19.59	9.88	-6.72
		3A	3B	3C	3D				
	AIC	7.32	9.32	11.33	-5.96				
	BIC	6.98	9.82	12.66	-3.79				

Table 8.9: Pramlintide pharmacodynamics AIC and BIC results. The asterisks (*) highlight the lowest value in each row.

will be smoother but will remain for a longer time in the case of a high protein content (Gingras et al., 2018). These discrepancies could be caused by differences in the meal composition (Table 8.8). For instance, meals reported by Hinshaw et al. (2016) contain more carbohydrates and less protein than those reported by Woerle et al. (2008), which may explain the larger and more rapid peak observed in Hinshaw data (Paterson et al., 2015).

However, we also found that a single set of parameters for the pramlintide model could not explain the transformation in both datasets. Some preliminary identifications were carried out as a cross-validation, similar to STAGE-IV1 and STAGE-IV2 (Section 8.2.1). Nevertheless, the identification of one of the datasets had unsatisfactory results in the validation performed with the other one. How the pramlintide effect is affected by meal composition is out of the scope of this work since no suitable data is available. Consequently, independent identifications were carried out for each dataset (STAGE-PD1 with Woerle data and STAGE-PD2 with Hinshaw data), aiming to find a common model structure.

All model structures from Table 8.7 were identified for each dataset. AIC and BIC results are reported in Table 8.9. Of note, these values refer to identification results as opposed to the previously presented results since no validation data is available for this stage. Results for STAGE-PD1 show that the best structure to fit Woerle data is model 2D.

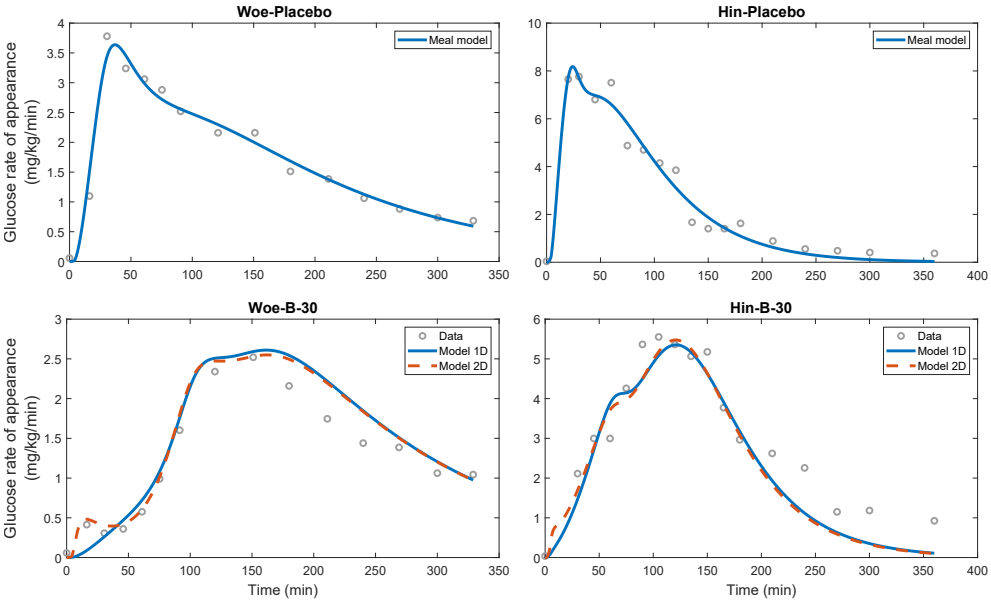

Figure 8.5: Glucose rate of appearance simulation results. Columns correspond to each dataset used (Woerle et al. (2008) data on the left column, and Hinshaw et al. (2016) on the right column). The upper row shows the meal model identification results for the trial arm of meal + placebo (STAGE-PD0). The bottom row presents the fit of PD model structures 1D and 2D to the meal + pramlintide data (STAGE-PD1 and STAGE-PD2, respectively).

However, for STAGE-PD2, the decision is split between 2D and 1D. Simulation results in Figure 8.5 (bottom row) show the responses obtained with both proposals. Although their AIC and BIC values are similar, the fit of 2D for Woerle data is closer to the data than model 1D. On the other hand, the results for both structures in Hinshaw data are fairly similar. Since our goal is to propose a structure that can adapt to different types of data, our proposed solution will be model 2D.

The behavior difference at the beginning of the simulation of the pramlintide models is mainly introduced by the parameter k_a, which represents the delay introduced by compartment $P_{\text{eff}}(t)$. It symbolizes the time it takes for pramlintide to be effective after its appearance in plasma. In the Woerle dataset, it has a value of around 12 minutes, whereas, for the Hinshaw data, the identified value is around 4 minutes. This allows observing the original glucose rate of appearance in the first samples of the simulation before the

pramlintide takes effect and slows down the glucose rise.

8.3 Results

Figure 8.6 presents an overview of the final proposed PK/PD pramlintide model. The equations that define it are listed next:

$$\dot{Q}_1(t) = a_s \cdot U_{sc}(t) - (k_{q1} + k_{q12}) \cdot Q_1(t) \tag{8.2a}$$
$$\dot{Q}_2(t) = k_{q12} \cdot Q_1(t) - k_{q2} \cdot Q_2(t) \tag{8.2b}$$
$$\dot{P}_1(t) = \big(k_{q1} \cdot Q_1(t) + k_{q2} \cdot Q_2(t)\big) - k_e \cdot P_1(t) \tag{8.2c}$$
$$P(t) = \frac{P_1(t)}{V_P} \tag{8.2d}$$
$$\dot{P}_{eff}(t) = k_a \cdot \big(P_1(t) - P_{eff}(t)\big) \tag{8.2e}$$
$$h(P_{eff}) = \frac{n \cdot P_{eff}^e}{d^e + P_{eff}^e} \tag{8.2f}$$

Equations (8.2a) and (8.2b) correspond to the subcutaneous PK (subcutaneous model 3A). Equation (8.2c) describes the intravenous kinetics (intravenous model 3), and Equation (8.2d) the plasma pramlintide concentration. Finally, equations (8.2e) and (8.2f) represent PD model 2D.

Then, applying function η (Equation (8.3a)) to the meal model, the equations for the states $Q_{sto2}(t)$ and $Q_{gut}(t)$ are modified so that the effect of pramlintide acts on the gastric emptying parameter:

$$\eta(P_{eff}) = \frac{1}{1 + h(P_{eff})} \tag{8.3a}$$
$$\dot{Q}_{sto2}(t) = k_{g21} \cdot Q_{sto1}(t) - \eta(P_{eff}) \cdot k_{empt}(Q_{sto}) \cdot Q_{sto2}(t) \tag{8.3b}$$
$$\dot{Q}_{gut}(t) = \eta(P_{eff}) \cdot k_{empt}(Q_{sto}) \cdot Q_{sto2}(t) - k_{abs} \cdot Q_{gut}(t) \tag{8.3c}$$

Table 8.10 includes the pramlintide model parameter units and descriptions. Additionally, the identified values from each selected model structure are also included.

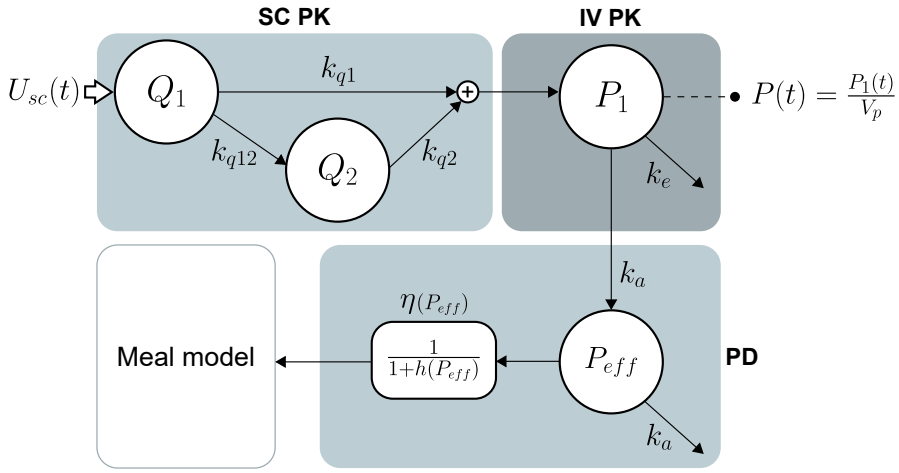

Figure 8.6: Pramlintide model proposal overview. The three main stages are represented: subcutaneous PK ((8.2a), (8.2b)), intravenous PK (8.2c) and PD ((8.3a), (8.2e), (8.2f)). The input to the system, $U_{sc}(t)$, is the subcutaneous pramlintide infusion. Pramlintide concentration in plasma is measured as $P(t)$. Pramlintide takes effect by modulating the glucose rate of appearance obtained through a meal model (7.11).

Symbol	Units	Value	Description
$U_{sc}(t)$	pmol/min	–	Pramlintide subcutaneous infusion
$Q_1(t)$	pmol	–	First subcutaneous compartment
$Q_2(t)$	pmol	–	Second subcutaneous compartment
$P_1(t)$	pmol	–	Plasma pramlintide compartment
$P(t)$	pmol/l	–	Plasma pramlintide volume
$P_{eff}(t)$	pmol	–	Pramlintide effect compartment
a_s	–	0.4235	Pramlintide bioavailability
k_{q1}	min^{-1}	0.0974	Rate from first subcutaneous compartment to plasma
k_{q12}	min^{-1}	0.1667	Rate from first to second subcutaneous compartment
k_{q2}	min^{-1}	0.0109	Rate from second compartment to plasma
k_e	min^{-1}	0.0322	Output rate from plasma compartment
V_P	l	31.549	Plasma distribution volume

Continued in next page

Continued from previous page

Symbol	Units	Value	Description
k_a	min^{-1}	(W) 0.0798, (H) 0.2671	Rate in the pramlintide effect compartment
n	-	(W) 76.662, (H) 15.156	Numerator coefficient in Hill equation from $h(P_{eff})$
d	pmol	(W) 960.87, (H) 908.01	Denominator in Hill equation from $h(P_{eff})$
e	-	(W) 4.5363, (H) 3.2745	Exponent in Hill equation from $h(P_{eff})$
$U_g(t)$	mg/min	–	Meal input rate
$Q_{sto1}(t)$	mg	–	Solid phase of glucose in the stomach
$Q_{sto2}(t)$	mg	–	Liquid phase of glucose in the stomach
$Q_{gut}(t)$	mg	–	Glucose mass in the intestine
k_{empt}	min^{-1}	–	Rate constant of gastric emptying
$R_a(t)$	mg/kg/min	–	Glucose rate of appearance in plasma
D	mg	–	Amount of ingested glucose
f	-	0.9	Fraction of intestinal absorption that appears in plasma
BW	kg	(W) 76, (H) 86	Body weight
b	%	(W) 0.8235, (H) 0.8355	Percentage of the dose for which k_{empt} decreases to $(k_{max} - k_{min})/2$
k_{abs}	min^{-1}	(W) 0.0547, (H) 0.2280	Rate constant of intestinal absorption
k_{min}	min^{-1}	(W) 0.0074, (H) 0.0196	k_{empt} minimum value
k_{max}	min^{-1}	(W) 0.0273, (H) 0.0350	k_{empt} maximum value
k_{g21}	min^{-1}	k_{max}	Grinding rate

Table 8.10: Pramlintide PK/PD model and meal model signals and parameters' descriptions and values. Meal model and pramlintide PD parameters have two values: the ones preceded by (W) correspond to values identified for data from Woerle et al. (2008), and the ones preceded by (H), from Hinshaw et al. (2016).

8.4 Discussion

A thorough validation was carried out in order to propose a pramlintide PK/PD model structure that would describe phenomena observed in clinical data. However, the validation had limitations, given the nature of the datasets used. The following paragraphs present a series of considerations over each of the model stages, a case study validation integrating the model in a T1D simulator, and a review of the limitations of this work.

The selected model for the intravenous PK stage simplifies the model proposed in Clodi et al. (1998). The three-compartment model has been reduced to a single compartment, providing an adequate description of infusion and bolus data from people with T1D. Of note, the fit for the higher dose (300 μg) is the least accurate. However, no other works found in the literature use such big intravenous doses for pramlintide therapy, and it is far from the doses tested in insulin-pramlintide AP systems (see Section 2.3.3).

Subcutaneous PK is one of the most relevant stages since most current therapies and clinical trials administer pramlintide subcutaneously. The model's fit to the identification data is accurate (results not shown), but some disparities exist in the fitting of the validation data (see Figure 8.4). Subcutaneous doses of 30 μg were the primary data of interest since the open loop use of pramlintide typically administers a 30 μg bolus alongside meals. In fact, all works used in this chapter include at least a 30 μg dose. However, average values of plasma pramlintide present some differences across the clinical trials. Most of them report peak plasma pramlintide values between 30 and 40 pmol/l after a 30 μg dose. Conversely, the data from Chase et al. (2009) and Hassan and Heptulla (2009) show plasma values up to 50-60 pmol/l. This magnitude difference could be because the study participants were adolescents instead of adults. The proposed model was fitted using data from adult patients aggregated datasets (data from Kong et al. (1998), see Table 8.1). Therefore, it is reasonable that the model describes the Cha-30 and Has-30 responses more poorly than the other sets. Hence, to further develop the proposed model, a variety of data from different cohorts would help define these differences.

Regarding the PD stage, the behavior of the two selected datasets (from Woerle et al. (2008) and Hinshaw et al. (2016)) was rather different. Nevertheless, even if a single set of parameters could not describe both signals, it was possible to find a single shared model structure. The resulting structure (whose main components are an extra compartment and a Hill equation) allows modulating the shape of the glucose rate of appearance after a meal as a function of the amount of plasma pramlintide.

Validation of the effect of pramlintide on gastric emptying using glucose rate of appearance data has an upside and a downside. The positive aspect is that it allows focusing

on glucose evolution caused solely by meal ingestion. On the other hand, the glucose rate of appearance is reconstructed based on glucose readings, meaning it is an approximation of the actual signal.

Different parameter sets had to be identified for each dataset used based on the information provided by the placebo arm of the clinical trials. An even more physiologically-accurate meal model could have better captured both datasets' behavior. Goyal et al. (2019) stated that the gastric emptying rate depends on the physical characteristics and the caloric density of meals. Focusing on the caloric content, one would expect gastric emptying in the dataset from Hinshaw et al. (2016) to be slower. However, glucose in Woerle et al. (2008) data takes almost 300 minutes to get to half its peak values, whereas, in the former, that time is around 175 minutes. Such a difference does not seem to be explained by meal composition. It could be explained by differences in caloric density (i.e., solids take longer to digest, and liquids leave the stomach faster). Nevertheless, more data is needed to include this kind of effect in the present model.

The pramlintide proposed model was integrated into an extended version of the UVA/Padova simulator, which implements the glucoregulatory model proposed by Dalla Man (Dalla Man et al., 2014). The objective of this test was to observe whether the addition of the pramlintide model would result in coherent glucose responses after its integration into the T1D simulator. Figure 8.7 shows the result of a 24-hour simulation for the ten virtual patients available in the simulator. The pramlintide model parameters were maintained the same for the cohort. Specifically, the parameters identified for the Woerle dataset were used (see Table 8.10). The simulation scenario included three meals (40, 80, and 60 g of carbohydrates). In order to observe the contribution introduced by the pramlintide model, two simulations were carried out with the same scenario: with and without pramlintide (labeled "Insulin + Pramlintide" and "Insulin" in Figure 8.7, respectively). In the simulation with pramlintide, a 1-min 30 μg pramlintide bolus was administered alongside each meal, as well as an insulin bolus. The simulation shows a delay of the glucose postprandial peak, as well as a reduction of the maximum glucose concentration, similar to the effects reported both in Woerle et al. (2008) and Hinshaw et al. (2016).

Some known physiological effects of amylin were not tested in the model proposed structures due to the data limitations. These effects include inhibition of glucagon secretion (Lutz, 2022) and the "hypoglycemic override" (Young, 2005), whereby amylin has no effect in hypoglycemia conditions since hypoglycemia accelerates gastric emptying to raise glucose levels as soon as possible. This mechanism could be introduced in future simulators as a heuristic rule that deactivates pramlintide effect depending on glucose values. However, the available data did not describe these phenomena, so it was not

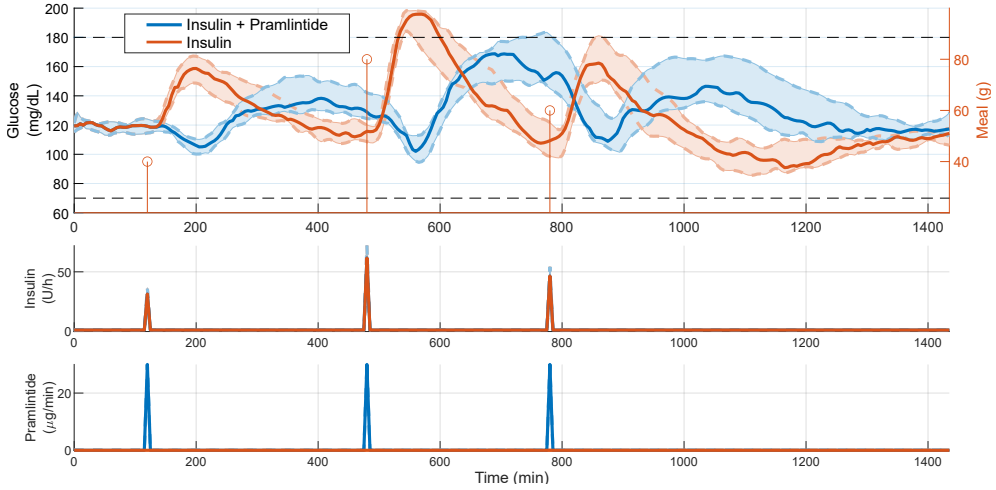

Figure 8.7: Simulation results after integrating the proposed pramlintide model into the T1D UVA/Padova simulator. Upper graph depicts plasma glucose, middle graph depicts insulin administration, and bottom graph depicts pramlintide administration. Continuous lines represent the mean of the results obtained for the cohort of 10 virtual patients. Shaded areas enclose standard deviation. Results in orange represent a simulation where only insulin was administered (basal infusion and prandial boluses). Results in blue represent a simulation where a 30 μg pramlintide bolus was administered alongside insulin prandial boluses. The simulation scenario consisted of three meals, denoted by circles in the upper graph.

possible to include them in the modeling process. Another limitation of this work is the use of RMSE as an assessment metric for parameter identification. There was no a priori knowledge about most of the model parameters, which can be troublesome in the identification process.

8.5 Conclusion

This chapter provides an advancement in the description of pramlintide PK/PD. A novel model is proposed that offers an easy-to-implement modulation of the gastric emptying rate as a function of plasma pramlintide concentration. The main limitation is the scarcity of the data used. Without access to complete individual datasets of patients' data, identifications and validations had to be carried out using aggregated value. Hence, no virtual cohort can be

developed. However, the presented model provides an overview of pramlintide behavior, using a simpler than other proposals in the literature, reducing the risk of overfitting. These developments open the door to enhance and improve the proposal with additional dynamics and individual data validation.

Chapter 9

Conclusions and future work

This final chapter presents the overall conclusions of this thesis and the considered research lines for future work. The publications derived from the contributions summarized here are listed in the next chapter, "List of publications".

9.1 Thesis general conclusions

This thesis has been focused on modeling and simulators related to T1D and AP systems. Given the utmost importance of providing accurate simulators for the accurate development of AP control algorithms, this thesis aimed to contribute to these simulators, providing new models for the design of adjunctive therapies using pramlintide and exploring new ways of describing glucagon dynamics following a more physiology-focused approach. Hence, in this thesis three main contributions have been presented:

- An analysis of literature on both T1D management and AP systems and glucoregulatory models for T1D.
- A model of glucagon effect based on glucagon receptor dynamics.
- A preliminary PK/PD pramlintide model.

The first part of the thesis was devoted to gathering the state of the art of diabetes technology, analyzing first the normal process of glucose homeostasis in order to observe better the implications of T1D. Then, diabetes therapies were reviewed, giving way to AP systems. Several reviews of clinical trials using SHAP systems show its contributions in reducing time in hypoglycemia and increasing time in normoglycemia, especially during the night period. However, there are several challenges to overcome, and DHAP contributes to solving some of them. Insulin-glucagon AP systems are especially effective in preventing hypoglycemia episodes during exercise, whereas insulin-pramlintide systems help to reduce time in hyperglycemia and improve overall time in range, although more extensive studies are needed to get the most of the hormone in combination with the AP system. Using both adjunctive hormones has the limitation of adding to the patients' device burden, so future developments need to address this concern, for instance improving the development of dual-chamber pumps.

The second chapter of the first part provided an overview of the most relevant models used for T1D in the literature, as well as some of the works extended from them, focusing on their structural differences. This lead to the analysis of how the glucagon effect is defined in the literature. Even if the interactions between α-cells and β-cells are known, few works in the literature contemplate an interaction between insulin and glucagon concentrations. The chapter lastly listed the only four pramlintide models available in the literature, of which only one of them is a complete PK/PD model.

The second part of the thesis included the proposal of the EGP model including glucagon effect modulated by receptors (Chapter 4), followed by the first validation, where clinical data with single glucagon doses (100, 200, and 300 μg) was used to evaluate the model performance (Chapter 5), and the second validation (Chapter 6) where the dataset included two consecutive glucagon doses (100 and 500 μg) in two different settings (low or high-content CHO diet).

The validations followed a shared procedure: identifying the model's parameters as well as the parameters of a selection of EGP models used as comparators and assessing their performance based on the RMSE obtained against the clinical data. The main difference among the successive validations was the identification strategy. The proposed glucagon model was able to provide a lower RMSE compared to the selected EGP definitions in every validation carried out in this thesis. The proof-of-concept results in Validation 1 were presented in Furió-Novejarque et al. (2022b). Results for the preliminary validation were exposed in Furió-Novejarque et al. (2022a), and finally, the conclusive results obtained with this dataset led to the publication of a paper in Furió-Novejarque et al. (2023b). The results and procedures followed in Validation 2 were presented in Furió-Novejarque et al.

(2023a). The final definition of the model adds two compartments to the baseline model and comprises five identifiable parameters. The potential interaction between glucagon and insulin could not be evaluated with the available data; hence, it was not modeled.

The final part of the thesis was devoted to the pramlintide model proposal. Pramlintide background was more limited compared to glucagon, given the lack of precedent models and the absence of individual clinical data. A preliminary version of the model was presented in Miragall et al. (2023). However, further developments were carried out, assessing different structures and assessing the most adequate combinations based on AIC and BIC results using data from the literature. The final proposal simplifies both the PK and the PD submodels compared to the other precedents in the literature. The results have been published in a journal paper (Furió-Novejarque et al., 2024).

The thesis has successfully contributed to the understanding of glucagon effect on glucose and pramlintide mechanisms, providing useful results to the field that will be incorporated in future T1D simulators.

9.2 Future work

After the results obtained in this work, several research lines and developments have opened up:

- First and foremost, the development of a simulator that integrates the presented models. This would require integrating the models, which are already implemented, into a unique software suite. Additionally, a virtual cohort has to be generated that can be produced sampling parameter sets from the parameter distributions generated from the identifications in this work. For convenience, a user interface could be implemented to facilitate the configuration of the scenarios and the simulations' execution, as well as the display of the results.

- A refinement of the pramlintide model, especially focused on the PD stage, given the limitations observed in the results of Chapter 8. Gaining access to some dataset with individual data of a clinical trial using pramlintide would be the first step.

- In a similar way, the glucagon model could be further enhanced given the possibility of analyzing the saturation of glucagon caused by high insulin levels. Also, the potential proposal of a PK model that includes the nonlinearity observed in plasma glucagon when administering bigger glucagon doses. The effect was slightly

apparent in Validation 1 with the 300 μg dose, but it became an issue in Validation 2 with the 500 μg dose.

- Given the interest rise in adjunctive therapies, as shown in Chapter 2, a possible continuation of the work could focus on the modeling of other adjunctive therapies (e.g., GLP-1 or SGLT inhibitors) to incorporate their effect into T1D simulators.

- Given the variability of gastric emptying, depending on the consistency of the meals (liquid versus solid) or their composition (fat, protein, carbohydrates), a meal model including these variables would be an interesting development. In this sense, a collaboration with the Food Technology Institute at Universitat Politècnica de València is being explored, to perform studies with emulators of chemical reactions in the digestive system.

- A current great interest in the T1D area is the need for customizable simulators that could account for the variability observed in the patients' day to day (e.g., including sex differences or stress effects). In the context in the new project in the team, DIABETEXX, several clinical studies will be performed to gather knowledge on sex differences and influence of the menstrual cycle in women related to exercise and meal challenges, producing data of great value for this purpose.

Chapter 10

List of publications

"Si tienes cosas, cosas tienes". — Dra. Vanessa Moscardó.

Listed below are the publications and other works resulted from this thesis.

Journal articles

- **Furió-Novejarque, C.**, Sala-Mira, I., Ranjan, A.G., Nørgaard, K., Díez, J.L., Jørgensen, J.B., Bondia, J. Analysis on the contribution of glucagon receptors to glucose dynamics in type 1 diabetes. *IFAC Journal of Systems and Control* – Invited to Special Issue. *Under review*.

- Sanz, R., Sala-Mira, I., **Furió-Novejarque, C.**, García, P., Díez, J.L., Bondia, J. A Customizable Fully-Autonomous Artificial Pancreas with Coordinated Insulin, Glucagon and Rescue Carbohydrates. *Under review*.

- **Furió-Novejarque, C.**, Sala-Mira, I., Díez, J.L., Bondia, J. A model of subcutaneous pramlintide pharmacokinetics and its effect on gastric emptying: Proof-of-concept

based on populational data. *Computer Methods and Programs in Biomedicine*, 244 Article 107968. doi:10.1016/j.cmpb.2023.107968 Impact factor = 6.1

- **Furió-Novejarque, C.**, Sanz, R., Ritschel, T. K. S., Reenberg, A., Ranjan, A. G., Nørgaard, K., Díez, J. L., Jørgensen, J.B., and Bondia, J. (2023). Modeling the effect of glucagon on endogenous glucose production in type 1 diabetes: On the role of glucagon receptor dynamics. *Computers in Biology and Medicine*, 154 Article 106605. doi:10.1016/j.compbiomed.2023.106605 Impact Factor = 7.7

- Viñals, C., Beneyto, A., Martín-SanJosé, J.F., **Furió-Novejarque, C.**, Bertachi, A., Bondia, J., Vehi, J., Conget, I., and Giménez, M. (2021). Artificial Pancreas with Carbohydrate Suggestion Performance for Unannounced and Announced Exercise in Type 1 Diabetes. *Journal of Clinical Endocrinology and Metabolism*, 106(1):55–63. doi:10.1210/clinem/dgaa562 Impact Factor = 5.8

Conference papers

- **Furió-Novejarque, C.**, Sala-Mira, I.,Ranjan, A.G.,Nørgaard, K.,Díez, J.L., Jørgensen, J.B., Bondia, J. (2023). Validation of a model of glucagon action including glucagon receptor dynamics under consecutive doses in low and high-carb diets. *22nd World Congress of the International Federation of Automatic Control (IFAC WC 2023). Yokohama (Japan)*. IFAC-PapersOnLine, 56(2):9666–9671. doi: 10.1016/j.ifacol.2023.10.275

- **Furió-Novejarque, C.**, Sanz, R., Reenberg, A. T., Ritschel, T. K. S., Ranjan, A. G., Nørgaard, K., Díez, J. L., Jørgensen, J. B., and Bondia, J. (2022). Assessment of a new model of glucagon action with glucagon receptor dynamics. *10th Vienna International Conference on Mathematical Modelling (MATHMOD 2022). Viena (Austria)*. IFAC-PapersOnLine, 55(20):647–652. doi:10.1016/j.ifacol.2022.09.169

Abstracts and posters

- Sanz, R., Sala-Mira, I., **Furió-Novejarque, C.**, García, P., Díez, J.L., Bondia, J. (2024) Flex-AP: A novel announcement-free automated insulin delivery system with flexible architecture. *17th International Conference on Advanced Technologies & Treatments for Diabetes (ATTD 2024). Florence (Italy)*.

- Miragall, J., **Furió-Novejarque, C.**, Sala-Mira, I., Díez,J.L., Bondia, J. (2023). A new pharmacokinetics and pharmacodynamics model of subcutaneous pramlintide infusion. *16th International Conference on Advanced Technologies & Treatments for Diabetes (ATTD 2023). Berlin (Germany)*. In Diabetes Technology and Therapeutics, 25(S2):A-136. doi:10.1089/dia.2023.2525.abstracts

- **Furió-Novejarque, C.**, Sanz, R., Reenberg, A., Ritschel, T., Ranjan, A., Díez, J.L., Jørgensen, J.B., and Bondia, J. (2022). Validation of a novel model of glucagon effect including glucagon receptor dynamics. *15th International Conference on Advanced Technologies & Treatments for Diabetes (ATTD 2022). Barcelona (Spain)*. In Diabetes Technology and Therapeutics, 24(S1):A-27. doi:10.1089/dia.2022.2525.abstracts

- **Furió Novejarque, C.** Modelado fisiológico de la produción endógena de glucosa considerando receptores de glucagón. (2022) *VII Encuentro de estudiantes de doctorado*. Universitat Politècnica de València.

- Viñals, C., Beneyto A., Martín-SanJosé, J.F., **Furió-Novejarque, C.**, Bertachi, A., Bondia, J., Vehí J., Conget, I., Giménez, M. (2020) Automatic control of blood glucose under announced and unannounnced exercise using a new multivariable closed loop controller with automatic carbohydrate suggestion and mitigation module. *13th International Conference on Advanced Technologies & Treatments for Diabetes (ATTD 2020). Madrid (Spain)*. In Diabetes Technology and Therapeutics. 22(S1):A-36. doi:10.1089/dia.2020.2525.abstracts

- **Furió Novejarque, C.** Estrategias de control coordinado no lineal para el páncreas artificial bihormonal. (2019) *VI Encuentro de estudiantes de doctorado*. Universitat Politècnica de València.

Bibliography

Aberer, F., Pieber, T.R., Eckstein, M.L., Sourij, H., and Moser, O. (2022). Glucose-Lowering Therapy beyond Insulin in Type 1 Diabetes: A Narrative Review on Existing Evidence from Randomized Controlled Trials and Clinical Perspective. *Pharmaceutics*, 14(6):1–22, doi:10.3390/pharmaceutics14061180. (Cited on page 26).

Abitbol, A., Rabasa-Lhoret, R., Messier, V., Legault, L., Smaoui, M., Cohen, N., and Haidar, A. (2018). Overnight Glucose Control with Dual- and Single-Hormone Artificial Pancreas in Type 1 Diabetes with Hypoglycemia Unawareness: A Randomized Controlled Trial. *Diabetes Technology and Therapeutics*, 20(3):189–196, doi:10.1089/dia.2017.0353. (Cited on pages 37 and 38).

Adis (2003). Pramlintide. *BioDrugs*, 17(1):73–79, doi:10.2165/00063030-200317010-00008. (Cited on pages 25 and 26).

Ahren, B., Adner, N., Svartberg, J., Petrella, E., Holst, J.J., and Gutniak, M.K. (2002). Antidiabetogenic effect of the human amylin analogue, pramlintide, in Type 1 diabetes is not mediated by GLP-1. *Diabetic Medicine*, 19(9):790–792, doi:10.1046/j.1464-5491.2002.00657_1.x. (Cited on pages 181 and 190).

Ajmera, I., Swat, M., Laibe, C., Novére, N.L., and Chelliah, V. (2013). The impact of mathematical modeling on the understanding of diabetes and related complications. *CPT: Pharmacometrics and Systems Pharmacology*, 2(7), doi:10.1038/psp.2013.30. (Cited on pages 51, 52 and 53).

Almurashi, A.M., Rodriguez, E., and Garg, S.K. (2023). Emerging Diabetes Technologies: Continuous Glucose Monitors/Artificial Pancreases. *Journal of the Indian Institute of Science*, 103(1):205–230, doi:10.1007/s41745-022-00348-3. (Cited on page 21).

Andersen, G., Eloy, R., Famulla, S., Heise, T., Meiffren, G., Seroussi, C., Gaudier, M., Mégret, C., Chan, Y.P., Soula, O., and Riddle, M. (2023). A co-formulation of pramlintide and insulin A21G (ADO09) improves postprandial glucose and short-term control of mean glucose, time in range, and body weight versus insulin aspart in adults with type 1 diabetes. *Diabetes, Obesity and Metabolism*, 25(5):1241–1248, doi:10.1111/dom.14972. (Cited on page 26).

Andersen, G., Meiffren, G., Famulla, S., Heise, T., Ranson, A., Seroussi, C., Eloy, R., Gaudier, M., Charvet, R., Chan, Y., Soula, O., and DeVries, J.H. (2021). ADO09, a co-formulation of the amylin analogue pramlintide and the insulin analogue A21G, lowers postprandial blood glucose versus insulin lispro in type 1 diabetes. *Diabetes, Obesity and Metabolism*, 23(4):961–970, doi:10.1111/dom.14302. (Cited on page 26).

Anderson, D.H. (1983). *Compartmental Modeling and Tracer Kinetics*, volume 50 of *Lecture Notes in Biomathematics*. Springer Berlin Heidelberg, Berlin, Heidelberg. (Cited on page 52).

Ang, K. and Sherr, J.L. (2017). Moving beyond subcutaneous insulin: The application of adjunctive therapies to the treatment of type 1 diabetes. *Expert Opinion on Drug Delivery*, 14(9):1113–1131, doi:10.1080/17425247.2017.1360862. (Cited on pages 26 and 27).

Aussedat, B., Dupire-Angel, M., Gifford, R., Klein, J.C., Wilson, G.S., and Reach, G. (2000). Interstitial glucose concentration and glycemia: implications for continuous subcutaneous glucose monitoring. *American Journal of Physiology-Endocrinology and Metabolism*, 278(4):E716–E728, doi:10.1152/ajpendo.2000.278.4.E716. (Cited on page 19).

Avgerinos, I., Manolopoulos, A., Michailidis, T., Kitsios, K., Liakos, A., Karagiannis, T., Dimitrakopoulos, K., Matthews, D.R., Tsapas, A., and Bekiari, E. (2021). Comparative efficacy and safety of glucose-lowering drugs as adjunctive therapy for adults with type 1 diabetes: A systematic review and network meta-analysis. *Diabetes, Obesity and Metabolism*, 23(3):822–831, doi:10.1111/dom.14291. (Cited on page 26).

Bakhtiani, P., El Youssef, J., Duell, A., Branigan, D., Jacobs, P., Lasarev, M., Castle, J., and Ward, W. (2015). Factors affecting the success of glucagon delivered during an automated closed-loop system in type 1 diabetes. *Journal of Diabetes and its Complications*, 29(1):93–98, doi:10.1016/j.jdiacomp.2014.09.001. (Cited on page 39).

Bakhtiani, P.A., Zhao, L.M., El Youssef, J., Castle, J.R., and Ward, W.K. (2013). A review of artificial pancreas technologies with an emphasis on bi-hormonal therapy. *Diabetes, Obesity and Metabolism*, 15(12):1065–1070, doi:10.1111/dom.12107. (Cited on page 36).

Balsa-Canto, E., Alonso, A.A., and Banga, J.R. (2010). An iterative identification procedure for dynamic modeling of biochemical networks. *BMC Systems Biology*, 4(1):11, doi:10.1186/1752-0509-4-11. (Cited on pages 51, 101, 102 and 103).

Balsa-Canto, E., Henriques, D., Gábor, A., and Banga, J.R. (2016). AMIGO2, a toolbox for dynamic modeling, optimization and control in systems biology. *Bioinformatics*, 32(21):3357–3359, doi:10.1093/bioinformatics/btw411. (Cited on page 103).

Banarer, S., McGregor, V.P., and Cryer, P.E. (2002). Intraislet hyperinsulinemia prevents the glucagon response to hypoglycemia despite an intact autonomic response. *Diabetes*, 51(4):958–965, doi:10.2337/diabetes.51.4.958. (Cited on page 16).

Bano, G. (2013). Glucose homeostasis, obesity and diabetes. *Best Practice and Research: Clinical Obstetrics and Gynaecology*, 27(5):715–726, doi:10.1016/j.bpobgyn.2013.02.007. (Cited on page 11).

Barreiro, X.R. and Villaverde, A.F. (2023). On the Origins and Rarity of Locally but Not Globally Identifiable Parameters in Biological Modeling. *IEEE Access*, 11(May):65457–65467, doi:10.1109/ACCESS.2023.3288998. (Cited on page 102).

Basu, R., Di Camillo, B., Toffolo, G., Basu, A., Shah, P., Vella, A., Rizza, R., and Cobelli, C. (2003). Use of a novel triple-tracer approach to assess postprandial glucose metabolism. *American Journal of Physiology-Endocrinology and Metabolism*, 284(1):E55–E69, doi:10.1152/ajpendo.00190.2001. (Cited on page 190).

Bauer, S., Hay, M., Amilhon, B., Jean, A., and Moyse, E. (2005). In vivo neurogenesis in the dorsal vagal complex of the adult rat brainstem. *Neuroscience*, 130(1):75–90, doi:10.1016/j.neuroscience.2004.08.047. (Cited on page 164).

Beato-Víbora, P.I. and Arroyo-Díez, F.J. (2019). New uses and formulations of glucagon for hypoglycaemia. *Drugs in Context*, 8:1–10, doi:10.7573/dic.212599. (Cited on page 23).

Bekiari, E., Kitsios, K., Thabit, H., Tauschmann, M., Athanasiadou, E., Karagiannis, T., Haidich, A.B., Hovorka, R., and Tsapas, A. (2018). Artificial pancreas treatment for outpatients with type 1 diabetes: systematic review and meta-analysis. *BMJ*, 361:k1310, doi:10.1136/bmj.k1310. (Cited on pages 31 and 37).

Bélanger, P., Couturier, K., Latour, M.G., and Lavoie, J.M. (2000). Effects of supranormal liver glycogen content on hyperglucagonemia-induced liver glycogen breakdown. *European Journal of Applied Physiology*, 83:328–335, doi:10.1007/s004210000286. (Cited on pages 16 and 136).

Benam, K.D., Khoshamadi, H., Åm, M.K., Stavdahl, Ø., Gros, S., and Fougner, A.L. (2023). Identifiable prediction animal model for the bi-hormonal intraperitoneal artificial pancreas. *Journal of Process Control*, 121:13–29, doi:10.1016/j.jprocont.2022.11.008. (Cited on page 73).

Berger, M. and Rodbard, D. (1989). Computer Simulation of Plasma Insulin and Glucose Dynamics After Subcutaneous Insulin Injection. *Diabetes Care*, 12(10):725–736, doi:10.2337/diacare.12.10.725. (Cited on page 68).

Bergman, R.N. (2005). Minimal Model: Perspective from 2005. *Hormone Research in Paediatrics*, 64(Suppl. 3):8–15, doi:10.1159/000089312. (Cited on pages 55 and 56).

Bergman, R.N., Ider, Y.Z., Bowden, C.R., and Cobelli, C. (1979). Quantitative estimation of insulin sensitivity. *The American journal of physiology*, 236(6):E667–77, doi:10.1152/ajpendo.1979.236.6.E667. (Cited on pages 55, 56 and 276).

Bergman, R.N., Phillips, L.S., and Cobelli, C. (1981). Physiologic evaluation of factors controlling glucose tolerance in man. Measurement of insulin sensitivity and β-cell glucose sensitivity from the response to intravenous glucose. *Journal of Clinical Investigation*, 68(6):1456–1467, doi:10.1172/JCI110398. (Cited on pages 55, 60, 71, 90 and 276).

Biester, T., Kordonouri, O., and Danne, T. (2019). Beyond type 2 diabetes: sodium glucose co-transporter-inhibition in type 1 diabetes. *Diabetes, Obesity and Metabolism*, 21(S2):53–61, doi:10.1111/dom.13659. (Cited on page 28).

Biester, T., Muller, I., von dem Berge, T., Atlas, E., Nimri, R., Phillip, M., Battelino, T., Bratina, N., Dovc, K., Scheerer, M.F., Kordonouri, O., and Danne, T. (2021). Add-on therapy with dapagliflozin under full closed loop control improves time in range in adolescents and young adults with type 1 diabetes: The DAPADream study. *Diabetes, Obesity and Metabolism*, 23(2):599–608, doi:10.1111/dom.14258. (Cited on page 46).

Blauw, H., Joannet Onvlee, A., Klaassen, M., van Bon, A.C., and Hans Devries, J. (2021). Fully Closed Loop Glucose Control With a Bihormonal Artificial Pancreas in Adults With Type 1 Diabetes: An Outpatient, Randomized, Crossover Trial. *Diabetes Care*, 44(3):836–838, doi:10.2337/DC20-2106. (Cited on page 41).

Blauw, H., Keith-Hynes, P., Koops, R., and DeVries, J.H. (2016a). A Review of Safety and Design Requirements of the Artificial Pancreas. *Annals of Biomedical Engineering*, 44(11):3158–3172, doi:10.1007/s10439-016-1679-2. (Cited on page 33).

Blauw, H., van Bon, A.C., Koops, R., and DeVries, J.H. (2016b). Performance and safety of an integrated bihormonal artificial pancreas for fully automated glucose control at home. *Diabetes, Obesity and Metabolism*, 18(7):671–677, doi:10.1111/dom.12663. (Cited on pages 30 and 41).

Blauw, H., Wendl, I., DeVries, J.H., Heise, T., and Jax, T. (2016c). Pharmacokinetics and pharmacodynamics of various glucagon dosages at different blood glucose levels. *Diabetes, Obesity and Metabolism*, 18(1):34–39, doi:10.1111/dom.12571. (Cited on pages 39 and 136).

Blonde, L., Umpierrez, G.E., Reddy, S.S., McGill, J.B., Berga, S.L., Bush, M., Chandrasekaran, S., DeFronzo, R.A., Einhorn, D., Galindo, R.J., Gardner, T.W., Garg, R., Garvey, W.T., Hirsch, I.B., Hurley, D.L., Izuora, K., Kosiborod, M., Olson, D., Patel, S.B., Pop-Busui, R., Sadhu, A.R., Samson, S.L., Stec, C., Tamborlane, W.V., Tuttle, K.R., Twining, C., Vella, A., Vellanki, P., and Weber, S.L. (2022). American Association of Clinical Endocrinology Clinical Practice Guideline: Developing a Diabetes Mellitus Comprehensive Care Plan—2022 Update. *Endocrine Practice*, 28(10):923–1049, doi:10.1016/j.eprac.2022.08.002. (Cited on pages 21, 22, 23, 24, 25, 26, 27 and 28).

Böhm, S.K., Grady, E.F., and Bunnett, N.W. (1997). Regulatory mechanisms that modulate signalling by G-protein-coupled receptors. *Biochemical Journal*, 322(1):1–18, doi:10.1042/bj3220001. (Cited on page 83).

Bosi, E., Choudhary, P., de Valk, H.W., Lablanche, S., Castañeda, J., de Portu, S., Da Silva, J., Ré, R., Vorrink-de Groot, L., Shin, J., Kaufman, F.R., Cohen, O., Laurenzi, A., Caretto, A., Slatterly, D., Henderson-Wilson, M., Weisnagel, S.J., Dubé, M.C., Julien, V.È., Trevisan, R., Lepore, G., Bellante, R., Hramiak, I., Spaic, T., Driscoll, M., Borot, S., Clergeot, A., Khiat, L., Hammond, P., Ray, S., Dinning, L., Tonolo, G., Manconi, A., Ledda, M.S., de Ranitz, W., Silvius, B., Wojtusciszyn, A., Farret, A., Vriesendorp, T., Immeker-de Jong, F., van der Linden, J., Brink, H.S., Alkemade, M., Schaepelynck-Belicar, P., Galie, S., Tréglia, C., Benhamou, P.Y., Haddouche, M., Hoogma, R., Leelarathna, L., Shaju, A., and James, L. (2019). Efficacy and safety of suspend-before-low insulin pump technology in hypoglycaemia-prone adults with type 1 diabetes (SMILE): an open-label randomised controlled trial. *The Lancet Diabetes and Endocrinology*, 7(6):462–472, doi:10.1016/S2213-8587(19)30150-0. (Cited on page 30).

Boyle, C.N., Zheng, Y., and Lutz, T.A. (2022). Mediators of Amylin Action in Metabolic Control. *Journal of Clinical Medicine*, 11(8), doi:10.3390/jcm11082207. (Cited on page 165).

Breton, M.D. (2008). Physical activity-the major unaccounted impediment to closed loop control. *Journal of Diabetes Science and Technology*, 2(1):169–174, doi:10.1177/193229680800200127. (Cited on page 56).

Cardona-Hernandez, R., Dôvc, K., Biester, T., Ekhlaspour, L., Macedoni, M., Tauschmann, M., and Mameli, C. (2023). New therapies towards a better glycemic control in youths with type 1 diabetes. *Pharmacological Research*, 195(August):106882, doi:10.1016/j.phrs.2023.106882. (Cited on page 28).

Castellanos, L.E., Balliro, C.A., Sherwood, J.S., Jafri, R., Hillard, M.A., Greaux, E., Selagamsetty, R., Zheng, H., El-Khatib, F.H., Damiano, E.R., and Russell, S.J. (2021). Performance of the Insulin-Only iLet Bionic Pancreas and the Bihormonal iLet Using Dasiglucagon in Adults With Type 1 Diabetes in a Home-Use Setting. *Diabetes Care*, 44(6):e118–e120, doi:10.2337/dc20-1086. (Cited on pages 38 and 41).

Castle, J.R., Engle, J.M., El Youssef, J., Massoud, R.G., Yuen, K.C., Kagan, R., and Ward, W.K. (2010a). Novel use of glucagon in a closed-loop system for prevention of hypoglycemia in type 1 diabetes. *Diabetes Care*, 33(6):1282–1287, doi:10.2337/dc09-2254. (Cited on page 36).

Castle, J.R., Engle, J.M., Youssef, J.E., Massoud, R.G., and Ward, W.K. (2010b). Factors Influencing the Effectiveness of Glucagon for Preventing Hypoglycemia. *Journal of Diabetes Science and Technology*, 4(6):1305–1310, doi:10.1177/193229681000400603. (Cited on pages 37, 38 and 39).

Castle, J.R., Youssef, J.E., Bakhtiani, P.A., Cai, Y., Stobbe, J.M., Branigan, D., Ramsey, K., Jacobs, P., Reddy, R., Woods, M., and Ward, W.K. (2015). Effect of repeated glucagon doses on hepatic glycogen in type 1 Diabetes: Implications for a bihormonal Closed-Loop system. *Diabetes Care*, 38(11):2115–2119, doi:10.2337/dc15-0754. (Cited on pages 39, 40, 128 and 136).

Castle, J.R., Youssef, J.E., Wilson, L.M., Reddy, R., Resalat, N., Branigan, D., Ramsey, K., Leitschuh, J., Rajhbeharrysingh, U., Senf, B., Sugerman, S.M., Gabo, V., and Jacobs, P.G. (2018). Randomized outpatient trial of single- and dual-hormone closed-loop systems that adapt to exercise using wearable sensors. *Diabetes Care*, 41(7):1471–1477, doi:10.2337/dc18-0228. (Cited on pages 37 and 38).

Chandrasekhar, A. and Padhi, R. (2023). Blood Glucose Regulation Models in Artificial Pancreas for Type-1 Diabetic Patients. *Journal of the Indian Institute of Science*, 103(1):353–364, doi:10.1007/s41745-023-00362-z. (Cited on page 54).

Chase, H.P., Lutz, K., Pencek, R., Zhang, B., and Porter, L. (2009). Pramlintide Lowered Glucose Excursions and Was Well-Tolerated in Adolescents with Type 1 Diabetes: Results from a Randomized, Single-Blind, Placebo-Controlled, Crossover Study. *Journal of Pediatrics*, 155(3):369–373, doi:10.1016/j.jpeds.2009.03.012. (Cited on pages 181, 190 and 197).

Chiş, O., Banga, J.R., and Balsa-Canto, E. (2011a). GenSSI: A software toolbox for structural identifiability analysis of biological models. *Bioinformatics*, 27(18):2610–2611, doi:10.1093/bioinformatics/btr431. (Cited on pages 103 and 176).

Chiş, O.T., Banga, J.R., and Balsa-Canto, E. (2011b). Structural Identifiability of Systems Biology Models: A Critical Comparison of Methods. *PLoS ONE*, 6(11):e27755, doi:10.1371/journal.pone.0027755. (Cited on page 102).

Clodi, M., Thomaseth, K., Pacini, G., Hermann, K., Kautzky-Willer, A., Waldhäusl, W., Prager, R., and Ludvik, B. (1998). Distribution and kinetics of amylin in humans. *American Journal of Physiology-Endocrinology and Metabolism*, 274(5):E903–E908, doi:10.1152/ajpendo.1998.274.5.E903. (Cited on pages xv, 74, 75, 166 and 197).

Cobelli, C., Caumo, A., and Omenetto, M. (1999). Minimal model S G overestimation and S I underestimation: improved accuracy by a Bayesian two-compartment model. *American Journal of Physiology-Endocrinology and Metabolism*, 277(3):E481–E488, doi:10.1152/ajpendo.1999.277.3.E481. (Cited on page 56).

Cobelli, C. and Dalla Man, C. (2022). Minimal and Maximal Models to Quantitate Glucose Metabolism: Tools to Measure, to Simulate and to Run in Silico Clinical Trials. *Journal of Diabetes Science and Technology*, 16(5):1270–1298, doi:10.1177/19322968211015268. (Cited on page 69).

Cohan, P. and Peters, A.L. (2010). Therapy of Type 1 Diabetes Mellitus. In *Principles of Diabetes Mellitus*, pages 709–729. Springer US, Boston, MA. (Cited on pages 19 and 21).

Colburn, W.A., Gottlieb, A.B., Koda, J., and Kolterman, O.G. (1996). Pharmacokinetics and Pharmacodynamics of AC137 (25,28,29 Tripro-Amylin, Human) After Intravenous Bolus and Infusion Doses in Patients with Insulin-Dependent Diabetes. *The Journal of Clinical Pharmacology*, 36(1):13–24, doi:10.1002/j.1552-4604.1996.tb04147.x. (Cited on pages 75, 181, 184 and 186).

Collyns, O.J., Meier, R.A., Betts, Z.L., Chan, D.S., Frampton, C., Frewen, C.M., Hewapathirana, N.M., Jones, S.D., Roy, A., Grosman, B., Kurtz, N., Shin, J., Vigersky, R.A., Wheeler, B.J., and de Bock, M.I. (2021). Improved glycemic outcomes with medtronic minimed advanced hybrid closed-loop delivery: Results from a randomized crossover trial comparing automated insulin delivery with predictive low glucose suspend in peoplewithtype1diabetes. *Diabetes Care*, 44(4):969–975, doi:10.2337/dc20-2250. (Cited on page 30).

Colmegna, P. and Sánchez Peña, R.S. (2014). Analysis of three T1DM simulation models for evaluating robust closed-loop controllers. *Computer Methods and Programs in Biomedicine*, 113(1):371–382, doi:10.1016/j.cmpb.2013.09.020. (Cited on page 70).

Cooperberg, B.A. and Cryer, P.E. (2009). β-Cell–Mediated Signaling Predominates Over Direct α-Cell Signaling in the Regulation of Glucagon Secretion in Humans. *Diabetes Care*, 32(12):2275–2280, doi:10.2337/dc09-0798. (Cited on page 15).

Cooperberg, B.A. and Cryer, P.E. (2010). Insulin reciprocally regulates glucagon secretion in humans. *Diabetes*, 59(11):2936–2940, doi:10.2337/db10-0728. (Cited on page 16).

Cornish-Bowden, A. (2015). One hundred years of Michaelis–Menten kinetics. *Perspectives in Science*, 4:3–9, doi:10.1016/j.pisc.2014.12.002. (Cited on page 72).

Cryer, P., Davis, S., and Shamoon, H. (2003). Hypoglycemia in diabetes. *Diabetes Care*, 26(6):1902–1912, doi:10.2337/diacare.26.6.1902. (Cited on pages 20 and 28).

Cryer, P.E. (2001). Hypoglycemia-associated autonomic failure in diabetes. *American Journal of Physiology-Endocrinology and Metabolism*, 281(6):E1115–E1121, doi:10.1152/ajpendo.2001.281.6.E1115. (Cited on pages 13, 14 and 20).

Dalla Man, C., Camilleri, M., and Cobelli, C. (2006). A system model of oral glucose absorption: Validation on gold standard data. *IEEE Transactions on Biomedical Engineering*, 53(12):2472–2478, doi:10.1109/TBME.2006.883792. (Cited on pages 65, 171, 191 and 273).

Dalla Man, C., Micheletto, F., Lv, D., Breton, M., Kovatchev, B., and Cobelli, C. (2014). The UVA/PADOVA type 1 diabetes simulator: New features. *Journal of Diabetes Science and Technology*, 8(1):26–34, doi:10.1177/1932296813514502. (Cited on pages 63, 66, 70, 198 and 273).

Dalla Man, C., Rizza, R.A., and Cobelli, C. (2007). Meal Simulation Model of the Glucose-Insulin System. *IEEE Transactions on Biomedical Engineering*, 54(10):1740–1749, doi:10.1109/TBME.2007.893506. (Cited on page 273).

Domingo-Lopez, D.A., Lattanzi, G., H. J. Schreiber, L., Wallace, E.J., Wylie, R., O'Sullivan, J., Dolan, E.B., and Duffy, G.P. (2022). Medical devices, smart drug delivery, wearables and technology for the treatment of Diabetes Mellitus. *Advanced Drug Delivery Reviews*, 185:114280, doi:10.1016/j.addr.2022.114280. (Cited on page 21).

Dormand, J. and Prince, P. (1980). A family of embedded Runge-Kutta formulae. *Journal of Computational and Applied Mathematics*, 6(1):19–26, doi:10.1016/0771-050X(80)90013-3. (Cited on page 102).

Drucker, D.J., Dritselis, A., and Kirkpatrick, P. (2010). Liraglutide. *Nature Reviews Drug Discovery*, 9(4):267–268, doi:10.1038/nrd3148. (Cited on pages 27 and 28).

Edelman, S.V., Schroeder, B.E., and Frias, J.P. (2007). Pramlintide acetate in the treatment of Type 2 and Type 1 diabetes mellitus. *Expert Review of Endocrinology & Metabolism*, 2(1):9–18, doi:10.1586/17446651.2.1.9. (Cited on page 161).

Edgerton, D.S., Moore, M.C., Gregory, J.M., Kraft, G., and Cherrington, A.D. (2021). Importance of the route of insulin delivery to its control of glucose metabolism. *American Journal of Physiology - Regulatory Integrative and Comparative Physiology*, 320(5):E891–E897, doi:10.1152/AJPENDO.00628.2020. (Cited on page 33).

El-Khatib, F.H., Balliro, C., Hillard, M.A., Magyar, K.L., Ekhlaspour, L., Sinha, M., Mondesir, D., Esmaeili, A., Hartigan, C., Thompson, M.J., Malkani, S., Lock, J.P., Harlan, D.M., Clinton, P., Frank, E., Wilson, D.M., DeSalvo, D., Norlander, L., Ly, T., Buckingham, B.A., Diner, J., Dezube, M., Young, L.A., Goley, A., Kirkman, M.S., Buse, J.B., Zheng, H., Selagamsetty, R.R., Damiano, E.R., and Russell, S.J. (2017). Home use of a bihormonal bionic pancreas versus insulin pump therapy in adults with type 1 diabetes: a multicentre randomised crossover trial. *The Lancet*, 389(10067):369–380, doi:10.1016/S0140-6736(16)32567-3. (Cited on page 41).

El-Khatib, F.H., Russell, S.J., Nathan, D.M., Sutherlin, R.G., and Damiano, E.R. (2010). A Bihormonal Closed-Loop Artificial Pancreas for Type 1 Diabetes. *Science Translational Medicine*, 2(27):27ra27, doi:10.1126/scitranslmed.3000619. (Cited on page 36).

El Youssef, J., Castle, J.R., Bakhtiani, P.A., Haidar, A., Branigan, D.L., Breen, M., and Ward, W.K. (2014). Quantification of the Glycemic Response to Microdoses of Subcutaneous Glucagon at Varying Insulin Levels. *Diabetes Care*, 37(11):3054–3060, doi:10.2337/dc14-0803. (Cited on pages 40, 71, 91, 97, 110 and 128).

El Youssef, J., Castle, J.R., Branigan, D.L., Massoud, R.G., Breen, M.E., Jacobs, P.G., Bequette, B.W., and Ward, W.K. (2011). A Controlled Study of the Effectiveness of an

Adaptive Closed-Loop Algorithm to Minimize Corticosteroid-Induced Stress Hyperglycemia in Type 1 Diabetes. *Journal of Diabetes Science and Technology*, 5(6):1312–1326, doi:10.1177/193229681100500602. (Cited on page 34).

Emami, A., Youssef, J.E., Rabasa-Lhoret, R., Pineau, J., Castle, J.R., and Haidar, A. (2017). Modeling Glucagon Action in Patients with Type 1 Diabetes. *IEEE Journal of Biomedical and Health Informatics*, 21(4):1163–1171, doi:10.1109/JBHI.2016.2593630. (Cited on pages 71, 96, 97, 98 and 99).

Fabietti, P.G., Canonico, V., Federici, M.O., Benedetti, M.M., and Sarti, E. (2006). Control oriented model of insulin and glucose dynamics in type 1 diabetics. *Medical and Biological Engineering and Computing*, 44(1-2):69–78, doi:10.1007/s11517-005-0012-2. (Cited on pages 57, 60 and 282).

Fabra, E.M., Díez, J.L., Bondia, J., and Sanz, A.J.L. (2021). A comprehensive review of continuous glucose monitoring accuracy during exercise periods. *Sensors (Switzerland)*, 21(2):1–19, doi:10.3390/s21020479. (Cited on page 33).

Faggionato, E., Laurenti, M.C., Vella, A., and Man, C.D. (2023). Nonlinear Mixed Effects Modeling of Glucagon Kinetics in Healthy Subjects. *IEEE Transactions on Biomedical Engineering*, 70(9):2733–2740, doi:10.1109/TBME.2023.3262974. (Cited on page 177).

Fang, J., Landersdorfer, C.B., Cirincione, B., and Jusko, W.J. (2013). Study Reanalysis Using a Mechanism-Based Pharmacokinetic/Pharmacodynamic Model of Pramlintide in Subjects with Type 1 Diabetes. *The AAPS Journal*, 15(1):15–29, doi:10.1208/s12248-012-9409-7. (Cited on pages 75, 171, 180 and 184).

Fang, Z., Liu, M., Tao, J., Li, C., Zou, F., and Zhang, W. (2022). Efficacy and safety of closed-loop insulin delivery versus sensor-augmented pump in the treatment of adults with type 1 diabetes: a systematic review and meta-analysis of randomized-controlled trials. *Journal of Endocrinological Investigation*, 45(3):471–481, doi:10.1007/s40618-021-01674-6. (Cited on page 30).

Fineman, M.S., Koda, J.E., Shen, L.Z., Strobel, S.A., Maggs, D.G., Weyer, C., and Kolterman, O.G. (2002). The human amylin analog, pramlintide, corrects postprandial hyperglucagonemia in patients with type 1 diabetes. *Metabolism: Clinical and Experimental*, 51(5):636–641, doi:10.1053/meta.2002.32022. (Cited on page 25).

Forlenza, G.P., McVean, J., Beck, R.W., Bauza, C., Bailey, R., Buckingham, B., Dimeglio, L.A., Sherr, J.L., Clements, M., Neyman, A., Evans-Molina, C., Sims, E.K., Messer,

L.H., Ekhlaspour, L., McDonough, R., Van Name, M., Rojas, D., Beasley, S., Dubose, S., Kollman, C., and Moran, A. (2023). Effect of Verapamil on Pancreatic Beta Cell Function in Newly Diagnosed Pediatric Type 1 Diabetes: A Randomized Clinical Trial. *Jama*, 329(12):990–999, doi:10.1001/jama.2023.2064. (Cited on page 28).

Furió-Novejarque, C., Sala-Mira, I., Díez, J.L., and Bondia, J. (2024). A model of subcutaneous pramlintide pharmacokinetics and its effect on gastric emptying: Proof-of-concept based on populational data. *Computer Methods and Programs in Biomedicine*, 244(September 2023):107968, doi:10.1016/j.cmpb.2023.107968. (Cited on page 203).

Furió-Novejarque, C., Sala-Mira, I., Ranjan, A.G., Nørgaard, K., Díez, J.L., Jørgensen, J.B., and Bondia, J. (2023a). Validation of a model of glucagon action including glucagon receptor dynamics under consecutive doses in low and high-carb diets. *IFAC-PapersOnLine*, 56(2):9666–9671, doi:10.1016/j.ifacol.2023.10.275. (Cited on pages 202 and 267).

Furió-Novejarque, C., Sanz, R., Reenberg, A., Ritschel, T., Ranjan, A., Díez, J.L., Jørgensen, J., and Bondia, J. (2022a). Validation of a novel model of glucagon effect including glucagon receptor dynamics. *Diabetes Technology and Therapeutics*, 24(S1):A–27, doi:10.1089/dia.2022.2525.abstracts. (Cited on pages 110 and 202).

Furió-Novejarque, C., Sanz, R., Reenberg, A.T., Ritschel, T.K., Ranjan, A.G., Nørgaard, K., Díez, J.L., Jørgensen, J.B., and Bondia, J. (2022b). Assessment of a new model of glucagon action with glucagon receptor dynamics. *IFAC-PapersOnLine*, 55(20):647–652, doi:10.1016/j.ifacol.2022.09.169. (Cited on pages 110 and 202).

Furió-Novejarque, C., Sanz, R., Ritschel, T.K., Reenberg, A.T., Ranjan, A.G., Nørgaard, K., Díez, J.l., Bagterp, J., and Bondia, J. (2023b). Modeling the effect of glucagon on endogenous glucose production in type 1 diabetes: On the role of glucagon receptor dynamics. *Computers in Biology and Medicine*, 154(January):106605, doi:10.1016/j.compbiomed.2023.106605. (Cited on pages 122, 202 and 267).

Gamarra, E. and Trimboli, P. (2023). Menstrual Cycle, Glucose Control and Insulin Sensitivity in Type 1 Diabetes: A Systematic Review. *Journal of Personalized Medicine*, 13(2):374, doi:10.3390/jpm13020374. (Cited on page 34).

Garcia-Tirado, J., Farhy, L., Nass, R., Kollar, L., Clancy-Oliveri, M., Basu, R., Kovatchev, B., and Basu, A. (2022). Automated Insulin Delivery with SGLT2i Combination Therapy in Type 1 Diabetes. *Diabetes Technology and Therapeutics*, 24(7):461–470, doi:10.1089/dia.2021.0542. (Cited on pages 28 and 47).

Garcia-Tirado, J., Zuluaga-Bedoya, C., and Breton, M.D. (2018). Identifiability Analysis of Three Control-Oriented Models for Use in Artificial Pancreas Systems. *Journal of Diabetes Science and Technology*, 12(5):937–952, doi:10.1177/1932296818788873. (Cited on page 103).

Gavin, J.R., Roth, J., Neville, D.M., de Meyts, P., and Buell, D.N. (1974). Insulin dependent regulation of insulin receptor concentrations: A direct demonstration in cell culture. *Proceedings of the National Academy of Sciences of the United States of America*, 71(1):84–88, doi:10.1073/pnas.71.1.84. (Cited on page 83).

Gerich, J.E. (1988). Glucose Counterregulation and Its Impact on Diabetes Mellitus. *Diabetes*, 37(12):1608–1617, doi:10.2337/diab.37.12.1608. (Cited on pages 14 and 20).

Gerich, J.E. (1993). Control of glycaemia. *Baillière's Clinical Endocrinology and Metabolism*, 7(3):551–586, doi:10.1016/S0950-351X(05)80207-1. (Cited on page 11).

Gerich, J.E., Langlois, M., Noacco, C., Karam, J.H., and Forsham, P.H. (1973). Lack of glucagon response to hypoglycemia in diabetes: Evidence for an intrinsic pancreatic alpha cell defect. *Science*, 182(4108):171–173, doi:10.1126/science.182.4108.171. (Cited on page 18).

Giménez, M., Khunti, K., Matsuhisa, M., Chenji, S., Syring, K., and Yan, Y. (2023). Systematic Literature Review and Indirect Treatment Comparison of Three Ready-to-Use Glucagon Treatments for Severe Hypoglycemia. *Diabetes Therapy*, 14(11):1757–1769, doi:10.1007/s13300-023-01466-6. (Cited on page 24).

Gingell, J.J., Rees, T.A., Hendrikse, E.R., Siow, A., Rennison, D., Scotter, J., Harris, P.W., Brimble, M.A., Walker, C.S., and Hay, D.L. (2020). Distinct Patterns of Internalization of Different Calcitonin Gene-Related Peptide Receptors. *ACS Pharmacology and Translational Science*, 3(2):296–304, doi:10.1021/acsptsci.9b00089. (Cited on page 163).

Gingras, V., Bonato, L., Messier, V., Roy-Fleming, A., Smaoui, M.R., Ladouceur, M., and Rabasa-Lhoret, R. (2018). Impact of macronutrient content of meals on postprandial glucose control in the context of closed-loop insulin delivery: A randomized cross-over study. *Diabetes, Obesity and Metabolism*, 20(11):2695–2699, doi:10.1111/dom.13445. (Cited on page 192).

Glezer, S., Hovelmann, U., Teng, S., Lamers, D., Odoul, M., Correia, J., Zijlstra, E., Gaudier, M., Soula, O., and Duracher, D. (2018). BioChaperone Glucagon (BCG), a Stable Ready-to-Use Liquid Glucagon Formulation, Is Well Tolerated and Quickly Restores Eug-

lycemia after Insulin-Induced Hypoglycemia. *Diabetes*, 67(Supplement_1):305–OR, doi:10.2337/db18-305-OR. (Cited on page 23).

Goldfine, I.D. (1975). Binding of insulin to thymocytes from suckling and hypophysectomized rats: Evidence for two mechanisms regulating insulin sensitivity. *Endocrinology*, 97(4):948–954, doi:10.1210/endo-97-4-948. (Cited on page 83).

González-Vélez, V., Dupont, G., Gil, A., González, A., and Quesada, I. (2012). Model for glucagon secretion by pancreatic α-cells. *PLoS ONE*, 7(3):1–11, doi:10.1371/journal.pone.0032282. (Cited on page 86).

Goutelle, S., Maurin, M., Rougier, F., Barbaut, X., Bourguignon, L., Ducher, M., and Maire, P. (2008). The Hill equation: A review of its capabilities in pharmacological modelling. *Fundamental and Clinical Pharmacology*, 22(6):633–648, doi:10.1111/j.1472-8206.2008.00633.x. (Cited on page 174).

Goyal, R.K., Guo, Y., and Mashimo, H. (2019). Advances in the physiology of gastric emptying. *Neurogastroenterology and Motility*, 31(4):1–14, doi:10.1111/nmo.13546. (Cited on page 198).

Graf, C.J., Woodworth, J.R., Seger, M.E., Holcombe, J.H., Bowsher, R.R., and Lynch, R. (1999). Pharmacokinetic and glucodynamic comparisons of recombinant and animal-source glucagon after IV, IM, and SC injection in healthy volunteers. *Journal of Pharmaceutical Sciences*, 88(10):991–995, doi:10.1021/js99007p. (Cited on pages 36 and 109).

Guyton, J.R., Foster, R.O., Soeldner, J.S., Tan, M.H., Kahn, C.B., Koncz, L., and Gleason, R.E. (1978). A model of glucose-insulin homeostasis in man that incorporates the heterogeneous fast pool theory of pancreatic insulin release. *Diabetes*, 27(10):1027–1042, doi:10.2337/diab.27.10.1027. (Cited on page 68).

Haidar, A. (2016). The Artificial Pancreas: How Closed-Loop Control Is Revolutionizing Diabetes. *IEEE Control Systems*, 36(5):28–47, doi:10.1109/MCS.2016.2584318. (Cited on pages 29, 34 and 54).

Haidar, A. (2019). Insulin-and-glucagon artificial pancreas versus insulin-alone artificial pancreas: A short review. *Diabetes Spectrum*, 32(3):215–221, doi:10.2337/ds18-0097. (Cited on page 37).

Haidar, A., Duval, C., Legault, L., and Rabasa-Lhoret, R. (2013a). Pharmacokinetics of insulin aspart and glucagon in type 1 diabetes during closed-loop operation. *Journal of*

Diabetes Science and Technology, 7(6):1507–1512, doi:10.1177/193229681300700610. (Cited on pages 64 and 275).

Haidar, A., Elleri, D., Kumareswaran, K., Leelarathna, L., Allen, J.M., Caldwell, K., Murphy, H.R., Wilinska, M.E., Acerini, C.L., Evans, M.L., Dunger, D.B., Nodale, M., and Hovorka, R. (2013b). Pharmacokinetics of insulin aspart in pump-treated subjectswith type 1 diabetes: Reproducibility and effect ofage,weight, and duration of diabetes. *Diabetes Care*, 36(10):173–174, doi:10.2337/dc13-0485. (Cited on page 34).

Haidar, A., Legault, L., Matteau-Pelletier, L., Messier, V., Dallaire, M., Ladouceur, M., and Rabasa-Lhoret, R. (2015a). Outpatient overnight glucose control with dual-hormone artificial pancreas, single-hormone artificial pancreas, or conventional insulin pump therapy in children and adolescents with type 1 diabetes: An open-label, randomised controlled trial. *The Lancet Diabetes and Endocrinology*, 3(8):595–604, doi:10.1016/S2213-8587(15)00141-2. (Cited on pages 37 and 38).

Haidar, A., Legault, L., Messier, V., Mitre, T.M., Leroux, C., and Rabasa-Lhoret, R. (2015b). Comparison of dual-hormone artificial pancreas, single-hormone artificial pancreas, and conventional insulin pump therapy for glycaemic control in patients with type 1 diabetes: An open-label randomised controlled crossover trial. *The Lancet Diabetes and Endocrinology*, 3(1):17–26, doi:10.1016/S2213-8587(14)70226-8. (Cited on pages 37 and 38).

Haidar, A., Lovblom, L.E., Cardinez, N., Gouchie-Provencher, N., Orszag, A., Tsoukas, M.A., Falappa, C.M., Jafar, A., Ghanbari, M., Eldelekli, D., Rutkowski, J., Yale, J.F., and Perkins, B.A. (2022). Empagliflozin add-on therapy to closed-loop insulin delivery in type 1 diabetes: a 2×2 factorial randomized crossover trial. *Nature Medicine*, 28(6):1269–1276, doi:10.1038/s41591-022-01805-3. (Cited on page 47).

Haidar, A., Messier, V., Legault, L., Ladouceur, M., and Rabasa-Lhoret, R. (2017). Outpatient 60-hour day-and-night glucose control with dual-hormone artificial pancreas, single-hormone artificial pancreas, or sensor-augmented pump therapy in adults with type 1 diabetes: An open-label, randomised, crossover, controlled trial. *Diabetes, Obesity and Metabolism*, 19(5):713–720, doi:10.1111/dom.12880. (Cited on pages 37 and 38).

Haidar, A., Smaoui, M.R., Legault, L., and Rabasa-Lhoret, R. (2016). The role of glucagon in the artificial pancreas. *The Lancet Diabetes and Endocrinology*, 4(6):476–479, doi:10.1016/S2213-8587(16)30006-7. (Cited on pages 36, 37 and 38).

Haidar, A., Tsoukas, M.A., Bernier-Twardy, S., Yale, J.F., Rutkowski, J., Bossy, A., Pytka, E., El Fathi, A., Strauss, N., and Legault, L. (2020). A novel dual-hormone insulin- and-

pramlintide artificial pancreas for type 1 diabetes: A randomized controlled crossover trial. *Diabetes Care*, 43(3):597–606, doi:10.2337/dc19-1922. (Cited on pages 43, 44 and 161).

Haidar, A., Wilinska, M.E., Graveston, J.A., and Hovorka, R. (2013c). Stochastic virtual population of subjects with type 1 diabetes for the assessment of closed-loop glucose controllers. *IEEE Transactions on Biomedical Engineering*, 60(12):3524–3533, doi:10.1109/TBME.2013.2272736. (Cited on pages 64 and 275).

Haidar, A., Yale, J.F., Lovblom, L.E., Cardinez, N., Orszag, A., Falappa, C.M., Gouchie-Provencher, N., Tsoukas, M.A., El Fathi, A., Rene, J., Eldelekli, D., Lanctôt, S.O., Scarr, D., and Perkins, B.A. (2021). Reducing the need for carbohydrate counting in type 1 diabetes using closed-loop automated insulin delivery (artificial pancreas) and empagliflozin: A randomized, controlled, non-inferiority, crossover pilot trial. *Diabetes, Obesity and Metabolism*, 23(6):1272–1281, doi:10.1111/dom.14335. (Cited on page 47).

Hallschmid, M. (2021). Intranasal insulin. *Journal of Neuroendocrinology*, 33(4):1–13, doi:10.1111/jne.12934. (Cited on page 22).

Harris, K., Boland, C., Meade, L., and Battise, D. (2018). Adjunctive therapy for glucose control in patients with type 1 diabetes. *Diabetes, Metabolic Syndrome and Obesity*, 11:159–173, doi:10.2147/DMSO.S141700. (Cited on page 26).

Harvey, R.A., Dassau, E., Zisser, H., Seborg, D.E., Jovanovič, L., and Doyle, F.J. (2012). Design of the Health Monitoring System for the Artificial Pancreas: Low Glucose Prediction Module. *Journal of Diabetes Science and Technology*, 6(6):1345–1354, doi:10.1177/193229681200600613. (Cited on page 30).

Hassan, K. and Heptulla, R.A. (2009). Reducing postprandial hyperglycemia with adjuvant premeal pramlintide and postmeal insulin in children with type 1 diabetes mellitus. *Pediatric Diabetes*, 10(4):264–268, doi:10.1111/j.1399-5448.2008.00490.x. (Cited on pages 181, 190 and 197).

Hawkes, C.P., De Leon, D.D., and Rickels, M.R. (2019). Novel Preparations of Glucagon for the Prevention and Treatment of Hypoglycemia. *Current Diabetes Reports*, 19(10):97, doi:10.1007/s11892-019-1216-4. (Cited on page 23).

Hay, D.L., Chen, S., Lutz, T.A., Parkes, D.G., and Roth, J.D. (2015). Amylin: Pharmacology, Physiology, and Clinical Potential. *Pharmacological Reviews*, 67(3):564–600, doi:10.1124/pr.115.010629. (Cited on pages 14, 18, 162, 163 and 164).

Hay, D.L., Garelja, M.L., Poyner, D.R., and Walker, C.S. (2018). Update on the pharmacology of calcitonin/CGRP family of peptides: IUPHAR Review 25. *British Journal of Pharmacology*, 175(1):3–17, doi:10.1111/bph.14075. (Cited on page 162).

Haymond, M.W., DuBose, S.N., Rickels, M.R., Wolpert, H., Shah, V.N., Sherr, J.L., Weinstock, R.S., Agarwal, S., Verdejo, A.S., Cummins, M.J., Newswanger, B., Beck, R.W., Polsky, S., Beatson, C., Brackett, S., Toschi, E., Edwards, S., Castillo, A.A., Bzdick, S., Tichy, E., Zgorski, M., Steffen, A., Markman, E., Dalton-Bakes, C., Peleckis, A., Prestrelski, S., and Strange, P. (2017). Efficacy and safety of mini-dose glucagon for treatment of nonsevere hypoglycemia in adults with type 1 diabetes. *Journal of Clinical Endocrinology and Metabolism*, 102(8):2994–3001, doi:10.1210/jc.2017-00591. (Cited on pages 23, 24 and 136).

Haymond, M.W., Redondo, M.J., McKay, S., Cummins, M.J., Newswanger, B., Kinzell, J., and Prestrelski, S. (2016). Nonaqueous, mini-dose glucagon for treatment of mild hypoglycemia in adults with type 1 diabetes: A dose-seeking study. *Diabetes Care*, 39(3):465–468, doi:10.2337/dc15-2124. (Cited on page 23).

Haymond, M.W. and Schreiner, B. (2001). Mini-dose glucagon rescue for hypoglycemia in children with type 1 diabetes. *Diabetes Care*, 24(4):643–645, doi:10.2337/diacare.24.4.643. (Cited on pages 24 and 136).

Heinemann, L. (2002). Variability of Insulin Absorption and Insulin Action. *Diabetes Technology and Therapeutics*, 4(5):673–682, doi:10.1089/152091502320798312. (Cited on page 114).

Hepp, K.D., Langley, J., Von Funcke, H.J., Renner, R., and Kemmler, W. (1975). Increased insulin binding capacity of liver membranes from diabetic Chinese hamsters. *Nature*, 258(5531):154, doi:10.1038/258154a0. (Cited on page 83).

Hernández-Ordoñez, M. and Campos-Delgado, D.U. (2008). An extension to the compartmental model of type 1 diabetic patients to reproduce exercise periods with glycogen depletion and replenishment. *Journal of Biomechanics*, 41(4):744–752, doi:10.1016/j.jbiomech.2007.11.028. (Cited on page 59).

Herrero, P., Georgiou, P., Oliver, N., Reddy, M., Johnston, D., and Toumazou, C. (2013). A Composite Model of Glucagon–Glucose Dynamics for In Silico Testing of Bihormonal Glucose Controllers. *Journal of Diabetes Science and Technology*, 7(4):941–951, doi:10.1177/193229681300700416. (Cited on pages 59, 60, 70 and 277).

Hinshaw, L., Mallad, A., Man, C.D., Basu, R., Cobelli, C., Carter, R.E., Kudva, Y.C., and Basu, A. (2015). Glucagon sensitivity and clearance in type 1 diabetes: Insights from in vivo and in silico experiments. *American Journal of Physiology - Endocrinology and Metabolism*, 309(5):E474–E486, doi:10.1152/ajpendo.00236.2015. (Cited on page 72).

Hinshaw, L., Schiavon, M., Dadlani, V., Mallad, A., Dalla Man, C., Bharucha, A., Basu, R., Geske, J.R., Carter, R.E., Cobelli, C., Basu, A., and Kudva, Y.C. (2016). Effect of Pramlintide on Postprandial Glucose Fluxes in Type 1 Diabetes. *The Journal of Clinical Endocrinology and Metabolism*, 101(5):1954–1962, doi:10.1210/jc.2015-3952. (Cited on pages 161, 182, 191, 192, 193, 196, 197 and 198).

Horowitz, M., Jones, K.L., Akkermans, L.M.A., and Samsom, M. (2004). Gastric Function. In *Gastrointestinal Function in Diabetes Mellitus*, pages 117–176. Wiley. (Cited on page 164).

Hövelmann, U., Bysted, B.V., Mouritzen, U., Macchi, F., Lamers, D., Kronshage, B., Møller, D.V., and Heise, T. (2018). Pharmacokinetic and pharmacodynamic characteristics of dasiglucagon, a novel soluble and stable glucagon analog. *Diabetes Care*, 41(3):531–537, doi:10.2337/dc17-1402. (Cited on pages 23 and 140).

Hövelmann, U., Olsen, M.B., Mouritzen, U., Lamers, D., Kronshage, B., and Heise, T. (2019). Low doses of dasiglucagon consistently increase plasma glucose levels from hypoglycaemia and euglycaemia in people with type 1 diabetes mellitus. *Diabetes, Obesity and Metabolism*, 21(3):601–610, doi:10.1111/dom.13562. (Cited on pages 23 and 24).

Hovorka, R. (2011). Closed-loop insulin delivery: From bench to clinical practice. *Nature Reviews Endocrinology*, 7(7):385–395, doi:10.1038/nrendo.2011.32. (Cited on page 33).

Hovorka, R., Canonico, V., Chassin, L.J., Haueter, U., Massi-Benedetti, M., Federici, M.O., Pieber, T.R., Schaller, H.C., Schaupp, L., Vering, T., and Wilinska, M.E. (2004). Nonlinear model predictive control of glucose concentration in subjects with type 1 diabetes. *Physiological Measurement*, 25(4):905–920, doi:10.1088/0967-3334/25/4/010. (Cited on pages 58, 59, 171 and 268).

Hovorka, R., Shojaee-Moradie, F., Carroll, P.V., Chassin, L.J., Gowrie, I.J., Jackson, N.C., Tudor, R.S., Margot Umpleby, A., and Jones, R.H. (2002). Partitioning glucose distribution/transport, disposal, and endogenous production during IVGTT. *American Journal of Physiology - Endocrinology and Metabolism*, 282(5):992–1007, doi:10.1152/ajpendo.00304.2001. (Cited on pages 57, 91, 93 and 268).

Huffman, D.M., McLean, G.W., and Seagrove, M.A. (2009). Continuous subcutaneous pramlintide infusion therapy in patients with type 1 diabetes: observations

from a pilot study. *Endocrine practice : official journal of the American College of Endocrinology and the American Association of Clinical Endocrinologists*, 15(7):689–695, doi:10.4158/EP09044.ORR1. (Cited on pages 43 and 180).

Hwang, J.H., Perseghin, G., Rothman, D.L., Cline, G.W., Magnusson, I., Petersen, K.F., and Shulman, G.I. (1995). Impaired net hepatic glycogen synthesis in insulin-dependent diabetic subjects during mixed meal ingestion: A 13C nuclear magnetic resonance spectroscopy study. *Journal of Clinical Investigation*, 95(2):783–787, doi:10.1172/JCI117727. (Cited on page 18).

IDF (2022). IDF Atlas Reports. Technical report. (Cited on page 16).

Ilkowitz, J.T., Katikaneni, R., Cantwell, M., Ramchandani, N., and Heptulla, R.A. (2016). Adjuvant liraglutide and insulin versus insulin monotherapy in the closed-loop system in type 1 diabetes: A randomized open-labeled crossover design trial. *Journal of Diabetes Science and Technology*, 10(5):1108–1114, doi:10.1177/1932296816647976. (Cited on page 46).

Infante, M., Baidal, D.A., Rickels, M.R., Fabbri, A., Skyler, J.S., Alejandro, R., and Ricordi, C. (2021). Dual-hormone artificial pancreas for management of type 1 diabetes: Recent progress and future directions. *Artificial Organs*, 45(9):968–986, doi:10.1111/aor.14023. (Cited on page 42).

Insel, P.A., Kramer, K.J., Sherwin, R.S., Liljenquist, J.E., Tobin, J.D., Andres, R., and Berman, M. (1974). Modeling the insulin-glucose system in man. *Federation proceedings*, 33(7):1865–8. (Cited on page 64).

Ishikawa, Y. and Homcy, C.J. (1997). The adenylyl cyclases as integrators of transmembrane signal transduction. *Circulation Research*, 80(3):297–304, doi:10.1161/01.RES.80.3.297. (Cited on page 85).

Jackson, M. and Castle, J.R. (2020). Where Do We Stand with Closed-Loop Systems and Their Challenges? *Diabetes Technology and Therapeutics*, 22(7):485–491, doi:10.1089/dia.2019.0469. (Cited on page 33).

Jacobs, P. (2019). Virtual Patient Population Model. (Cited on page 59).

Jacobs, P.G., Resalat, N., Youssef, J.E., Reddy, R., Branigan, D., Preiser, N., Condon, J., and Castle, J. (2015). Incorporating an exercise detection, grading, and hormone dosing algorithm into the artificial pancreas using accelerometry and heart rate. *Journal of*

Diabetes Science and Technology, 9(6):1175–1184, doi:10.1177/1932296815609371. (Cited on pages 59, 96, 98, 99 and 270).

JDRF (2022). Type 1 Diabetes Index. (Cited on page 16).

Jones, R.W. (2019). Glucagon Control Strategies for the Bi-hormonal Artificial Pancreas. In *2019 14th IEEE Conference on Industrial Electronics and Applications (ICIEA)*, pages 1051–1056. IEEE. (Cited on page 36).

Kahn, C.R., Neville, D.M., and Roth, J. (1973). Insulin-Receptor Interaction in the Obese-Hyperglycemic Mouse. *Journal of Biological Chemistry*, 248(1):244–250, doi:10.1016/s0021-9258(19)44468-2. (Cited on page 83).

Kanderian, S.S., Weinzimer, S.A., and Steil, G.M. (2012). The identifiable virtual patient model: Comparison of simulation and clinical closed-loop study results. *Journal of Diabetes Science and Technology*, 6(2):371–379, doi:10.1177/193229681200600223. (Cited on pages 61, 64, 168 and 278).

Karageorgiou, V., Papaioannou, T.G., Bellos, I., Alexandraki, K., Tentolouris, N., Stefanadis, C., Chrousos, G.P., and Tousoulis, D. (2019). Effectiveness of artificial pancreas in the non-adult population: A systematic review and network meta-analysis. *Metabolism: Clinical and Experimental*, 90:20–30, doi:10.1016/j.metabol.2018.10.002. (Cited on page 30).

Katsuura, G., Asakawa, A., and Inui, A. (2002). Roles of pancreatic polypeptide in regulation of food intake. *Peptides*, 23(2):323–329, doi:10.1016/S0196-9781(01)00604-0. (Cited on page 12).

Kelly, R.A., Fitches, M.J., Webb, S.D., Pop, S.R., and Chidlow, S.J. (2019). Modelling the effects of glucagon during glucose tolerance testing. *Theoretical Biology and Medical Modelling*, 16(1):1–17, doi:10.1186/s12976-019-0115-3. (Cited on pages 57, 60, 70 and 279).

Kim, T.K. and Eberwine, J.H. (2010). Mammalian cell transfection: The present and the future. *Analytical and Bioanalytical Chemistry*, 397(8):3173–3178, doi:10.1007/s00216-010-3821-6. (Cited on page 84).

Kobayati, A., Haidar, A., and Tsoukas, M.A. (2022). Glucagon-like peptide-1 receptor agonists as adjunctive treatment for type 1 diabetes: Renewed opportunities through tailored approaches? *Diabetes, Obesity and Metabolism*, 24(5):769–787, doi:10.1111/dom.14637. (Cited on page 46).

Koenig, J.A. (2004). Assessment of receptor internalization and recycling. *Methods in molecular biology (Clifton, N.J.)*, 259:249–273, doi:10.1385/1-59259-754-8:249. (Cited on page 82).

Kolterman, O.G., Schwartz, S., Corder, C., Levy, B., Klaff, L., Peterson, J., and Gottlieb, A. (1996). Effect of 14 days' subcutaneous administration of the human amylin analogue, pramlintide (AC137), on an intravenous insulin challenge and response to a standard liquid meal in patients with IDDM. *Diabetologia*, 39(4):492–499, doi:10.1007/BF00400683. (Cited on pages 161, 181, 188 and 190).

Kong, M.F., King, P., Macdonald, I.A., Stubbs, T.A., Perkins, A.C., Blackshaw, P.E., Moyses, C., and Tattersall, R.B. (1997). Infusion of pramlintide, a human amylin analogue, delays gastric emptying in men with IDDM. *Diabetologia*, 40(1):82–88, doi:10.1007/s001250050646. (Cited on page 161).

Kong, M.F., Stubbs, T.A., King, P., Macdonald, I.A., Lambourne, J.E., Blackshaw, P.E., Perkins, A.C., and Tattersall, R.B. (1998). The effect of single doses of pramlintide on gastric emptying of two meals in men with IDDM. *Diabetologia*, 41(5):577–583, doi:10.1007/s001250050949. (Cited on pages 25, 181, 188 and 197).

Kono, T. and Barham, F.W. (1971). The Relationship between the Insulin-binding Capacity of Fat Cells and the Cellular Response to Insulin. *Journal of Biological Chemistry*, 246(20):6210–6216, doi:10.1016/S0021-9258(18)61777-6. (Cited on page 87).

Kovatchev, B.P., Breton, M., Dalla Man, C., and Cobelli, C. (2009). In Silico Preclinical Trials: A Proof of Concept in Closed-Loop Control of Type 1 Diabetes. *Journal of Diabetes Science and Technology*, 3(1):44–55, doi:10.1177/193229680900300106. (Cited on pages 53 and 65).

Kovatchev, B.P., Farhy, L.S., Cox, D.J., Straume, M., Yankov, V.I., Gonder-Frederick, L.A., and Clarke, W.L. (1999). Modeling Insulin-Glucose Dynamics during Insulin Induced Hypoglycemia. Evaluation of Glucose Counterregulation. *Journal of Theoretical Medicine*, 1(4):313–323, doi:10.1080/10273669908833028. (Cited on page 66).

Kovatchev, B.P., Patek, S.D., Ortiz, E.A., and Breton, M.D. (2015). Assessing sensor accuracy for non-adjunct use of continuous glucose monitoring. *Diabetes Technology and Therapeutics*, 17(3):177–186, doi:10.1089/dia.2014.0272. (Cited on page 33).

Krilov, L., Nguyen, A., Miyazaki, T., Unson, C.G., and Bouscarel, B. (2008). Glucagon receptor recycling: Role of carboxyl terminus, β-arrestins, and cytoskeleton. *American Journal*

of Physiology - Cell Physiology, 295(5):1230–1237, doi:10.1152/ajpcell.00240.2008. (Cited on page 84).

Kruger, D.F. and Gloster, M.A. (2004). Pramlintide for the treatment of insulin-requiring diabetes mellitus: Rationale and review of clinical data. *Drugs*, 64(13):1419–1432, doi:10.2165/00003495-200464130-00003. (Cited on page 13).

Kulcu, E., Tamada, J.A., Reach, G., Potts, R.O., and Lesho, M.J. (2003). Physiological differences between interstitial glucose and blood glucose measured in human subjects. *Diabetes Care*, 26(8):2405–2409, doi:10.2337/diacare.26.8.2405. (Cited on page 19).

Kushner, T., Bequette, B.W., Cameron, F., Forlenza, G., Maahs, D., and Sankaranarayanan, S. (2019). Models, Devices, Properties, and Verification of Artificial Pancreas Systems. In *Automated Reasoning for Systems Biology and Medicine*, pages 93–131. (Cited on page 54).

Lakshman, R., Boughton, C., and Hovorka, R. (2023). The changing landscape of automated insulin delivery in the management of type 1 diabetes. *Endocrine Connections*, 12(8):e230132, doi:10.1530/EC-23-0132. (Cited on page 32).

Langford, B.E., Evans, M., Haskins-Coulter, T., O'Connor, M., Cant, H.E., Eddowes, L.A., Edmonds, C., and Tank, A. (2020). Systematic literature review and network meta-analysis of sodium-glucose co-transporter inhibitors vs metformin as add-on to insulin in type 1 diabetes. *Diabetes, Obesity and Metabolism*, 22(1):39–50, doi:10.1111/dom.13863. (Cited on page 28).

Laugesen, C., Ranjan, A.G., Schmidt, S., and Nørgaard, K. (2022). Low-Dose Dasiglucagon Versus Oral Glucose for Prevention of Insulin-Induced Hypoglycemia in People With Type 1 Diabetes: A Phase 2, Randomized, Three-Arm Crossover Study. *Diabetes Care*, 45(6):1391–1399, doi:10.2337/dc21-2304. (Cited on pages 25 and 136).

Laugesen, C., Ranjan, A.G., Schmidt, S., and Nørgaard, K. (2023). Pen-administered low-dose dasiglucagon vs usual care for prevention and treatment of non-severe hypoglycaemia in people with type 1 diabetes during free-living conditions: a Phase II, randomised, open-label, two-period crossover trial. *Diabetologia*, 66(7):1208–1217, doi:10.1007/s00125-023-05909-4. (Cited on page 23).

Lehmann, E., Deutsch, T., Carson, E., and Sönksen, P. (1994). AIDA: an interactive diabetes advisor. *Computer Methods and Programs in Biomedicine*, 41(3-4):183–203, doi:10.1016/0169-2607(94)90054-X. (Cited on page 68).

Lehmann, E.D. and Deutsch, T. (1992). A physiological model of glucose-insulin interaction in type 1 diabetes mellitus. *Journal of Biomedical Engineering*, 14(3):235–242, doi:10.1016/0141-5425(92)90058-S. (Cited on page 68).

Lehmann, E.D., Tarín, C., Bondia, J., Teufel, E., and Deutsch, T. (2007). Incorporating a Generic Model of Subcutaneous Insulin Absorption into the AIDA v4 Diabetes Simulator. *Journal of Diabetes Science and Technology*, 1(3):423–435, doi:10.1177/193229680700100317. (Cited on page 68).

Leu, J.P. and Zonszein, J. (2010). Diagnostic Criteria and Classification of Diabetes. In *Principles of Diabetes Mellitus*, pages 107–115. Springer US, Boston, MA. (Cited on page 16).

Levetan, C., Want, L.L., Weyer, C., Strobel, S.A., Crean, J., Wang, Y., Maggs, D.G., Kolterman, O.G., Chandran, M., Mudaliar, S.R., and Henry, R.R. (2003). Impact of pramlintide on glucose fluctuations and postprandial glucose, glucagon, and triglyceride excursions among patients with type 1 diabetes intensively treated with insulin pumps. *Diabetes Care*, 26(1):1–8, doi:10.2337/diacare.26.1.1. (Cited on page 25).

Lindkvist, E.B., Laugesen, C., Reenberg, A.T., Ritschel, T.K.S., Svensson, J., Jørgensen, J.B., Nørgaard, K., and Ranjan, A.G. (2023). Performance of a dual-hormone closed-loop system versus insulin-only closed-loop system in adolescents with type 1 diabetes. A single-blind, randomized, controlled, crossover trial. *Frontiers in Endocrinology*, 14(January):1–10, doi:10.3389/fendo.2023.1073388. (Cited on page 38).

Liu, W. and Tang, F. (2008). Modeling a simplified regulatory system of blood glucose at molecular levels. *Journal of Theoretical Biology*, 252(4):608–620, doi:10.1016/j.jtbi.2008.02.021. (Cited on pages 68 and 87).

Lutz, T.A. (2022). Creating the amylin story. *Appetite*, 172(February):105965, doi:10.1016/j.appet.2022.105965. (Cited on pages 161, 171, 189 and 198).

Lv, D., Breton, M.D., and Farhy, L.S. (2013). Pharmacokinetics modeling of exogenous glucagon in Type 1 diabetes mellitus patients. *Diabetes Technology and Therapeutics*, 15(11):935–941, doi:10.1089/dia.2013.0150. (Cited on pages 59 and 177).

Ly, T.T., Nicholas, J.A., Retterath, A., Lim, E.M., Davis, E.A., and Jones, T.W. (2013). Effect of sensor-augmented insulin pump therapy and automated insulin suspension vs standard insulin pump therapy on hypoglycemia in patients with type 1 diabetes: A randomized clinical trial. *Jama*, 310(12):1240–1247, doi:10.1001/jama.2013.277818. (Cited on page 30).

Majdpour, D., Tsoukas, M.A., Yale, J.F., El Fathi, A., Rutkowski, J., Rene, J., Garfield, N., Legault, L., and Haidar, A. (2021). Fully Automated Artificial Pancreas for Adults With Type 1 Diabetes Using Multiple Hormones: Exploratory Experiments. *Canadian Journal of Diabetes*, 45(8):734–742, doi:10.1016/j.jcjd.2021.02.002. (Cited on page 47).

Masroor, S., van Dongen, M.G., Alvarez-Jimenez, R., Burggraaf, K., Peletier, L.A., and Peletier, M.A. (2019). Mathematical modeling of the glucagon challenge test. *Journal of Pharmacokinetics and Pharmacodynamics*, 46(6):553–564, doi:10.1007/s10928-019-09655-2. (Cited on pages 87, 88, 90 and 114).

Mauvais-Jarvis, F. (2018). Gender differences in glucose homeostasis and diabetes. *Physiology and Behavior*, 187(August 2017):20–23, doi:10.1016/j.physbeh.2017.08.016. (Cited on page 34).

McCall, A.L. and Farhy, L.S. (2013). Treating Type 1 diabetes: From strategies for insulin delivery to dual hormonal control. *Minerva Endocrinologica*, 38(2):145–163. (Cited on pages 21, 22, 33 and 54).

McCoy, S., Kabadi, M., Kabadi, U., and Birkenholz, M. (1995). More Uniform Diurnal Blood Glucose Control and a Reduction in Daily Insulin Dosage on Addition of Glibenclamide to Insulin in Type 1 Diabetes Mellitus: Role of Enhanced Insulin Sensitivity. *Diabetic Medicine*, 12(10):880–884, doi:10.1111/j.1464-5491.1995.tb00390.x. (Cited on page 28).

McGough, J.J. and Faraone, S.V. (2009). Estimating the size of treatment effects: moving beyond p values. *Psychiatry (Edgmont)*, 6(10):21–9. (Cited on page 117).

McKay, M.D., Beckman, R.J., and Conover, W.J. (2000). A comparison of three methods for selecting values of input variables in the analysis of output from a computer code. *Technometrics*, 42(1):55–61, doi:10.1080/00401706.2000.10485979. (Cited on page 101).

McQueen, J. (2005). Pramlintide acetate. *American Journal of Health-System Pharmacy*, 62(22):2363–2372, doi:10.2146/ajhp050341. (Cited on pages 25 and 26).

Megyesi, K., Kahn, C.R., Roth, J., Neville, D.M., Nissley, S.P., Humbel, R.E., and Froesch, E.R. (1975). The NSILA-s receptor in liver plasma membranes. Characterization and comparison with the insulin receptor. *Journal of Biological Chemistry*, 250(23):8990–8996, doi:10.1016/s0021-9258(19)40683-2. (Cited on page 87).

Micheletto, F., Dalla Man, C., Kolterman, O., Chiquette, E., Herrmann, K., Schirra, J., Kovatchev, B., and Cobelli, C. (2013). In silico design of optimal ratio for co-administration

of pramlintide and insulin in type 1 diabetes. *Diabetes Technology and Therapeutics*, 15(10):802–809, doi:10.1089/dia.2013.0054. (Cited on pages 77 and 171).

Miragall, J., Furió-Novejarque, C., Sala-Mira, I., Díez, J.L., and Bondia, J. (2023). A new pharmacokinetics and pharmacodynamics model of subcutaneous pramlintide infusion. *Diabetes Technology and Therapeutics*, 25(S2):A–136, doi:10.1089/dia.2023.2525.abstracts. (Cited on page 203).

Mitrakou, A., Ryan, C., Veneman, T., Mokan, M., Jenssen, T., Kiss, I., Durrant, J., Cryer, P., and Gerich, J. (1991). Hierarchy of glycemic thresholds for counterregulatory hormone secretion, symptoms, and cerebral dysfunction. *American Journal of Physiology-Endocrinology and Metabolism*, 260(1):E67–E74, doi:10.1152/ajpendo.1991.260.1.E67. (Cited on page 15).

Mohanty, R.R. and Das, S. (2017). Inhaled insulin - current direction of insulin research. *Journal of Clinical and Diagnostic Research*, 11(4):OE01–OE02, doi:10.7860/JCDR/2017/23626.9732. (Cited on page 22).

Moscardó García, V. (2019). *Contributions to modelling and control for improved hypoglycaemia and variability mitigation by dual-hormone artificial pancreas systems*. PhD thesis, Universitat Politècnica de València, Valencia (Spain). (Cited on page 176).

Müller, T.D., Finan, B., Clemmensen, C., Di Marchi, R.D., and Tschöp, M.H. (2017). The new biology and pharmacology of glucagon. *Physiological Reviews*, 97(2):721–766, doi:10.1152/physrev.00025.2016. (Cited on pages 10, 14, 16, 17 and 85).

Müller, T.D., Nogueiras, R., Andermann, M.L., Andrews, Z.B., Anker, S.D., Argente, J., Batterham, R.L., Benoit, S.C., Bowers, C.Y., Broglio, F., Casanueva, F.F., D'Alessio, D., Depoortere, I., Geliebter, A., Ghigo, E., Cole, P.A., Cowley, M., Cummings, D.E., Dagher, A., Diano, S., Dickson, S.L., Diéguez, C., Granata, R., Grill, H.J., Grove, K., Habegger, K.M., Heppner, K., Heiman, M.L., Holsen, L., Holst, B., Inui, A., Jansson, J.O., Kirchner, H., Korbonits, M., Laferrère, B., LeRoux, C.W., Lopez, M., Morin, S., Nakazato, M., Nass, R., Perez-Tilve, D., Pfluger, P.T., Schwartz, T.W., Seeley, R.J., Sleeman, M., Sun, Y., Sussel, L., Tong, J., Thorner, M.O., van der Lely, A.J., van der Ploeg, L.H., Zigman, J.M., Kojima, M., Kangawa, K., Smith, R.G., Horvath, T., and Tschöp, M.H. (2015). Ghrelin. *Molecular Metabolism*, 4(6):437–460, doi:10.1016/j.molmet.2015.03.005. (Cited on page 12).

Neelakanta, P.S. (2006). A Complex System Model of Glucose Regulatory Metabolism. *Complex Systems*, 16:343–367. (Cited on page 68).

Neelakanta, P.S., Sudhakar, R., and DeGroff, D. (1991). Langevin machine: a neural network based on stochastically justifiable sigmoidal function. *Biological Cybernetics*, 65(5):331–338, doi:10.1007/BF00216966. (Cited on page 69).

Nocedal, J. and Wright, S.J. (2006). *Numerical optimization*. (Cited on page 101).

Nordlie, R.C., Foster, J.D., and Lange, A.J. (1999). Regulation of glucose production by the liver. *Annual Review of Nutrition*, 19(1):379–406, doi:10.1146/annurev.nutr.19.1.379. (Cited on page 10).

Nyholm, B., Brock, B., Ørskov, L., and Schmitz, O. (2001). Amylin receptor agonists: a novel pharmacological approach in the management of insulin-treated diabetes mellitus. *Expert Opinion on Investigational Drugs*, 10(9):1641–1652, doi:10.1517/13543784.10.9.1641. (Cited on page 162).

Nyholm, B., Møller, N., Gravholt, C.H., Orskov, L., Mengel, A., Bryan, G., Moyses, C., Alberti, K.G., and Schmitz, O. (1996). Acute effects of the human amylin analog AC137 on basal and insulin-stimulated euglycemic and hypoglycemic fuel metabolism in patients with insulin-dependent diabetes mellitus. *The Journal of Clinical Endocrinology and Metabolism*, 81(3):1083–1089, doi:10.1210/jcem.81.3.8772580. (Cited on page 16).

Nyholm, B., Ørskov, L., Hove, K.Y., Gravholt, C.H., Møller, N., George, K., Alberti, M.M., Moyses, C., Kolterman, O., and Schmitz, O. (1999). The amylin analog pramlintide improves glycemic control and reduces postprandial glucagon concentrations in patients with type 1 diabetes mellitus. *Metabolism: Clinical and Experimental*, 48(7):935–941, doi:10.1016/S0026-0495(99)90232-9. (Cited on page 25).

Ovalle, F., Grimes, T., Xu, G., Patel, A.J., Grayson, T.B., Thielen, L.A., Li, P., and Shalev, A. (2018). Verapamil and beta cell function in adults with recent-onset type 1 diabetes. *Nature Medicine*, 24(8):1108–1112, doi:10.1038/s41591-018-0089-4. (Cited on page 28).

Pasqua, M.R., Jafar, A., Kobayati, A., Tsoukas, M.A., and Haidar, A. (2022). Low-Dose Empagliflozin as Adjunct to Hybrid Closed-Loop Insulin Therapy in Adults With Suboptimally Controlled Type 1 Diabetes: A Randomized Crossover Controlled Trial. *Diabetes Care*, 46(1):165–172, doi:10.2337/dc22-0490. (Cited on page 47).

Patek, S.D., Lv, D., Ortiz, E.A., Hughes-Karvetski, C., Kulkarni, S., Zhang, Q., and Breton, M.D. (2016). Empirical Representation of Blood Glucose Variability in a Compartmental Model. In *Prediction Methods for Blood Glucose Concentration*, pages 133–157. (Cited on page 56).

Paterson, M., Bell, K.J., O'Connell, S.M., Smart, C.E., Shafat, A., and King, B. (2015). The Role of Dietary Protein and Fat in Glycaemic Control in Type 1 Diabetes: Implications for Intensive Diabetes Management. *Current Diabetes Reports*, 15(9):1–9, doi:10.1007/s11892-015-0630-5. (Cited on page 192).

Patil, M., Deshmukh, N.J., Patel, M., and Sangle, G.V. (2020). Glucagon-based therapy: Past, present and future. *Peptides*, 127(October 2019):170296, doi:10.1016/j.peptides.2020.170296. (Cited on page 23).

Payne, V.A., Arden, C., Wu, C., Lange, A.J., and Agius, L. (2005). Dual Role of Phosphofructokinase-2/Fructose Bisphosphatase-2 in Regulating the Compartmentation and Expression of Glucokinase in Hepatocytes. *Diabetes*, 54(7):1949–1957, doi:10.2337/diabetes.54.7.1949. (Cited on page 85).

Peters, T.M. and Haidar, A. (2018). Dual-hormone artificial pancreas: benefits and limitations compared with single-hormone systems. *Diabetic Medicine*, 35(4):450–459, doi:10.1111/dme.13581. (Cited on pages 34 and 36).

Pham, H. (2019). A new criterion for model selection. *Mathematics*, 7(12):1–12, doi:10.3390/MATH7121215. (Cited on pages 176 and 177).

Pittas, A.G., Westcott, G.P., and Balk, E.M. (2015). Efficacy, safety, and patient acceptability of Technosphere inhaled insulin for people with diabetes: A systematic review and meta-analysis. *The Lancet Diabetes and Endocrinology*, 3(11):886–894, doi:10.1016/S2213-8587(15)00280-6. (Cited on page 21).

Pontiroli, A.E. (2015). Intranasal Glucagon. *Journal of Diabetes Science and Technology*, 9(1):38–43, doi:10.1177/1932296814557518. (Cited on page 23).

Qiao, Y.C., Ling, W., Pan, Y.H., Chen, Y.L., Zhou, D., Huang, Y.M., Zhang, X.X., and Zhao, H.L. (2017). Efficacy and safety of pramlintide injection adjunct to insulin therapy in patients with type 1 diabetes mellitus: A systematic review and meta-analysis. *Oncotarget*, 8(39):66504–66515, doi:10.18632/oncotarget.16008. (Cited on page 25).

Quiroz, G. (2019). The evolution of control algorithms in artificial pancreas: A historical perspective. *Annual Reviews in Control*, 48:222–232, doi:10.1016/j.arcontrol.2019.07.004. (Cited on page 32).

Ramkissoon, C.M., Aufderheide, B., Bequette, B.W., and Palerm, C.C. (2014). A Model of Glucose-Insulin-Pramlintide Pharmacokinetics and Pharmacodynamics

in Type I Diabetes. *Journal of Diabetes Science and Technology*, 8(3):529–542, doi:10.1177/1932296813517323. (Cited on pages 75, 166, 169, 171 and 180).

Ranjan, A., Nørgaard, K., Tetzschner, R., Steineck, I.I.K., Clausen, T.R., Holst, J.J., Madsbad, S., and Schmidt, S. (2018). Effects of precedingethanol intake on glucose response to low-dose glucagon in individuals with type 1 diabetes: A Randomized, placebo-controlled, crossover study. *Diabetes Care*, 41(4):797–806, doi:10.2337/dc17-1458. (Cited on page 40).

Ranjan, A., Schmidt, S., Damm-Frydenberg, C., Steineck, I., Clausen, T.R., Holst, J.J., Madsbad, S., and Nørgaard, K. (2017). Low-Carbohydrate Diet Impairs the Effect of Glucagon in the Treatment of Insulin-Induced Mild Hypoglycemia: A Randomized Crossover Study. *Diabetes Care*, 40(1):132–135, doi:10.2337/dc16-1472. (Cited on pages 40, 128, 134, 135 and 137).

Ranjan, A., Schmidt, S., Madsbad, S., Holst, J.J., and Nørgaard, K. (2016). Effects of subcutaneous, low-dose glucagon on insulin-induced mild hypoglycaemia in patients with insulin pump treated type 1 diabetes. *Diabetes, Obesity and Metabolism*, 18(4):410–418, doi:10.1111/dom.12627. (Cited on pages 24, 108, 109, 128 and 136).

Ranjan, A.G., Schmidt, S., and Nørgaard, K. (2021). Glucagon for hypoglycaemia treatment in type 1 diabetes. *Diabetes/Metabolism Research and Reviews*, 37(5):1–12, doi:10.1002/dmrr.3409. (Cited on page 24).

Rashid, M., Samadi, S., Sevil, M., Hajizadeh, I., Kolodziej, P., Hobbs, N., Maloney, Z., Brandt, R., Feng, J., Park, M., Quinn, L., and Cinar, A. (2019). Simulation software for assessment of nonlinear and adaptive multivariable control algorithms: Glucose–insulin dynamics in Type 1 diabetes. *Computers and Chemical Engineering*, 130:106565, doi:10.1016/j.compchemeng.2019.106565. (Cited on pages 63, 65 and 281).

Rathee, S. and Nilam (2017). ODE models for the management of diabetes: A review. *International Journal of Diabetes in Developing Countries*, 37(1):4–15, doi:10.1007/s13410-016-0475-8. (Cited on page 69).

Ratner, R.E., Dickey, R., Fineman, M., Maggs, D.G., Shen, L., Strobel, S.A., Weyer, C., and Kolterman, O.G. (2004). Amylin replacement with pramlintide as an adjunct to insulin therapy improves long-term glycaemic and weight control in Type 1 diabetes mellitus: A 1-year, randomized controlled trial. *Diabetic Medicine*, 21(11):1204–1212, doi:10.1111/j.1464-5491.2004.01319.x. (Cited on page 25).

Reiband, H.K., Schmidt, S., Ranjan, A., Holst, J.J., Madsbad, S., and Nørgaard, K. (2015). Dual-hormone treatment with insulin and glucagon in patients with type 1 diabetes.

Diabetes/Metabolism Research and Reviews, 31(7):672–679, doi:10.1002/dmrr.2632. (Cited on page 18).

Renard, E. (2008). Insulin delivery route for the artificial pancreas: Subcutaneous, intraperitoneal, or intravenous? Pros and cons. *Journal of Diabetes Science and Technology*, 2(4):735–738, doi:10.1177/193229680800200429. (Cited on page 22).

Reno, C.M., Litvin, M., Clark, A.L., and Fisher, S.J. (2013). Defective Counterregulation and Hypoglycemia Unawareness in Diabetes. Mechanisms and Emerging Treatments. *Endocrinology and Metabolism Clinics of North America*, 42(1):15–38, doi:10.1016/j.ecl.2012.11.005. (Cited on page 13).

Renukuntla, V.S., Ramchandani, N., Trast, J., Cantwell, M., and Heptulla, R.A. (2014). Role of Glucagon-like peptide-1 analogue versus Amylin as an adjuvant therapy in type 1 diabetes in a closed loop setting with ePID algorithm. *Journal of Diabetes Science and Technology*, 8(5):1011–1017, doi:10.1177/1932296814542153. (Cited on page 45).

Resalat, N., Youssef, J.E., Tyler, N., Castle, J., and Jacobs, P.G. (2019). A statistical virtual patient population for the glucoregulatory system in type 1 diabetes with integrated exercise model. *PLoS ONE*, 14(7):e0217301, doi:10.1371/journal.pone.0217301. (Cited on pages 59, 62, 70, 96, 98 and 270).

Rickels, M.R., DuBose, S.N., Toschi, E., Beck, R.W., Verdejo, A.S., Wolpert, H., Cummins, M.J., Newswanger, B., and Riddell, M.C. (2018). Mini-dose Glucagon as a novel approach to prevent exercise-induced hypoglycemia in type 1 diabetes. *Diabetes Care*, 41(9):1909–1916, doi:10.2337/dc18-0051. (Cited on page 23).

Riddell, M.C., Gallen, I.W., Smart, C.E., Taplin, C.E., Adolfsson, P., Lumb, A.N., Kowalski, A., Rabasa-Lhoret, R., McCrimmon, R.J., Hume, C., Annan, F., Fournier, P.A., Graham, C., Bode, B., Galassetti, P., Jones, T.W., Millán, I.S., Heise, T., Peters, A.L., Petz, A., and Laffel, L.M. (2017). Exercise management in type 1 diabetes: a consensus statement. *The Lancet Diabetes and Endocrinology*, 5(5):377–390, doi:10.1016/S2213-8587(17)30014-1. (Cited on pages 10 and 34).

Riddle, M.C., Nahra, R., Han, J., Castle, J., Hanavan, K., Hompesch, M., Huffman, D., Strange, P., and Ohman, P. (2018). Control of postprandial hyperglycemia in type 1 diabetes by 24-hour fixed-dose coadministration of pramlintide and regular human insulin: A randomized, two-way crossover study. *Diabetes Care*, 41(11):2346–2352, doi:10.2337/dc18-1091. (Cited on page 43).

Rimmington, F. (2020). Pharmacokinetics and pharmacodynamics. *Southern African Journal of Anaesthesia and Analgesia*, 26(6):S153–S156, doi:10.36303/SAJAA.2020.26.6.S3.2562. (Cited on pages 52 and 53).

Rodbell, M., Krans, H.M.J., Pohl, S.L., and Birnbaumer, L. (1971). The Glucagon-sensitive Adenyl Cyclase System in Plasma Membranes of Rat Liver. *Journal of Biological Chemistry*, 246(6):1872–1876, doi:10.1016/S0021-9258(18)62389-0. (Cited on page 89).

Röder, P.V., Wu, B., Liu, Y., and Han, W. (2016). Pancreatic regulation of glucose homeostasis. *Experimental & Molecular Medicine*, 48(3):e219–e219, doi:10.1038/emm.2016.6. (Cited on pages 12, 13 and 28).

Rodriguez, L.M., Mason, K.J., Haymond, M.W., and Heptulla, R.A. (2007). The role of prandial pramlintide in the treatment of adolescents with type 1 diabetes. *Pediatric Research*, 62(6):746–749, doi:10.1203/PDR.0b013e318159af8c. (Cited on page 180).

Rohatgi, A. (2022). WebPlotDigitizer. (Cited on page 180).

Ronald Kahn, C. (1976). Membrane receptors for hormones and neurotransmitters. *Journal of Cell Biology*, 70(2):261–286, doi:10.1083/jcb.70.2.261. (Cited on pages 82, 87 and 89).

Roy, A. and Parker, R.S. (2006). Dynamic Modeling of Free Fatty Acid, Glucose, and Insulin: An Extended "Minimal Model". *Diabetes Technology & Therapeutics*, 8(6):617–626, doi:10.1089/dia.2006.8.617. (Cited on page 56).

Roy, A. and Parker, R.S. (2007). Dynamic modeling of exercise effects on plasma glucose and insulin levels. *Journal of Diabetes Science and Technology*, 1(3):338–347, doi:10.1177/193229680700100305. (Cited on page 56).

Russell, S.J., El-Khatib, F.H., Nathan, D.M., and Damiano, E.R. (2010). Efficacy determinants of subcutaneous microdose glucagon during closed-loop control. *Journal of Diabetes Science and Technology*, 4(6):1288–1304, doi:10.1177/193229681000400602. (Cited on page 39).

Russell, S.J., Hillard, M.A., Balliro, C., Magyar, K.L., Selagamsetty, R., Sinha, M., Grennan, K., Mondesir, D., Ehklaspour, L., Zheng, H., Damiano, E.R., and El-Khatib, F.H. (2016). Day and night glycaemic control with a bionic pancreas versus conventional insulin pump therapy in preadolescent children with type 1 diabetes: A randomised crossover trial. *The Lancet Diabetes and Endocrinology*, 4(3):233–243, doi:10.1016/S2213-8587(15)00489-1. (Cited on page 41).

Sala Mira, I. (2023). *New Contributions Towards Meal and Exercise Announcement-Free Artificial Pancreas Systems*. PhD thesis, Universitat Politècnica de València, Valencia (Spain). (Cited on page 34).

Salway, J. (1993). *Metabolism at a glance*. Blackwell. (Cited on pages 10 and 85).

Samsom, M., Szarka, L.A., Camilleri, M., Vella, A., Zinsmeister, A.R., and Rizza, R.A. (2000). Pramlintide, an amylin analog, selectively delays gastric emptying: potential role of vagal inhibition. *American Journal of Physiology-Gastrointestinal and Liver Physiology*, 278(6):G946–G951, doi:10.1152/ajpgi.2000.278.6.G946. (Cited on page 163).

Schaller, S. (2014). *Automated Optimal Glycaemic Control using a Physiology-Based Pharmacokinetic/Pharmacodynamic model*. PhD thesis. (Cited on pages 69 and 86).

Schaller, S., Willmann, S., Lippert, J., Schaupp, L., Pieber, T., Schuppert, A., and Eissing, T. (2013). A Generic Integrated Physiologically based Whole-body Model of the Glucose-Insulin-Glucagon Regulatory System. *CPT: Pharmacometrics & Systems Pharmacology*, 2(8):1–10, doi:10.1038/psp.2013.40. (Cited on page 69).

Schönauer, M. and Thomas, A. (2010). Sensor-augmented pump therapy - On the way to artificial pancreas. *Avances en Diabetologia*, 26(3):143–146, doi:10.1016/S1134-3230(10)63002-5. (Cited on page 19).

Sedaghat, A.R., Sherman, A., and Quon, M.J. (2002). A mathematical model of metabolic insulin signaling pathways. *American Journal of Physiology - Endocrinology and Metabolism*, 283(5):1084–1101, doi:10.1152/ajpendo.00571.2001. (Cited on pages 68 and 89).

Sharma, A. and Jusko, W.J. (1998). Characteristics of indirect pharmacodynamic models and applications to clinical drug responses. *British Journal of Clinical Pharmacology*, 45(3):229–239, doi:10.1046/j.1365-2125.1998.00676.x. (Cited on page 75).

Sherr, J.L., Patel, N.S., Michaud, C.I., Palau-Collazo, M.M., Van Name, M.A., Tamborlane, W.V., Cengiz, E., Carria, L.R., Tichy, E.M., and Weinzimer, S.A. (2016). Mitigating meal-related glycemic excursions in an insulin-sparing manner during closed-loop insulin delivery: The beneficial effects of adjunctive pramlintide and liraglutide. *Diabetes Care*, 39(7):1127–1134, doi:10.2337/dc16-0089. (Cited on page 45).

Shrayyef, M.Z. and Gerich, J.E. (2010). Normal Glucose Homeostasis. In *Principles of Diabetes Mellitus*, volume 53, pages 19–35. Springer US, Boston, MA. (Cited on pages 10, 15 and 34).

Silvestre, R.A., Rodríguez-Gallardo, J., Jodka, C., Parkes, D.G., Pittner, R.A., Young, A.A., and Marco, J. (2001). Selective amylin inhibition of the glucagon response to arginine is extrinsic to the pancreas. *American Journal of Physiology-Endocrinology and Metabolism*, 280(3):E443–E449, doi:10.1152/ajpendo.2001.280.3.E443. (Cited on page 16).

Smaoui, M.R., Rabasa-Lhoret, R., and Haidar, A. (2020a). Development platform for artificial pancreas algorithms. *PLOS ONE*, 15(12):e0243139, doi:10.1371/journal.pone.0243139. (Cited on pages 62, 64, 72, 98, 170 and 275).

Smaoui, M.R., Rabasa-Lhoret, R., and Haidar, A. (2020b). Ulna (t1dclinic.com/ulna.php). (Cited on pages 64 and 98).

Sorensen, J.T. (1985). *A physiologic model of glucose metabolism in man and its use to design and assess improved insulin therapies for diabetes*. PhD thesis. (Cited on page 69).

Srinivasan, S., Ekhlaspour, L., and Cengiz, E. (2021). Adjunctive Therapies to Optimize Closed-loop Glucose Control. *Journal of Diabetes Science and Technology*, 15(6):1243–1251, doi:10.1177/19322968211032701. (Cited on pages 25, 27, 46 and 49).

Steil, G., Clark, B., Kanderian, S., and Rebrin, K. (2005). Modeling Insulin Action for Development of a Closed-Loop Artificial Pancreas. *Diabetes Technology & Therapeutics*, 7(1):94–108, doi:10.1089/dia.2005.7.94. (Cited on page 69).

Strasser, A., Wittmann, H.J., and Seifert, R. (2017). Binding Kinetics and Pathways of Ligands to GPCRs. *Trends in Pharmacological Sciences*, 38(8):717–732, doi:10.1016/j.tips.2017.05.005. (Cited on page 89).

Svendby, S.R. (2016). *Mathematical Modelling of Heart Rate During Cycling Exercise. MS Thesis*. PhD thesis. (Cited on page 65).

Svoboda, M., Tastenoy, M., Vertongen, P., and Robberecht, P. (1994). Relative quantitative analysis of glucagon receptor mRNA in rat tissues. *Molecular and Cellular Endocrinology*, 105(2):131–137, doi:10.1016/0303-7207(94)90162-7. (Cited on page 84).

Taleb, N., Emami, A., Suppere, C., Messier, V., Legault, L., Ladouceur, M., Chiasson, J.L., Haidar, A., and Rabasa-Lhoret, R. (2016). Efficacy of single-hormone and dual-hormone artificial pancreas during continuous and interval exercise in adult patients with type 1 diabetes: randomised controlled crossover trial. *Diabetologia*, 59(12):2561–2571, doi:10.1007/s00125-016-4107-0. (Cited on pages 37 and 38).

Tanenbaum, M.L. and Commissariat, P.V. (2023). Experience with burdens of diabetes device use that affect uptake and optimal use in people with type 1 diabetes. *Endocrine Connections*, 12(10):e230193, doi:10.1530/EC-23-0193. (Cited on page 42).

Tarín, C., Teufel, E., Picó, J., Bondia, J., and Pfleiderer, H.J. (2005). Comprehensive pharmacokinetic model of insulin glargine and other insulin formulations. *IEEE Transactions on Biomedical Engineering*, 52(12):1994–2005, doi:10.1109/TBME.2005.857681. (Cited on page 69).

Tašić, J., Takács, M., and Kovács, L. (2022). Control Engineering Methods for Blood Glucose Levels Regulation. *Acta Polytechnica Hungarica*, 19(7):127–152, doi:10.12700/aph.19.7.2022.7.7. (Cited on page 32).

Teigen, I.A. (2023). *Doctoral thesis The Bihormonal Artificial Pancreas : New Perspectives on the Pharmacokinetics and Pharmacodynamics of Glucagon*. PhD thesis. (Cited on page 73).

Thomas, A. and Heinemann, L. (2022). Algorithms for Automated Insulin Delivery: An Overview. *Journal of Diabetes Science and Technology*, 16(5):1228–1238, doi:10.1177/19322968211008442. (Cited on page 32).

Thompson, R.G., Pearson, L., and Kolterman, O.G. (1997a). Effects of 4 weeks' administration of pramlintide, a human amylin analogue, on glycaemia control in patients with IDDM: effects on plasma glucose profiles and serum fructosamine concentrations. *Diabetologia*, 40(11):1278–1285, doi:10.1007/s001250050821. (Cited on page 25).

Thompson, R.G., Peterson, J., Gottlieb, A., and Mullane, J. (1997b). Effects of pramlintide, an analog of human amylin, on plasma glucose profiles in patients with IDDM: results of a multicenter trial. *Diabetes*, 46(4):632–6. (Cited on page 180).

Torres-Castaño, A., Rivero-Santana, A., Perestelo-Pérez, L., Duarte-Díaz, A., Abt-Sacks, A., Ramos-García, V., Álvarez-Pérez, Y., Wäagner, A.M., Rigla, M., and Serrano-Aguilar, P. (2022). Dual-Hormone Insulin-and-Pramlintide Artificial Pancreas for Type 1 Diabetes: A Systematic Review. *Applied Sciences (Switzerland)*, 12(20):1–15, doi:10.3390/app122010262. (Cited on page 44).

Trout, K.K., Rickels, M.R., Schutta, M.H., Petrova, M., Freeman, E.W., Tkacs, N.C., and Teff, K.L. (2007). Menstrual cycle effects on insulin sensitivity in women with type 1 diabetes: A pilot study. *Diabetes Technology and Therapeutics*, 9(2):176–182, doi:10.1089/dia.2006.0004. (Cited on page 34).

Tsoukas, M.A., Cohen, E., Legault, L., von Oettingen, J.E., Yale, J.F., Vallis, M., Odabassian, M., El Fathi, A., Rutkowski, J., Jafar, A., Ghanbari, M., Gouchie-Provencher, N., René, J., Palisaitis, E., and Haidar, A. (2021a). Alleviating carbohydrate counting with a FiASP-plus-pramlintide closed-loop delivery system (artificial pancreas): Feasibility and pilot studies. *Diabetes, Obesity and Metabolism*, 23(9):2090–2098, doi:10.1111/dom.14447. (Cited on page 44).

Tsoukas, M.A., Majdpour, D., Yale, J.F., Fathi, A.E., Garfield, N., Rutkowski, J., Rene, J., Legault, L., and Haidar, A. (2021b). A fully artificial pancreas versus a hybrid artificial pancreas for type 1 diabetes: a single-centre, open-label, randomised controlled, crossover, non-inferiority trial. *The Lancet Digital Health*, 3(11):e723–e732, doi:10.1016/S2589-7500(21)00139-4. (Cited on pages 43, 44 and 161).

Underland, L.J., Ilkowitz, J.T., Katikaneni, R., Dowd, A., and Heptulla, R.A. (2017). Use of Sitagliptin with Closed-Loop Technology to Decrease Postprandial Blood Glucose in Type 1 Diabetes. *Journal of Diabetes Science and Technology*, 11(3):602–610, doi:10.1177/1932296817699847. (Cited on page 46).

Unger, R.H. and Cherrington, A.D. (2012). Glucagonocentric restructuring of diabetes: A pathophysiologic and therapeutic makeover. *Journal of Clinical Investigation*, 122(1):4–12, doi:10.1172/JCI60016. (Cited on page 18).

Van Bon, A.C., Luijf, Y.M., Koebrugge, R., Koops, R., Hoekstra, J.B., and Devries, J.H. (2014). Feasibility of a portable bihormonal closed-loop system to control glucose excursions at home under free-living conditions for 48 Hours. *Diabetes Technology and Therapeutics*, 16(3):131–136, doi:10.1089/dia.2013.0166. (Cited on page 41).

Van Dongen, M.G., Geerts, B.F., Bhanot, S., Morgan, E.S., De Kam, M.L., Moerland, M., Romijn, J.A., Cohen, A.F., and Burggraaf, J. (2014). Characterization of a standardized glucagon challenge test as a pharmacodynamic tool in pharmacological research. *Hormone and Metabolic Research*, 46(4):269–273, doi:10.1055/s-0033-1363223. (Cited on page 89).

Van Dongen, M.G., Geerts, B.F., Morgan, E.S., Brandt, T.A., De Kam, M.L., Romijn, J.A., Cohen, A.F., Bhanot, S., and Burggraaf, J. (2015). First proof of pharmacology in humans of a novel glucagon receptor antisense drug. *Journal of Clinical Pharmacology*, 55(3):298–306, doi:10.1002/jcph.396. (Cited on pages 89 and 90).

Van Schaftingen, E. and Gerin, I. (2002). The glucose-6-phosphatase system. *Biochemical Journal*, 362(3):513, doi:10.1042/0264-6021:3620513. (Cited on page 85).

van Sloun, B., Goossens, G.H., Erdõs, B., O'Donovan, S.D., Singh-Povel, C.M., Geurts, J.M., van Riel, N.A., and Arts, I.C. (2023). E-DES-PROT: A novel computational model to describe the effects of amino acids and protein on postprandial glucose and insulin dynamics in humans. *iScience*, 26(3):106218, doi:10.1016/j.isci.2023.106218. (Cited on page 177).

Viñals, C., Beneyto, A., Martín-SanJosé, J.F., Furió-Novejarque, C., Bertachi, A., Bondia, J., Vehi, J., Conget, I., and Giménez, M. (2021). Artificial Pancreas with Carbohydrate Suggestion Performance for Unannounced and Announced Exercise in Type 1 Diabetes. *Journal of Clinical Endocrinology and Metabolism*, 106(1):55–63, doi:10.1210/clinem/dgaa562. (Cited on page 3).

Visentin, R., Campos-Náñez, E., Schiavon, M., Lv, D., Vettoretti, M., Breton, M., Kovatchev, B.P., Dalla Man, C., and Cobelli, C. (2018). The UVA/Padova Type 1 Diabetes Simulator Goes From Single Meal to Single Day. *Journal of Diabetes Science and Technology*, 12(2):273–281, doi:10.1177/1932296818757747. (Cited on page 66).

Visentin, R., Man, C.D., and Cobelli, C. (2016). One-Day Bayesian Cloning of Type 1 Diabetes Subjects: Toward a Single-Day UVA/Padova Type 1 Diabetes Simulator. *IEEE Transactions on Biomedical Engineering*, 63(11):2416–2424, doi:10.1109/TBME.2016.2535241. (Cited on page 138).

von Scholten, B.J., Kreiner, F.F., Gough, S.C., and von Herrath, M. (2021). Current and future therapies for type 1 diabetes. *Diabetologia*, 64(5):1037–1048, doi:10.1007/s00125-021-05398-3. (Cited on pages 26, 27 and 28).

Wahren, J., Ekberg, K., Johansson, J., Henriksson, M., Pramanik, A., Johansson, B.L., Rigler, R., and Jörnvall, H. (2000). Role of C-peptide in human physiology. *American Journal of Physiology-Endocrinology and Metabolism*, 278(5):E759–E768, doi:10.1152/ajpendo.2000.278.5.E759. (Cited on page 12).

Walter, E. and Lecourtier, Y. (1982). Global approaches to identifiability testing for linear and nonlinear state space models. *Mathematics and Computers in Simulation*, 24(6):472–482, doi:10.1016/0378-4754(82)90645-0. (Cited on page 176).

Wang, H., Xu, J., Lazarovici, P., Quirion, R., and Zheng, W. (2018). cAMP Response Element-Binding Protein (CREB): A Possible Signaling Molecule Link in the Pathophysiology of Schizophrenia. *Frontiers in Molecular Neuroscience*, 11(August):1–14, doi:10.3389/fnmol.2018.00255. (Cited on page 85).

Ware, J. and Hovorka, R. (2022). Recent advances in closed-loop insulin delivery. *Metabolism*, 127:154953, doi:10.1016/j.metabol.2021.154953. (Cited on page 32).

Weinzimer, S.A., Sherr, J.L., Cengiz, E., Kim, G., Ruiz, J.L., Carria, L., Voskanyan, G., Roy, A., and Tamborlane, W.V. (2012). Effect of pramlintide on prandial glycemic excursions during closed-loop control in adolescents and young adults with type 1 diabetes. *Diabetes Care*, 35(10):1994–1999, doi:10.2337/dc12-0330. (Cited on page 43).

Weisman, A., Bai, J.W., Cardinez, M., Kramer, C.K., and Perkins, B.A. (2017). Effect of artificial pancreas systems on glycaemic control in patients with type 1 diabetes: a systematic review and meta-analysis of outpatient randomised controlled trials. *The Lancet Diabetes and Endocrinology*, 5(7):501–512, doi:10.1016/S2213-8587(17)30167-5. (Cited on pages 30 and 37).

Weissberg-Benchell, J., Hessler, D., Fisher, L., Russell, S.J., and Polonsky, W.H. (2017). Impact of an Automated Bihormonal Delivery System on Psychosocial Outcomes in Adults with Type 1 Diabetes. *Diabetes Technology and Therapeutics*, 19(12):723–729, doi:10.1089/dia.2017.0174. (Cited on page 42).

Wendt, S.L., Ranjan, A., Kloppenborg, J., Knudsen, B., Juul, J., Nørgaard, K., and Bagterp, J. (2017a). Simulating clinical studies of the glucoregulatory system: in vivo meets in silico. Technical report. (Cited on pages 112, 252 and 267).

Wendt, S.L., Ranjan, A., Møller, J.K., Schmidt, S., Knudsen, C.B., Holst, J.J., Madsbad, S., Madsen, H., Nørgaard, K., and Jørgensen, J.B. (2017b). Cross-Validation of a Glucose-Insulin-Glucagon Pharmacodynamics Model for Simulation Using Data From Patients With Type 1 Diabetes. *Journal of diabetes science and technology*, 11(6):1101–1111, doi:10.1177/1932296817693254. (Cited on pages 58, 61, 91, 93, 96, 98, 99, 110, 138 and 267).

Weyer, C., Fineman, M.S., Strobel, S., Shen, L., Data, J., Kolterman, O.G., and Sylvestri, M.F. (2005). Properties of pramlintide and insulin upon mixing. *American Journal of Health-System Pharmacy*, 62(8):816–822, doi:10.1093/ajhp/62.8.816. (Cited on page 26).

Weyer, C., Gottlieb, A., Kim, D.D., Lutz, K., Schwartz, S., Gutierrez, M., Wang, Y., Ruggles, J.A., Kolterman, O.G., and Maggs, D.G. (2003). Pramlintide Reduces Postprandial Glucose Excursions When Added to Regular Insulin or Insulin Lispro in Subjects With Type 1 Diabetes. *Diabetes Care*, 26(11):3074–3079, doi:10.2337/diacare.26.11.3074. (Cited on pages 25 and 180).

Weyer, C., Maggs, D., Young, A., and Kolterman, O. (2001). Amylin Replacement With Pramlintide as an Adjunct to Insulin Therapy in Type 1 and Type 2 Diabetes Mellitus:

A Physiological Approach Toward Improved Metabolic Control. *Current Pharmaceutical Design*, 7(14):1353–1373, doi:10.2174/1381612013397357. (Cited on pages 26, 42, 163, 164 and 180).

Wilinska, M.E., Chassin, L.J., Acerini, C.L., Allen, J.M., Dunger, D.B., and Hovorka, R. (2010). Simulation environment to evaluate closed-loop insulin delivery systems in type 1 diabetes. *Journal of Diabetes Science and Technology*, 4(1):132–144, doi:10.1177/193229681000400117. (Cited on pages 58, 61, 64, 168 and 268).

Wilinska, M.E., Chassin, L.J., Schaller, H.C., Schaupp, L., Pieber, T.R., and Hovorka, R. (2005). Insulin kinetics in type-1 diabetes: Continuous and bolus delivery of rapid acting insulin. *IEEE Transactions on Biomedical Engineering*, 52(1):3–12, doi:10.1109/TBME.2004.839639. (Cited on pages 58, 75, 138, 169 and 177).

Wilinska, M.E. and Hovorka, R. (2014). Simulation Models for In-Silico Evaluation of Closed-Loop Insulin Delivery Systems in Type 1 Diabetes. In *Data-driven Modeling for Diabetes*, pages 131–149. (Cited on page 54).

Wilson, L.M. and Castle, J.R. (2018). Stable Liquid Glucagon: Beyond Emergency Hypoglycemia Rescue. *Journal of Diabetes Science and Technology*, 12(4):847–853, doi:10.1177/1932296818757795. (Cited on page 23).

Wilson, L.M., Jacobs, P.G., and Castle, J.R. (2020a). Role of Glucagon in Automated Insulin Delivery. *Endocrinology and Metabolism Clinics of North America*, 49(1):179–202, doi:10.1016/j.ecl.2019.10.008. (Cited on pages 36, 37 and 41).

Wilson, L.M., Jacobs, P.G., Ramsey, K.L., Resalat, N., Reddy, R., Branigan, D., Leitschuh, J., Gabo, V., Guillot, F., Senf, B., El Youssef, J., Steineck, I.I.K., Tyler, N.S., and Castle, J.R. (2020b). Dual-hormone closed-loop system using a liquid stable glucagon formulation versus insulin-only closed-loop system compared with a predictive low glucose suspend system: An open-label, outpatient, single-center, crossover, randomized controlled trial. *Diabetes Care*, 43(11):2721–2729, doi:10.2337/dc19-2267. (Cited on page 38).

Woerle, H.J., Albrecht, M., Linke, R., Zschau, S., Neumann, C., Nicolaus, M., Gerich, J.E., Göke, B., and Schirra, J. (2008). Impaired hyperglycemia-induced delay in gastric emptying in patients with type 1 diabetes deficient for islet amyloid polypeptide. *Diabetes Care*, 31(12):2325–2331, doi:10.2337/dc07-2446. (Cited on pages 77, 171, 182, 191, 192, 193, 196, 197 and 198).

Woerle, H.J., Meyer, C., Dostou, J.M., Gosmanov, N.R., Islam, N., Popa, E., Wittlin, S.D., Welle, S.L., and Gerich, J.E. (2003). Pathways for glucose disposal after meal ingestion

in humans. *American Journal of Physiology-Endocrinology and Metabolism*, 284(4):E716–E725, doi:10.1152/ajpendo.00365.2002. (Cited on page 10).

Woods, S.C., Lutz, T.A., Geary, N., and Langhans, W. (2006). Pancreatic signals controlling food intake; insulin, glucagon and amylin. *Philosophical Transactions of the Royal Society B: Biological Sciences*, 361(1471):1219–1235, doi:10.1098/rstb.2006.1858. (Cited on pages 12, 15 and 162).

Wu, Z., Lebbar, M., Taleb, N., Legault, L., Messier, V., and Rabasa-Lhoret, R. (2023). Comparing dual-hormone and single-hormone automated insulin delivery systems on nocturnal glucose management among children and adolescents with type 1 diabetes: A pooled analysis. *Diabetes, Obesity and Metabolism*, 25(1):310–313, doi:10.1111/dom.14850. (Cited on page 37).

Xie, J. (2018). Simglucose v0.2.1. (Cited on page 66).

Yang, J., Kalhan, S.C., and Hanson, R.W. (2009). What is the metabolic role of phosphoenolpyruvate carboxykinase? *Journal of Biological Chemistry*, 284(40):27025–27029, doi:10.1074/jbc.R109.040543. (Cited on page 85).

Young, A. (2005). Inhibition of Gastric Emptying. *Advances in Pharmacology*, 52(1):99–121, doi:10.1016/S1054-3589(05)52006-4. (Cited on pages 14, 163, 164 and 198).

Yu, S.S., Lefkowitz, R.J., and Hausdorff, W.P. (1993). β-Adrenergic receptor sequestration. A potential mechanism of receptor resensitization. *Journal of Biological Chemistry*, 268(1):337–341, doi:10.1016/s0021-9258(18)54155-7. (Cited on page 82).

Zeng, B., Jia, H., Gao, L., Yang, Q., Yu, K., and Sun, F. (2022). Dual-hormone artificial pancreas for glucose control in type 1 diabetes: A meta-analysis. *Diabetes, Obesity and Metabolism*, 24(10):1967–1975, doi:10.1111/dom.14781. (Cited on page 38).

Zhou, K. and Isaacs, D. (2022). Closed-Loop Artificial Pancreas Therapy for Type 1 Diabetes. *Current Cardiology Reports*, 24(9):1159–1167, doi:10.1007/s11886-022-01733-1. (Cited on page 32).

Part IV

Appendices

Appendix A

Parameter values

A.1 Preliminary validation

A.2 Validation 1

A.3 Validation 2

Proof-of-concept - Receptors EGP								
Patient	1	2	3	4	5	6	7	8
$k_{on} \cdot 10^{-4}$	0.37	1.16	0.51	0.19	0.10	0.23	0.57	0.23
V_r	64	120	138	85	70	85	200	65
$K_r \cdot 10^{-4}$	184.0	1777.7	812.7	152.4	108.2	190.9	2706.2	146.1
$S_I \cdot 10^{-4}$	170	100	277	100	100	300	484	500
EGP_0	7.0	10.0	10.0	6.0	5.6	10.0	10.0	2.5
$S_{T\text{-}A} \cdot 10^{-4}$	29.98	38.28	45.91	15.62	33.66	45.46	41.44	50.00
$S_{T\text{-}B} \cdot 10^{-4}$	34.98	25.12	31.09	22.71	25.69	17.37	38.94	28.68
$S_{T\text{-}C} \cdot 10^{-4}$	36.75	17.50	50.00	17.67	37.70	39.81	10.00	50.00
$S_{D\text{-}A} \cdot 10^{-4}$	5.99	4.31	1.00	1.00	1.00	2.54	2.93	1.00
$S_{D\text{-}B} \cdot 10^{-4}$	6.00	6.00	2.99	1.85	1.10	6.00	1.71	1.00
$S_{D\text{-}C} \cdot 10^{-4}$	3.20	1.00	5.35	1.04	1.37	3.45	3.10	6.00
$Q_{20\text{-}A}$	1873	1862	2500	933	2500	2500	1804	2348
$Q_{20\text{-}B}$	2500	1190	1655	2500	1286	1231	2500	1311
$Q_{20\text{-}C}$	2285	1188	1517	500	1677	2500	757	1389

Table A.1: Proof-of-concept validation identified parameter values for the Receptors EGP model. S_t, S_d, and Q_{20} were adjusted per visit in the dataset (A, B, C).

Proof-of-concept - DTU EGP								
Patient	1	2	3	4	5	6	7	8
E_{max}	85.26	85.26	100.00	99.18	76.34	100.00	100.00	74.36
C_{E50}	802.0	1000.0	538.3	573.6	696.7	418.0	1000.0	999.7
$S_E \cdot 10^{-4}$	10.0	10.0	152.7	10.0	10.0	270.8	355.5	10.0
$S_{T\text{-}A} \cdot 10^{-4}$	12.95	17.96	43.55	11.11	25.53	42.85	42.58	16.24
$S_{T\text{-}B} \cdot 10^{-4}$	31.20	40.46	34.06	20.07	21.42	18.14	13.40	14.18
$S_{T\text{-}C} \cdot 10^{-4}$	40.84	38.39	50.00	17.95	37.65	35.80	45.33	50.00
$S_{D\text{-}A} \cdot 10^{-4}$	4.01	2.76	1.16	1.09	1.00	2.27	4.29	1.00
$S_{D\text{-}B} \cdot 10^{-4}$	5.89	3.78	2.43	2.20	1.74	6.00	4.08	3.75
$S_{D\text{-}C} \cdot 10^{-4}$	2.94	1.00	6.00	1.49	2.05	4.00	4.62	6.00
$Q_{20\text{-}A}$	1040	1081	2500	654	1940	2500	1987	1035
$Q_{20\text{-}B}$	2378	2024	1771	2268	1103	1437	1304	607
$Q_{20\text{-}C}$	2500	2500	1739	500	1647	2500	2086	1117

Table A.2: Proof-of-concept validation identified parameter values for the DTU EGP model. S_t, S_d, and Q_{20} were adjusted per visit in the dataset (A, B, C).

Patient	1	2	3	4	5	6	7	8
G_{GNG}	6	6	6	6	6	6	6	6
V	160	160	160	160	160	160	160	160
W	54	81	87	73	50	69	72	59
F_{01}	14.2	15.5	12.0	14.2	13.8	12.8	13.1	13.4
$k_{12} \cdot 10^{-4}$	244	397	281	358	285	213	238	289
$k_{a1} \cdot 10^{-4}$	16	18	15	47	15	18	10	37
$k_{a2} \cdot 10^{-4}$	522	548	517	624	495	437	353	518
$k_{a3} \cdot 10^{-4}$	215	327	235	178	231	68	74	154
t_{max}	57.6	40.8	48.5	68.5	57.3	67.9	46.5	55.4
$Cl_{F,I}$	18.9	14.8	17.3	23.7	18.5	17.4	24.6	26.8
$k_1 \cdot 10^{-4}$	420	220	380	350	560	580	350	520
$k_{2\text{-}A}$	0.14	0.10	0.19	0.25	0.26	0.06	0.28	0.09
$k_{2\text{-}B}$	0.14	0.12	0.19	0.25	0.41	0.06	0.28	0.14
$k_{2\text{-}C}$	0.14	0.50	0.17	0.25	0.19	0.07	0.09	0.06
$Cl_{F,C\text{-}A}$	94.0	114.0	200.0	136.0	106.0	159.0	125.0	91.0
$Cl_{F,C\text{-}B}$	94.0	75.6	200.0	136.0	97.8	159.0	125.0	78.0
$Cl_{F,C\text{-}C}$	94.0	90.1	130.6	136.0	84.8	89.5	86.8	68.7

Table A.3: Common parameter values in the preliminary validation and Validation 1. Gray shaded cells highlight parameters taken from Wendt et al. (2017a). Glucagon PK parameters k_2 and $Cl_{F,C}$ were adjusted per visit (A,B,C) if necessary to improve the fit to the plasma glucagon data.

Preliminary validation - Receptors EGP								
Patient	1	2	3	4	5	6	7	8
$k_{on} \cdot 10^{-4}$	0.37	1.16	0.51	0.19	0.10	0.23	0.57	0.23
V_r	63.86	120.45	137.57	85.30	69.96	85.32	200.00	64.72
$K_r \cdot 10^{-4}$	184.0	1777.7	812.7	152.4	108.2	190.9	2706.2	146.1
$S_I \cdot 10^{-4}$	170	100	277	100	100	300	484	500
EGP_0	7.0	10.0	10.0	6.0	5.6	10.0	10.0	2.5
$S_{T\text{-}A} \cdot 10^{-4}$	29.98	38.28	45.91	15.62	33.66	45.46	41.44	50.00
$S_{T\text{-}B} \cdot 10^{-4}$	34.98	25.12	31.09	22.71	25.69	17.37	38.94	28.68
$S_{T\text{-}C} \cdot 10^{-4}$	36.75	17.50	50.00	17.67	37.70	39.81	10.00	50.00
$S_{D\text{-}A} \cdot 10^{-4}$	5.99	4.31	1.00	1.00	1.00	2.54	2.93	1.00
$S_{D\text{-}B} \cdot 10^{-4}$	6.00	6.00	2.99	1.85	1.10	6.00	1.71	1.00
$S_{D\text{-}C} \cdot 10^{-4}$	3.20	1.00	5.35	1.04	1.37	3.45	3.10	6.00
$Q_{20\text{-}A}$	1873	1862	2500	933	2500	2500	1804	2348
$Q_{20\text{-}B}$	2500	1190	1655	2500	1286	1231	2500	1311
$Q_{20\text{-}C}$	2285	1188	1517	500	1677	2500	757	1389

Table A.4: Preliminary validation identified parameter values for the Receptors EGP model. S_t, S_d, and Q_{20} were adjusted per visit in the dataset (A, B, C).

Preliminary validation - DTU EGP								
Patient	1	2	3	4	5	6	7	8
E_{max}	87.63	80.60	100.00	92.04	74.50	100.00	99.98	62.57
C_{E50}	829.9	1000.0	636.2	475.1	540.5	437.9	999.3	592.5
$S_E \cdot 10^{-4}$	10.0	10.0	129.7	10.0	10.0	252.5	312.7	10.3
G_{GNG}	6.74	6.82	7.52	5.20	4.92	6.83	2.88	4.07
$S_{T\text{-}A} \cdot 10^{-4}$	12.80	15.15	38.37	12.35	33.66	43.17	47.84	28.00
$S_{T\text{-}B} \cdot 10^{-4}$	33.59	36.11	28.03	21.83	27.16	19.60	21.40	19.69
$S_{T\text{-}C} \cdot 10^{-4}$	41.45	40.30	50.00	18.07	43.36	36.37	49.21	50.00
$S_{D\text{-}A} \cdot 10^{-4}$	6.00	3.83	1.71	1.00	1.00	2.61	1.94	1.00
$S_{D\text{-}B} \cdot 10^{-4}$	6.00	4.19	3.66	1.99	1.41	6.00	1.02	2.08
$S_{D\text{-}C} \cdot 10^{-4}$	3.53	1.00	6.00	1.41	1.85	4.41	1.83	6.00
$Q_{20\text{-}A}$	1035	965	2197	754	2500	2500	2279	1645
$Q_{20\text{-}B}$	2485	1811	1513	2462	1330	1409	1904	939
$Q_{20\text{-}C}$	2500	2500	1559	500	1902	2500	2314	1268

Table A.5: Preliminary validation identified parameter values for the DTU EGP model. S_t, S_d, and Q_{20} were adjusted per visit in the dataset (A, B, C).

Preliminary validation - McGill EGP								
Patient	1	2	3	4	5	6	7	8
T	0.050	0.061	0.236	0.137	0.038	0.298	0.075	0.037
$K_{Gd} \cdot 10^{-3}$	289.3	1.1	1.3	262.4	9516.1	163.9	1.1	8333.7
$T_{Gd} \cdot 10^{-3}$	146.02	1.10	1.93	706.76	298.01	530.85	1.13	104.44
$S \cdot 10^{-4}$	100.05	100.00	392.87	100.24	100.38	500.00	331.61	100.09
G_{ng}	7.8	7.0	7.1	7.3	8.6	7.6	4.7	6.2
$S_{T\text{-}A} \cdot 10^{-4}$	10.01	10.00	44.45	10.04	10.01	19.62	25.27	47.87
$S_{T\text{-}B} \cdot 10^{-4}$	22.74	29.03	30.84	22.43	16.78	22.19	10.00	12.67
$S_{T\text{-}C} \cdot 10^{-4}$	43.45	41.67	50.00	26.02	49.97	38.97	50.00	50.00
$S_{D\text{-}A} \cdot 10^{-4}$	1.00	2.77	1.40	1.01	1.00	1.73	2.17	1.00
$S_{D\text{-}B} \cdot 10^{-4}$	6.00	4.13	3.20	2.15	3.55	6.00	1.83	1.01
$S_{D\text{-}C} \cdot 10^{-4}$	3.35	1.00	6.00	1.36	2.31	3.66	3.56	6.00
$Q_{20\text{-}A}$	669	688	2500	680	863	1071	1362	2497
$Q_{20\text{-}B}$	1519	1471	1644	2447	850	1486	1173	500
$Q_{20\text{-}C}$	2500	2500	1625	579	1861	2500	2251	1223

Table A.6: Preliminary validation identified parameter values for the McGill EGP model. S_t, S_d, and Q_{20} were adjusted per visit in the dataset (A, B, C).

Preliminary validation - OHSU EGP								
Patient	1	2	3	4	5	6	7	8
$k_{g3} \cdot 10^{-6}$	8.62	3.47	15.41	10.05	5.96	9.63	4.16	10.68
k_d	9.60	37.54	43.11	15.07	6.15	23.37	50.00	20.08
k_c	0.32	1.00	1.00	0.20	0.26	0.68	0.85	0.90
$S_f \cdot 10^{-6}$	1.20	1.08	99.77	5.15	1.06	2.46	99.70	1.43
EGP_0	7.8	7.1	8.7	7.3	8.4	9.8	3.9	7.7
$S_{T\text{-}A} \cdot 10^{-4}$	10.00	10.00	47.25	10.01	10.00	28.66	32.43	10.27
$S_{T\text{-}B} \cdot 10^{-4}$	25.38	34.43	15.74	22.69	16.06	10.00	32.14	12.88
$S_{T\text{-}C} \cdot 10^{-4}$	42.98	41.91	50.00	24.39	50.00	43.71	42.28	50.00
$S_{D\text{-}A} \cdot 10^{-4}$	1.00	3.36	1.48	1.00	1.00	3.42	1.47	1.00
$S_{D\text{-}B} \cdot 10^{-4}$	6.00	4.07	4.60	2.18	3.50	6.00	1.97	4.32
$S_{D\text{-}C} \cdot 10^{-4}$	3.23	1.00	6.00	1.38	2.44	4.48	1.65	6.00
$Q_{20\text{-}A}$	670	703	2500	677	870	1626	1650	823
$Q_{20\text{-}B}$	1745	1700	982	2485	843	804	2500	500
$Q_{20\text{-}C}$	2500	2500	1450	515	1794	2500	2003	932

Table A.7: Preliminary validation identified parameter values for the OHSU EGP model. S_t, S_d, and Q_{20} were adjusted per visit in the dataset (A, B, C).

Validation 1 - Receptors EGP								
Patient	1	2	3	4	5	6	7	8
$k_{on} \cdot 10^{-4}$	0.02	0.53	0.13	0.10	0.01	0.05	0.17	0.01
V_r	135.08	199.77	194.91	80.10	101.32	109.06	199.98	102.86
$K_r \cdot 10^{-4}$	85.7	2190.2	347.6	165.2	28.6	79.0	1036.9	16.2
$S_I \cdot 10^{-4}$	220	204	100	101	103	100	433	634
EGP_0	8.0	9.1	10.0	9.9	6.1	10.0	4.7	3.9

Table A.8: Validation 1 identified parameter values for the Receptors EGP model.

Validation 1 - DTU EGP								
Patient	1	2	3	4	5	6	7	8
E_{max}	99.98	74.73	99.97	79.06	95.71	100.00	88.58	99.98
C_{E50}	899.8	999.1	447.3	735.4	987.4	641.7	1000.0	631.1
$S_E \cdot 10^{-4}$	132.6	10.3	10.2	11.7	29.8	10.0	213.5	88.6
G_{GNG}	5.5	5.8	8.0	7.6	5.0	9.5	2.7	1.0

Table A.9: Validation 1 identified parameter values for the DTU EGP model.

Validation 1 - McGill EGP								
Patient	1	2	3	4	5	6	7	8
T	0.053	0.054	0.201	0.068	0.031	0.173	0.050	0.064
$K_{Gd} \cdot 10^{-3}$	264.8	2.5	6883.7	813.6	6692.0	92.1	6651.7	66.2
$T_{Gd} \cdot 10^{-3}$	192.82	4.66	432.09	365.05	553.75	416.48	2.17	555.98
$S \cdot 10^{-4}$	100.08	100.10	280.01	100.73	108.80	382.17	100.36	100.07
G_{ng}	7.4	6.1	9.1	9.3	6.8	10.0	3.2	4.9

Table A.10: Validation 1 identified parameter values for the McGill EGP model.

Validation 1 - OHSU EGP								
Patient	1	2	3	4	5	6	7	8
$k_{g3} \cdot 10^{-6}$	8.25	9.81	9.93	10.74	9.45	12.32	10.59	13.33
k_d	0.26	1.00	0.34	0.27	0.20	0.32	1.00	0.13
$k_c \cdot 10^{-3}$	1.62	7.46	3.59	1.63	1.14	1.69	14.31	1.46
$S_f \cdot 10^{-6}$	8.16	9.19	68.86	10.49	9.40	99.80	94.07	13.54
EGP_0	7.4	6.1	9.9	9.1	6.8	11.9	3.2	5.0

Table A.11: Validation 1 identified parameter values for the OHSU EGP model.

Validation 1 - common parameters								
Patient	1	2	3	4	5	6	7	8
$S_{T\text{-}A} \cdot 10^{-4}$	11.28	18.89	56.24	1.60	24.57	55.01	46.54	55.32
$S_{T\text{-}B} \cdot 10^{-4}$	28.25	30.46	38.26	7.43	21.87	6.20	41.22	43.23
$S_{T\text{-}C} \cdot 10^{-4}$	49.21	35.89	88.97	1.12	48.45	47.74	42.82	90.09
$S_{D\text{-}A} \cdot 10^{-4}$	1.81	1.52	2.08	0.12	0.10	2.79	1.46	0.63
$S_{D\text{-}B} \cdot 10^{-4}$	5.45	3.16	5.32	2.74	0.96	201.94	1.54	2.60
$S_{D\text{-}C} \cdot 10^{-4}$	3.08	0.28	5.97	3550.33	1.52	4.69	1.23	9.71
$Q_{20\text{-}A}$	860	1038	2990	218	1822	3000	2190	2503
$Q_{20\text{-}B}$	2061	1508	1939	802	1126	3000	3000	2177
$Q_{20\text{-}C}$	2999	2178	2992	121	1979	3000	2042	2999

Table A.12: Validation 1 identified common parameter values from the base model.

Validation 2 - Receptors EGP											
	Patient	1	2	3	4	5	6	7	8	9	10
Method A	$k_{on} \cdot 10^{-4}$	0.01	0.06	0.08	0.08	0.02	0.23	0.04	0.02	0.07	0.04
	V_r	92.65	57.44	57.46	55.02	111.57	55.03	117.81	55.00	55.14	96.87
	$K_r \cdot 10^{-4}$	49.0	105.5	119.3	131.3	120.6	114.0	115.1	13.5	98.1	304.1
	$S_I \cdot 10^{-4}$	80	80	81	81	116	761	592	761	755	80
	EGP_0	8.8	8.6	8.5	10.0	8.4	12.0	12.0	3.1	10.7	12.0
Method B	$k_{on} \cdot 10^{-4}$	0.07	0.23	0.11	0.30	0.07	0.52	0.53	0.10	0.02	0.27
	V_r	45.39	61.72	59.55	60.03	41.86	62.81	217.70	40.06	46.49	111.42
	$K_r \cdot 10^{-4}$	8.1	639.4	147.6	359.4	212.8	491.2	2516.9	68.6	8.3	2031.6
	$S_I \cdot 10^{-4}$	172	50	50	59	70	337	416	277	415	162
	EGP_0	15.0	12.8	12.9	12.2	15.0	15.0	15.0	7.2	12.3	11.4
Method C	$k_{on} \cdot 10^{-4}$	0.01	0.23	0.14	0.29	0.14	0.47	0.54	0.10	0.07	0.29
	$V_{r\text{-}L}$	40.07	67.48	40.05	49.00	40.07	50.96	201.74	63.67	40.12	72.93
	$V_{r\text{-}H}$	69.34	59.85	57.69	55.40	282.67	70.45	264.04	40.05	107.82	65.22
	$K_r \cdot 10^{-4}$	9.2	629.3	116.5	283.2	1468.1	413.6	3014.7	63.9	161.7	1192.1
	$S_I \cdot 10^{-4}$	98	50	131	157	144	170	408	149	50	158
	EGP_0	15.0	12.7	13.5	13.1	15.0	15.0	15.0	8.7	15.0	11.4

Table A.13: Validation 2 identified parameter values for the Receptors EGP model, for the three identification methods used (A,B,C). Subscripts *L* and *H* indicate differentiation of visits L and H, respectively.

		Validation 2 - DTU EGP									
	Patient	1	2	3	4	5	6	7	8	9	10
Method A	E_{max}	77.79	59.82	59.79	59.82	75.36	59.79	98.42	59.78	59.90	59.78
	C_{E50}	1187.4	898.8	428.6	1030.6	1199.6	600.1	1199.9	357.9	1100.1	1199.9
	$S_E \cdot 10^{-4}$	64.3	8.0	256.1	26.0	125.8	255.8	8.0	255.7	18.9	256.0
	G_{GNG}	4.8	8.1	6.6	10.1	6.0	8.8	1.3	0.9	3.6	10.6
Method B	E_{max}	149.72	37.37	62.26	40.60	37.52	37.36	37.36	39.07	67.67	40.24
	C_{E50}	223.7	517.5	457.0	380.9	361.5	323.8	403.7	223.8	224.4	1485.9
	$S_E \cdot 10^{-4}$	137.6	186.2	289.7	12.8	310.7	6.3	320.3	320.1	312.6	10.6
	G_{GNG}	7.6	11.9	12.1	12.0	12.8	11.0	4.8	5.1	6.9	10.3
Method C	$E_{max\text{-}L}$	76.57	39.09	45.17	37.52	37.37	37.36	37.39	62.41	38.09	39.78
	$E_{max\text{-}H}$	149.14	37.39	55.77	40.52	119.75	47.58	40.18	44.19	91.29	40.44
	C_{E50}	223.7	438.6	223.9	267.9	1499.6	236.0	559.6	223.7	445.7	1495.8
	$S_E \cdot 10^{-4}$	139.0	242.9	283.1	209.4	320.3	320.3	319.5	320.0	306.4	7.4
	G_{GNG}	5.6	11.7	10.8	11.2	11.6	13.3	5.2	7.4	14.1	10.3

Table A.14: Validation 2 identified parameter values for the DTU EGP model, for the three identification methods used (A,B,C). Subscripts *L* and *H* indicate differentiation of visits L and H, respectively.

Validation 2 - McGill EGP											
	Patient	1	2	3	4	5	6	7	8	9	10
Method A	T	0.040	0.032	0.024	0.024	0.033	0.024	0.032	0.027	0.025	0.024
	$K_{Gd} \cdot 10^{-3}$	24.5	21.6	321.7	33.5	17.9	6362.8	70.2	41.5	80.2	6.5
	$T_{Gd} \cdot 10^{-3}$	651.13	241.07	106.83	179.12	279.86	88.09	235.38	529.98	212.76	665.11
	$S \cdot 10^{-4}$	81.78	256.38	288.93	337.79	80.09	213.98	80.08	80.31	136.52	371.46
	G_{ng}	6.0	10.3	12.0	12.0	7.2	12.0	5.9	5.9	5.7	12.0
Method B	T	0.255	0.017	0.048	0.026	0.015	0.017	0.016	0.022	0.042	0.015
	$K_{Gd} \cdot 10^{-3}$	216.6	2.1	57.4	6.2	219.5	1.7	1.8	12.2	40.4	1.6
	$T_{Gd} \cdot 10^{-3}$	832.89	3.38	155.15	11.15	103.21	3.05	2.14	817.93	821.70	797.83
	$S \cdot 10^{-4}$	159.63	259.05	573.15	565.58	51.62	50.08	50.06	50.45	52.32	446.41
	G_{ng}	11.3	12.5	14.4	14.0	13.4	12.0	5.9	6.0	9.3	10.4
Method C	T_L	0.110	0.021	0.040	0.027	0.015	0.025	0.015	0.037	0.042	0.015
	T_H	0.302	0.020	0.048	0.024	0.161	0.051	0.025	0.039	0.100	0.025
	$K_{Gd} \cdot 10^{-3}$	197.5	3.0	8.4	6.2	780.8	1.8	1.6	19.8	51.4	1.5
	$T_{Gd} \cdot 10^{-3}$	830.84	7.17	815.09	10.34	46.49	3.99	778.01	681.67	809.78	826.96
	$S \cdot 10^{-4}$	163.02	303.49	572.79	548.57	453.22	573.13	171.97	291.07	567.76	572.80
	G_{ng}	9.1	12.5	15.0	14.1	11.9	14.8	5.9	8.3	15.0	10.3

Table A.15: Validation 2 identified parameter values for the McGill EGP model, for the three identification methods used (A,B,C). Subscripts L and H indicate differentiation of visits L and H, respectively.

		Validation 2 - OHSU EGP									
	Patient	1	2	3	4	5	6	7	8	9	10
Method A	$k_{g3} \cdot 10^{-6}$	10.12	10.27	10.30	10.01	10.58	10.31	10.34	10.29	10.22	10.16
	k_d	0.31	0.50	0.67	0.73	0.57	0.56	0.20	0.23	0.25	0.68
	$k_c \cdot 10^{-3}$	1.03	0.96	0.91	0.91	2.13	0.91	0.91	0.91	0.92	0.91
	$S_f \cdot 10^{-6}$	82.12	118.09	37.98	42.01	31.16	20.22	22.33	12.74	29.16	20.47
	EGP_0	6.1	10.1	11.9	12.2	7.2	12.0	5.9	5.5	5.5	12.0
Method B	$k_{g3} \cdot 10^{-6}$	9.65	9.11	9.08	9.08	9.07	9.35	9.17	9.07	8.96	9.12
	k_d	0.22	1.50	0.49	1.44	0.63	1.50	1.50	0.26	0.15	1.47
	$k_c \cdot 10^{-3}$	0.57	1.30	0.57	1.25	0.61	2.09	3.82	0.68	0.57	1.42
	$S_f \cdot 10^{-6}$	148.62	148.66	147.33	53.18	135.89	147.10	148.90	23.48	29.28	135.15
	EGP_0	11.9	12.5	14.8	14.0	13.5	12.0	5.9	6.1	9.4	10.4
Method C	$k_{g3} \cdot 10^{-6}$	9.32	9.08	9.08	9.08	9.17	9.14	9.09	9.09	8.75	9.10
	k_d	0.18	1.49	1.10	1.44	0.48	1.50	1.48	0.27	0.39	1.49
	$k_c \cdot 10^{-3}$	0.57	1.31	1.08	1.21	0.57	1.50	3.45	0.71	0.58	1.41
	$S_f \cdot 10^{-6}$	148.13	91.62	142.96	27.52	149.04	140.06	128.77	41.39	17.19	146.47
	$EGP_{0\text{-}L}$	9.8	12.9	15.5	14.5	11.4	14.8	5.7	9.0	14.4	10.4
	$EGP_{0\text{-}H}$	9.2	12.4	15.3	14.1	12.6	14.8	6.2	8.3	16.6	10.4

Table A.16: Validation 2 identified parameter values for the OHSU EGP model, for the three identification methods used (A,B,C). Subscripts *L* and *H* indicate differentiation of visits L and H, respectively.

	Validation 2 common parameters									
	Patient	1	2	3	4	5	6	7	8	9	10
Method A	F_{01}	14.5	15.3	9.6	9.6	9.6	17.5	9.6	9.7	10.2	9.6
	$k_{12} \cdot 10^{-4}$	473	170	170	183	409	170	262	240	171	171
	$k_{a1} \cdot 10^{-4}$	8	20	8	56	10	8	54	18	8	20
	$k_{a2} \cdot 10^{-4}$	679	748	287	748	282	283	389	747	299	283
	$k_{a3} \cdot 10^{-4}$	386	54	54	54	94	54	67	54	81	54
	$S_{T\text{-}L} \cdot 10^{-4}$	13.74	39.41	77.36	50.20	108.10	108.09	108.10	108.08	75.45	108.05
	$S_{T\text{-}H} \cdot 10^{-4}$	0.92	34.34	47.84	44.74	9.01	102.31	63.63	47.74	0.93	9.79
	$S_{D\text{-}L} \cdot 10^{-4}$	1.02	2.66	6.44	12.86	4.61	0.51	2.50	0.09	0.32	6.17
	$S_{D\text{-}H} \cdot 10^{-4}$	4.85	0.08	1.46	3.17	29.58	0.31	1.12	0.98	0.24	4199.38
Method B	F_{01}	6.0	12.6	6.0	14.1	6.0	6.0	6.0	10.2	6.0	6.1
	$k_{12} \cdot 10^{-4}$	595	595	341	595	595	344	595	107	107	595
	$k_{a1} \cdot 10^{-4}$	70	70	9	70	70	37	63	24	70	65
	$k_{a2} \cdot 10^{-4}$	435	718	392	933	214	229	715	177	929	177
	$k_{a3} \cdot 10^{-4}$	213	34	34	35	232	215	490	36	144	71
	$S_{T\text{-}L} \cdot 10^{-4}$	135.11	18.43	135.09	58.43	24.50	68.71	76.17	18.81	135.09	44.33
	$S_{T\text{-}H} \cdot 10^{-4}$	10.94	2.53	32.22	4.29	20.75	37.03	12.56	7.86	21.97	12.40
	$S_{D\text{-}L} \cdot 10^{-4}$	1.45	24.79	11.36	20.93	30.48	11.61	4.64	4.74	0.57	56.16
	$S_{D\text{-}H} \cdot 10^{-4}$	5.68	168.46	31.27	4421.85	22.79	36.73	18.69	3.40	9.41	360.93
Method C	F_{01}	6.0	12.4	6.0	14.1	6.0	6.0	6.0	13.5	6.0	6.6
	$k_{12} \cdot 10^{-4}$	595	592	595	595	595	595	595	595	595	595
	$k_{a1} \cdot 10^{-4}$	70	66	30	70	70	44	70	19	27	67
	$k_{a2} \cdot 10^{-4}$	444	501	936	933	241	177	922	177	518	187
	$k_{a3} \cdot 10^{-4}$	221	34	34	35	110	47	489	34	34	69
	$S_{T\text{-}L} \cdot 10^{-4}$	44.00	21.45	33.79	54.70	20.37	49.88	57.27	109.40	15.24	41.60
	$S_{T\text{-}H} \cdot 10^{-4}$	9.94	2.74	26.13	4.36	23.25	71.05	14.75	34.12	71.92	11.24
	$S_{D\text{-}L} \cdot 10^{-4}$	2.26	22.67	139.18	22.68	31.14	39.98	5.30	7.37	5237.60	56.29
	$S_{D\text{-}H} \cdot 10^{-4}$	5.26	133.39	70.94	4738.53	17.15	34.09	15.62	2.84	22.79	466.17

Table A.17: Validation 2 identified common parameter values from the base model.

Validation 2 PK parameters										
Patient	1	2	3	4	5	6	7	8	9	10
V	160	160	160	160	160	160	160	160	160	160
W	75	75	75	75	75	75	75	75	75	75
t_{max}	102.8	75.3	90.5	54.7	53.1	91.7	75.3	69.9	64.8	56.3
$Cl_{F,I}$	4.7	15.9	6.3	25.4	21.0	12.4	20.7	15.9	20.1	29.5
$k_1 \cdot 10^{-4}$	638	352	638	638	283	531	387	423	596	341
$k_{2L\text{-}100}$	0.11	0.14	0.11	0.05	**0.15**	0.15	0.47	0.12	0.05	0.37
$k_{2L\text{-}500}$	0.09	0.06	0.05	0.09	**0.15**	0.06	0.14	0.13	0.03	0.30
$k_{2H\text{-}100}$	0.34	0.55	0.16	0.15	**0.05**	**0.05**	0.14	0.36	0.05	**0.05**
$k_{2H\text{-}500}$	0.10	0.08	0.06	0.07	**0.05**	**0.05**	0.04	0.14	0.21	**0.05**
$Cl_{F,C\,L\text{-}100}$	99.6	79.0	**56.7**	138.0	104.0	96.1	103.0	81.0	64.5	89.3
$Cl_{F,C\,L\text{-}500}$	79.7	47.4	**56.7**	69.0	67.6	57.6	41.2	36.4	64.5	53.6
$Cl_{F,C\,H\text{-}100}$	99.6	79.0	56.7	138.0	104.0	96.1	103.0	81.0	64.5	89.3
$Cl_{F,C\,H\text{-}500}$	74.7	47.4	39.7	48.3	67.6	76.9	61.8	64.8	83.8	98.2

Table A.18: Validation 2 PK identified parameter values. Shaded cells highlight fixed values.

Appendix B

T1D models

This chapter provides a description of the states and parameters of the selection of models reviewed in Chapter 3. Tables have sections corresponding to each subsystem in the model. Values in blue represent inputs to the system. A collection of tables at the end of the document accompanies this chapter, where the complete equations for each model are reported. The models included in this chapter are:

B.1 Receptors proposal

	Magnitude	Units	Description
Insulin subsystem	u_I	U/min	Insulin infusion (as a deviation from basal)
	$X_1(t)$	U	Insulin mass due to exogenous dosing in subcutaneous tissue
	$X_2(t)$	U	Insulin mass due to exogenous dosing in plasma
	$I(t)$	mU/l	Insulin plasma concentration
	t_{max}	min	Time from dose to maximum plasma concentration
	W	kg	Weight
	$Cl_{F,I}$	ml/kg/min	Apparent insulin clearance
	I_b	mU/l	Basal insulin concentration
Glucagon subsystem	u_C	pg/min	Glucagon infusion (as a deviation from basal)
	$Z_1(t)$	pg	Glucagon mass due to exogenous dosing in subcutaneous tissue
	$Z_2(t)$	pg	Glucagon mass due to exogenous dosing in plasma
	$C(t)$	pg/ml	Glucagon concentration in plasma
	k_1, k_2	min^{-1}	Absorption elimination rate constants
	$Cl_{F,C}$	ml/kg/min	Apparent glucagon clearance
	C_b	pg/ml	Basal glucagon concentration
Glucose subsystem	$x_1(t)$	mU/l	Effect of insulin on glucose distribution
	$x_2(t)$	mU/l	Effect of insulin on glucose disposal
	$x_3(t)$	mU/l	Effect of insulin on EGP
	$EGP(t)$	μmol/kg/min	Endogenous glucose production
	$Q_1(t)$	μmol/kg	Glucose mass in the accessible compartment
	$Q_2(t)$	μmol/kg	Glucose mass in the non-accessible compartment
	$G(t)$	mmol/l	Blood glucose
	k_{a1}, k_{a2}, k_{a3}	min^{-1}	Deactivation rate constants
	F_{01}	μmol/kg/min	Insulin-independent glucose flux
	F_R	μmol/kg/min	Renal glucose clearance
	S_T	min^{-1}/(mU/l)	Insulin sensitivity to glucose transport
	S_D	min^{-1}/(mU/l)	Insulin sensitivity to glucose disposal
	k_{12}	min^{-1}	Transfer rate constant from the nonaccessible to the accessible compartment
	V	ml/kg	Glucose distribution volume

Continued in next page

Continued from previous page

	Magnitude	Units	Description
EGP subsystem	$r(t), r_C(t)$	unitless	Normalized amount of free and bonded receptors
	$F_{hgp}(t)$	μmol/kg/min	Hepatic glucose production
	k_{off}	min^{-1}	Dissociation rate
	k_{rec}	min^{-1}	Recycling rate
	k_{in}	min^{-1}	Internalization rate of the glucagon-bonded receptor
	k_{on}	$(\text{pg/min})^{-1}$	Association rate of glucagon to the receptor
	V_h	ml	Volume of the hepatic interstitial space
	K_r	unitless	Apparent dissociation constant
	V_r	μmol/kg/min	Maximal glucagon-dependent hepatic glucose production rate
	EGP_0	μmol/kg/min	EGP extrapolated to zero insulin concentration
	S_I	$(\text{mU/l})^{-1}$	Hepatic insulin sensitivity

References: Furió-Novejarque et al. (2023b,a)

Table B.1: Units and description of the states and parameters in the PK/PD model proposal.

B.2 Wendt model

This model uses the same equations for the insulin subsystem, glucagon subsystem and glucose subsystem as the receptors proposal, hence, only the EGP subsystem is added here.

	Magnitude	Units	Description
EGP	$G_{gg}(t)$	μmol/kg/min	Glucose production due to glycogenolysis
	S_E	l/mU	Insulin sensitivity on glycogenolysis
	E_{max}	μmol/kg/min	Maximum EGP at basal insulin concentration
	G_{GNG}	μmol/kg/min	Glucose production due to gluconeogenesis
	C_{E50}	pg/ml	Glucagon concentration yielding half of maximum EGP

References: Wendt et al. (2017b,a)

Table B.2: Units and description of the states and parameters in the DTU model.

B.3 Hovorka model

	Magnitude	Units	Description
Insulin subsystem	u_I	U/h	Insulin administration (bolus and infusion)
	$S_1(t)$	U	Absorption of subcutaneously administered insulin
	$S_2(t)$	U	Absorption of subcutaneously administered insulin
	$I(t)$	mU/l	Plasma insulin concentration
	$t_{max,I}$	min	Time-to-maximum insulin absorption
	V_I	l/kg	Insulin distribution volume
	k_e	min^{-1}	Insulin elimination from plasma
Glucose subsystem	$Q_1(t)$	mmol/kg	Mass of glucose in the accessible compartment
	$Q_2(t)$	mmol/kg	Mass of glucose in the non-accessible compartment
	$G(t)$	mmol/l	Glucose concentration
	$x_1(t)$	mU/l	Remote effects of insulin on glucose distribution/transport
	$x_2(t)$	mU/l	Remote effects of insulin on glucose disposal
	$x_3(t)$	mU/l	Remote effects of insulin on EGP
	F_{01}^c	mmol/kg/min	Non-insulin-dependent glucose flux
	F_R	mmol/kg/min	Renal glucose clearance
	k_{12}	min^{-1}	Transfer rate (non-accessible to accessible compartment)
	EGP_0	mmol/kg/min	EGP extrapolated to the zero insulin concentration
	k_{a1}, k_{a2}, k_{a3}	min^{-1}	Deactivation rate constants
	S_{IT}	min^{-1} per mU/l	Insulin sensitivity of distribution/transport
	S_{ID}	min^{-1} per mU/l	Insulin sensitivity of disposal
	S_{IE}	min^{-1} per mU/l	Insulin sensitivity of EGP
	k_{b1}, k_{b2}, k_{b3}	min^{-2} per mU/l	Activation rate constant
	V_G	l/kg	Distribution volume of the accessible compartment
Meal subs.	D_G	g	Amount of carbohydrates
	U_G	mmol/l	Gut absorption rate
	A_G	unitless	Carbohydrate availability
	Bio	%	Bioavailability of CHO
	$t_{max,G}$	min	Time-of-maximum glucose R_a in the accessible comp.

References: Hovorka et al. (2002, 2004); Wilinska et al. (2010)

Table B.3: Units and description of the states and parameters in the Hovorka model.

B.4 Jacobs model

	Magnitude	Units	Description
Insulin subsystem	u_I	mU/kg/min	Insulin infusion rate
	$S_1(t)$	mU/kg	Insulin mass in compartment 1
	$S_2(t)$	mU/kg	Insulin mass in compartment 2
	$I(t)$	mU/l	Plasma insulin concentration
	t_{max}	min	Time-to-maximum absorption
	V_I	l/kg	Distribution volume
	k_e	min^{-1}	Insulin elimination rate
Glucagon subsystem	u_g	mg/kg/min	Glucagon basal rate
	$X_{1g}(t)$	mg/kg	Glucagon mass compartment 1
	$X_{2g}(t)$	mg/kg	Glucagon mass compartment 2
	$X_{3g}(t)$	mg/kg	Plasma glucagon mass
	$Y(t)$	unitless	Effect of glucagon on EGP
	$Z(t)$	unitless	Derivative of $Y(t)$
	k_{1g}	min^{-1}	Constant transfer rate
	k_{ge1}	min^{-1}	Elimination rate from the inaccessible compartment
	k_{2g}	min^{-1}	Constant transfer rate
	k_{ge2}	min^{-1}	Elimination rate from the accessible compartment
	k_c	min^{-1}	Clearance rate of glucagon from the remote compartment
	k_g	$(\text{ng/l})^{-1}\text{min}^{-1}$	Constant $k_g = \frac{10^6 k_c S_{fGG}}{V_{dGG}}$
	S_{fGG}	$(\text{ng/l})^{-1}\text{min}^{-1}$	Glucagon sensitivity factor
	V_{dGG}	l/kg	Glucagon volume of distribution
Meal subs.	D_G	mmol/kg	Carbohydrate intake
	U_G	mmol/kg/min	Glucose absorption rate from meals
	t_0	min	Meal announcement time
	A_G	unitless	Carbohydrate bioavailability
	$t_{max,G}$	min	Time-to-maximum appearance rate of glucose in Q_1
EGP	k_{g3}	unitless	Contribution of $Z(t)$ to glucagon action
	EGP_0	mmol/kg/min	Basal EGP at a theoretical zero insulin concentration
	$Q_1(t)$	mmol/kg	Mass of glucose in the accessible (plasma) comp.
	$Q_2(t)$	mmol/kg	Mass of glucose in the non-accessible (interstitial) comp.

Continued in next page

Continued from previous page

	Magnitude	Units	Description
Glucose subsystem	$X_1(t)$	min^{-1}	Effects of insulin on glucose distribution
	$X_2(t)$	min^{-1}	Effects of insulin on glucose disposal
	$X_3(t)$	-	Effects of insulin on suppression of EGP
	F_{01}^c	mmol/kg/min	Non-insulin mediated glucose flux
	F_R	mmol/kg/min	Renal glucose clearance
	k_{a1}, k_{a2}, k_{a3}	min^{-1}	Appearance and elimination rates
	S_{f1}, S_{f2}, S_{f3}	min^{-1} per mU/l	Insulin sensitivity factors
	k_{12}	min^{-1}	Transfer rate (non-accessible to accessible compartment)
Exercise subsystem	PVO_2^{max}	%	Percentage of maximum oxygen consumption during exercise
	PAMM	%	Percentage of active muscle mass
	Γ_{PGUA}	mg/min	Glucose uptake from active tissues
	Γ_{HGPA}	mg/min	Glucose production from active tissues (identical value to Γ_{PGUA})
	$\Gamma_{\overline{PGUA}}$	mg/min	Peripheral glucose uptake from active tissues
	M_{HGP}	%	Percentage increment with respect to the basal hepatic glucose production
	M_{PIU}	%	Increment of peripheral insulin uptake
	M_{PGU}	%	Percentage increment with respect to the basal peripheral glucose uptake
	$S_{fi\text{-}EX}$	min^{-1} per mU/l	Exercise insulin sensitivity factors ($i \in 1, 2, 3$)
	$PAMM$	%	Percentage of active muscular mass

References: Resalat et al. (2019); Jacobs et al. (2015)

Table B.4: Units and description of the states and parameters in the Jacobs model.

B.5 Dalla Man Model

	Magnitude	Units	Description
Insulin subsystem	IRR	pmol/kg/min	Insulin infusion rate
	$I_{sc1}(t)$	pmol/kg	Insulin mass in the first subcutaneous compartment
	$I_{sc2}(t)$	pmol/kg	Insulin mass in the second subcutaneous compartment
	$R_{ai}(t)$	pmol/kg/min	Insulin rate of appearance
	$I_p(t)$	pmol/kg	Insulin mass in plasma
	$I_l(t)$	pmol/kg	Insulin mass in liver
	$I(t)$	pmol/l	Plasma insulin concentration
	k_d	min^{-1}	Rate parameter
	k_{a1}	min^{-1}	Rate parameter
	k_{a2}	min^{-1}	Rate parameter
	m_1	min^{-1}	Rate parameter
	m_2	min^{-1}	Rate parameter
	m_3	min^{-1}	Rate parameter
	m_4	min^{-1}	Rate parameter
	V_I	l/kg	Insulin distribution volume
Glucagon subsystem	H_{inf}	pg/ml/min	Glucagon infusion rate
	$H_{sc1}(t)$	pg/ml	Glucagon concentration in the subcutaneous space
	$H_{sc2}(t)$	pg/ml	Glucagon concentration in the subcutaneous space
	$Ra_H(t)$	pg/ml/min	Subcutaneous glucagon rate of appearance
	$H(t)$	pg/ml	Plasma glucagon concentration
	$SR_H(t)$	pg/ml/min	Glucagon secretion
	$SR^s_H(t)$	pg/ml/min	First component contributing to glucagon secretion
	$SR^d_H(t)$	pg/ml/min	Second component contributing to glucagon secretion
	SR^b_H	pg/ml/min	Glucagon secretion basal value
	n	min^{-1}	Clearance rate
	σ		Alpha-cell responsivity to glucose level
	σ_2		Alpha-cell responsivity to glucose level
	$1/\rho$		Delay between static glucagon secretion and plasma glucose
	δ		Alpha-cell response to glucose rate of change
	k_{h1}	min^{-1}	Parameter describing subcutaneous glucagon kinetics

Continued in next page

Continued from previous page

	Magnitude	Units	Description
	k_{h2}	min^{-1}	Parameter describing subcutaneous glucagon kinetics
	k_{h3}	min^{-1}	Parameter describing subcutaneous glucagon kinetics
EGP subsystem	$X_H(t)$	pg/ml	Delayed glucagon action on EGP
	$I'(t)$	pmol/l	
	$X_L(t)$	pmol/l	Delayed insulin action in the liver
	k_H	min^{-1}	Delay between glucagon concentration and action
	H_b	pg/ml	Steady state plasma glucagon concentration
	k_i	min^{-1}	Rate parameter
	k_{p1}	mg/kg/min	Extrapolated EGP at zero glucose and insulin
	k_{p2}	min^{-1}	Liver glucose effectiveness
	k_{p3}	mg/kg/min per pmol/l	Parameter governing amplitude of insulin action on the liver
	ξ	mg/kg/min per pg/ml	Liver responsivity to glucagon
Meals subsystem	D	mg	Amount of ingested glucose
	$Q_{sto1}(t)$	mg	Solid phase of glucose in the stomach
	$Q_{sto2}(t)$	mg	Liquid phase of glucose in the stomach
	$Q_{sto}(t)$	mg	Amount of glucose in the stomach
	$Q_{gut}(t)$	mg	Glucose mass in the intestine
	$Ra(t)$	mg/kg/min	Glucose rate of appearance in plasma
	k_{gri}	min^{-1}	Grinding rate
	k_{empt}	min^{-1}	Rate constant of gastric emptying
	k_{abs}	min^{-1}	Rate constant of intestinal absorption
	k_{min}	min^{-1}	k_{empt} maximum value
	k_{max}	min^{-1}	k_{empt} minimum value
	α	unitless	k_{empt} decrease rate $\left(\alpha = \frac{5}{2 \cdot D \cdot (1-b)}\right)$
	b	%	Percentage of the dose for which k_{empt} decreases at $(k_{max} - k_{min})/2$
	β	unitless	k_{empt} increase/recovery rate $\left(\beta = \frac{5}{2 \cdot D \cdot c}\right)$
	c	%	Percentage of the dose for which k_{empt} is back to $(k_{max} - k_{min})/2$
	f	unitless	Fraction of intestinal absorption which actually appears in plasma
	BW	kg	Body weight

Continued in next page

Continued from previous page

	Magnitude	Units	Description
Glucose subsystem	$G_p(t)$	mg/kg	Plasma glucose mass
	$G_t(t)$	mg/kg	Glucose mass in tissue
	$G(t)$	mg/dl	Plasma glucose concentration
	$risk(t)$	unitless	Risk function
	$E(t)$	mg/kg/min	Renal excretion
	$U_{id}(t)$	mg/kg/min	Insulin-dependent utilization
	$X(t)$	pmol/l	Insulin action on glucose utilization
	U_{ii}	mg/kg/min	Insulin-independent utilization (glucose uptake by the brain and erythrocytes)
	k_{e1}	min^{-1}	Glomerular filtration rate
	k_{e2}	mg/kg	Renal threshold of glucose
	k_1	min^{-1}	Rate parameter
	k_2	min^{-1}	Rate parameter
	V_G	dl/kg	Glucose distribution volume
	V_{m0}	mg/kg/min	Rate parameter
	V_{mx}	mg/kg/min	Rate parameter quantifying peripheral insulin action
	r_1	l/pmol	Model parameter
	r_2	unitless	Model parameter
	K_{m0}	mg/kg	Rate parameter
	p_{2U}	min^{-1}	Rate constant of insulin action on the peripheral glucose utilization
	G_{th}	mg/dl	Hypoglycemic threshold (set at 60 mg/dl)
	I_b	pmol/l	Basal insulin

References: Dalla Man et al. (2006, 2007, 2014)

Table B.5: Units and description of the states and parameters in the Dalla Man model.

B.6 Haidar model

	Magnitude	Units	Description
Insulin subsystem	u_I	U/min	Insulin infusion rate
	$Q_{is1}(t)$	U	Insulin mass in the 1^{st} slow compartment
	$Q_{is2}(t)$	U	Insulin mass in the 2^{nd} slow compartment
	$Q_{if1}(t)$	U	Insulin mass in the 1^{st} fast compartment
	$Q_{if2}(t)$	U	Insulin mass in the 2^{nd} fast compartment
	$Q_i(t)$	U	Insulin mass in plasma
	$I(t)$	mU/l	Plasma insulin concentration
	p_i	unitless	Portion of subcutaneous insulin absorbed through the slow channel
	k_{is1}, k_{is2}	min^{-1}	Transfer rates
	k_{if}	min^{-1}	Transfer rate
	k_e	min^{-1}	Fractional clearance rate
	c_i	U/min	Background insulin appearance
	$I_m(t)$	unitless	Piecewise function describing time-varying components of insulin kinetics (30-min segments)
	V_i	ml/kg	Insulin distribution volume
	w	kg	Weight
Glucagon subsystem	$u_g(t)$	unit/min	Glucagon infusion
	$Q_{g1}(t)$	unit	Glucagon mass in the first subcutaneous compartment
	$Q_{g2}(t)$	unit	Glucagon mass in the second subcutaneous compartment
	$C_p(t)$	mU/l	Glucagon concentration in plasma
	$t_{g_{max}}$	min	Time-to-peak plasma glucagon concentration
	MCR_g	ml/kg/min	Metabolic clearance rate
	C_b	mU/l	Basal glucagon concentration
EGP	S_g		Glucagon sensitivity
	S_e	10^{-4} per mU/l	Insulin sensitivity of EGP
	$Q_1(t)$	μmol/kg	Mass of glucose in the accessible compartment
	$Q_2(t)$	μmol/kg	Mass of glucose in the non-accessible compartment
	$G(t)$	mmol/l	Glucose concentration

Continued in next page

Continued from previous page

	Magnitude	Units	Description
Glucose subsystem	$G_s(t)$	mmol/l	Interstitial glucose concentration
	$x_1(t)$	min^{-1}	Delayed effects of insulin on glucose distribution
	$x_2(t)$	min^{-1}	Delayed effects of insulin on glucose disposal
	$x_3(t)$	min^{-1}	Delayed effects of insulin on EGP
	F_{01}^c	μmmol/kg/min	Non-insulin-dependent glucose utilization
	$F_g(t)$	unitless	Piecewise function for glucose's time-varying characteristics (15-min segments)
	k_{12}	min^{-1}	Transfer rate (non-accessible to accessible compartment)
	S_t	$10^4 \times$ /min per mU/l	Insulin sensitivity on glucose distribution
	S_d	$10^4 \times$ /min per mU/l	Insulin sensitivity on glucose disposal
	k_{a1}, k_{a2}, k_{a3}	min^{-1}	Time constants
	V	l/kg	Glucose distribution volume
	k_s	l/min	Time constant
Meal subsystem	CHO	g	Amount of carbohydrates
	$U_{m1}(t)$	μmol/kg/min	Glucose appearance in the 1^{st} absorption channel
	$U_{m2}(t)$	μmol/kg/min	Glucose appearance in the 2^{nd} absorption channel
	$U_m(t)$	μmol/kg/min	Total glucose appearance
	k_m	min^{-1}	Transfer rate parameter
	d	min	Delay associated with the second absorption channel
	$f_m(t)$	unitless	Piecewise function for variability on absorption profiles (15-min segments)
	p_m	unitless	Portion of the meal absorbed through the 1^{st} channel

References: Haidar et al. (2013c,a); Smaoui et al. (2020a)

Table B.6: Units and description of the states and parameters in the Haidar model.

B.7 Bergman - Minimal model

	Magnitude	Units	Description
Insulin subsystem	u_I	U/h	Insulin administration
	$I(t)$	μU/ml	Plasma insulin
	$X(t)$	μU/ml	Interstitial comparment
	p_2	min^{-1}	Output rate of the remote insulin compartment (k_3)
	p_3	min^{-1}	Input rate to the $X(t)$ compartment ($k_2(k_4 + k_6)$)
	S_I	min^{-1}/μU per ml	Insulin sensitivity, equal to - p_3/p_2
	h	mg/dl	Glucose threshold
	n	min^{-1}	Time constant for insulin disappearance
Glucose	$G(t)$	mg/dl	Plasma glucose
	p_1	min^{-1}	Output rates from the G(t) compartments ($-(k_1 + k_5)$)
	G_b	mg/dl	Basal glucose
	γ	unitless	Increase proportion by which glucose exceeds h

References: Bergman et al. (1979, 1981)

Table B.7: Units and description of the states and parameters in the Bergman model.

B.8 Herrero model

	Magnitude	Units	Description
Insulin subsystem	u	μU/kg	Subcutaneous insulin infusion
	$S_1(t)$	μU	First compartment of subcutaneous insulin absorption
	$S_2(t)$	μU	Second compartment of subcutaneous insulin absorption
	$I(t)$	μU/ml	Plasma insulin concentration
	V_I	ml/kg	Distribution volume of plasma insulin
	t_{maxI}	min	Time-to-maximum insulin absorption
	k_e	min^{-1}	First-order decay rate for insulin in plasma
	I_b	μU/ml	Basal insulin concentration
	w	ng/kg	Subcutaneous glucagon infusion
	$Z_1(t)$	ng	First compartment of subcutaneous glucagon absorption

Continued in next page

Continued from previous page

	Magnitude	Units	Description
Glucagon subs.	$Z_2(t)$	ng	Second compartment of subcutaneous glucagon absorption
	$N(t)$	pg/ml	Plasma glucagon concentration
	V_N	ml/kg	Distribution volume of plasma glucagon
	t_{maxN}	min	Time-to-maximum glucagon absorption
	k_N	min^{-1}	First-order decay rate for glucagon in plasma
	N_b	pg/ml	Basal glucagon concentration
EGP	$Y(t)$	min^{-1}	Glucagon action on glucose production
	p_3	min^{-1}	Rate constant describing dynamics of glucagon action
	S_N	min^{-1} per pg/ml	Glucagon sensitivity
Glucose subs.	$G(t)$	mg/dl	Plasma glucose
	$X(t)$	min^{-1}	Insulin action on glucose production and disposal
	S_G	min^{-1}	Fractional glucose effectiveness
	p_2	min^{-1}	Rate constant describing dynamics of insulin action
	S_I	min^{-1} per μU/ml	Insulin sensitivity
	V	dl/kg	Glucose distribution volume
Meal subs.	D_G	mg	Amount of carbohydrates
	$F(t)$	mg/min/kg	Glucose appearance in the first compartment
	$R_A(t)$	mg/min/kg	Rate of glucose appearance
	A_G	unitless	Carbohydrate bioavailability
	τ_m	min	Peak time of meal glucose appearance, different for each meal

References: Herrero et al. (2013)

Table B.8: Units and description of the states and parameters in the Herrero model.

B.9 Kanderian - IVP model

	Magnitude	Units	Description
Insulin	ID	μU/min	Insulin administration (bolus and infusion)
	$I_{sc}(t)$	μU/ml	Subcutaneous insulin concentration
	$I_p(t)$	μU/ml	Plasma insulin concentration
	τ_1, τ_2	min	PK time constants
	C_I	ml/min	Insulin clearance
Glucose subsystem	$G(t)$	mg/dl	Plasma glucose
	$G_{ISF}(t)$	mg/dl	Glucose concentration in the interstitial fluid
	$I_{eff}(t)$	min^{-1}	Insulin effect
	$GEZI$	min^{-1}	Glucose effectiveness at zero insulin
	EGP	mg/dl/min	Endogenous glucose production
	p_2	min^{-1}	Time constant for insulin action
	S_I	ml/μU/min	Insulin sensitivity
	τ_{SEN}	min	Interstitial fluid delay (fixed to 10 min)
Meal subs.	C_H	g	Amount of carbohydrates
	$R_A(t)$	mg/dl/min	Rate of glucose appearance
	V_G	dl	Glucose distribution volume
	τ_m	min	Peak time of meal glucose appearance, different for each meal
References: Kanderian et al. (2012)			

Table B.9: Units and description of the states and parameters in the IVP model.

B.10 Kelly model

	Magnitude	Units	Description
Insulin subsystem	I_{inf}	μU/ml	Insulin infusion
	$I(t)$	μU/ml	Plasma insulin concentration
	I_b	μU/ml	Baseline plasma insulin concentration
	I_0	μU/ml	Theoretical value of insulin concentration at $t = 0$
	p_4	min^{-1}	Rate of insulin disappearance from plasma
	p_5	$\mu\text{U/ml min}^{-2}\,(\text{mg/dl})^{-1}$	Rate of second phase insulin secretion (glucose dependent)
Glucagon subsystem	$E(t)$	pg/ml	Plasma glucagon concentration
	$Y(t)$	min^{-1}	Interstitial glucagon activity
	E_b	ng/l	Baseline plasma glucagon concentration
	p_6	min^{-1}	Rate of glucagon disappearance from plasma
	p_7	$\text{ng/l min}^{-2}\,(\text{mg/dl})^{-1}$	Rate of excess plasma glucagon stimulated glucagon activity
	p_8	min^{-1}	Rate of clearance of interstitial glucagon
	p_9	$\text{min}^{-1}\,(\text{ng/l})^{-1}$	Rate of excess plasma glucagon stimulated glucose activity
	p_{11}	ng/l min^{-1}	Maximum rate at which insulin suppresses glucagon secretion
	δ	$\text{mg/dl min}^{-1}\,(\text{ng/l})^{-1}$	Glucagon effectiveness
Glucose subsystem	G_{inf}	mg/dl	Glucose infusion
	$G(t)$	mg/dl	Plasma glucose
	$X(t)$	min^{-1}	Interstitial insulin activity
	G_b	mg/dl	Baseline plasma glucose concentration
	G_0	mg/dl	Theoretical value of glucose concentration at $t = 0$
	p_2	min^{-1}	Rate of clearance of interstitial insulin
	p_3	$\text{min}^{-2}\,(\mu\text{U/ml})^{-1}$	Rate of clearance of interstitial insulin
	p_1	min^{-1}	Glucose effectiveness

References: Kelly et al. (2019)

Table B.10: Units and description of the states and parameters in the Kelly model.

B.11 Cinar model

	Magnitude	Units	Description
Insulin subsystem	u	mU/min	Insulin infusion rate
	$S_1(t)$	mU	Insulin mass in subcutaneous compartment 1
	$S_2(t)$	mU	Insulin mass in subcutaneous compartment 2
	$I(t)$	mU/l	Plasma insulin concentration
	$t_{max,I}$	min	Time-to-maximum insulin absorption
	V_I	l/kg	Insulin distribution volume
	k_e	min^{-1}	Insulin elimination rate
Meals subs.	D	mg/mmol	Carbohydrate intake (regular meal)
	DH	mg/mmol	Carbohydrate intake (fast-acting rescue)
	U_G	mmol/kg/min	Glucose absorption rate from meals
	A_G	unitless	Carbohydrate bioavailability
	$t_{max,G}$	min	Time-to-maximum appearance rate of glucose in the bloodstream
Glucose subsystem	$Q_1(t)$	mmol	Glucose in the bloodstream (accessible compartment)
	$Q_2(t)$	mmol	Glucose in the peripheral tissue (non-accessible compartment)
	$G_{sub}(t)$	mmol/l	Subcutaneous glucose concentration
	$x_1(t)$	min^{-1}	Effects of insulin on glucose distribution
	$x_2(t)$	min^{-1}	Effects of insulin on glucose disposal
	$x_3(t)$	min^{-1}	Effects of insulin on suppression of EGP
	F_{01}^c	mmol/kg/min	Non-insulin-dependent glucose flux
	F_R	mmol/kg/min	Renal glucose clearance
	EGP_0	mmol/kg/min	Extrapolated EGP at zero insulin concentration
	V_G	l/kg	Glucose distribution volume
	τ_G	min	Time constant for bloodstream to the interstitial tissues
	a	unitless	Exercise parameter
	β	mmol/min	Exercise-induced insulin-independent glucose uptake rate
	α	unitless	Exercise-induced insulin action
	k_{a1}, k_{a2}, k_{a3}	min^{-1}	Appearance and elimination rates
	k_{b1}, k_{b2}, k_{b3}	min^{-1} per mU/l	Activation rates
	k_{12}	min^{-1}	Transfer rate

Continued in next page

Continued from previous page

	Magnitude	Units	Description
Exercise subsystem	HR	BPM	Heart rate
	$E_1(t)$	BPM	Short-term exercise effect
	$T_E(t)$	min	Characteristic time for long term exercise effect
	$E_2(t)$	unitless	Long-term exercise effect
	t_{HR}	min	Exercise parameter
	t_{in}	min	Exercise parameter
	n	unitless	Exercise parameter
	t_{ex}	min	Exercise parameter
	c_1	min	Exercise parameter
	c_2	min	Exercise parameter
	HR_{base}	BPM	Basal heart rate

References: Rashid et al. (2019)

Table B.11: Units and description of the states and parameters in the Cinar model.

B.12 Fabietti model

	Magnitude	Units	Description
Insulin subsystem	V_{sc}	μU/h	Rate of insulin subcutaneous infusion or bolus
	V_{iv}	μU/h	Rate of insulin intravenous infusion
	$S(t)$	μU/h	Release rate to plasma compartment
	$I(t)$	μU/ml	Plasma insulin concentration
	T_i	h	Diffusion in the subcutaneous compartment
	K_i	ml/h	Constant related to the plasma distribution volume
	T_{xi}	h	Diffusion in the plasma compartment
	G_{iv}	mmol/h	Intravenous glucose administration
	$G(t)$	mmol/l	Blood glucose concentration
	$Y(t)$	mmol/l	Glucose concentration in the interstitial compartment
	$X(t)$	μU/ml	Equivalent insulin concentration in the remote compartment
	$E_g(t)$	mmol/h	Glucose contribution from ingested food

Continued in next page

Continued from previous page

	Magnitude	Units	Description
Glucose subsystem	$E_b(t)$	mmol/h	Hepatic glucose release
	$E_r(t)$	mmol/h	Renal clearance
	P_{circ}	unitless	Coefficient of the circadian variation of insulin sensitivity
	A_c, P_c	unitless	Amplitude and phase of the circadian rhythm
	T_{yg}	h	Time constant
	T_{gy}	h	Time constant
	V_g	l	Glucose distribution volume
	M_i	h	Insulin-independent metabolism
	T_m	h	Diffusion in the remote compartment
	K_{yg}	unitless	Rate between the distribution volumes of the interstitial and blood compartments
	K_{is}	ml/μU/h	Insulin sensitivity
Meal subsystem	R_i	mmol/h	Rate of carbohydrate ingestion during meals
	$A_g(t)$	mmol/h	Rate of glucose appearance in blood from sugar
	$A_s(t)$	mmol/h	Rate of glucose appearance in blood from fast absorption starch
	$A_m(t)$	mmol/h	Rate of glucose appearance in blood from slow absorption starch
	F_s	unitless	Starch fraction in the total meal carbohydrate amount
	G_g	unitless	Second-order filter transfer function
	G_s	unitless	Third-order filter transfer function
	G_m	unitless	Fourth-order filter transfer function
	F_m	unitless	Fraction of mixed meal in the starch absorption model

References: Fabietti et al. (2006)

Table B.12: Units and description of the states and parameters in the Fabietti model.

B.13 Models equations

	Bergman model	Kelly model	Fabietti model
Insulin	$\dot{I}(t) = \gamma(G(t) - h)t - nI(t)$	$\dot{I}(t) = -p_4\left(I(t) - I_b\right) + p_5(G(t) - G_b)^+ t + I_{inf}(t)$	$\dot{S}(t) = \frac{1}{T_i}\left(-S(t) - V_{sc}(t)\right)$ $\dot{I}(t) = \frac{1}{T_{xi}}\left(-I(t) + K_i\left(V_{iv}(t) + S(t)\right)\right)$
Glucgn.		$\dot{E}(t) = -p_6\left(E(t) - E_b\right) + p_7\left(G_b - G(t)\right)^+ t$ $- p_{11}\tanh\alpha(I(t) - I_b)$	
EGP		$\dot{Y}(t) = -p_8 Y(t) + p_9\left(E(t) - E_b\right)^+$	
Glucose	$\dot{X}(t) = p_2 X(t) + p_3 I(t)$ $\dot{G}(t) = -\left(S_G + X(t)\right)G(t) - S_G G_b$	$\dot{X}(t) = -p_2 X(t) + p_3(I(t) - I_b)$ $\dot{G}(t) = -p_1\left(G(t) - G_b\right)$ $+ \left(Y(t) - X(t)\right)G(t) + G_{inf}(t)$	$\dot{X}(t) = \frac{1}{T_m}\left(-X(t) + I(t)\right)$ $\dot{G}(t) = -\frac{G(t)}{T_{yg}} + \frac{Y(t)}{T_{gy}}$ $+ \frac{1}{V_g}\left(-M_i + E_g(t) + E_b(t) + G_{iv}(t)\right) - E_r(t)$ $\dot{Y}(t) = K_{yg}\left(\frac{G(t)}{T_{yg}} - \frac{Y(t)}{T_{gy}}\right) - K_{is}P_{circ}X(t)Y(t)$ $P_{circ} = 1 + A_c\sin\left(\frac{\pi t}{12} + P_c\right)$
Meals			$E_g(t) = A_g + A_s + A_m$ $A_g(s) = (1 - F_s)G_g(s)R_i(s)$ $A_s(s) = F_s(1 - F_m)G_s(s)R_i(s)$ $A_m(s) = F_s F_m G_m(s)R_i(s)$

Hovorka model

Insulin

$$\dot{S}_1(t) = u_I(t) - \frac{S_1(t)}{t_{max,I}}$$
$$\dot{S}_2(t) = \frac{S_1(t)}{t_{max,I}} - \frac{S_2(t)}{t_{max,I}}$$
$$\dot{I}(t) = \frac{S_2(t)/t_{max,I}}{V_I} - k_e I(t)$$

EGP

$$EGP(t) = EGP_0(1 - x_3(t))$$

Glucose

$$\dot{x}_1(t) = -k_{a1}x_1(t) + S_{IT}k_{a1}I(t)$$
$$\dot{x}_2(t) = -k_{a2}x_2(t) + S_{ID}k_{a2}I(t)$$
$$\dot{x}_3(t) = -k_{a3}x_3(t) + S_{IE}k_{a3}I(t)$$
$$\dot{Q}_1(t) = -F_{01}^c - F_R - x_1(t)Q_1(t) + k_{12}Q_2(t) + EGP(t) + U_G(t)$$
$$\dot{Q}_2(t) = x_1(t)Q_1(t) - [k_{12} + x_2(t)]\,Q_2(t)$$
$$G(t) = \frac{Q_1(t)}{V_G}$$

For every definition of F_{01}^c and F_R :

$$F_{01}^c = \begin{cases} F_{01} & \text{if } G \geq 4.5 \text{ mmol/l} \\ F_{01}G/4.5 & \text{otherwise} \end{cases}$$

$$F_R = \begin{cases} 0.003(G-9)V_G & \text{if } G \geq 9 \text{ mmol/l} \\ 0 & \text{otherwise} \end{cases}$$

Meals

Hovorka2004:

$$U_G(t) = \frac{D_G A_G t e^{-t/t_{max,G}}}{t_{max,G}^2}$$

Willinska2010:

$$\dot{G}_1(t) = -\frac{G_1(t)}{t_{max}} + Bio \cdot D$$
$$\dot{G}_2(t) = \frac{G_1(t)}{t_{max}} - \frac{G_2(t)}{t_{max}}$$
$$U_G(t) = G_2/t_{max}$$

	Receptors model	Wendt model	Herrero model
Insulin	$\dot{S}_1(t) = u_I(t) - \frac{S_1(t)}{t_{max}}$ $\dot{S}_2(t) = \frac{S_1(t)}{t_{max}} - \frac{S_2(t)}{t_{max}}$ $I(t) = \frac{1}{t_{max}} \frac{S_2(t)}{W \cdot Cl_{F,I}} \cdot 10^6 + I_b$	$\dot{S}_1(t) = u_I(t) - \frac{S_1(t)}{t_{max}}$ $\dot{S}_2(t) = \frac{S_1(t)}{t_{max}} - \frac{S_2(t)}{t_{max}}$ $I(t) = \frac{1}{t_{max}} \frac{S_2(t)}{W \cdot Cl_{F,I}} \cdot 10^6 + I_b$	$\dot{S}_1(t) = u(t) - \frac{S_1(t)}{t_{maxI}}$ $\dot{S}_2(t) = \frac{S_1(t) - S_2(t)}{t_{maxI}}$ $\dot{I}(t) = -k_e I(t) + \frac{S_2(t)}{V_I t_{maxI}}$
Glucagon	$\dot{Z}_1(t) = u_C(t) - k_1 Z_1(t)$ $\dot{Z}_2(t) = k_1 Z_1(t) - k_2 Z_2(t)$ $C(t) = \frac{k_2 Z_2(t)}{W \cdot Cl_{F,C}} + C_b$	$\dot{Z}_1(t) = u_C(t) - k_1 Z_1(t)$ $\dot{Z}_2(t) = k_1 Z_1(t) - k_2 Z_2(t)$ $C(t) = \frac{k_2 Z_2(t)}{W \cdot Cl_{F,C}} + C_b$	$\dot{Z}_1(t) = w(t) + \frac{Z_1(t)}{t_{maxN}}$ $\dot{Z}_2(t) = \frac{Z_1(t) - Z_2(t)}{t_{maxN}}$ $\dot{N}(t) = -k_N N(t) + \frac{Z_2(t)}{V_N t_{maxN}}$
EGP	$\dot{r}(t) = -k_{on} V_h C(t) r(t) + k_{off} r_c(t) + k_{rec}(1 - r(t) - r_c(t))$ $\dot{r}_c(t) = k_{on} V_h C(t) r(t) - k_{off} r_c(t) - k_{in} r_c(t)$ $F_{hgp}(t) = \frac{V_r r_c(t)}{K_r + r_c(t)}$ $EGP(t) = F_{hgp}(t) + EGP_0(1 - S_I x_3(t))$	$G_{GG}(t) = \frac{1 - S_e x_3(t)}{1 - S_e I_b} \left((E_{max} - G_{GNG}) \frac{C(t)}{C_{E50} + C(t)} \right)$ $EGP(t) = G_{GG}(t) + G_{GNG}$	$\dot{Y}(t) = -p_3 Y(t) + p_3 S_N (N(t) - N_b)$ $p_3 = k_8, \qquad S_N = \frac{k_7}{k_8} k_9$
Glucose	$\dot{x}_1(t) = -k_{a1} [x_1(t) - I(t)]$ $\dot{x}_2(t) = -k_{a2} [x_2(t) - I(t)]$ $\dot{x}_3(t) = -k_{a3} [x_3(t) - I(t)]$ $\dot{Q}_1(t) = -F_{01} - F_R - S_T x_1(t) Q_1(t) + k_{12} Q_2(t) + EGP(t)$ $\dot{Q}_2(t) = S_T x_1(t) Q_1(t) - [k_{12} + S_D x_2(t)] Q_2(t)$ $G(t) = \frac{Q_1(t)}{V}$	$\dot{x}_1(t) = -k_{a1} [x_1(t) - I(t)]$ $\dot{x}_2(t) = -k_{a2} [x_2(t) - I(t)]$ $\dot{x}_3(t) = -k_{a3} [x_3(t) - I(t)]$ $\dot{Q}_1(t) = -F_{01} - F_R - S_T x_1(t) Q_1(t) + k_{12} Q_2(t) + EGP(t)$ $\dot{Q}_2(t) = S_T x_1(t) Q_1(t) - [k_{12} + S_D x_2(t)] Q_2(t)$ $G(t) = \frac{Q_1(t)}{V}$	$\dot{X}(t) = p_2 X(t) + p_3 S_I (I(t) - I_b)$ $S_I = \frac{k_2}{k_3} (k_4 + k_6), \quad p_2 = k_3$ $\dot{G}(t) = -(S_G + X(t) - Y(t)) G(t) + S_G G_b + \frac{R_a(t)}{V}$ $S_G = k_1 + k_5$
Meals			$\dot{F}(t) = \frac{1}{t_{maxG}} (-F(t) + A_G D_G)$ $\dot{R}_a(t) = \frac{1}{t_{maxG}} (-R_a(t) + F(t))$

	Jacobs model	Haidar model
Insulin	$\dot{S}_1(t) = u_I - \frac{S_1(t)}{t_{max}}$ $\dot{S}_2(t) = \frac{S_1(t)}{t_{max}} - \frac{S_2(t)}{t_{max}}$ $\dot{I}(t) = \frac{S_2(t)}{t_{max} V_I} - k_e I(t)$	$\dot{Q}_{is1}(t) = u_i(t) p_i - Q_{is1}(t) k_{is1}$ $\dot{Q}_{is2}(t) = Q_{is1}(t) k_{is1} - Q_{is2}(t) k_{is2}$ $\dot{Q}_{if1}(t) = u_i(t)(1 - p_i) - Q_{if1}(t) k_{if}$ $\dot{Q}_{if2}(t) = Q_{if1}(t) k_{if} - Q_{if2}(t) k_{if}$ $\dot{Q}_i(t) = (Q_{is2}(t) k_{is2} + Q_{if2} k_{if2}) I_m(t) - Q_i(t) k_e + c_i, \qquad I_p(t) = \frac{Q_i(t)}{V_i \omega} \cdot 10^6$
Glucagon	$\dot{X}_{1g}(t) = -(k_{1g} + k_{ge1}) X_{1g}(t) + u_g(t)$ $\dot{X}_{2g}(t) = k_{1g} X_{1g}(t) - k_{2g} X_{2g}(t)$ $\dot{X}_{3g}(t) = k_{2g} X_{2g}(t) - k_{ge2} X_{3g}(t)$ $\dot{Y}(t) = \frac{10^6 \times k_c \times S_{fGC}}{V_{dGG}} X_{3g}(t) - k_c Y(t) = k_g X_{3g}(t) - k_c Y(t)$ $Z(t) = \dot{Y}(t) \rightarrow \dot{Z}(t) = k_g k_{2g} X_{2g}(t) - k_g k_{ge2} X_{3g}(t) - k_c Z(t)$	$\dot{Q}_{g1}(t) = u_g(t) - \frac{Q_{g1}(t)}{t_{gmax}}$ $\dot{Q}_{g2}(t) = \frac{Q_{g1}(t)}{t_{gmax}} - \frac{Q_{g2}(t)}{t_{gmax}}$ $C_p(t) = \frac{1}{t_{gmax}} \cdot \frac{Q_{g2}(t)}{\omega \mathrm{MCR}_g} \cdot 10^6 + C_b$
EGP	$EGP(t) = EGP_0(1 - X_3(t) + Y(t) + k_{g3} Z(t))$	$EGP(t) = \begin{cases} C_p(t) S_g (1 - x_3(t) S_e) & \text{if } x_3(t) < 1 \\ 0 & \text{if } x_3(t) \geq 1 \end{cases}$
Glucose	$\dot{X}_1(t) = -k_{a1} X_1(t) + S_{f1} k_{a1} I(t)$ $\dot{X}_2(t) = -k_{a2} X_2(t) + S_{f2} k_{a2} I(t)$ $\dot{X}_3(t) = -k_{a3} X_3(t) + S_{f3} k_{a3} I(t)$ $\dot{Q}_1(t) = -F_{01}^c - F_R - X_1(t) Q_1(t) + k_{12} Q_2(t) + EGP(t) + U_G(t)$ $\dot{Q}_2(t) = X_1(t) Q_1(t) - k_{12} Q_2(t) - X_2(t) Q_2(t)$	$\dot{x}_1(t) = -k_{a1} x_1(t) + k_{a1} I(t)$ $\dot{x}_2(t) = -k_{a2} x_2(t) + k_{a2} I(t)$ $\dot{x}_3(t) = -k_{a3} x_3(t) + k_{a3} I(t)$ $\dot{Q}_1(t) = -F_{01} \frac{Q_1(t)/V}{1 + Q_1(t)/V} - x_1(t) S_t Q_1(t) + k_{12} Q_2(t) + EGP(t) + F_g(t) + U_m(t)$ $\dot{Q}_2(t) = x_1(t) S_t Q_1(t) - [k_{12} + x_2(t) S_d]\, Q_2(t)$ $G(t) = \frac{Q_1(t)}{V}$ $\dot{G}_s(t) = -k_s G_s(t) + k_s G(t)$
Meals	$U_G(t) = \frac{D_G A_G (t - t_0) e^{\frac{t - t_0}{t_{max,G}}}}{t_{max,G}^2}$	$U_{m1}(t) = k_m^2 t e^{-k_m t} \frac{CHO \cdot 5551}{\omega}$ $U_{m2}(t) = \begin{cases} k_m^2 (t - d) e^{-k_m (t-d)} \frac{CHO \cdot 5551}{\omega} (1 - p_m) & \text{if } t > d \\ 0 & \text{otherwise} \end{cases}$ $U_m(t) = (U_{m1}(t) + U_{m2}(t)) f_m(t)$
Exercise	$S_{f1-EX} = M_{PGU} M_{PIU} S_{f1}, \quad S_{f2-EX} = M_{PGU} M_{PIU} S_{f2}, \quad S_{f3-EX} = M_{HGP} S_{f3}$ $M_{PGU} = 1 + \frac{\Gamma_{PGUA}(t) \times PAMM}{35}$ $M_{PIU} = 1 + 2.4 \times PAMM$ $M_{HGP} = 1 + \frac{\Gamma_{HGPA}(t) \times PAMM}{155}$ $\dot{\Gamma}_{PGUA}(t) = -\frac{1}{30} \Gamma_{PGUA}(t) + \frac{1}{30} \Gamma_{\overline{PGUA}}$ $\Gamma_{\overline{PGUA}} = 0.006\,(PVO_2^{max})^2 + 1.2264\,(PVO_2^{max}) - 10.1958$	

	IVP model	Cinar model
Insulin	$\dot{I}_{sc}(t) = -\frac{I_{sc}(t)}{\tau_1} + \frac{1}{\tau_1}\frac{ID(t)}{C_I}$ $\dot{I}_p(t) = -\frac{I_p(t)}{\tau_2} + \frac{I_{sc}(t)}{\tau_2}$	$\dot{S}_1(t) = u(t) - \frac{S_1(t)}{t_{max,I}}$ $\dot{S}_2(t) = \frac{S_1(t)}{t_{max,I}} - \frac{S_2(t)}{t_{max,I}}$ $\dot{I}(t) = \frac{S_2(t)}{V_I t_{max}} - k_e I(t)$
EGP		$EGP(t) = EGP_0(1 - x_3(t))$
Glucose	$\dot{I}_{eff}(t) = -p_2 I_{eff}(t) + p_2 S_I I_p(t)$ $\dot{G}(t) = -(\text{GEZI} + I_{eff}(t))G(t) + \text{EGP} + R_A(t)$ $\dot{G}_{ISF}(t) = -\frac{G_{ISF}(t)}{\tau_{SEN}} + \frac{G(t)}{\tau_{SEN}}$	$\dot{X}_1(t) = -k_{a1}X_1(t) + k_{b1}I(t)$ $\dot{X}_2(t) = -k_{a2}X_2(t) + k_{b2}I(t)$ $\dot{X}_3(t) = -k_{a3}X_3(t) + k_{b3}I(t)$ $\dot{Q}_1(t) = -F_{01}^c - F_R - (1+\alpha E_2(t)^2)X_1(t)Q_1(t) + k_{12}Q_2(t) + EGP(t) + U_G(t)$ $\dot{Q}_2(t) = (1+\alpha E_2(t)^2)X_1(t)Q_1(t) - k_{12}Q_2(t) - (1+\alpha E_2(t)^2)X_2(t)Q_2(t) - \beta\frac{E_1(t)}{HR_{base}}$
Meals	$R_A(t) = \frac{C_G(t)}{V_G\tau_m^2} \cdot t \cdot e^{\frac{t}{\tau_m}}$	$\dot{D}_1(t) = A_G D(t) - \frac{D_1(t)}{t_{max,G}}$ $\dot{D}_2(t) = \frac{D_1(t)}{t_{max,G}} - \frac{D_2(t)}{t_{max,G}}$ $\dot{DH}_1(t) = A_G DH(t) - \frac{DH_1(t)}{t_{max,g}}, \quad t_{max,g} = \frac{t_{max,G}}{2}$ $\dot{DH}_2(t) = \frac{DH_1(t)}{t_{max,g}} - \frac{DH_2(t)}{t_{max,g}}$ $U_G(t) = \frac{D_2(t)}{t_{max,G}} + \frac{DH_2(t)}{t_{max,g}}$
Exercise		$\dot{E}_1(t) = \frac{1}{t_{HR}}\left[\Delta HR(t) - E_1(t)\right], \quad f\left(E_1(t)\right) = \frac{\left(\frac{E_1(t)}{a \cdot HR_{base}}\right)^n}{1 + \left(\frac{E_1(t)}{a \cdot HR_{base}}\right)^n}$ $\dot{T}_E(t) = \frac{1}{t_{ex}}\left[c_1 f\left(E_1(t)\right) + c_2 - T_E(t)\right]$ $\dot{E}_2(t) = -\left[\frac{f\left(E_1(t)\right)}{t_{in}} + \frac{1}{T_E(t)}\right] \cdot E_2(t) + \frac{f\left(E_1(t)\right)}{t_{in}} \cdot \frac{1}{T_E(t)}c_1 + c_2$

Dalla Man model

Insulin

$$\dot{I}_{sc1}(t) = -(k_d + k_{a1})I_{sc1}(t) + IIR(t)$$
$$\dot{I}_{sc2}(t) = k_d I_{sc1}(t) - k_{a2} I_{sc2}(t)$$
$$R_{ai}(t) = k_{a1} I_{sc1}(t) + k_{a2} I_{sc2}(t)$$
$$\dot{I}_p(t) = -(m_2 + m_4)I_p(t) + m_1 I_l(t) + R_{ai}(t)$$
$$\dot{I}_l(t) = -(m_1 + m_3)I_l(t) + m_2 I_p(t)$$
$$I(t) = \frac{I_p(t)}{V_I}$$

Glucagon

$$\dot{H}_{sc1}(t) = -(k_{h1} + k_{h2})H_{sc1}(t) + H_{inf}(t)$$
$$\dot{H}_{sc2}(t) = k_{h1} H_{sc1}(t) - k_{h3} H_{sc2}(t)$$
$$Ra_H(t) = k_{h3} H_{sc2}(t)$$
$$SR_H(t) = SR^s_H(t) + SR^d_H(t)$$
$$\dot{H}(t) = -nH(t) + SR_H(t) + Ra_H(t)$$

$$\dot{SR}^S_H(t) = \begin{cases} -\rho \cdot \left[SR^S_H(t) - \max\left(\sigma_2 \cdot [G_{th} - G(t)] + SR^b_H, 0\right)\right] & \text{if } G(t) \geq G_b \\ -\rho \cdot \left[SR^S_H(t) - \max\left(\frac{\sigma \cdot [Gth - G(t)]}{I(t)+1} + SR^b_H, 0\right)\right] & \text{if } G(t) < G_b \end{cases}$$
$$SR^d_H(t) = \delta \cdot \max\left(-\frac{\mathrm{d}G(t)}{\mathrm{d}t}, 0\right)$$

EGP

$$\dot{X}_H(t) = -k_H X_H(t) + k_H \cdot max\left[(H(t) - H_b), 0\right]$$
$$\dot{I}'(t) = -k_i \cdot \left[I'(t) - I(t)\right]$$
$$\dot{X}_L(t) = -k_i \cdot \left[X_L(t) - I'(t)\right]$$
$$EGP(t) = k_{p1} - k_{p2} G_p(t) - k_{p3} X_L(t) + \xi X_H(t)$$

Glucose

$$\dot{G}_p(t) = -U_{ii} - E(t) - k_1 G_p(t) + k_2 G_t(t) + EGP(t) + Ra(t)$$
$$\dot{G}_t(t) = k_1 G_p(t) - k_2 G_t(t) - U_{id}(t)$$
$$G(t) = \frac{G_p(t)}{V_G}$$
$$U_{id}(t) = \frac{[V_{m0} + V_{mx} X(t)(1 + r_1 \cdot risk)] \cdot G_t(t)}{K_{m0} + G_t(t)}$$
$$\dot{X}(t) = -p_{2U} X(t) + p_{2U}\left[I(t) - I_b\right]$$

$$risk = \begin{cases} 0 & \text{if } G \geq G_b \\ 10 \cdot [f(G)]^2 & \text{if } G_{th} \leq G < G_b \\ 10 \cdot [f(G_{th})]^2 & \text{if } G < G_{th} \end{cases}$$
$$f(G) = log(G/G_b)^{r_2}$$
$$E(t) = \begin{cases} k_{e1} \cdot [G_p(t) - k_{e2}] & \text{if } G_p(t) > k_{e2} \\ 0 & \text{if } G_p(t) \leq k_{e2} \end{cases}$$

Meals

$$\dot{Q}_{sto1}(t) = -k_{gri} \cdot Q_{sto1}(t) + D \cdot \delta(t)$$
$$\dot{Q}_{sto2}(t) = -k_{empt}(Q_{sto}) \cdot Q_{sto2}(t) + k_{gri} \cdot Q_{sto1}(t)$$
$$Q_{sto}(t) = Q_{sto1}(t) + Q_{sto2}(t)$$
$$\dot{Q}_{gut}(t) = -k_{abs} \cdot Q_{gut}(t) + k_{empt}(Q_{sto}) \cdot Q_{sto2}(t)$$
$$Ra(t) = \frac{f \cdot k_{abs} \cdot Q_{gut}(t)}{BW}$$

$$k_{empt}(Q_{sto}) = k_{min} + \frac{k_{max} - k_{min}}{2} \cdot \{tanh\left[\alpha\left(Q_{sto}(t) - b \cdot D\right)\right] - tanh\left[\beta\left(Q_{sto}(t) - c \cdot D\right)\right] + 2\}$$